



# **Improvement of Base and Soil Construction Quality by Using Intelligent Compaction Technology**

**Research Report 0-6740-1**

**TxDOT Project Number 0-6740**

**Conducted for:  
Texas Department of Transportation  
in cooperation with  
Federal Highway Administration**

**February 2014**

Center for Transportation Infrastructure Systems  
The University of Texas at El Paso  
El Paso, TX 79968  
(915) 747-6925  
<http://ctis.utep.edu>

## TECHNICAL REPORT STANDARD TITLE PAGE

|  |   |  |           |
|--|---|--|-----------|
| 1. Report No.<br><b>FHWA/TX-13/0-6740-1</b>  | 2. Government Accession No.                                 | 3. Recipient's Catalog No.   |           |
| 4. Title and Subtitle<br><b>Improvement of Base and Soil Construction Quality by Using Intelligent Compaction Technology</b>   |   | 5. Report Date<br><b>February 2014</b>   |           |
|  |   | 6. Performing Organization Code  |           |
| 7. Author(s)<br><b>A.K. Siddagangaiah, R. Aldouri, S. Nazarian, C.M. Chang, and A. Puppala</b>   |   | 8. Performing Organization Report No.<br><b>TX 0-6740-1</b>  |           |
| 9. Performing Organization Name and Address<br><b>Center for Transportation Infrastructure Systems<br/>The University of Texas at El Paso<br/>El Paso, Texas 79968-0516</b>  |   | 10. Work Unit No.  |           |
|  |   | 11. Contract or Grant No.<br><b>Project No. 0-6740</b>   |           |
| 12. Sponsoring Agency Name and Address<br><b>Texas Department of Transportation<br/>Research and Technology Implementation Office<br/>P.O. Box 5080<br/>Austin, Texas 78763-5080</b>   |   | 13. Type of Report and Period Covered<br><b>Technical Report<br/>Nov. 1, 2012 –Nov. 30, 2013</b>   |           |
|  |   | 14. Sponsoring Agency Code   |           |
| 15. Supplementary Notes<br><b>Research Performed in cooperation with TxDOT and the Federal Highway Administration<br/>Research Study Title: Improvement of Construction Quality Control by Using Intelligent Compaction Technology for Base and Soil</b>   |   |  |           |
| 16. Abstract<br><b>TxDOT current practice for field compaction quality control and acceptance of base and soil layers is to determine the compacted density and moisture content by nuclear density gauge (NDG). TxDOT has considered several stiffness-based devices to replace density measurement because stiffness parameters are more relevant to pavement design. Since both density and stiffness measurements are truly spot tests, they cannot represent the quality and uniformity of compaction in a continuous manner. Intelligent compaction (IC) technique is a fast-developing technology for base and soil compaction quality control and acceptance. Proof rolling subgrade and base using the intelligent compaction rollers after completing compaction can effectively identify the weak spots and significantly improve the uniformity of the compacted layers. In this report, guidelines and test protocols for the use of intelligent compaction to improve the process of accepting compacted materials are evaluated, and prototype specifications are proposed.</b> |   |  |           |
| 17. Key Words<br><b>Intelligent compaction, Geomaterial, Strength, Modulus, Structural analysis</b>  |   | 18. Distribution Statement<br><b>No restrictions. This document is available to the public through the National Technical service, 5285 Port Royal Road, Springfield, Virginia 22161, <a href="http://www.ntis.gov">www.ntis.gov</a></b> |           |
| 19. Security Classif. (of this report)<br><b>Unclassified</b>  | 20. Security Classif. (of this page)<br><b>Unclassified</b> | 21. No. of Pages<br><b>178</b>   | 22. Price |

**Improvement of Base and Soil Construction Quality by  
Using Intelligent Compaction Technology**

by

**Anjan Kumar Siddagangaiah, PhD  
Raed Aldouri, PhD  
Cesar Tirado, PhD  
Soheil Nazarian, PhD, PE  
Carlos M. Chang, PhD, PE  
and  
Anand Puppala, PhD, PE**

**Research Project TX-0-6740**

**Conducted for  
Texas Department of Transportation  
in cooperation with  
Federal Highway Administration**

**Research Report TX 0-6740-1**

**Center for Transportation Infrastructure Systems  
The University of Texas at El Paso  
El Paso, TX 79968-0516**

## **DISCLAIMERS**

The contents of this report reflect the view of the authors who are responsible for the facts and the accuracy of the data presented herein. The contents do not necessarily reflect the official views or policies of the Texas Department of Transportation or the Federal Highway Administration. This report does not constitute a standard, a specification or a regulation.

The material contained in this report is experimental in nature and is published for informational purposes only. Any discrepancies with official views or policies of the Texas Department of Transportation or the Federal Highway Administration should be discussed with the appropriate Austin Division prior to implementation of the procedures or results.

## **NOT INTENDED FOR CONSTRUCTION, BIDDING, OR PERMIT PURPOSES**

Anjan Kumar Siddagangaiah, PhD  
Raed Aldouri, PhD  
Cesar Tirado, PhD  
Soheil Nazarian, PhD, PE (66495)  
Carlos M. Chang, PhD, PE  
Anand Puppala, PhD, PE

## **Acknowledgements**

The authors would like to express their sincere appreciation to the Project Management Committee of this project, consisting of Jimmy Si, Richard Williammee, Wade Blackmon, Victor Goebel, Charles Gurganus and Carlos Peralez for their support.

We are grateful to a number of employees of the Fort Worth District, especially Mike Rogers, Ben McCleery, David Fowler and John Poskey for their assistance in field testing. The help from Brown and Gay, Lane Construction and Prater Construction Company is also acknowledged.

We are also grateful to a number of undergraduate and graduate students from UTEP and UT-Arlington for their assistance in the project.

## **Abstract**

TxDOT's current practice for field compaction quality control and acceptance of base and soil layers is to determine the compacted density and moisture content by nuclear density gauge (NDG). TxDOT has considered several stiffness-based devices to replace density measurement because stiffness parameters are more relevant to pavement design. Since both density and stiffness measurements are truly spot tests, they cannot represent the quality and uniformity of compaction in a continuous manner. Intelligent Compaction (IC) is a fast-developing technology for base and soil compaction quality control and acceptance. Proof rolling subgrade and base using the intelligent compaction rollers after completing compaction can effectively identify the weak spots and significantly improve the uniformity of the compacted layers. In this report, guidelines and test protocols for the use of intelligent compaction to improve the process of accepting compacted materials are evaluated, and prototype specifications are proposed.

## **Implementation Statement**

In this report, a number of recommendations have been made to improve the general quality of compaction for subgrade and base construction. At this time, the recommendations should be implemented in a number of new and ongoing projects to confirm their applicability and to adjust the limits and/or criteria recommended. As part of the implementation, a guide should be developed to disseminate to the TxDOT staff. The specific items to be implemented include:

- (1) developing and deploying a training program for the TxDOT engineers and inspectors,
- (2) supporting the districts in implementing the IC technology in their districts,
- (3) implementing a field monitoring program to quantify the long-term benefits of the IC technology, and
- (4) assisting the Construction Division (CST) in evaluating and incorporating the new IC specification for inclusion in the new specification book.

# Table of Contents

|  |    |
|--|----|
| List of Figures.....   | vi |
| List of Tables.....  | ix |
| Chapter 1.....   | 1  |
| Introduction.....  | 1  |
| Objective.....   | 1  |
| Organization of Report .....   | 2  |
| Chapter 2.....   | 4  |
| Background and Information Search .....                                      | 4  |
| Introduction.....  | 4  |
| Advantages of Intelligent Compaction .....                                   | 4  |
| Challenges with Intelligent Compaction.....                                  | 4  |
| Modulus of Compacted Geomaterials .....                                      | 5  |
| Factors Impacting Modulus of Compacted Geomaterials .....                    | 5  |
| Intelligent Compaction Systems .....   | 6  |
| Data Collection in Intelligent Compaction Roller .....                       | 6  |
| Field Evaluation of Intelligent Compaction.....                              | 7  |
| Field Evaluation Devices for Spot Tests.....                                 | 7  |
| Existing Specifications.....   | 8  |
| IC Technology as Quality Control (QC) and Quality Acceptance (QA) Tools..... | 8  |
| Influence of Geomaterial Types on Quality Acceptance .....                   | 8  |
| Applicable Roller Types .....  | 14 |
| Effective Timing for Conducting IC-based Acceptance Testing.....             | 15 |
| Minimum Thickness of Layer for Quality Acceptance .....                      | 15 |
| Roller and Instrumentation Parameters for Robust Quality Acceptance .....    | 15 |
| Acceptance Testing.....  | 18 |
| Target Value Selection.....  | 18 |
| Limitations of Existing Guidelines for Development of Specifications.....    | 19 |
| Geostatistics in Intelligent Compaction .....                                | 20 |
| Numerical Analysis of Intelligent Compaction .....                           | 23 |
| Best Practices and their Impact on Compaction Process .....                  | 23 |
| Best Practices for Quality Control and Acceptance.....                       | 29 |
| Chapter 3.....   | 31 |
| Numerical Analysis of Soil-Roller Interaction .....                          | 31 |

|  |     |
|--|-----|
| Introduction.....  | 31  |
| Finite Element Modeling of Roller Compactor .....                | 31  |
| Parametric Study.....  | 33  |
| Depth of Influence .....   | 33  |
| Stiffness.....   | 36  |
| Finite Element Modeling of Light Weight Deflectometer (LWD)..... | 39  |
| Depth of Influence .....   | 40  |
| LWD Modulus .....  | 45  |
| Chapter 4.....   | 48  |
| Experimental Study.....  | 48  |
| Introduction.....  | 48  |
| Project Location.....  | 48  |
| Laboratory Test Results .....                                    | 48  |
| Test Program.....  | 53  |
| Field Studies.....   | 53  |
| Chapter 5.....   | 68  |
| Practical Observations .....                                     | 68  |
| Roller Measurement Target Values .....                           | 68  |
| Spatial Variability .....  | 72  |
| Site Preparation.....  | 72  |
| Analyses of Roller Measurements .....                            | 74  |
| GPS System Check and Calibration .....                           | 77  |
| Geospatial and Geostatistical Analyses .....                     | 77  |
| Training.....  | 80  |
| Chapter 6.....   | 81  |
| Modification of Prototype Specification.....                     | 81  |
| Introduction.....  | 81  |
| Traditional Tests and Sampling Frequencies.....                  | 81  |
| Means of Setting Target Values.....                              | 82  |
| Chapter 7.....   | 89  |
| Conclusions and Recommendations .....                            | 89  |
| REFERENCES .....   | 91  |
| Appendix A.....  | 95  |
| Appendix B.....  | 131 |
| Appendix C.....  | 145 |
| Appendix D.....  | 150 |
| Appendix E.....  | 159 |

## List of Figures

|  |    |
|--|----|
| Figure 1.1 – Flow Chart of Research Activities .....   | 3  |
| Figure 2.1 – Definitions of Modulus.....   | 5  |
| Figure 2.2 – Representation of Roller Drum and Soil Interaction (Anderegg et al., 2006).....   | 6  |
| Figure 2.3 – Three Basic Types of Behaviors (a) Continuous Contact (b) Periodic Loss of Contact (c) Bouncing or Rocking (Anderegg and Kaufmann, 2004) .....      | 7  |
| Figure 2.4 – A Histogram Showing CCV Values and their Occurrence in IC Technology with Descriptive Statistics (VEDA v2). .....                                   | 21 |
| Figure 2.5 – A Semivariogram of CCV Data from CCV Values (VEDA v2).....  | 21 |
| Figure 2.6 – Proofing Data Example Showing Spatial Variations in the CCV Values .....  | 21 |
| Figure 2.7 – Variation in Modulus as a Function of Compaction and Testing Moisture Contents.....   | 30 |
| Figure 2.8 – Variation in Modulus as a Function of Difference in Compaction and Testing Moisture Contents .....  | 30 |
| Figure 3.1 – FE Modeling of Roller and Pavement Structure .....  | 32 |
| Figure 3.2 – Roller to Soil Contact .....  | 32 |
| Figure 3.3 – Vertical Stress Distribution for a Pavement Structure with a 6 in. Base.....  | 34 |
| Figure 3.4 – Response Profiles for a Pavement Structure with a 6 in. Base..... (Base Modulus of 45 ksi and Varying Subgrade Modulus). .....                      | 34 |
| Figure 3.5 – Depth of Influence in terms of Vertical Stress at Varying Stress Level and Varying Base Thickness. ....   | 35 |
| Figure 3.6 – Depth of Influence at a 10% of the Surface Vertical Peak Stress for Varying Base and Subgrade Moduli. ....  | 36 |
| Figure 3.7 – Depth of Influence at a 10% of the Surface Peak Deflection with Varying Base and Subgrade Moduli. ....  | 37 |
| Figure 3.8 – Hysteresis Loops for the Calculation of Tangent and Secant Stiffness and Modulus for a 6-in. Base, $E_{BASE} = 45$ ksi and $E_{SUBG} = 15$ ksi..... | 37 |
| Figure 3.9 – Tangent and Secant Stiffness and Moduli for a 6-in. base, $E_{BASE} = 45$ ksi and Varying Subgrade Moduli. ....                                     | 38 |
| Figure 3.10 – Roller Stiffness Parameters as a Function of Base to Subgrade Modulus Ratio .....  | 39 |
| Figure 3.11 – Schematic Views of LWD Devices and Finite Element Model of Zorn LWD .....  | 40 |
| Figure 3.12 – Vertical Stress Distributions of LWD Impact on a Section with a 6 in. Thick Base .....   | 41 |

|   |    |
|---|----|
| Figure 3.13 – Vertical Stress Contour Plots of LWD Impact under Different Layer Combinations.....   | 42 |
| Figure 3.14 – Depth Profiles of Vertical Deformations for a Section with a 6 in. Thick Base.....  | 43 |
| Figure 3.15 – Depth of Influence at a Stress Level of 10% of the Surface Peak Stress .....  | 43 |
| Figure 3.16 – Depth of Influence at a Level of 10% of the Surface Peak Stress for Deflection .....  | 44 |
| Figure 3.17 – Surface Deflection Moduli for Different Layer Combinations .....  | 45 |
| Figure 3.18 – Relationship of $M_s$ and $E_{LWD}$ under Different Layer Combinations.....   | 46 |
| Figure 4.1 – Locations of Field Evaluation Sites.....   | 49 |
| Figure 4.2 – Illustration of Test Sections in SH 267 Site .....   | 50 |
| Figure 4.3 – Illustration of Test Sections along IH 35W Site.....   | 51 |
| Figure 4.4 – Gradation Curves of Geomaterials .....   | 51 |
| Figure 4.5 – Variation of Laboratory MR and FFRC Modulus with Moisture Content.....   | 52 |
| Figure 4.6 – Test Locations on Embankment and Subgrade Layer of SH 267 Site .....   | 53 |
| Figure 4.7 – Test Locations on Base Layer of SH 267 Project.....  | 54 |
| Figure 4.8 – Test Locations on Lime-Treated Subgrade of SH 267 Project.....   | 55 |
| Figure 4.9 – Test Locations on Embankment and Subgrade along IH 35W Section .....   | 55 |
| Figure 4.10 – Spatial Variations of NDG Moisture Contents and Dry Densities of Embankment.....  | 56 |
| Figure 4.11 – Spatial Variations of Moisture Content and Dry Density with NDG Immediately after Compaction of Subgrade Layer .....                    | 57 |
| Figure 4.12 – Variations of Average NDG Moisture Contents and Dry Densities with Number of Passes of Roller during Compaction of Subgrade Layer ..... | 57 |
| Figure 4.13 – Variations of Measured Moduli of Embankment Layer.....  | 58 |
| Figure 4.14 – Spatial Variations of Measured Moduli immediately after Compaction of Subgrade.....   | 58 |
| Figure 4.15 – Variations of Measured Moduli between Passes of IC Roller .....   | 59 |
| Figure 4.16 – Variations of CMV before and after Compaction of Subgrade.....  | 60 |
| Figure 4.17 – Distributions of CMVs with Passes for Different SH 267 Subgrade Sections.....   | 60 |
| Figure 4.18 – Influence of Subgrade Lift Placement for Subgrade Sections.....   | 61 |
| Figure 4.19 – Influence of Time on Roller Measurement Values for Subgrade Sections .....  | 62 |
| Figure 4.20 – Distributions of CMV with Passes for Production Section .....   | 62 |
| Figure 4.21 – Relations between the NDG Dry Density and the CMV for Subgrade Sections of SH 267.....  | 65 |
| Figure 4.22 – Relations between the LWD Modulus and the CMV for Different Sections of Subgrade.....   | 66 |
| Figure 4.23 – Relations between the PSPA Modulus and the CMV for Different Sections of Subgrade.....  | 67 |
| Figure 5.1 – Process of Estimating Optimal Passes and Target Roller Measurement Values.....   | 68 |
| Figure 5.2 – Target RMV estimation Process for Dry Subgrade Section of SH 267 Site .....  | 69 |
| Figure 5.3 – Target RMV Estimation Process for OMC Subgrade Section of SH 267 Site .....  | 70 |
| Figure 5.4 – Target RMV estimation Process for Wet Subgrade Section of SH 267 Site.....   | 71 |
| Figure 5.5 – Variation in Roller Measurements with Compaction Process.....  | 72 |
| Figure 5.6 – Distributions of Measurements for a Production Section.....  | 73 |
| Figure 5.7 – Distribution of Speed with Different Rollers .....   | 74 |

|   |    |
|---|----|
| Figure 5.8 – Subgrade Site at SH 267 .....  | 75 |
| Figure 5.9 – Distribution of Roller Measurements on the Dry Subgrade Section of SH 267 ....   | 75 |
| Figure 5.10 – Flow Chart Representation of Data Processing and Analysis using ArcGIS .....  | 76 |
| Figure 5.11 – Gridded Roller Measurement Values for Subgrade Section at SH 267 .....  | 76 |
| Figure 5.12 – IC Roller Calibration .....   | 77 |
| Figure 5.13 – Histogram of Roller Measurements on IH 35W Subgrade .....   | 78 |
| Figure 5.14 – Semivariogram Constructed with Roller Measurement Values (CMV) .....  | 78 |
| Figure 5.15 – Comparison of Data Predicted Using Kriging and Observed .....   | 79 |
| Figure 5.16 – Kriging Method to Identify the Weak Locations .....   | 79 |
| Figure 5.17 – Variation in Roller Measurements Using Kriging.....   | 80 |
| Figure 5.18 – Kriged Surface with Spot Test Points .....  | 80 |
| Figure 6.1 – Suggested Sample Size for Different Devices.....   | 82 |
| Figure 6.2 – Relation of Simulated Roller and LWD Moduli .....  | 83 |
| Figure 6.3 – Relation of the Simulated and NCHRP 10-84 Estimated LWD Moduli.....  | 83 |
| Figure 6.4 – Variation of the CMV before Lift Placement.....  | 84 |
| Figure 6.5 – Variation of the CMV after Placement and Compaction of the Next Lift .....   | 84 |
| Figure 6.6 – Variation of the Differences in CMVs ( $\Delta$ CMV) After Placement and<br>Compaction of the Next Lift and Foundation Layer .....     | 84 |
| Figure 6.7 – Variation of the Differences in the CMVs ( $\Delta$ CMV) After Placement and<br>Compaction of the Next Lift and Foundation Layer ..... | 85 |
| Figure 6.8 – Comparison of the Different Acceptance Scenarios .....   | 88 |

## List of Tables

|   |    |
|---|----|
| Table 2.1 - Commercially Available roller Measurement Values (Mooney et al., 2010) .....                              | 7  |
| Table 2.2 - Summary of Quality Control and in situ Correlations.....  | 9  |
| Table 2.3 - Advantages and Disadvantages of Modulus-Based Devices<br>(Nazarian et al., 2011).....                     | 11 |
| Table 2.4 - Advantages and Disadvantages of Moisture/Density Devices<br>(Nazarian et al., 2011).....                  | 12 |
| Table 2.5 - Summary of Existing Intelligent Compaction Specifications .....   | 13 |
| Table 2.6 - IC in Quality Control and Quality Acceptance Testing .....  | 14 |
| Table 2.7 - Influence of Geomaterials Types on Quality Acceptance .....   | 14 |
| Table 2.8 - TxDOT Approved IC Rollers.....  | 15 |
| Table 2.9 - Data Elements.....  | 16 |
| Table 2.10 - Specifications for Control Strips .....  | 17 |
| Table 2.11 - Specifications for Acceptance Testing .....  | 18 |
| Table 2.12 - Geostatistics in Intelligent Compaction.....   | 22 |
| Table 2.13 - Summary of Finite Element Studies for the Modeling of Roller Compaction.....                             | 24 |
| Table 3.1 - Pavement Sections Properties.....   | 33 |
| Table 4.1 - Index Properties of Geomaterials .....  | 49 |
| Table 4.2 - Laboratory Results of MR and FFRC Tests of Geomaterials .....   | 52 |
| Table 4.3 - Comparisons of Average Moisture Contents of Subgrade with Different Devices .                             | 57 |
| Table 4.4 - Average Moduli from Different Sections.....   | 58 |
| Table 4.5 - Descriptive Statistics of NDT Devices on Different Sections of SH 267 Site .....                          | 63 |
| Table 4.6 - Descriptive Statistics of NDT Devices on Different Sections of IH 35W Site .....                          | 64 |
| Table 6.1 - Analyses of Variability of Modulus-Based Devices .....  | 81 |
| Table 6.2 - Contribution of each Variability Parameter to the Total Variability of the<br>Modulus-Based Devices ..... | 81 |
| Table 6.3 - Estimated Target Moduli of the Different Devices .....  | 83 |
| Table 6.4 - Descriptive Statistics of the NDT Devices on the Different Sections<br>of SH 267 Site.....                | 86 |
| Table 6.5 - Descriptive Statistics of the NDT Devices on the Different Sections<br>of IH 35W Site.....                | 86 |



# Chapter 1

## Introduction

Intelligent Compaction (IC) is a fast-developing technology for soil and base compaction quality control. It is a continuous assessment of mechanistic soil and base properties (stiffness, modulus) through roller parameters (frequency, amplitude and speed) integrated with global positioning system (GPS) to provide a complete compaction and geographic information (Mooney et al., 2010). European countries have implemented specifications for IC technology for soils and bases. Many pilot studies in the United States have been carried out to understand and implement the IC technology (Mooney et al., 2010).

The Texas Department of Transportation's (TxDOT) current practice for field compaction quality control and acceptance for soil and base layers is to determine the compacted density and occasionally moisture content by nuclear density gauge (NDG). TxDOT has considered several stiffness-based devices to replace density measurement because stiffness parameters are more relevant to and used in pavement design. Since both density and stiffness measurements are spot tests, they cannot represent the quality and uniformity of compaction in a continuous manner.

Proof rolling is currently specified by TxDOT as a way of evaluating the uniformity of the compacted materials. Proof rolling subgrade and base using the intelligent compaction rollers after completing compaction can effectively identify the weak spots and significantly improve the uniformity of the compacted layers. Even though TxDOT has participated in a Federal Highway Administration (FHWA)-led pooled fund study and funded a few studies to implement the IC technology, there are still obstacles and gaps that need to be explored and overcome in order to fully employ IC technology in day-to-day compaction and quality control/quality assurance (QC/QA) operations.

### Objective

The primary objective of this project is to improve the process of accepting compacted geomaterials using IC technology to ensure quality, performance and durability. The tasks include:

- Evaluating available instrumented rollers on how the data are obtained and how accurately and at what level of sensitivity the stiffness or modulus are measured by these instruments.
- Establishing correlation(s) between the IC data collected by the rollers and measurements of in-situ stiffness or modulus, moisture content and possibly density.
- Developing test protocols for the application of IC and instrumented rollers.
- Developing acceptance procedures and draft specification for the use of the IC equipment on subgrade soils, embankment and bases.

To achieve these objectives, a number of tasks were proposed and completed. A flow chart of the progression of these tasks is shown in Figure 1.1. The first step of the process was to identify the sites in TxDOT districts that benefit the most from using local materials and to investigate the methods and

criteria that the districts currently use to incorporate intelligent compaction in construction. The local soil and bases from the sites that might benefit the most from this study were selected for comprehensive testing and evaluation. The second step of the process consisted of extensive performance-based laboratory tests to determine the relationship between the laboratory and field testing, to establish target modulus and also to use appropriate constitutive material properties in the structural analyses.

### **Organization of Report**

Aside from this introductory chapter, the report consists of six chapters. Chapter 2 contains the background and information searched from the previous work done for the purpose of using intelligent compaction for road construction.

Chapter 3 presents the numerical analysis of soil interaction under the stresses experienced during compaction by roller drum and testing using nondestructive devices (spot tests). For numerical analysis, the topics include the sensitivity study in order to understand the parameters that influence the response of soil and base layers under roller and spot tests. Several factors such as modulus, thickness and combination of soil and base layers are comprehensively evaluated to provide a means of understanding the depth of influence of roller drum vibrations and spot test.

Chapter 4 outlines the research and test procedures for developing the prototype specifications to use intelligent compaction technology for soils and bases. The topics discussed in that Chapter are selection of construction sites, field and laboratory testing programs, which include setting up the roller instrumentation, minimum GPS requirements, spot testing, index property tests, repeated load triaxial tests and free-free resonant column (FFRC) tests. Also the results from the laboratory and field studies and their relationships with roller measurements are discussed.

Chapter 5 presents the practical lessons learned during the field studies and from the data analysis. The topics discussed in that Chapter are selection of roller measurement target values, sensitivity of roller measurements, and spatial variability of spot test results, calibration of GPS system, geostatistical analysis and the training required.

Chapter 6 presents the proposed modification of the prototype specification addressing the test and sampling frequencies, alternate methods of setting roller target values, and establishing acceptance criteria for spot testing and roller measurements.

Chapter 7 contains the summary and conclusions of the research as well as recommendations for changing TxDOT policies and future study.

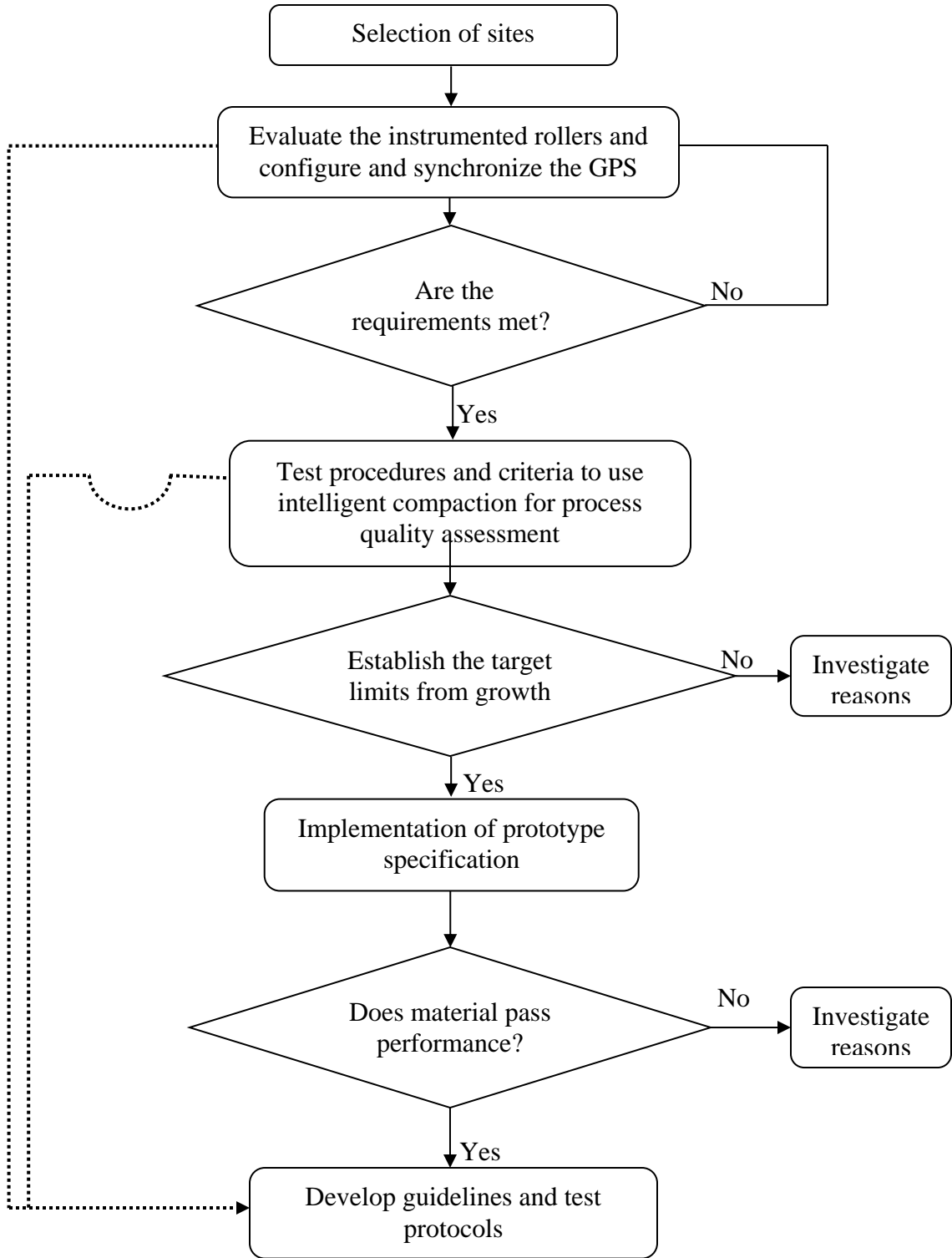


**Figure 1.1 - Flow Chart of Research Activities**

## Chapter 2

### Background and Information Search

#### Introduction

As the first task of the research project, an extensive literature review on the use of intelligent compaction technology for roadway soils and bases was conducted. The results from the information search are documented in this chapter.

#### Advantages of Intelligent Compaction

The advantages of intelligent compaction have been investigated by several groups (e.g., Anderegg and Koufman, 2004; White et al., 2006; Hossian et al., 2006; Peterson et al., 2006; Mooney et al., 2010; Gallivan et al., 2011 and Chang et al., 2012). The advantages are summarized as listed below:

- a) Improved quality of compaction/uniformity
- b) Reduced over/under compaction costs
- c) Reduced time of compaction
- d) Identification of soft or weak spots
- e) Increased lifetime of the roller
- f) Integration of design, construction and performance

#### Challenges with Intelligent Compaction

The challenges in implementing the intelligent compaction for quality control and assurance are primarily evaluating the influence of machine operating conditions and underlying heterogeneity on the roller measurement values. The tasks to be accomplished for the successful implementation of the intelligent compaction for quality control and assurance of soil and base materials are identified as below (Peterson et al., 2006 and Mooney et al., 2010):

- a) Correlation of the in situ measurements with the roller measurement values
- b) Influence of moisture content variation
- c) Consideration of density and moisture along with roller measurement values
- d) Uncertainty in spatial pairing of point measurements and roller measurement values
- e) Intrinsic measurement errors associated with roller measurement values and in situ point test measurements

## Modulus of Compacted Geomaterials

It would be beneficial to distinguish between the terms “modulus” and “stiffness.” As reflected in Figure 2.1, modulus is the ratio of a measured strain and an applied stress. Modulus of a material can vary between an initial tangent modulus,  $E_{\max}$ , to a secant modulus ( $E_1$  through  $E_3$ ) depending on the magnitude of stresses applied. Stiffness, which is defined as the deformation of a material under an applied load, is not a unique material property but the response of a pavement system to load. With different levels of approximation, the modulus can be estimated from the stiffness given the layer properties, the dimensions of applied load, and a model that estimates the response of the pavement system.

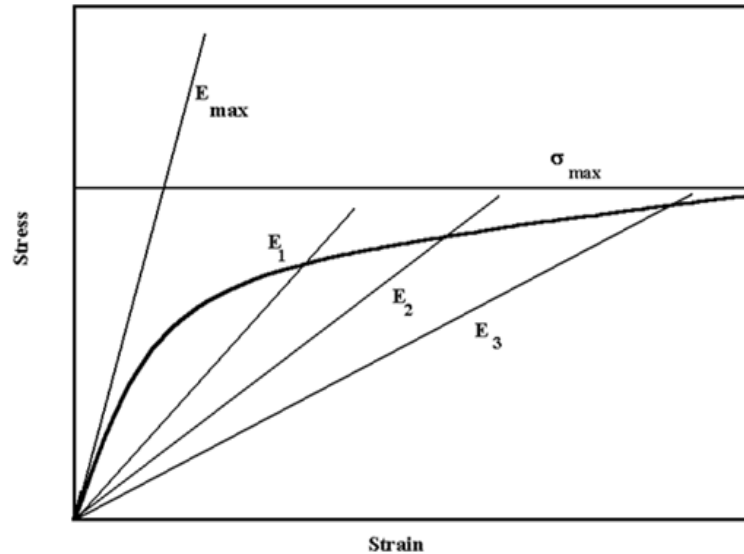


Figure 2.1 -Definitions of Modulus

### Factors Impacting Modulus of Compacted Geomaterials

There is a consensus on the major factors that could affect the modulus of geomaterials (Puppala, 2008). These factors generally include the stress state, moisture content (including degree of saturation or suction), stress history, density, gradation and Atterberg limits.

**State of Stress:** The impact of the state of stress on modulus is well-known. Even though simple in concept, the dependency of the modulus on the state of stress brings about practical complications in the context of this study. The modulus or stiffness of a geomaterial placed in a pavement section is not a unique value and depends on the underlying and/or overlying layers and the device used to measure the modulus (Nazarian et al., 2011).

**Moisture Content:** Excellent reviews of the impact of moisture content on modulus can be found in Richter (2006), Cary and Zapata (2010) and Siekmeier (2011). Typically an increase in moisture content will decrease matric suction, and hence, will decrease the modulus. Several recent studies have demonstrated that the difference between the moisture content at compaction and testing impacts the modulus more than the moisture content at the time of compaction (Khoury and Zaman, 2004; Pacheco and Nazarian, 2011).

**Density:** The impact of density on modulus has not been studied as extensively as the impact of moisture content. A strong correlation between modulus and density has not been observed in many field studies (Mooney et al., 2010; and Von Quintus et al., 2010). Pacheco and Nazarian (2011) attributed the lack of a strong correlation to the complex interaction between the moisture content, density and degree of saturation of a given material.

**Gradation and Plasticity:** The impact of gradation and plasticity on modulus have been extensively qualified (Richter, 2006; Puppala, 2008) and to a lesser extent quantified. In general, as the plasticity of the material or the percent fines increases, the modulus decreases.

**Short-term Behaviors of Geomaterials:** The short-term behavior of compacted geomaterials along a drying path is of more practical interest for quality management. The increase in moisture during construction is usually due to precipitation, which will interrupt the construction and may require re-compaction of the layer. The amount of work related to short-term behaviors of exposed geomaterials has been limited to a few studies such as Khoury and Zaman (2004) and Pacheco and Nazarian (2011).

**Intelligent Compaction Systems**

The roller measurement value (RMV) is basically derived from the vibratory drum and soil interaction relations. Figure 2.2 shows the typical representation of the model and the force displacement relations (Anderegg et al., 2006). The roller and soil are represented with the combinations of spring and dashpot models.

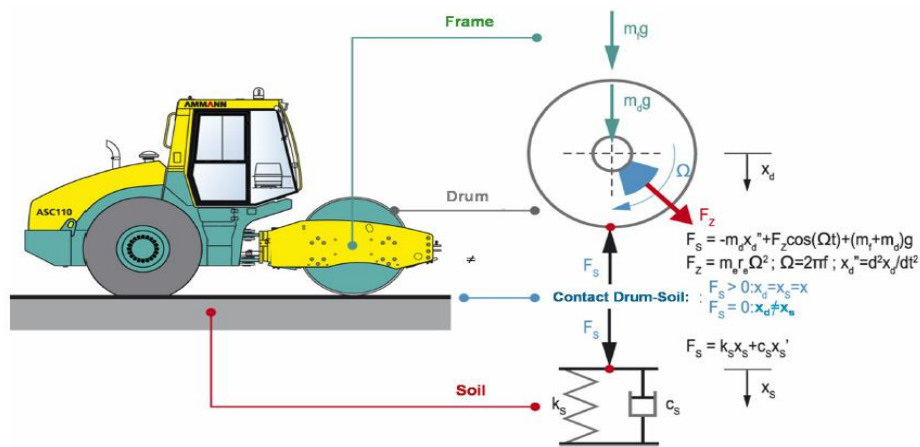


**Figure 2.2 -Representation of Roller Drum and Soil Interaction (Anderegg et al., 2006)**

The compaction of a material using an intelligent compaction roller is controlled with the continuous feedback of the roller measurement values. Three different modes of roller drum and soil interactions are shown in Figure 2.3 (Anderegg and Koufman, 2004). The continuous contact between the roller drum and the soil is established during the early stage of compaction. Partial loss of contact is observed during the stiffening of the compacting layer. The bouncing behavior is normally experienced when the stiffness of the soil increases or attains the maximum stiffness. Working in double-jump is undesirable and is likely to degrade the compaction performance, loosen already compacted areas, and shorten the life of the roller (Briaud and Seo, 2003).

**Data Collection in Intelligent Compaction Roller**

The intelligent roller compactors include sensors to measure vibration characteristics or rolling resistance of the drum, onboard electronics to record and process sensor output and record the compaction level. The onboard GPS system records the geospatial information. The data measurements and location details are stored in a data storage system (Peterson et al., 2006, Mooney and Adam, 2007). The data storage system and measurement value vary with the type and make of the intelligent roller compactor. The descriptions of roller measurement values are discussed in detail in Mooney et al. (2010). The different data measurement units used for compaction control are listed in Table 2.1.

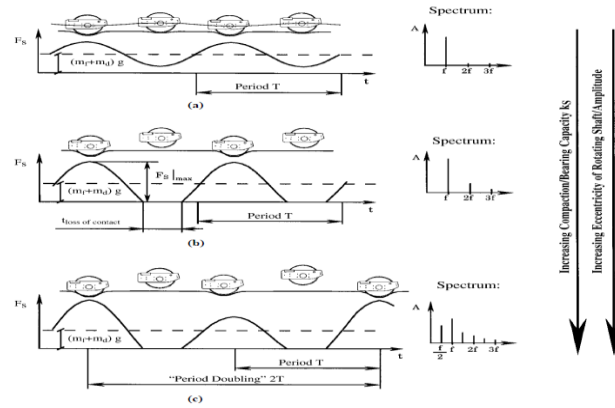


**Figure 2.3 - Three Basic Types of Behaviors (a) Continuous Contact (b) Periodic Loss of Contact (c) Bouncing or Rocking (Anderegg and Kaufmann, 2004)**

**Table 2.1 - Commercially Available roller Measurement Values (Mooney et al., 2010)**

| Measurement Value                              | Manufactures                      | Parameters Used  | Relations Used   |
|--|-----------------------------------|--|--|
| <b>Compaction Meter Value (CMV)</b>            | Dynapac, Caterpillar, Hamm, Volvo | Ratio of vertical drum acceleration amplitudes at fundamental vibration frequency and its first harmonic   | $CMV = c \frac{A_{2\Omega}}{A_{\Omega}}$<br>Where $c$ is constant around 300, $A_{2\Omega}$ is the amplitude of second harmonic, $A_{\Omega}$ is amplitude of fundamental frequency  |
| <b>Compaction Control Value (CCV)</b>          | Sakai                             | Algebraic relationship of multiple vertical drum vibration amplitudes, including fundamental frequency, and multiple harmonics and sub harmonics | $CCV = \frac{A_1 + A_3 + A_4 + A_5 + A_6}{A_1 + A_2}$<br>Where $A_i$ are amplitudes at the excitation frequencies  |
| <b>Stiffness, <math>K_s</math></b>             | Ammann                            | Vertical drum displacement, drum-soil contact force  | $k_s = \Omega^2 \left[ m_d + \frac{m_o e_o \cos(\theta)}{z_d} \right]$<br>Where $m_d$ is drum mass, $m_o e_o$ is eccentric mass moment, $\theta$ is phase angle, $z_d$ is drum displacement, $\Omega$ is frequency   |
| <b>Vibration Modulus, <math>E_{vib}</math></b> | Bomag                             | Vertical drum displacement, drum-soil contact force  | $z_d = \frac{2 \times (1 - \nu^2)}{\pi \times E_{vib}} \times \frac{F_s}{L} \times \left( 1.8864 + \ln \frac{L}{b} \right)$<br>where $F_s$ is drum soil interaction force, $L$ is the drum length, $b$ is contact width, $\nu$ is Poisson ratio, $z_d$ is drum displacement    |
| <b>Machine Drive Power (MDP)</b>               | Caterpillar                       | Difference of gross power and the power associated with sloping grade and machine loss   | $MDP = P_g - WV \left[ \sin \theta + \frac{a}{g} \right] - (mV + b)$<br>where $P_g$ is gross power, $W$ is roller weight, $a$ is acceleration, $g$ is acceleration due to gravity, $\theta$ is slope angle, $V$ is roller velocity, $m$ and $b$ are internal loss coefficients |

### Field Evaluation of Intelligent Compaction

Studies have been carried out to evaluate the roller measurement values for the compaction quality management of different pavement layers and embankment soils. Research has also been carried out to correlate the roller measurement values with the in situ point test measurements. Table 2.2 summarizes various studies and their significant findings.

### Field Evaluation Devices for Spot Tests

Table 2.3 contains a list of most common portable modulus-based devices available in the market. A detailed compilation of the literature review for each device is included in Nazarian et al. (2011). The most common advantages and disadvantages of each device are summarized in Table 2.3. The nuclear density gauge (NDG) is still the most widely-used device for measuring moisture content. The field of

measuring moisture and density with non-nuclear devices is evolving quite rapidly. Improvements to software and hardware are also being implemented on a number of existing devices. A few devices that estimate the moisture content and/or density of the compacted geomaterials are included in Table 2.4. Spot test devices that are described in detail in Nazarian et al. (2011). A number of less used and known devices are also available (Sebesta et al., 2012).

### **Existing Specifications**

The existing European specifications and pilot studies in United States are explained in detail in White et al. (2007) and Mooney et al. (2010). Brief background and summary of the existing specifications are given in Table 2.5. The minimum equipment requirements in IC specifications are discussed in the subsequent section.

### **IC Technology as Quality Control (QC) and Quality Acceptance (QA) Tools**

Different manufacturers recommend different roller measurement values (RMVs). Irrespective of the RMV used, the vertical, longitudinal and transverse heterogeneity of the underlying soil strata is the most important factor influencing the RMVs and the modulus-based spot test results. The correlations developed with the RMVs and the spot tests change whenever there is a change in the underlying condition. The heterogeneity stems from the change in material type, compaction effort and moisture contents at the time of compaction and testing (Nazarian et al., 2011). The depth of influence for a regular (11 to 15 ton) roller is reported to vary between 2.5 ft to 4 ft (Mooney et al., 2010). Hence, the RMVs measured will reflect the composite stiffness of the geomaterials up to a depth of 2.5 ft to 4 ft. However, the spot tests typically reflect the material property up to a depth of 0.5 ft to 1 ft (Mooney et al., 2010).

Table 2.6 summarizes the findings from selected studies in use of the IC in quality control and acceptance testing. Whenever there is a high variability in the underlying ground strata, the use of IC for quality control and acceptance might be challenging. Research studies have recommended construction of individual test strips whenever the variability in the underlying ground conditions is high.

### **Influence of Geomaterial Types on Quality Acceptance**

Table 2.7 presents the findings from the selected studies on influence of geomaterials on RMVs. The IC specification is applicable to both cohesive and cohesionless soil and base materials. However, several studies (e.g., Mooney et al. 2010; and Hossian et al., 2006) have demonstrated that the RMVs are less reliable on cohesive soils if careful attention is not paid to soil moisture content variations. It is also important to account for the soil moisture variation for the stabilized materials. The European specifications limit the fine content (<0.06 mm) for materials compacted using IC technology. Also, Sweden specifications limit the fines content to 7%. Hence, the IC technology is by default used predominantly for cohesionless soils (Mooney et al., 2010).

**Table 2.2 - Summary of Quality Control and in situ Correlations**

| Reference                          | Objective and scope   | Key findings/comments  |
|------------------------------------|---|--|
| <b>White et al., 2005</b>          | Evaluated the utilization of intelligent rollers in real time compaction monitoring. A pilot field study was carried out in Illinois on a cohesive glacial till soil. Spot measurements of density, moisture content, and DCP and Clegg impact hammer values were correlated to roller measurement values.                            | The variation in the machine drive power was observed to be the result of inherent soil and moisture variations in the compacted layer. The compaction effort was found to be significant only up to a depth of 40 cm. Consideration of moisture content in the regression analysis resulted in a better understanding of measurements and correlation between them. |
| <b>White et al., 2006</b>          | Evaluated the relationship between machine drive power and measures of soil compaction at a test section in Peoria, Illinois. Two moisture contents were adopted. Vibratory pad foot roller was used. Well-graded silty sand was evaluated with nuclear gauge, moisture meter and DCP.  | Demonstrated the use of machine drive power as a tool for compaction control. Variability of DCP index reduced with increase in roller passes.   |
| <b>Anderegg et al., 2006</b>       | Demonstrated the compaction monitoring using single drum vibratory intelligent compactor.   | Linear relation with high correlation was established between moduli from the plate bearing tests and roller measurement values.   |
| <b>Mooney et al., 2006</b>         | Investigated the influence of heterogeneity on vibratory roller compactor response in Colorado. Lift thickness and moisture content were also considered along with varying depth to bedrock. A double smooth drum roller was used. The soil type was poorly graded sand (A-1-b) and DCP was used for the point measurements.         | Roller parameters found to be sensitive to underlying stiffness when operated near resonance. At higher frequencies the roller parameters were insensitive to changes in the underlying soil conditions.   |
| <b>Hossian et al., 2006</b>        | Demonstrated intelligent compaction control concepts in identifying soft spots in Kansas. The relation of roller measured stiffness with density and moisture content was established. A single drum vibratory roller was used. Soil type was clayey sand and nuclear gauge, moisture meter and DCP were used for point measurements. | Poor correlation was observed between the roller measurement values and the CBR from DCP due to empirical nature. The target stiffness values needs to be function of the dry density since both high and low densities results in lower IC roller stiffness. Authors also showed the limitations of QC based on dry density alone.                                  |
| <b>Petersen and Peterson, 2006</b> | Compared CMV with the point test measurements such as LWD, DCP and Geogauge   | The roller measurements vary greatly with point measurements. The variation in the roller measurements is due to the difference in the area of measurements between drum and sensors of spot tests, and the response is greatly influenced by moisture, material and support.  |
| <b>White and Thompson, 2008</b>    | Evaluated compaction meter value and machine drive power with five different types of subbase materials including RAP in Illinois. Single drum intelligent roller with Clegg Impact tester, SSG, LWD, DCP and PLT were used as compaction control tools.  | Machine drive power was observed to be more variable as compared to compaction meter value. Multivariate analyses may be used to relate the roller measured values and in situ point test values.  |
| <b>Mooney and Rinehart, 2007</b>   | Explored relationship between vibration characteristics and soil properties in a test section in Denver. Double drum smooth intelligent compactor was used.   | Heterogeneity causes significant challenge to vibration based assessment of soil properties. Roller measurements for QC/QA were found to be greatly influenced by the stress dependent nature of soil.   |
| <b>Rahman et al., 2007</b>         | Studied the use of subgrade stiffness obtained from the IC technology using Bomag single smooth steel drum variocontrol intelligent roller. Three sections were considered in Kansas.   | Demonstrated the potential benefits of IC technology in identifying weak areas of compaction. Revealed the sensitivity of the roller measurements to moisture content variation.   |

**Table 2.2 cont. -Summary of Quality Control and in situ Correlations**

| Reference   | Objective and scope   | Key findings/comments   |
|---|---|---|
| <b>White et al., 2011</b>   | Review of the field assessment studies and examining the factors influencing roller measurement values, correlations between the spot test measurements and spatial uniformity.                     | Roller measurement values are highly influenced by the variability of soil properties across the width of roller drum and moisture content. Establishing the target values, acceptance limits, correlations between field measurements being technology specific and based on local experience are the potential limitations of existing IC specifications. |
| <b>Gallivan et al., 2011</b>  | Evaluated the use of intelligent compaction for QC/QA   | Established the advantage of roller measurement values in detecting the deeper weak spots that cannot be identified with the density measurements.  |
| <b>Rahman et al., 2012</b>  | Developed correlations between the in situ measurements and roller measurement values in Kansas. Single drum intelligent roller was used along with nuclear gauge, SSG, LWD, DCP and PLT.           | Study showed that the change in layer modulus with depth is a potential source of problem to compare stiffness and modulus results from different test and roller measurement values.   |
| <b>Rinehart et al., 2012</b>  | Evaluated the European CCC specifications on a pilot project in Colorado. Pilot study was implemented on a 30 cm thick subbase, of 12 m width and 300 m long. Dynapac roller was used in the study. | Study recommends lowering the acceptance criteria using spot test results on the weak areas identified through roller based measurement values. For process and acceptance control, study recommends for additional analysis beyond correlation to establish roller compaction target values.   |
| CBR- California Bearing Ratio<br>RAP- Reclaimed Asphalt Pavement<br>CCC- Continuous Compaction Control<br>SSG- Soil Stiffness Gauge |   | LWD- Light Weight Deflectometer<br>DCP- Dynamic Cone Penetrometer<br>PLT- Plate Load Test   |

**Table 2.3 -Advantages and Disadvantages of Modulus-Based Devices (Nazarian et al., 2011)**

| <b>Device</b>   | <b>Description</b>  | <b>Advantages</b>   | <b>Disadvantages</b>  |
|---|---|---|---|
| <b>Clegg Impact Hammer (CIH)</b>                      | CIH measures the deceleration of a free falling mass or hammer from a set height onto a surface under test which is converted to strength/stiffness of geomaterial.   | CIH is simple to operate and correlations with CBR values are available.  | Possibility of boundary effects when calibrating with Proctor molds. Not strictly a stiffness/modulus measuring device.   |
| <b>Dynamic Cone Penetrometer (DCP)</b>                | DCP test involves driving a cone shaped probe into a geomaterial and measuring advancement of the device for several intervals of hammer drops. The rate of penetration of the probe is used to obtain layer thicknesses and moduli.                                    | Adapted by selected agencies in QA operations. Does not require extensive support software for evaluating test results. Can test multi-layers   | Takes time to perform a test. Not strictly a stiffness/modulus measuring device as the penetration rate has to go through two levels of empirical correlations to estimate modulus  |
| <b>Electro-Mechanical Stiffness Device (Geogauge)</b> | Geogauge provides stiffness property of a geomaterial by measuring applied force and resulting displacement induced by a small harmonic oscillator operating over a frequency of 100 to 200 Hz.   | Acceptable success rate in identifying areas with different physical conditions or anomalies. Simple training. Provides a reasonable estimate of laboratory measured moduli with proper calibration.  | Intimate contact between Geogauge and soil is difficult to achieve without thorough site preparation. Moduli do not represent stress levels that occur under truck loading. Underlying materials can influence results especially for relatively thin unbound layers. |
| <b>Portable Falling Weight Deflectometer (PFWD)</b>   | PFWD operates in a similar fashion to the FWD with one to three sensors. The FWD analysis method is applicable to PFWD as long as three sensors are used. PFWD with one sensor is often used with a so-called “forward-calculation” to estimate stiffness of the layer. | State of stress is closer to vehicular stresses than any other device. Pavement community is familiar with concept of deflection-based testing.   | Unable to consistently identify areas with anomalies. Underlying materials can influence results especially for relatively thin unbound layers. Any error in thickness of the layer being tested can result in large errors and variability in modulus.               |
| <b>Portable Seismic Property Analyzer (PSPA)</b>      | PSPA consists of two accelerometers and a source packaged into a hand-portable system. PSPA measures the linear elastic average modulus of a layer based on generating and detecting stress waves.  | Measures layer-specific modulus independent of thickness of layer. No backcalculation necessary. High success rate in identifying areas with different physical conditions or anomalies. Results can be calibrated to specific material being tested prior to construction when M-D relationship is measured in lab | Need to calibrate the test results to the material and site conditions under evaluation. Lowest repeatability, with a high standard deviation due to capability to detect anisotropic conditions.   |

**Table 2.4 - Advantages and Disadvantages of Moisture/Density Devices (Nazarian et al., 2011)**

| <b>Device</b>                                 | <b>Description</b>   | <b>Advantages</b>   | <b>Disadvantages</b>   |
|---|--|---|--|
| <b>Electrical Density Gauge (EDG)</b>         | EDG uses a radio signal between four spikes to measure capacitance, resistance, and impedance of the soil. These parameters are used to determine the density and water content of an unbound layer.   | Does not require a licensed technician.<br>Repeatable   | The necessity to run a series of lab and in situ tests for correlation purposes. Poor success rate in identifying areas with anomalies   |
| <b>Moisture + Density Indicator (M+DI)</b>    | <b>M+DI</b> utilizes time domain reflectometry (TDR) to measure voltage time histories of an electromagnetic step pulse at four soil spikes in the ground. The voltage time histories are analyzed to determine the water content and density of an unbound layer. | Requires no certified operators or safety training or instrument calibration.                                     | Prior calibration of the device for each specific soil using laboratory compaction molds is required.<br>May not be appropriate for aggregates or earth-rock mixtures that either interfere with penetration of the probes or have numerous and large void spaces.<br>Time required to conduct a test may be of concern. |
| <b>Soil Density Gauge (SDG)</b>               | SDG produces a radio-frequency electromagnetic field using a transmitter and receiver to estimate the in-place density, and moisture content of unbound pavement materials using electrical impedance spectroscopy (EIS).  | Requires no certified operators or safety training or instrument calibration.                                     | The technology is new and limited research has been performed using this device.   |
| <b>Speedy Moisture Tester (SMT)</b>           | SMT measures the moisture content of geomaterial by measuring the rise in gas pressure within an air-tight vessel containing a mix of soil sample and a calcium carbide reagent.   | Portable and requires no external power source.<br>Can measure many materials over a wide moisture content range. | Not suitable for all geomaterials, especially highly plastic clay soils<br>The reagent used is considered as a hazardous product<br>Compacted geomaterials have to be excavated before they can be tested.   |
| <b>Road-Bed Water Content Meter (DOT 600)</b> | DOT600 estimates the volumetric water content of soil samples by measuring the dielectric permittivity of the material.  | Sample bulk density and compaction force are monitored.<br>The system is completely portable.                     | The technology is new and limited research has been performed using this device<br>Prior calibration of the device for each specific soil is needed<br>Compacted geomaterials have to be excavated before they can be tested   |

**Table 2.5 - Summary of Existing Intelligent Compaction Specifications**

| Specification                 | Control section   | QC/QA   |
|-------------------------------|---|---|
| <b>Germany (1997)</b>         | Existing IC specifications are only for soils and embankments. Three 20 m long test strips should be selected as calibration sections. Develop the correlations between the roller MV and soil density or PLT modulus ( $E_{v2}$ ). The correlation coefficient shall be of minimum 0.70. Identify the roller MV target value (MV-TV) for the required density or modulus.  | 90% of all roller MVs shall be higher than MV-TV. To use CCC as a QA tool the soil type and the underlying stratigraphy should be homogeneous. The soil shall be reworked if density or modulus measurements made on the identified weak areas using CCC is not greater or equal to the desired value. Speed of the roller shall be constant.   |
| <b>Swedish (2004)</b>         | IC specifications are not recommended for subgrades since the base and subbase layers are considerable thick. Predominantly cohesionless soil compaction is monitored using IC.   | PLT at eight randomly locations within 5000 m <sup>2</sup> control area have to be carried out. Mean of compaction values for two inspection points $\geq 89\%$ for sub-base under base and for protective layers over 0.5 m thick; mean should be $\geq 90\%$ for bases. Required mean for two bearing capacity ratios varies depending on layer type.   |
| <b>ISSMGE/ Austria (2007)</b> | At least 100 m long and width equal to the site width and overlap of each roller shall be <10% of the drum width. Compaction shall continue until the mean measurement value of a pass is no more than 5% higher than the mean measurement value of the preceding pass. Roller measurement values shall be correlated to PLT. The correlation coefficient shall be greater than 0.70.   | The measured roller values shall be between 95 to 105% of PLT modulus values. Speed shall be constant between 2-6 km/h and frequency be constant within $\pm 2$ Hz.   |
| <b>FHWA (2012)</b>            | Test section should be of minimum 75 m long and 8 m wide. A minimum of 10 locations shall be used to measure nondestructive density or stiffness. Target values for the optimal passes shall be determined from the compaction curve between the roller values and number of passes. The pass where the measurement values do not increase by 5% is considered as the optimal pass. Target values (IC-MV) for required density shall be established from linear regression between the density and the roller measurement values. The variation in moisture content allowed is between -3 % and + 2 % of OMC. | The magnitude of the evaluation areas may vary but not less than 25,000 ft <sup>2</sup> . Around 90% of the construction area should meet the optimal number of roller passes and 70 % of the target values.  |
| <b>INDOT (2012)</b>           | Test section should be of minimum 30 m long and 6 m wide. The minimum thickness of the test section shall be 300 mm. The variation in moisture content allowed is between -3 % and + 2 % of the OMC. The target IC-MV should be established from the number of DCP blows required as determined in the laboratory.  | The compaction acceptance should be determined by DCP testing. The frequency of tests is one test for each 1000 cum for each lift. A minimum of 90% of the mapped construction area should have a minimum of 70 % of the target IC-MV.  |
| <b>MnDOT (2012)</b>           | At least 100 m x 10 m. Thickness shall be same as layer to be constructed. One control section for each type/source of material at site. Determine the optimum passes based on the stiffness increment. The total thickness of the granular layer shall be equal to planned granular layer thickness being constructed. Moisture content shall be varied from 65 to 100% of optimum.  | On all sections 90% of the IC stiffness measurements should be at least 90% of the target value prior to placing the next lift. If localized areas have IC stiffness of less than 80% of the target value, the areas shall be re-compacted. If a significant portion of the section is more than 30% in excess of the selected target value, the Engineer shall re-evaluate the target value (IC-TV). |

**Table 2.5 cont. - Summary of Existing Intelligent Compaction Specifications**

| Specification       | Control section  | QC/QA  |
|---------------------|--|--|
| <b>TxDOT (2012)</b> | Control strip of 150 ft in length and for full width for each layer type (minimum 25 ft). Density, moisture content, LWD stiffness and k-value measurement should be made after every 2 passes at a minimum of three locations. The roller measurement value that obtains at required moisture content and k-value for a minimum of 90% of the control strip area is the Target Value (MV-TV) for the material used to construct the course. Minimum k-value of 462 psi/in for 30-inch diameter plate on top of flexible base layers prior to placement of pavement surface shall be obtained for flexible base and top 12 inches of treated subgrade. | Minimum of 90 % of the area should have roller measurement values shall not be less than TV-1.5*SD (standard deviation). Additionally, local contiguous non-compliance areas not achieving RICM-TV must be no larger than 150 square feet. For lime treated soil and flexible base minimum of 3 tests per 10000 square yards shall be checked. |

**Table 2.6 - IC in Quality Control and Quality Acceptance Testing**

| Reference                         | Findings   |
|-----------------------------------|--|
| <b>White et al. (2005)</b>        | Statistical analysis of the data help to reduce the IC measurement variations, position error and explains the underlying support conditions   |
| <b>Hossain et al. (2006)</b>      | By continuous nature of stiffness measurements by IC rollers, it is possible to identify soft spots during production control and acceptance testing   |
| <b>Mooney and Rinehart (2007)</b> | The IC roller identified the weak areas that were not identified by a static proof roll test during acceptance testing   |
| <b>White et al. (2008)</b>        | The variations in the RMVs are important for interpreting layered soil conditions  |
| <b>Gallivan et al. (2011)</b>     | Minimal or inconsistent rolled areas are easily identified when IC roller is used for production control   |
| <b>Rahman et al. (2012)</b>       | Variability in soil properties is reduced when IC roller is used for production process. Proof rolling using IC roller identified poorly compacted locations. High variability in the stiffness measurements within a short distance contradicts the concept of uniform compaction using IC rollers. |

**Table 2.7 - Influence of Geomaterials Types on Quality Acceptance**

| Reference                    | Findings   |
|------------------------------|--|
| <b>Hossian et al. (2006)</b> | The influence of moisture content on the RMVs was found to be more pronounced for clay-type soils. |
| <b>White et al. (2008)</b>   | RMVs are dependent on the soil type  |
| <b>Rahman et al. (2012)</b>  | The LWD measured stiffness on fine graded soil control strip exhibit a high variability            |

**Applicable Roller Types**

Table 2.8 lists the TxDOT approved IC rollers. Vibratory single smooth (primarily) or pad drum (in some occasions) rollers are recommended for use with IC technology (e.g., MnDOT). The use of rollers with automatic feedback control is not encouraged for quality acceptance (Mooney et al. 2010). The roller parameters like amplitude, frequency and speed must remain constant during an acceptance pass. A forward rolling pattern is recommended for quality acceptance passes.

**Table 2.8 - TxDOT Approved IC Rollers**

| <b>Manufacturer</b>         | <b>Model Number</b>                            |
|-----------------------------|--|
| BOMAG America, Inc.         | BW 177DH-4 BVC, BW 213DH-4 BVC, BW 226DH-4 BVC |
| Case Construction Equipment | SV212, SV212 (PD)                              |
| Caterpillar, Inc.           | CS56, CS64, CS74, CS76, CS76 XT                |
| Dynapac USA, Inc.           | CA250D, CA260D, CA362D, CA512D                 |
| Sakai America, Inc.         | SV505CIS, SV510CIS, SV610CIS                   |

**Effective Timing for Conducting IC-based Acceptance Testing**

Limited research has been conducted on determining the effective timing for the IC-based acceptance testing. The timing for acceptance testing is critical, especially when the layer of interest is stabilized. Accounting for the moisture dependence of geomaterials is the most difficult task for developing relations between the RMVs and the in-situ behavior (Mooney and Adam, 2007). The variation of moisture from the time of compaction to the time for acceptance testing significantly influences the modulus measured using NDTs (Nazarian et al., 2011) or RMVs. Hence, it is important to consider the effective timing for conducting IC-based acceptance testing. The acceptance testing as close to the final roller pass as possible and 16 to 24 hrs after compaction is proposed in the literature. The main concern for modulus-based acceptance is the stabilized materials because they can stiffen rapidly and significantly shortly after the compaction. For stabilized layers, the acceptance testing is carried out after compaction and a day or two later. The proposed methodology for stabilized layers will help to investigate correlation between the spot test measurements and RMVs with time.

**Minimum Thickness of Layer for Quality Acceptance**

Mooney et al. (2010) indicate that acceptance based on RMV for thin lifts may be challenging. RMVs were found to be insensitive to thin lifts (6 in.) of stiff base material placed directly over a soft subgrade. However, the RMVs were more sensitive to thick lifts (>12 in.) over the soft subgrade. The roller stiffness sensitivity depends on the stiffness ratio of the materials for the layer thickness less than the depth of influence of the roller. According to Rinehart and Mooney (2009), the roller measured stiffness values were insensitive to thin stiff layers if the stiffness ratio was on the order of 10:1. However, for the layers with stiffness ratios on the order of 5:1, the RMVs were reasonably sensitive.

**Roller and Instrumentation Parameters for Robust Quality Acceptance**

The roller parameters required for a robust quality acceptance are (Mooney et al. 2010):

- RMV
- GPS Locational parameters
- Amplitude, frequency and speed of roller
- Direction of travel
- Feedback control on/off

Tables 2.9 lists the recommended values for the successful implementation of the IC technology for compaction quality management from several sources such as MnDOT, FHWA and INDOT. Table 2.10 summarizes different specifications for the construction of control strips.

**Table 2.9 - Data Elements**

| <b>Item</b> | <b>Date Field Name</b>                    | <b>Example of Data</b>            | <b>Recommended Values for This Study</b> |
|-------------|---|-----------------------------------|--|
| 1           | Date Stamp (YYYYMMDD)                     | 20080701                          | Variables to be recorded                 |
| 2           | Time Stamp<br>(HHMMSS.S –military format) | 090504.0<br>(9 hrs 5 min. 4.0 s.) |  |
| 3           | Longitude (decimal degrees)               | 94.85920403                       |  |
| 4           | Latitude (decimal degrees)                | 45.22777335                       |  |
| 5           | Easting (m)                               | 354048.3                          |  |
| 6           | Northing (m)                              | 5009934.9                         |  |
| 8           | Roller pass number                        | 2                                 |  |
| 9           | Direction index                           | 1 forward, 2 reverse              |  |
| 10          | Roller speed (km/h)                       | 2.5                               | 2.0-4.0                                  |
| 11          | Vibration ON                              | 1 for yes, 2 for no               | 1 for yes                                |
| 12          | Frequency (Hz)                            | 30                                | 25-35                                    |
| 13          | Amplitude (in.)                           | 0.02                              | 0.02-0.04                                |
| 14          | RMV                                       | 20.0                              | TBD                                      |

**Table 2.10 - Specifications for Control Strips**

| Source  | Test Strip Area (ftxft)         | Vibratory Roller Characteristics            |   |   |                | Approach   |
|---------|---------------------------------|---|---|---|----------------|--|
|         |                                 | Type  | Speed, mph  | Vibration Amplitude, mm                           | Frequency, vpm |  |
| TxDOT   | 150 X 25                        | See Table 2.8                               | Same during calibration and production compaction |   |                | Target value is RMV that obtains the required k-value for a minimum of 90% of the test area  |
| MnDOT   | 300 x 32                        | Smooth drum or pad foot vibratory roller    | Same during calibration and production compaction |   |                | Target RMV is achieved when additional passes do not result in a significant increase in stiffness values as determined by LWD.  |
| FHWA    | 225 x 24                        | Smooth drum or pad foot vibratory roller    | Same during calibration and production compaction |   |                | Target RMV is the point when the increase in the RMV between passes is less than 5% between successive passes<br>Production target RMV is established based on a linear regression relationship between (either density- or modulus-based) spot test results and corresponding RMVs. Minimum spot test requirement based on laboratory testing |
| INDOT   | 100 x 20                        | Smooth drum or pad foot vibratory roller    | Same during calibration and production compaction |   |                | IC roller shall be used on the test sections to establish the RMV that corresponds to the DCP test results. Minimum DCP index requirement based on laboratory testing  |
| ISSMGE  | 300 x full width of section     | Roller chosen by experience                 | 2-6   | Same during calibration and production compaction |                | Linear regression relationships between the point test results (PLT/LWD/MDD) and the RIMV results are used to establish the production target RMV.<br>For small projects based on RMV increment (up to < 5%)   |
| Austria | 300 X full width of site        | Single wheel smooth drum                    | 2-6   | Same during calibration and production compaction |                | Linear regression relationships between the point test results (PLT/LWD/MDD) and the RMV results are used to establish the production target RMV.<br>For small projects based on RMV increment (up to < 5%)  |
| Germany | Three test strips of 60 ft long | Single wheel smooth drum                    | Same during calibration and production compaction |   |                | Linear regression relationships between the point test results (PLT) and the RMV results are used to establish the production target RMV.  |
| Sweden  |                                 | Vibratory or oscillatory single drum roller | Not specified                                     |   |                | To identify the weak spots based on RMV  |

## Acceptance Testing

Table 2.11 summarizes different specifications for acceptance testing. The acceptance is typically based on spot tests performed at the weak areas identified using the target RICM-MV.

**Table 2.11 - Specifications for Acceptance Testing**

| Specifications             | Acceptance Criteria   |
|----------------------------|---|
| <b>TxDOT</b>               | Compact each lift until the RMV indicates that a minimum of 90% of the area has achieved the RTV minus 1.5 times the standard deviation. Local contiguous non-compliance areas not achieving RTV must be no larger than 150 ft <sup>2</sup> .   |
| <b>MnDOT</b>               | All segments shall be compacted so that at least 90% of the MVs are at least 90% of the moisture-corrected RTV prior to placing the next lift. All of the RMVs must be at least 80% of the moisture-corrected RTV. If a significant portion of the grade is more than 20% in excess of the selected moisture-corrected RTV, the Engineer shall reevaluate the selection of the RTV. |
| <b>FHWA</b>                | A minimum coverage of 90% of the individual construction area shall meet the optimal number of roller passes and 70% of the target RMV determined from test strips.   |
| <b>INDOT</b>               | A minimum of 90% of the construction area shall be mapped. A minimum of 70% of the mapped construction area shall exceed the target RMV.  |
| <b>ISSMGE/<br/>Austria</b> | The mean RMV must be $\geq ME^1$ (based on $1.05 * E_{LWD}^2$ )<br>100% of RMVs must be $\geq 0.8 MIN^3$ (based on $0.95 * E_{LWD}$ )<br>90% of RMVs must be $\geq MIN$ ( $0.95 * E_{LWD}$ )  |
| <b>Germany</b>             | 90% of all RMVs in an evaluation area must exceed the RTV.  |
| <b>Sweden</b>              | Swedish specifications use roller-integrated CCC to identify weak spots for PLT   |

<sup>1</sup>Mean RMV, <sup>2</sup>Modulus from LWD, <sup>3</sup>Min. RMV

## Target Value Selection

For an efficient utilization of the IC technology, it is desirable that the contractor reach the targeted compaction specification without over-compacting the material. The selection of the target value can either be tied to the pavement design parameters or obtained from field test strips. In general, the former option is more desirable than the latter. One of the impediments to the wide implementation of the IC technology has been the tedium and excessive efforts necessary to construct the test strips. The downside of tying the target values to the pavement design parameters are the need for upfront advanced laboratory testing (such as resilient modulus testing) and a lack of an algorithm to estimate the target value.

Nazarian et al. (2011) explain a process to select target values for devices that measure the response of the geomaterials (e.g., LWD, PLT and Geogauge) based on the pavement design parameters. The approach they proposed, especially for multi-layer earthwork, is to utilize a nonlinear structural algorithm. The nonlinear algorithm is used to develop straightforward relationships for estimating field target moduli from resilient modulus parameters ( $k_1$ - $k_3$ ) from Equation 2.1.

$$MR_{opt} = k_1 P_a \left[ \frac{\theta}{P_a} \right]^{k_2} \left[ \frac{\tau_{oct}}{P_a} + 1 \right]^{k_3} \quad (2.1)$$

**LWD:** The target modulus/deflection is set in a way that is compatible with the algorithm used during the structural design of the pavement. The following steps shall be used to set the target values:

**Step 1:** Determine the resilient modulus parameters of the layer under test and the underlying layer(s). In the order of preference, these values should be obtained from one of the options below.

**Step-2:** Convert the regression parameters  $k_1$  through  $k_3$  from Equation 2.1 to  $k'_1$  through  $k'_3$  using the following relationships:

$$k'_1 = k_1 e^{(-1.32 k_2)} \quad (2.2)$$

$$k'_2 = 1.88 k_2 \quad (2.3)$$

$$k'_3 = k_3 \quad (2.4)$$

**Step-3:** Calculate the effective modulus of the geomaterial,  $E_{eff}$ , from:

$$E_{eff} = [(1 - \nu^2) F / (\pi \cdot a \cdot d_{eff})] f \quad (2.5)$$

where  $a$  = radius of load plate,  $d_{eff}$  = peak deflection on top the compacted layer,  $\nu$  = Poisson's ratio of the geomaterials,  $f$  = plate rigidity factor.

**Step-4** Establishing Adjustment Factor,  $K_{adj}$ . Obtain,  $K_{adj}$ , from Equation 2.6 following the two step procedure described below:

$$K_{adj} = K_{lab-field} K_{moist} \quad (2.6)$$

where  $K_{lab-field}$  is an adjustment factor that accounts for differences in lab and field moduli at the same moisture content and density and  $K_{moist}$  is an adjustment factor for differences in the compaction and testing moisture contents. Estimate  $K_{lab-field}$  from the following relationship:

$$K_{lab-field} = (F_{env})^\lambda \quad (2.7)$$

where  $\lambda = -0.36$  and  $F_{env}$  is calculated from

$$\log F_{env} = \left[ (-0.40535) + \frac{1.20693}{1 + e^{0.68184 + 1.33194 \times \left( \frac{S - S_{opt}}{100} \right)}} \right] \quad (2.8)$$

where  $S_{opt}$  = degree of saturation at optimum moisture content and  $S$  = degree of saturation at compaction moisture content. Estimate  $K_{moist}$  in the following manner.

$$K_{moist} = e^{\eta(\omega_C - \omega_T)} \quad (2.9)$$

where:  $\eta = 0.18$  for fine-grained soils and 1.19 for unbound aggregates;  $\omega_T$  = moisture content at time of testing (in percent);  $\omega_C$  = moisture content at time of compaction (in percent);

**Step-5:** Estimate the adjusted modulus,  $E_{adj}$ , from:

$$E_{adj} = E_{eff} * K_{adj} \quad (2.10)$$

**PSPA:** The target modulus,  $E_{T-PSPA}$ , is directly determined from laboratory Free-Free Resonant Column (FFRC) test (conforming to ASTM C 215) results using the following equation:

$$E_{T-PSPA} = E_{FFRC-Lab} / [(1 + \nu)(1 - 2\nu)/(1 - \nu)] \quad (2.11)$$

where  $E_{FFRC-Lab}$  = measured modulus with the FFRC device on the laboratory specimen and  $\nu$  = Poisson's ratio of the material.

### Limitations of Existing Guidelines for Development of Specifications

White et al. (2011) conducted a thorough review of existing specifications for implementing intelligent compaction. That study noted that one of the major limitations of the existing intelligent compaction specifications is that the acceptance requirements (i.e., percent target value limits, acceptable variability, etc.) are technology specific and somewhat based on local experience. This limitation hinders widespread acceptance of these specifications into practice, as there are currently at least ten different IC technologies. White and Vennapusa (2004) have documented the following as the key attributes in order to generalize the acceptance of the intelligent compaction specification:

- a) Identification of the rollers and descriptions of their configurations,
- b) General guidelines for operations (speed, vibration frequency and amplitude, and track overlap)
- c) Records to be reported (time stamp, operations/mode, soil type, moisture content, layer thickness, etc.)
- d) Repeatability and reproducibility measurements for intelligent compaction values
- e) Ground conditions (smoothness, levelness, isolated soft/wet spots),
- f) Calibration procedures for rollers and selection of calibration areas,
- g) Regression analysis between intelligent compaction values and point measurements,
- h) Number and location of quality control (QC) and quality assurance (QA) tests,

- i) Operator training/certification, and
- j) Acceptance procedures/corrective actions based on achievement of minimum RMV target values and associated variability

### **Geostatistics in Intelligent Compaction**

Geostatistics are statistical techniques developed to analyze and predict values of a characteristic that is spatially distributed. It begins with a type of autocorrelation analysis called variography or semivariance analysis, in which the degree of spatial self-similarity is displayed as a variogram. A curve is fit to the variogram, and the equation that describes the curve, called the variogram model, is used to predict unsampled locations by kriging or conditional simulation. Kriging is a geostatistical method used for spatial interpolation and it is different from other methods because it can assess the quality of the prediction with estimated errors. Kriging uses the semivariogram to measure spatially correlated component or spatial dependence. This produces provide optimal unbiased estimates of the property across the entire spatial domain. The same analysis can also be performed with temporal data such as hourly or daily measures of some property to interpolate through time. Geostatistical analyses also provide tools for spatial data exploration, identification of data anomalies, evaluations of errors in prediction of surface models, statistical estimation and optimal surface creation.

Summary of studies on using geostatistics in evaluating the compaction quality are listed in Table 2.12. The use of geostatistics in IC as QA/AC tool in the acceptance of compacted soil will be more meaningful than just spot test because it can demonstrate the spatial variability of compaction and depict soft/hard spot areas that can be targeted for repeated compaction. Studies conducted by White et al. (2008), Vennapusa et al. (2010) and White et al. (2011) have proven the importance of conducting spatial analysis using geostatistics techniques rather than univariate statistics which can improve the visualization of the compaction non-uniformity. Vennapusa et al. (2010) demonstrated the use of variogram analysis in combination with conventional statistical analysis to effectively address the issue of non-uniformity in QC/QA during earthwork construction. A variogram is a plot of the average squared differences between data values as a function of separation or lag distance and is a common tool used in geostatistical studies to describe spatial variation (White et al., 2011).

Another field study by White et al. (2008) reported that variograms developed for two different spatial areas with similar univariate statistics (i.e., mean and standard deviation) showed distinctly different shapes of variograms with different spatial statistics, which illustrate the importance of spatial modeling to obtain better characterization of “non-uniformity” compared to using univariate statistics. This emphasizes the importance of dealing with “non-uniformity” in a spatial perspective rather than in a univariate statistics perspective.

The FHWA is recommending using Veda software which is developed to analyze data collected from GPS and roller monitoring and displays simple statistical graphs like a histogram of RMVs (Figure 2.4) and semivariogram (Figure 2.5) and spatial distribution of RMCs (Figure 2.6). The data can also be imported into GIS software like ESRI ArcGIS and analyzed using both spatial analysis tools and Geostatistical tools.

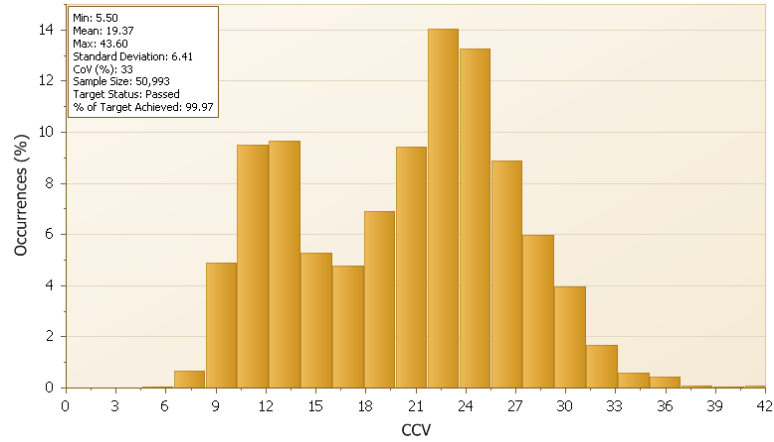


**Figure 2.4 -A Histogram Showing CCV Values and their Occurrence in IC Technology with Descriptive Statistics (VEDA v2).**

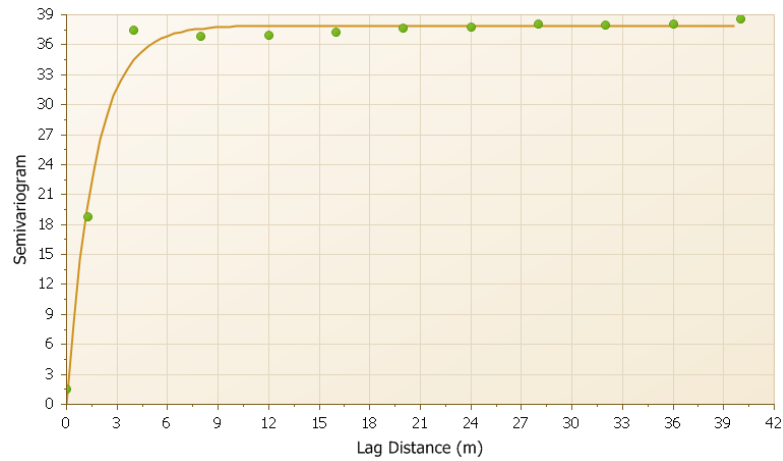


**Figure 2.5 -A Semivariogram of CCV Data from CCV Values (VEDA v2)**

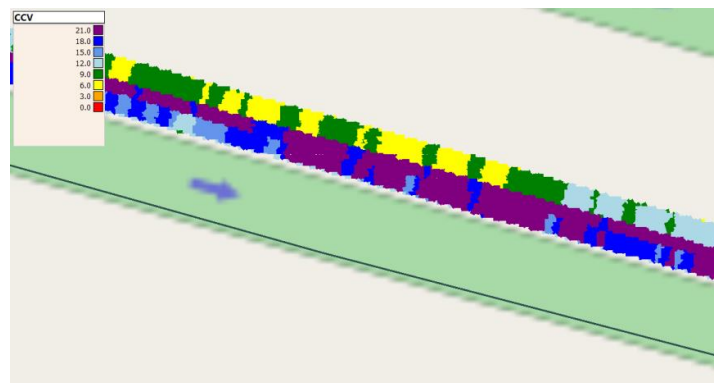


**Figure 2.6 -Proofing Data Example Showing Spatial Variations in the CCV Values (VEDA v2).**

**Table 2.12 - Geostatistics in Intelligent Compaction**

| Reference                     | Objective and scope  | Key findings/comments  |
|-------------------------------|--|--|
| <b>White et al., 2007</b>     | Evaluated the utilization of intelligent compaction monitoring for unbound materials in the field. Test sections with different site conditions, rollers with different data measurements and storage system were evaluated. | Study demonstrated the use of variogram models to effectively characterize the uniformity of compaction by quantifying spatial variability. The study showed that the range from a variogram plot can be potentially used as a maximum separation distance between spot tests measurements. Also study showed that to reduce any significant error, roller measurement values from the middle of drum shall be considered. |
| <b>Peterson et al., 2007</b>  | Evaluated the application of geostatistical tools to judge the adequacy of compaction and uniformity, assisting in the QC/QA process.  | Traditional descriptive statistics were found to be inadequate to address the concern of uniform compaction. The use of IC data and geostatistics help to identify and fix the problematic areas of poor compaction, which in turn improve the overall life cycle of pavements.  |
| <b>White et al., 2008</b>     | To characterize the uniformity of the compacted soil layer using intelligent compaction technology with variable feedback control.   | Findings from the study showed the limitations of univariate analysis in determining the uniformity of the compacted soil layer. Study identified the use of variogram model parameters to characterize the uniformity of compacted soil layer.  |
| <b>Vennapusa et al., 2010</b> | To quantify the non-uniformity using spatial referenced roller measurements  | Non-uniformity of compaction which cannot be explained with univariate analysis of roller measurements can be dealt with variogram analysis. Geostatistics can used to identify the areas of poor compaction and non-uniform conditions  |
| <b>White et al., 2011</b>     | Review of the field assessment studies and examined factors influencing the roller measurement values, correlations between the spot test measurements and spatial uniformity.   | Geostatistical analysis of roller measurement values facilitate construction process control and characterize variations and non-uniformity.   |

### **Numerical Analysis of Intelligent Compaction**

A few studies have been conducted using finite element modeling to assess compaction on pavements using IC rollers. Table 2.13 contains a summary of studies conducted modeling roller compaction on pavements or soils. In addition, two studies that discuss soil compaction due to wheel loading are included as part of the review of contact models, in this particular case of tire/terrain interaction. In general, the modeling considers layer thicknesses, material constitutive models, element types, load type, contact area, speed and the contact model between roller drum and pavement material.

### **Best Practices and their Impact on Compaction Process**

Traditionally the compaction process is aimed at achieving the target density at specified level of moisture content. The type of roller and lift thickness are selected based on the type of material and layer of pavement structure. The optimum number of passes to attain the desired level of density is determined based on the control section characteristics. The compaction effort is more or less maintained constant throughout the process (6 to 10 roller passes). These practices do not allow to monitor the compaction process and to vary the compaction effort during construction.

A number of studies investigated the correlation between the roller measurement values and the spot test measurements to evaluate the compaction uniformity. The best practice is to determine the target roller measurement value based on above correlations. The compaction process is monitored to meet the target value requirements. Individual agencies (Table 2.5) have identified their own limits of acceptance for target values to achieve compaction uniformity. Geostatistical analysis of roller measurement values facilitate process control and characterize non-uniformity of compaction.

The German specification recommends correlating three to five static plate load tests or density results for each control section to the roller measurement values. To establish the target roller measurement values the correlation coefficient must be greater than 0.7. However, there are no moisture content requirements. Most importantly to address the uniformity of compaction, the areas with roller measurement values lower than the target values should be distributed throughout the evaluation area. However, the definition of such distributed area is subjective (Mooney et al., 2010).

The Austrian/ISSME specifications are applicable to subgrade, subbase and base, and recycled materials (Mooney et al., 2010). Compaction is allowed with both static and vibratory rollers. However, dynamic measurements are needed for process control and acceptance. The target value is selected based on the minimum LWD modulus,  $E_{LWD}$ , or plate load test results  $EV_1$  requirements. Moisture content needs attention if the fines exceed 15%. The roller measurements for calibration and correlation development are valid only during continuous contact or partial loss of contact conditions (Figure 2.3).

The Swedish specifications for intelligent compaction are primarily for subbase and base layers (Mooney et al., 2010). The target values are established for the minimum requirements of plate load test results  $EV_2$ . Since the subbase and base layers are primarily granular materials (cohesionless soil), the moisture content requirements are not specified.

In addition to the general procedure for establishing the target values using intelligent compaction rollers, Minnesota specifications requires mapping subsurface before placing the layer. This will help to identify the weak areas to be corrected prior to compaction process. Also Minnesota specifications recommend to construct the control section with moisture near 65% and 95% of the optimum and to establish the correction factors for LWD testing.

**Table 2.13 - Summary of Finite Element Studies for the Modeling of Roller Compaction**

| Reference                    | Objective and Approach  | Concluding Remarks  | FE Model of Pavement   | Loading Type and Model  | Roller/Pavement Contact Model  |
|------------------------------|---|---|--|---|--|
| <b>ter Huerne (2004)</b>     | <ul style="list-style-type: none"> <li>Proposed an FEM for HMA rolling problem.</li> </ul>  | <ul style="list-style-type: none"> <li>Provided appropriate FE set up based on an interpolation procedure for getting right roller drum weight based on the measured layer thickness reduction.</li> <li>Recommendations to Rock material model (linear elastic with plastic behavior in accordance to critical state theory) available in DiekA code.</li> </ul> | <ul style="list-style-type: none"> <li>FEM code DiekA used.</li> <li>400 mm long model.</li> <li>Dense Asphalt Concrete (DAC) 0/16 used.</li> <li>Subbase of infinite material length.</li> <li>HMA modeled with an Arbitrary Lagrangian Eulerian (ALE) method.</li> </ul>   | <ul style="list-style-type: none"> <li>HAMM DV6.42 roller modeled as a free rotating rolling drum.</li> <li>Used rotated coordinate system for simulating roller drum.</li> </ul>   | <ul style="list-style-type: none"> <li>Suggests contour of drum modeled as rigid rotating boundary.</li> <li>Contact elements are four-node elements.</li> <li>Coulomb friction model in contact elements.</li> </ul>  |
| <b>Chiroux et al. (2005)</b> | <ul style="list-style-type: none"> <li>Soil interaction with a rigid wheel.</li> <li>Compared soil compaction wheel rut depth, and octahedral normal and shear stress of laboratory testing.</li> </ul> | <ul style="list-style-type: none"> <li>Modeled air void reduction process with FEM with reasonable accuracy in terms of deflections and stresses.</li> <li>Rebound found to be 25% of total deflection (not seen in their experiments).</li> </ul>  | <ul style="list-style-type: none"> <li>ABAQUS/Explicit.</li> <li>Two models: soil-bed and rigid rotating wheel</li> <li>Used half system.</li> <li>Soil was 7.2 m in length, 0.5 m height and 1.0 m in width.</li> <li>Relatively fine mesh density in the first 5 cm of soil under wheel.</li> <li>Soil used Drucker-Prager/cap model</li> <li>Hydrostatic pressure considered</li> </ul> | <ul style="list-style-type: none"> <li>Wheel, assumed to be rigid.</li> <li>Dimension: 54 in. diameter, 6 in. wide</li> <li>Used “R3D4” rigid 3D elements</li> <li>Weight of body applied through concentrated mass elements along perimeter of wheel.</li> <li>Two loadings of 5.8 and 11.6 kN (modeled weight of 2.9 and 5.8 kN due to half system).</li> <li>Translational velocity of 16.74 cm/s and 18.45 cm/s, respectively.</li> </ul> | <ul style="list-style-type: none"> <li>Contact surfaces at top of soil and outer surface of rigid wheel defined relative to each other by declaring them a “contact pair”.</li> <li>This technique allowed them to come in contact but not to cross each other.</li> <li>Rigid wheel loads soil by gradually applying gravitational acceleration to wheel through linear ramp.</li> <li>Friction interaction coefficient of 0.6 defined between surfaces.</li> </ul> |

**Table 2.13 cont. - Summary of Finite Element Studies for the Modeling of Roller Compaction**

| Reference  | Objective and Approach  | Concluding Remarks   | FE Model of Pavement  | Loading Type and Model  | Roller/Pavement Contact Model   |
|--|---|--|---|---|---|
| <p><b>Wang et al. (2007)</b></p>   | <ul style="list-style-type: none"> <li>• Provided an overview of the fundamental mechanisms of asphalt compaction.</li> <li>• Evaluated compaction mechanisms by means of the FEM and discrete element (DEM) models.</li> <li>• Evolution of Element Volume (EVOL) and Void Volume Fraction (VVF) used to evaluate the compaction.</li> </ul> | <ul style="list-style-type: none"> <li>• Modeled air void reduction process with FEM with reasonable accuracy.</li> <li>• DEM approach provided a fundamental understanding of particle kinematics, and relative binder/mastics to aggregate stiffness.</li> <li>• Both methods serve as guides for selection of compaction parameters.</li> </ul> | <ul style="list-style-type: none"> <li>• ABAQUS</li> <li>• Gurson-Tvergaard (1981) porous viscoplasticity model (Guler et al. 2002).</li> <li>• Considers the compaction of material in the view of its air void reduction resulting from the squeezing of aggregates and mastics.</li> <li>• This viscoplastic model considers hydrostatic components of stresses and strains and takes into effect void nucleation and growth.</li> </ul> | <ul style="list-style-type: none"> <li>• Modeled a roller, assumed to be rigid.</li> <li>• In addition to constant loading (5-20 kN) applied by the roller, a vibration force was included with smaller magnitude to the roller (sinusoidal function).</li> </ul> | <ul style="list-style-type: none"> <li>• Roller assumed to be rigid.</li> </ul>         |
| <p><b>Hügel et al. (2008), referring to a study carried by Kelm (2003)</b></p> | <ul style="list-style-type: none"> <li>• Modeling of compaction of soil by vibratory rollers on dry non-cohesive soils.</li> <li>• Calculate distribution of void ratio <math>e</math> of soil after single vehicle crossing.</li> </ul>  | <ul style="list-style-type: none"> <li>• Simulations helped optimize compaction and homogenization of non-cohesive soils.</li> </ul>   | <ul style="list-style-type: none"> <li>• ABAQUS/Explicit</li> <li>• Soil is modeled using hypoplastic constitutive models.</li> <li>• Subsoil section is discretized using continuum elements (C3D8R) with displacement degree of freedom, and far field uses infinite elements (CIN3D8).</li> </ul>  | <ul style="list-style-type: none"> <li>• Vibratory roller modeled as rigid surface linked with a point mass.</li> <li>• Horizontal velocity and vertical harmonic excitation of roller are predefined.</li> </ul>   | <ul style="list-style-type: none"> <li>• Roller drum modeled as rigid plate.</li> </ul> |

**Table 2.13 cont. - Summary of Finite Element Studies for the Modeling of Roller Compaction**

| Reference                 | Objective and Approach   | Concluding Remarks  | FE Model of Pavement   | Loading Type and Model   | Roller/Pavement Contact Model   |
|---------------------------|--|---|--|--|---|
| <b>Kim (2010)</b>         | <ul style="list-style-type: none"> <li>Modeling of IC rollers to estimate influence depth of soil compaction.</li> <li>Various drum types evaluated: cylindrical, triangular, Lanpac's (rounded triangular), pentagonal and Bomag's octagonal.</li> </ul>                  | <ul style="list-style-type: none"> <li>Width of contact area between drum and soil controls depth of compaction.</li> <li>Depth of compaction larger for IC rollers.</li> <li>Depth of compaction depends on stiffness of soil.</li> <li>Surface pressure controls degree of compaction (uneven for impact rollers).</li> </ul> | <ul style="list-style-type: none"> <li>3-D FE LS-DYNA</li> <li>Length of soil: 52.5 ft</li> <li>Planned compaction test length: 42 ft</li> <li>4 in. element size underneath roller</li> <li>Druker-Prager (simplified elastic perfectly plastic model).</li> <li>Contact friction of drum and soil based on soil external friction angle of 30°~35°.</li> </ul> | <ul style="list-style-type: none"> <li>Modeling of 24,000 lb drum</li> <li>Size: 1.50 m diameter, 2.20 m wide.</li> <li>Modeled with 4 in. thick rigid shell elements</li> <li>Beam element located axially in the middle of drum mesh moves at 10 km/h.</li> <li>Evaluated cylindrical, triangular, Lanpac's rounded triangular, pentagonal and Bomag's octagonal drums</li> </ul>  | <ul style="list-style-type: none"> <li>Roller shell and beam elements coupled as constrained rigid bodies.</li> <li>This coupling allows drum mesh to be rotate by friction force between drum and soil.</li> <li>Contact automatic surface to surface coupling added for contact between drum mesh and soil mesh.</li> <li>Soil treated as master material coupled drum and axis defined as slave material.</li> </ul> |
| <b>Xia and Pan (2010)</b> | <ul style="list-style-type: none"> <li>Modeling of vibratory asphalt compaction.</li> <li>Different compactor operations modeled to understand impact on compacted density.</li> <li>FE model used to predict spatial density change due to rolling compaction.</li> </ul> | <ul style="list-style-type: none"> <li>Vibratory asphalt compaction delivers better compaction to HMA layer.</li> <li>Vibration frequency important parameter for influencing final asphalt compaction.</li> </ul>  | <ul style="list-style-type: none"> <li>ABAQUS</li> <li>3-D FE</li> <li>10 m long, 3 m wide.</li> <li>Three layer system: 0.125 m HMA layer, 0.3 m base, and 2.0 m subgrade.</li> <li>Crushable foam model with volumetric hardening to model asphalt compaction</li> <li>Base and subgrade assumed to deform elastically.</li> </ul>                             | <ul style="list-style-type: none"> <li>Modeling of roller (non-vibratory and vibratory).</li> <li>Roller assumed to be a rigid body with a point mass element defined at the centroid.</li> <li>Roller dimensions: 3.44 m base, 1.3 m diameter, 1.72 m width.</li> <li>Load = 10.8 k (48 kN)</li> <li>Vibratory force frequency of 40 Hz.</li> <li>Eccentric mass moment of <math>m_0e_0 = 1.585 \text{ kg}\cdot\text{m}</math></li> </ul> | <ul style="list-style-type: none"> <li>Roller assumed to be rigid body.</li> </ul>  |

**Table 2.13 cont. - Summary of Finite Element Studies for the Modeling of Roller Compaction**

| Reference                                    | Objective and Approach  | Concluding Remarks   | FE Model of Pavement  | Loading Type and Model   | Roller/Pavement Contact Model   |
|--|---|--|---|--|---|
| <p><b>Patrick and Werkmeister (2010)</b></p> | <ul style="list-style-type: none"> <li>• Compaction of thick granular bases.</li> <li>• Compared theoretical stress and strain distribution under a vibratory roller and a standard heavy vehicle.</li> <li>• Evaluated thin AC surfaced granular pavements.</li> </ul> | <ul style="list-style-type: none"> <li>• Initial post-construction deformation of thin-surfaced granular pavement is affected by compaction level in the field, though rut would be relatively small.</li> <li>• Degree of compaction of 88% max. dry density (MDD) would not result in significant rutting of pavement.</li> <li>• FE indicates that max. vertical elastic and vertical compressive strains induced by 3 ton vibratory roller in upper part of base are smaller than those induced by a 40 kN dual wheel but higher for lower part of base course.</li> </ul> | <ul style="list-style-type: none"> <li>• ReFEM, 3-D FE</li> <li>• Used quarter model: FE section 2.4 m long × 4.0 m wide.</li> <li>• HMA and subgrade modeled as linear elastic.</li> <li>• Base course modeled using Dresden model.</li> </ul> | <ul style="list-style-type: none"> <li>• Smooth drum roller, Caterpillar CD 563C.</li> <li>• Load under a typical 3 metric ton vibratory roller drum for base course compaction.</li> <li>• Drum diameter 1.5 m, width 2.1 m.</li> <li>• Contact area: assumed 2.66 m long for high amplitude dynamic load with a width of 1.33 for low amplitude dynamic load.</li> <li>• High amplitude dynamic load 15.2 ton.</li> <li>• Elastic deformation of base course/subgrade assumed to be governed by parabolic load.</li> </ul> | <ul style="list-style-type: none"> <li>• Roller drum modeled as rigid plate (high stiffness <math>E = 320,000</math> MPa in transversal and vertical direction).</li> </ul> |

**Table 2.13 cont. - Summary of Finite Element Studies for the Modeling of Roller Compaction**

| Reference               | Objective and Approach   | Concluding Remarks  | FE Model of Pavement  | Loading Type and Model   | Roller/Pavement Contact Model   |
|-------------------------|--|---|---|--|---|
| <b>Xia (2011)</b>       | <ul style="list-style-type: none"> <li>• Tire/terrain interaction for off-road vehicle design.</li> <li>• Predict soil compaction and tire mobility.</li> </ul>  | <ul style="list-style-type: none"> <li>• Effects of tire inflation pressure, rolling speed and frictional property of tire/terrain interface on rolling radius, acceleration, torque and traction were obtained.</li> <li>• Proved that numerical model can serve as robust tool on predicting soil compaction.</li> </ul>  | <ul style="list-style-type: none"> <li>• ABAQUS/Explicit.</li> <li>• 3-D FE two layer system.</li> <li>• 12 m long, 3 m wide, 2 m deep.</li> <li>• Upper soil using Drucker-Prager/Cap model for soil compaction.</li> <li>• Stiffer lower soil modeled linear elastic.</li> </ul>  | <ul style="list-style-type: none"> <li>• Modeling of a tire with 981 mm diameter and 327 mm tread width.</li> <li>• Tire rubber modeled as compressible hyperelastic material and fiber reinforcement as linear elastic.</li> </ul>  | <ul style="list-style-type: none"> <li>• Simulation in two steps: first static followed by tire rolling over a deformable soil with an angular velocity at the tire axle.</li> <li>• Coulomb's friction law used to define friction between tire and ground.</li> </ul> |
| <b>Xu et al. (2012)</b> | <ul style="list-style-type: none"> <li>• Studied the effect of compaction uniformity on pavement performance.</li> <li>• Compared the effect of the HMA heterogeneity to a homogeneous HMA material on performance.</li> <li>• Peak pavement responses were used for pavement performance prediction using MEPDG distress models.</li> <li>• Determined Bomag ICMV, measurement of the vibration (dynamic) modulus of elasticity <math>E_{vib}</math> for pavement materials.</li> </ul> | <ul style="list-style-type: none"> <li>• Rutting of the nonuniform HMA model was higher than that of homogeneous HMA.</li> <li>• Fatigue life reduced in nonuniform HMA model.</li> <li>• A pavement section with lower mean value of layer moduli does not necessarily mean inferior performance since the effects from uniformity of material property may dominate other factors.</li> </ul> | <ul style="list-style-type: none"> <li>• ANSYS 12.1<sup>®</sup></li> <li>• 3-D FE model with heterogeneous HMA moduli as obtained from field IC measurements.</li> <li>• All pavement materials assumed linear elastic.</li> <li>• Spatially distributed moduli for heterogeneous HMA.</li> <li>• Dimensions: 770 ft long by 10 ft wide compaction lane similar to an IC construction project located on US 52 in Lafayette, IN.</li> <li>• The FE model: 105,798 elements, 117,100 nodes.</li> </ul> | <ul style="list-style-type: none"> <li>• Sinusoidal pulse with cycling period of 0.6 s, peak value of 9000 lb and pressure of 100 psi.</li> <li>• Contact area of 5.8 in. × 15.6 in., comprised by 3 elements.</li> <li>• Moved at a constant speed of 60 mph.</li> <li>• Step loading applied on element by element.</li> </ul> | <ul style="list-style-type: none"> <li>• None, pressure applied on AC layer.</li> </ul>   |

In summary, heterogeneity of the underlying layer, measurement depth and variation in moisture content were found to be the challenges to implement the IC technology (White et al., 2005, Mooney et al., 2006, Petersen and Peterson, 2006, Mooney and Rinehart, 2007). The stress dependent characteristic of the granular materials is a potential source of problem to compare stiffness and modulus results from different test and roller measurement values (Rinehart et al., 2012). Incorporation of moisture content, density and modulus measurements from the spot tests will improve to correlation between the roller measurement values and spot test results.

### **Best Practices for Quality Control and Acceptance**

Highway agencies in Europe and the United States have come up with their own specifications for quality control and acceptance of compaction using intelligent compaction technology (see Table 2.5). In general, the quality control and acceptance is based on achieving the target roller measurement values during process control and acceptance. Different methods practiced (Mooney et al., 2010) for establishing the target values in quality control and acceptance are as listed below:

- a) Establishing the required soil density or modulus value to be achieved in the field
- b) Calibrating the modulus and roller measurement values for moisture content variation
- c) Determining the target values consistent with the required density or modulus values
- d) Acceptance testing by comparing the roller measurement values with target values
- e) Acceptance based on the percentage change in the roller measurement values

The best practice is to maintain the constant speed and vibration amplitude during compaction process and acceptance. Specifications (Table 2.5) have come with different levels of acceptance and rejection. For control and acceptance testing roller should be in continuous contact or periodic loss of contact state with the placement.

Most of the specifications require the roller measurement values to be higher than 70 to 90% of the target values established from the control section for 90% of the area being considered. The weak areas not meeting the target value requirements are marked for rework or reconstruction. For acceptance of the compaction work, both roller measurement values and density or modulus are checked to meet the specified requirements.

For a particular type of soil, the important factors influencing the measurement values are moisture content, density and compaction energy. The nonlinear relation between the density and moisture content is well represented by a parabolic fit. Similar densities can be obtained at both dry and wet of optimum moisture contents. Even at same density, the modulus or stiffness values may not be comparable and hence the compaction control may not be possible with density measurements alone (Hossain et al., 2006). Also the variation in modulus and stiffness depends upon on the type of soil (cohesive or granular). White et al., (2005) have demonstrated the influence of moisture content on the density and stiffness measurements. The findings have shown that laboratory density and compaction energy required is significantly influenced by the moisture content. Similarly studies (Petersen and Peterson, 2006, Rahman et al., 2007) have also high lightened the importance of moisture content in developing target values.

Specifications in Austria recommend paying attention to moisture content variation if the fines exceed 15%. Similarly Minnesota specifications recommend calibrating the roller measurements values with moisture content variation.

Major findings from the ongoing NCHRP Project 10-84 (Nazarian et al, 2011) has shown that even though the traditional quality acceptance is based on ensuring adequate density, the parameters that control the stiffness of the layers the most are the moisture content at the time of compaction, the moisture content at the time of testing and the thickness of the lift during compaction. For example, Figure 2.7 demonstrates the variation of the modulus of a clayey soil compacted at OMC as well as wet and dry of OMC. The modulus increases as a specimen is allowed to dry. Figure 2.8 shows the variations

of the modulus normalized to modulus after 24 hrs of compaction with the difference in compaction and testing moisture contents for five diverse subgrades and a granular base. From these results, it is clear that the moisture content more than the density should be considered during the IC roller based acceptance. The NCHRP 10-84 specification, recommends that the following items should be emphasized:

- Modulus-based acceptance should be implemented in conjunction with as a restrict of a process control as possible since reasonably small changes in the moisture content will have significant impact on measured moduli.
- The density and moisture measurements can be considered as process control items, with modulus-based measurements being used for quality acceptance.
- The best results are obtained, when a moisture content measurement is carried out in conjunction with the modulus-based measurement.
- Highway agencies should consider incorporating the moisture content of the loose material before compaction in their process control.

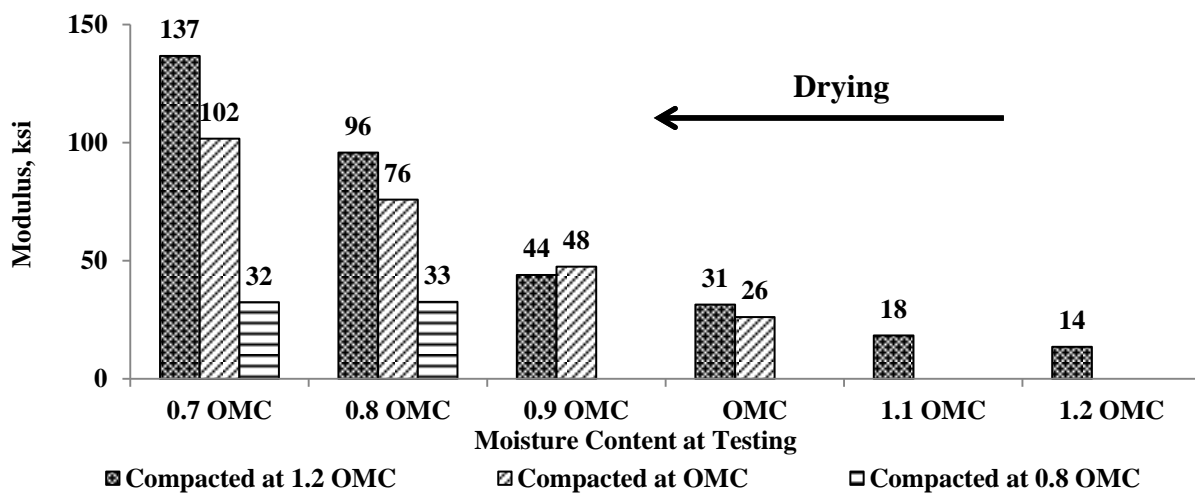


Figure 2.7 -Variation in Modulus as a Function of Compaction and Testing Moisture Contents

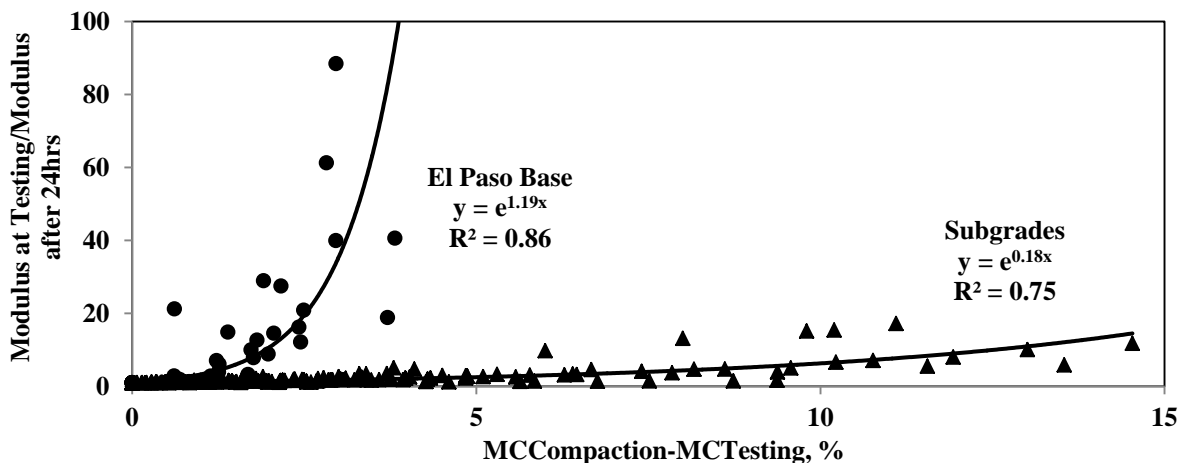


Figure 2.8 -Variation in Modulus as a Function of Difference in Compaction and Testing Moisture Contents

## Chapter 3

# Numerical Analysis of Soil-Roller Interaction

### Introduction

Pavement structures typically consist of several layers that progressively become stiffer and thinner as they are constructed from bottom to top. The depth of influence of a roller, which varies with the weight and dimensions of the roller and the frequency of the vibration, can be as deep as 6 to 7 ft (Mooney et al., 2010). It is intuitive that the thinner the layer that is being compacted becomes, the less influence it will have on the response of the roller. Due to the inevitable variability in moisture content and nonuniformity of the materials during compaction, there is a minimum layer thickness and modulus contrast that lend the IC roller response ineffective. What complicates the matter further are the facts that geomaterials, being embankment or base, behave quite nonlinearly under the heavy loads of the roller. Understanding the behavior of rollers benefits both the Contractor and TxDOT. The Contractor can utilize the results to optimize the roller setting to achieve compaction in the fewest possible passes (an incentive to adopt the technology) while TxDOT will benefit by minimizing the variability in the IC roller measurements (and as such more confidence in the acceptance results).

A large number of case studies of using the IC roller responses side-by-side with other modulus-based methods (e.g., light weight deflectometer (LWD), plate load test (PLT), Geogauge, Dynamic Cone Penetrometer (DCP), etc.) for acceptance are available in the literature. The results of these studies are mixed primarily because of lack of consideration of the roller-soil interaction. Numerical modeling of a roller and an LWD on a two-layered pavement system consisting of a base and subgrade is presented in this Chapter to address some of these concerns. The influence depth was numerically assessed. Though the weight and the roller parameters like amplitude and frequency of vibration may also significantly impact the responses of the rollers, due to time limitation, it is not addressed in this report.

### Finite Element Modeling of Roller Compactor

The numerical modeling of soil response due to roller compaction is rather complex. Thus, a dynamic finite element (FE) technique is necessary to evaluate the dynamic interaction of the roller with the soil or pavement system. For the purpose of this study, an FE analysis program called LS-DYNA was selected to address this need. LS-DYNA is a multi-purpose FE program that makes use of explicit and implicit time integration techniques.

A 3-D mesh was built for the FE modeling of a roller compacting the soil with a vibrating frequency. Figure 3.1 shows a 3-D view of the pavement structure and the roller. The roller was modeled with rigid shell elements and dimensions typical to common IC rollers (i.e., 80 in. wide and 30 in. in radius). Due to the size of the roller, the soil was modeled as 160 in. wide, 160 in. in length, and 100 in. in depth. A mesh consisting of brick elements with 2×2×2 in. dimensions was used for the pavement structure, totaling 320,000 elements. The roller was positioned at the center of the model. The roller was defined by 75,360 shell elements to better accommodate its nodes to be in contact with the soil's mesh. Both base

and subgrade materials were modeled linearly elastic. The interaction between the roller and the pavement structures was modeled using the automatic surface-to-surface contact option of LS-DYNA. Figure 3.2 shows the roller-to-surface contact.

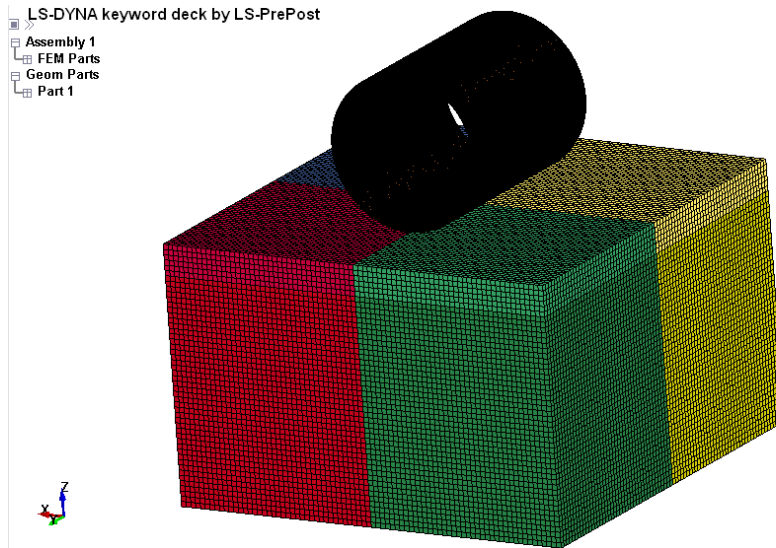


**Figure 3.1 - FE Modeling of Roller and Pavement Structure**

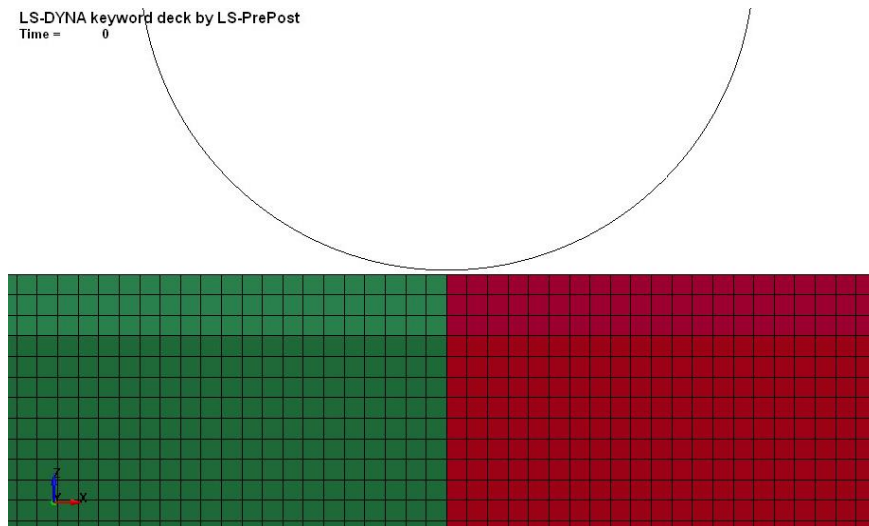


**Figure 3.2 – Roller to Soil Contact**

The vibratory loading of the roller was modeled using a 30 Hz sinusoidal load distributed on the roller with amplitude of 79 kips in addition to the 13 kips mass of the roller. The inertia of the soil, when modeled as a linear elastic material, will drive the roller in an upward motion in addition to the already existing upward direction of half the sinusoidal cycle. To prevent the roller's loss of contact and "jumping" away from the pavement, the vibratory load was shifted to avoid the change in direction of the load upwards by keeping the total load acting downwards at all times; however, the sinusoidal force amplitude was kept constant.

In addition to the geometric damping that occurs naturally in the model, Rayleigh damping was introduced to simulate material damping in the soil. The damping matrix  $[C]$  is defined by two parameters  $\alpha$  and  $\beta$  as defined in Equation 3.1.

$$[C] = \alpha[M] + \beta[K] \quad (3.1)$$

where  $[M]$  is the mass matrix,  $[K]$  is the stiffness matrix,  $\alpha$  and  $\beta$  were arbitrarily defined as 25 and 0.0002.

### Parametric Study

A parametric study to characterize the roller response consisted of the analysis of four cases of subgrade and 32 cases of two-layer pavement structures consisting of a base course and subgrade with combination of properties shown in Table 3.1.

**Table 3.1 Pavement Sections Properties**

| Pavement Layer         | Base                    | Subgrade      |
|------------------------|-------------------------|---------------|
| Thickness, H (in.)     | 0 (single layer), 6, 12 | -             |
| Modulus, E (ksi)       | 25, 45, 65, 85          | 5, 15, 25, 35 |
| Poisson's ratio, $\nu$ | 0.35                    | 0.35          |

The vibratory motion of the roller was maintained until the system reached a steady state solution. Pressure and displacement contours were generated for 1 ms during the analysis. Time history pavement responses were measured underneath the center of the roller. With that information, profiles of vertical deflection, stress and strain were determined during the roller vibration to calculate the depth of influence the loading has on the pavement structure.

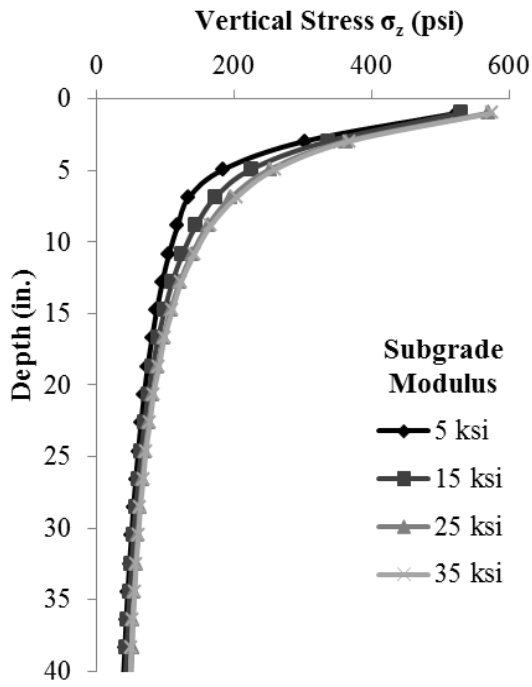
The profile of the peak vertical stress due to cyclic loading of the roller is shown in Figure 3.3 for a pavement section with a 6 in. thick base on top of subgrade. Figure 3.3a shows the stress profile for a base layer with a modulus of 45 ksi and subgrade with different moduli. Figure 3.3b shows the peak vertical stress profile for the same base layer thickness with a subgrade modulus of 15 ksi but different base moduli. The case of a pavement with no base, subgrade only, is also included. The vertical stress dissipates further within the first 12 in. below the surface if a base layer is used and diminishes with a similar rate for all pavements, particularly after 18 in. in depth. Similar to one-layered systems, in two-layered systems, the rate varies the most within a region 12 in. within the subgrade starting from the base-subgrade interface, located 6-in. underneath the surface.

Profiles of peak vertical strains and deformations are provided in Figure 3.4 for a 6 in. thick base layer with 45 ksi modulus, and varying subgrade moduli. Vertical strains and deflections increase as subgrade modulus decreases. Strains increase particularly when measured close to the base-subgrade interface. Influence depths can be determined from the profiles of peak responses. The depth of influence in terms of stress and deformation was investigated for the cases studied. In addition, the roller measured composite stiffness was determined.

### Depth of Influence

Depth of influence of soil compaction was calculated using the cyclic peak responses in terms of stress, strain and deflection. Mooney et al. (2010) suggests measurement depths of about 4 ft. Measurement depth,  $H_c$ , is reached when stress or strain decays to about 10% of the maximum vertical surface peak stress value,  $\sigma_{z,peak}$ , or peak strain value,  $\varepsilon_{z,peak}$ . The influence depth was measured based on the 10% of the peak soil response value in this study. Moreover, a level of 5% of the magnitude of the peak surface response was also considered.

(a) Base 45 ksi and varying subgrade modulus



(b) Subgrade 15 ksi and varying base modulus

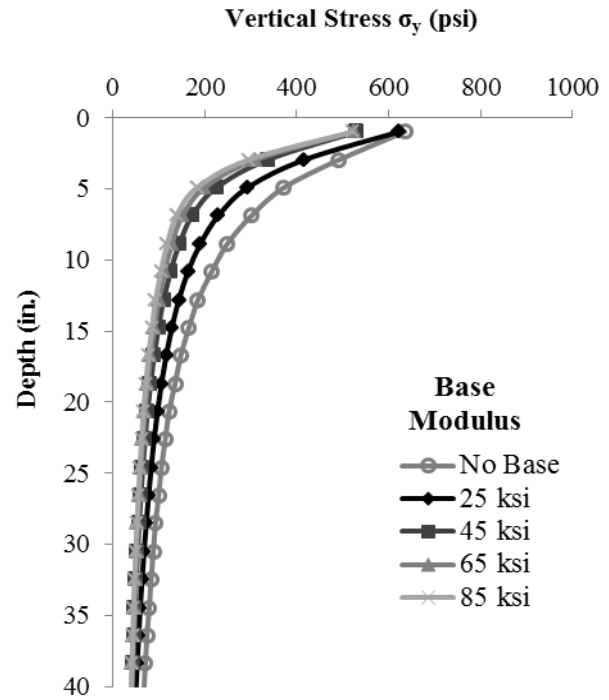
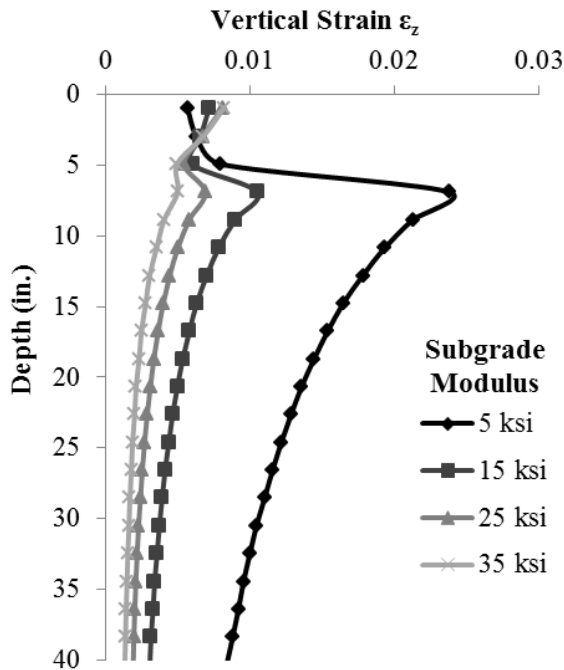


Figure 3.3 – Vertical Stress Distribution for a Pavement Structure with a 6 in. Base

(a) Vertical strain profile



(b) Deformation profile

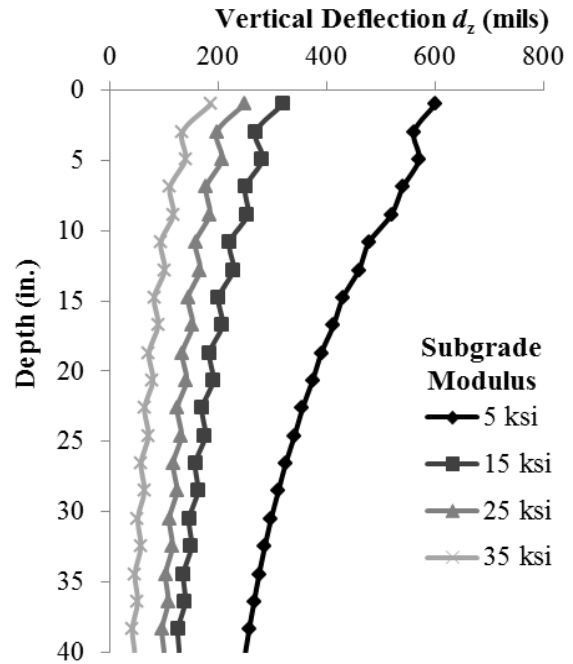
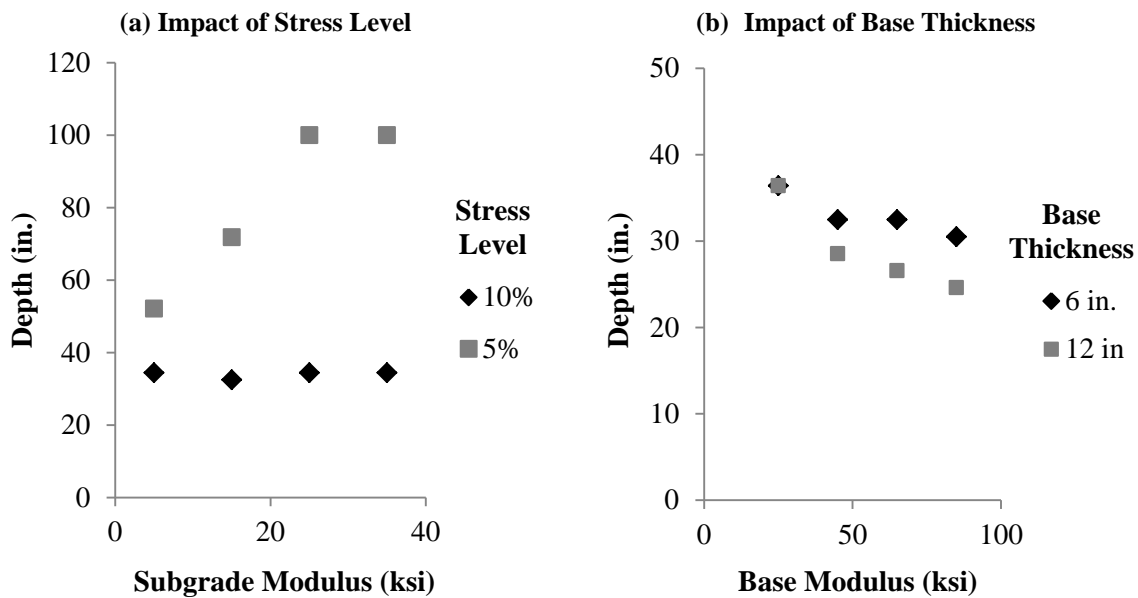


Figure 3.4 – Response Profiles for a Pavement Structure with a 6 in. Base (Base Modulus of 45 ksi and Varying Subgrade Modulus).

Figure 3.5a shows the depth of influence in terms of vertical stress for a pavement with a 6 in. thick base at different stress levels of the peak surface vertical stress at different subgrade moduli. The depth of influence for a 10% stress level remains fairly constant for different subgrade moduli at a depth of approximately 32 in. On the other hand, when stress level is further constrained to a lower value, the depth of strain increases as subgrade modulus increases. For the two highest subgrade moduli, the influence depth reached 100 in., which is set as the lower boundary of the model. Furthermore, as shown in Figure 3.3, the rate of change in stress beyond the stress level of 10% (i.e., beyond 30 in. in depth) is minimal. Thus, the 5% level of stress may occur deeper than 100 in.

The effects of base modulus and thickness on the depth of influence based on stress were also evaluated. Figure 3.5b shows the depth of influence for a stress level of 10% of the surface peak stress for both 6 in. and 12 in. base thickness and varying base moduli. A representative case is shown for a section with subgrade modulus of 15 ksi. From Figure 3.5b, the depth of influence decreases as base modulus and base thickness increases.



**Figure 3.5 – Depth of Influence in terms of Vertical Stress at Varying Stress Level and Varying Base Thickness.**

The effects of base and subgrade moduli were then evaluated for all cases. Figure 3.6a shows the influence depth in terms of vertical stress for all combinations of base and subgrade moduli, for a section with a base thickness of 6 in. at a 10% surface peak vertical stress. The depth of influence lies within 29 in. to 36 in. from the surface for the two-layer system. When no base is considered, the depth of influence increases up to 50 in. when a weak subgrade is used. The depth of influence for two-layer systems decreases as the base becomes stiffer, while the contribution of the subgrade modulus to depth of influence is less significant. Similar results are obtained for a base thickness of 12 in., as shown in Figure 3.6b. Generally, the depth of influence is somewhat similar for both base thicknesses; however, stresses dissipate slightly faster when a thicker base is used on less rigid subgrades.

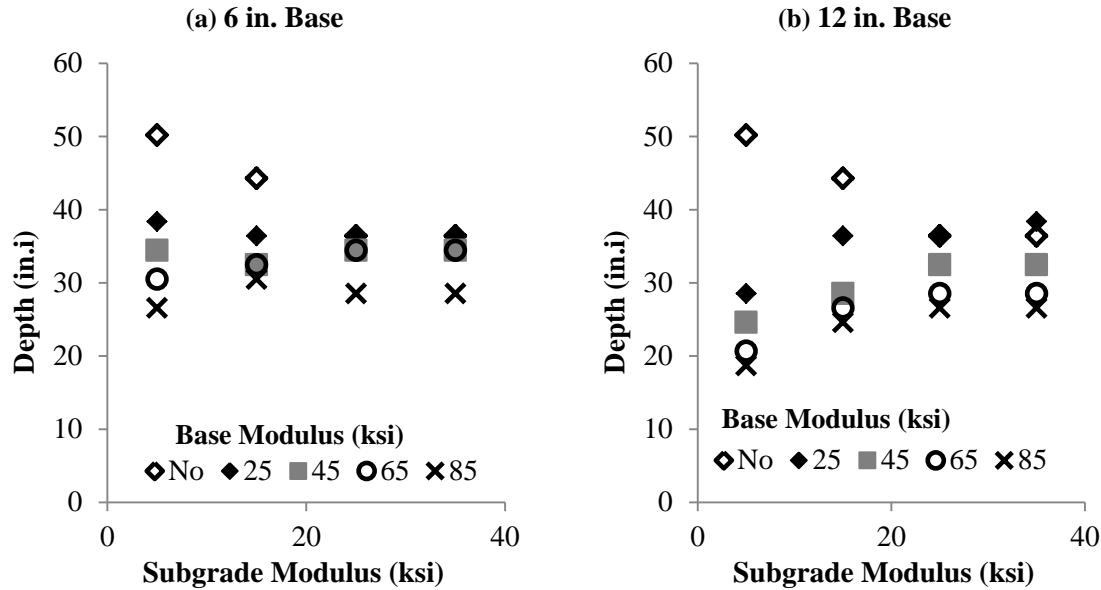


**Figure 3.6 – Depth of Influence at a 10% of the Surface Vertical Peak Stress for Varying Base and Subgrade Moduli.**

The influence depths in terms of deflection and strain were calculated for the same cases. Figure 3.7 shows the depths of influence at 10% of the surface peak deflections for sections with 6 in. and 12 in. base thickness and varying base and subgrade moduli. This depth varies between 73 in. and 85 in. from the surface in two-layer systems. When only the subgrade is analyzed, the depth of influence decreases close to 60 in. in weak subgrades. This occurs because larger surface deformations occur in weak subgrades which rapidly decrease close to the surface when compared to stiffer base layers and subgrades. Base and subgrade moduli had a slight impact on the influence depth, unlike base thickness that showed no significant influence. Depth of influence decreased slightly with lower base moduli and higher subgrade moduli. Base thickness had a slight impact on depth of influence only in the sections with low subgrade moduli. Nonetheless, the influence depth in terms of deflection did not vary much for any combination. A 5% level of deflection occurs deeper; however, it was not possible to predict it because of the model's boundary proximity.

It was not possible to predict the influence depths at 10% of peak surface vertical strain for all cases, since they extended beyond the model's depth of 100 in. Depth of influence at 10% of the selected surface peak response level (stress, deformation or strain) usually occurs at a point where the slope from the response vs. depth plot is approaching verticality, as shown in Figures 3.3 and 3.4. A response of 5% from the peak level occurs deeper, at a point where the slope is even closer to verticality. In the case of stress, Figure 3.4 shows that the stress decay rate decreases at depths occurring within a region of 15%-20% of the peak surface vertical stress. This range may suit better deflection and strain profiles. Particularly, when considering strain, the maximum peak occurring in the depth profile should be considered rather than the surface strain for determining the influence depth.

### Stiffness

Two soil stiffness parameters are determined from cyclic drum deformations in current practice. The force-displacement hysteresis loops are developed by plotting the time-varying contact force  $F_c$  versus drum displacement  $z_d$  (Mooney and Rinehart, 2009). In numerical analysis, the vertical forces transferred to the soil surface and the vertical deformations of the soil surface are used. Figure 3.8a shows a hysteresis loop for a pavement with a 6 in. thick base with 45 ksi modulus and 15 ksi subgrade modulus. Downward direction for displacement and compression for force are taken as positive. The secant

stiffness,  $k_s$ , is calculated from the point of zero dynamic displacement (under static loading) to the point of maximum displacement. This parameter is used by Case/Ammann (Mooney and Rinehart, 2009). The tangent stiffness,  $k_t$ , is measured from the loading portion of the curve as used by Bomag for determining  $E_{vib}$ .

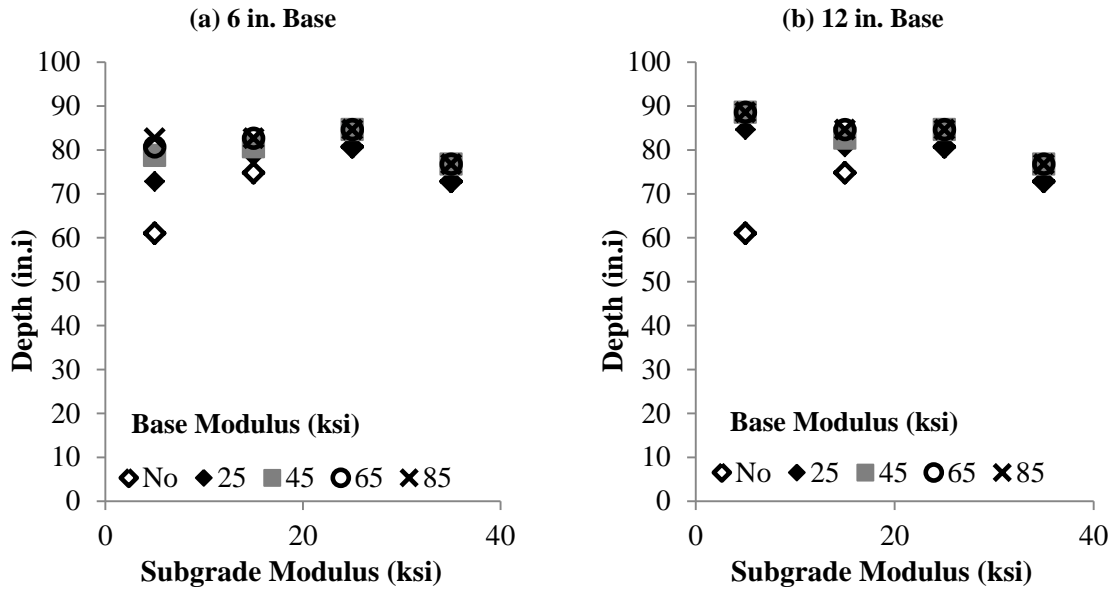


**Figure 3.7 – Depth of Influence at a 10% of the Surface Peak Deflection with Varying Base and Subgrade Moduli.**

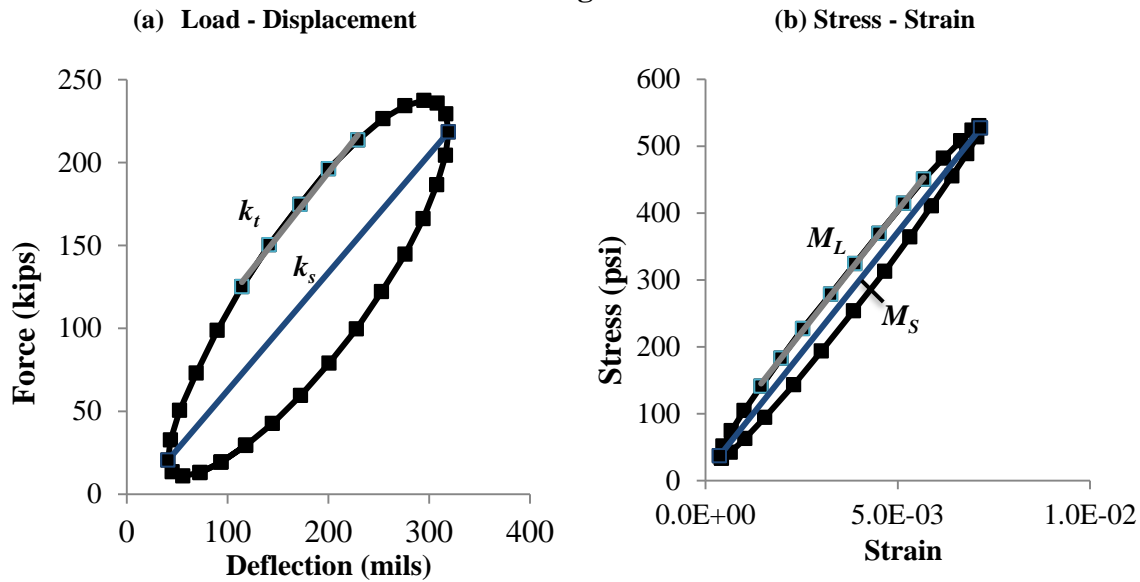
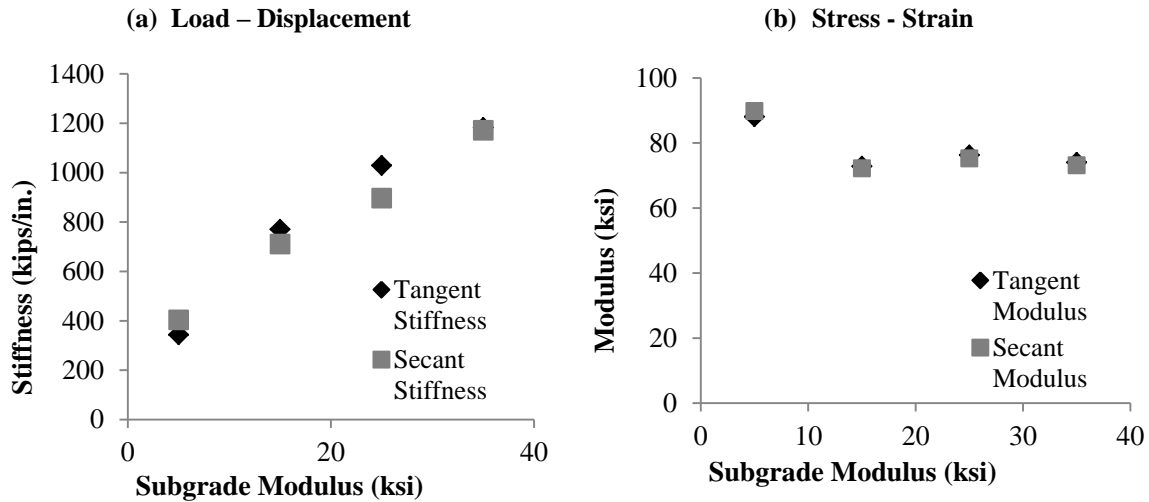


**Figure 3.8 – Hysteresis Loops for the Calculation of Tangent and Secant Stiffness and Modulus for a 6-in. Base,  $E_{BASE} = 45$  ksi and  $E_{SUBG} = 15$  ksi.**

Tangent and secant moduli can be obtained from the stress-strain  $\sigma_z$ - $\epsilon_z$  hysteresis loops. Figure 3.8b shows the  $\sigma_z$ - $\epsilon_z$  response to a vibratory roller pass. The secant modulus,  $M_s$ , is determined from zero  $\sigma_z$ - $\epsilon_z$  or the point of minimum through maximum  $\epsilon_z$ . The tangent modulus,  $M_L$ , is calculated similar to the

tangent stiffness. Figure 3.8b shows a hysteresis  $\sigma_z$ - $\epsilon_z$  loop for a pavement with a 6 in. thick base, 45 ksi base modulus and 15 ksi subgrade modulus. The compressive stresses and strains are taken as positive.

Figure 3.9 shows tangent and secant stiffness and moduli for a 6 in. thick base layer with modulus of 45 ksi and varying subgrade moduli. The stiffness increases as the subgrade modulus increases, as shown in Figure 3.9a. However, the tangent and secant moduli decrease as the subgrade modulus increases but remain fairly constant when the subgrade modulus exceeds 15 ksi, as shown in Figure 3.9b. No significant difference is apparent between the secant and tangent stiffness values or moduli.



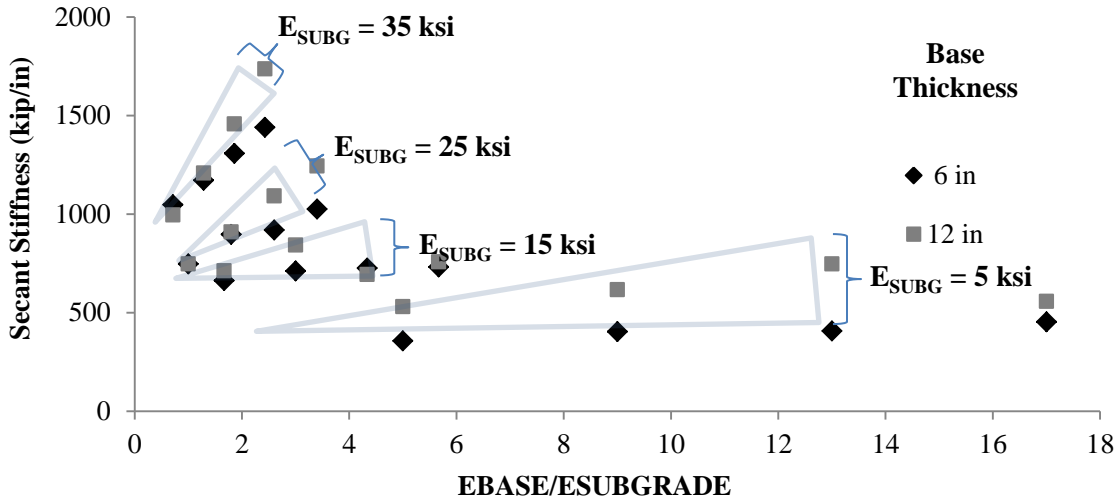
**Figure 3.9 – Tangent and Secant Stiffness and Moduli for a 6-in. base,  $E_{BASE} = 45$  ksi and Varying Subgrade Moduli.**

Figure 3.10a shows the secant stiffness against base-to-subgrade modulus ratio ( $E_{BASE}/E_{SUBG}$ ) for 6 and 12 in. thick base layers. The secant stiffness increases as the base and subgrade moduli increase. The secant stiffness also increases with base thickness. However, the stiffness growth rate is greater as the subgrade becomes stiffer. The secant stiffness does not seem to be considerably affected by the base modulus when the 6 in. base layer is laid on weak subgrades, yet for the 12 in. thick base the secant stiffness increases with higher base moduli, but oddly decreases at the largest  $E_{BASE}/E_{SUBG}$  ratio. This trend is currently under study as other parameters may be involved in the pavement response.

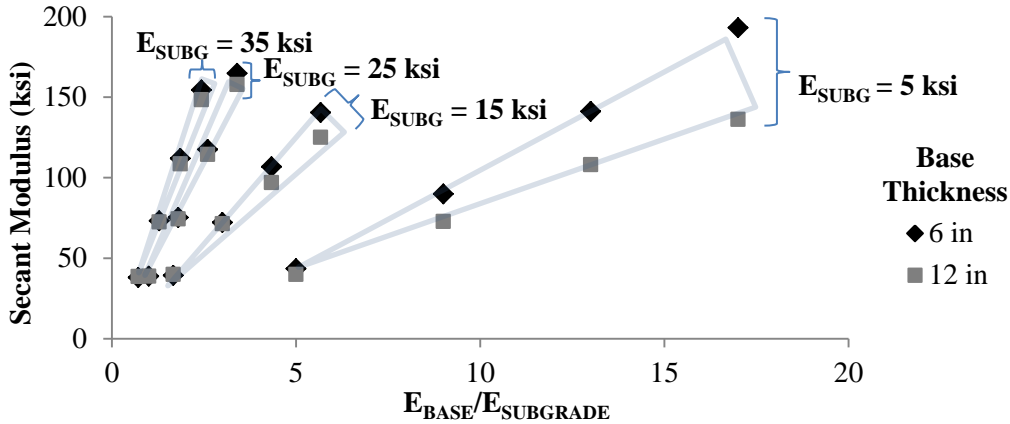
Figure 3.10b shows the secant modulus against base-to-subgrade modulus ratio ( $E_{BASE}/E_{SUBG}$ ) for 6 and 12 in. thick base layers. Similar to the stiffness, the secant modulus increases as the base modulus increases. The growth rate in modulus is greater as the subgrade becomes stiffer. Base thickness does not seem to affect the secant moduli when the base is laid on top of stiffer subgrades. However, the secant modulus increases more intensely on the 6 in. thick base than the 12 in. thick base as  $E_{BASE}/E_{SUBG}$  increases. This trend differs markedly from that one obtained for the secant stiffness. Additional studies are currently being conducted to determine the causes of this trend. The complexity of this problem hinders a simple interpretation since multiple variables are involved in the pavement response such as the roller's contact area and the dynamic nature of the analysis.

To show the effect of subgrade on the roller response of two-layer systems, a ratio was obtained between the secant modulus of the two-layer system ( $M_S$ ), i.e. the 6 and 12-in.-base pavements, to the secant modulus of its respective subgrade modeled as a single layer system ( $M_{S-SUBG}$ ). Figure 3.10c shows this  $M_S/M_{S-SUBG}$  ratio against base-to-subgrade modulus ratio ( $E_{BASE}/E_{SUBG}$ ) for 6 and 12 in. thick base layers. The ratio  $M_S/M_{S-SUBG}$  increases as  $E_{BASE}/E_{SUBG}$  increases indicating that the base has less impact on the secant modulus when laid on top of weak subgrades.

(a) Secant Stiffness



(b) Secant Modulus



(c) Ratio of Secant Moduli

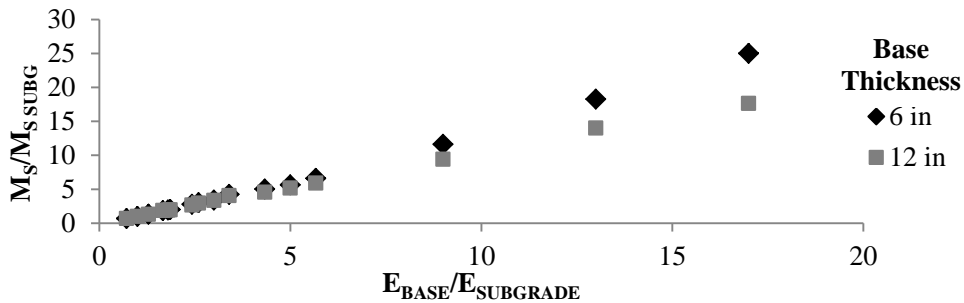
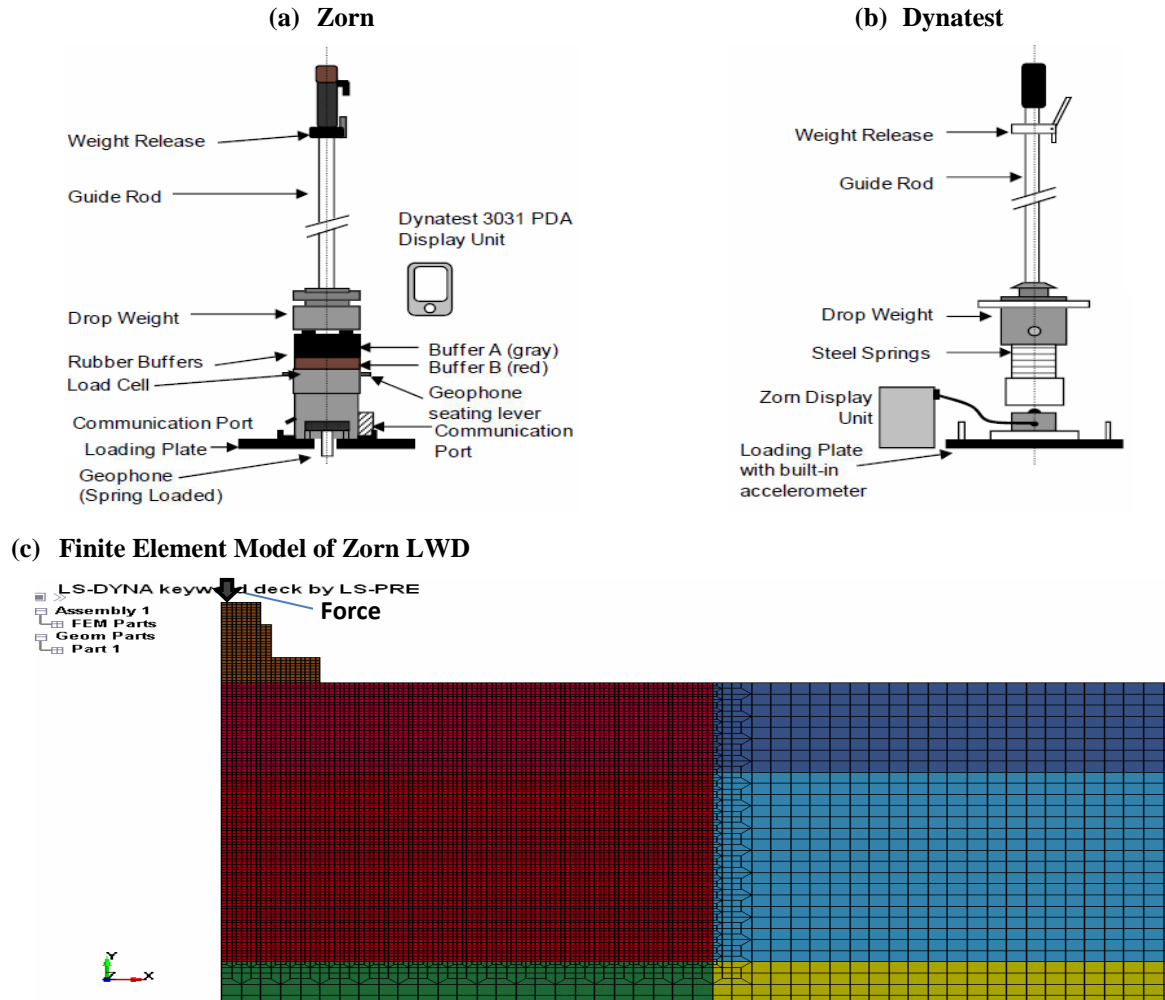


Figure 3.10 – Roller Stiffness Parameters as a Function of Base to Subgrade Modulus Ratio

**Finite Element Modeling of Light Weight Deflectometer (LWD)**

An axisymmetric dynamic linear elastic FE model was also developed using LS-DYNA to model the Light Weight Deflectometer (LWD) testing on top of a two-layer system consisting of a base layer and subgrade, using the same combination of properties shown in Table 3.1. The FE modeling of the LWD testing considered an automatic 2-D surface-to-surface contact model to assess the soil-plate interaction with the layered soil. The model used 0.2 in. square elements in the region directly under the LWD with a

mesh transition occurring at 20 in. depth to 0.8 in. square elements to optimize the computational speed. A total of 30,200 elements were used. The LWD plate was modeled using quad elements and impact force was applied at the top of the plate, as shown in Figure 3.11. The soil was modeled as 160 in. wide and 80 in. in depth. Both base and subgrade materials were modeled linearly elastic. The steel plate was modeled using a linear elastic model rather than rigid. The LWD impact was modeled using a 1500 lb force with pulse duration of 17 msec. Both Zorn and Dynatest LWDs were modeled. For the sake of brevity, only the Zorn's responses are provided in this report.



**Figure 3.11 – Schematic Views of LWD Devices and Finite Element Model of Zorn LWD**

A parametric study of the LWD impact response on the 32 cases of two-layered pavement structures consisting of a base course and subgrade with combination of properties shown in Table 3.1 was carried out. Pressure and displacement contours were generated for every 1 msec time interval. Time histories of responses were measured underneath the center of the plate and along the soil surface. With this information, profiles of vertical deflection, stress and strain were calculated during the plate impact to calculate the depth of influence the loading has on the pavement structure.

**Depth of Influence**

The profile of the peak vertical stress due to the LWD impact on a section with a 6 in. thick base above subgrade is shown in Figure 3.12. Figure 3.12a shows the stress profiles for a base layer with a modulus

of 45 ksi and subgrades with different moduli. Figure 3.12b shows the peak vertical stress profiles for the same base layer thickness with a subgrade modulus of 15 ksi but varying base moduli. A single layer system consisting of subgrade only is also included in Figure 3.12b. The vertical stress diminishes with a similar rate for all sections, particularly after a depth of 18 in. This behavior was similar to the roller-induced stresses with some differences.

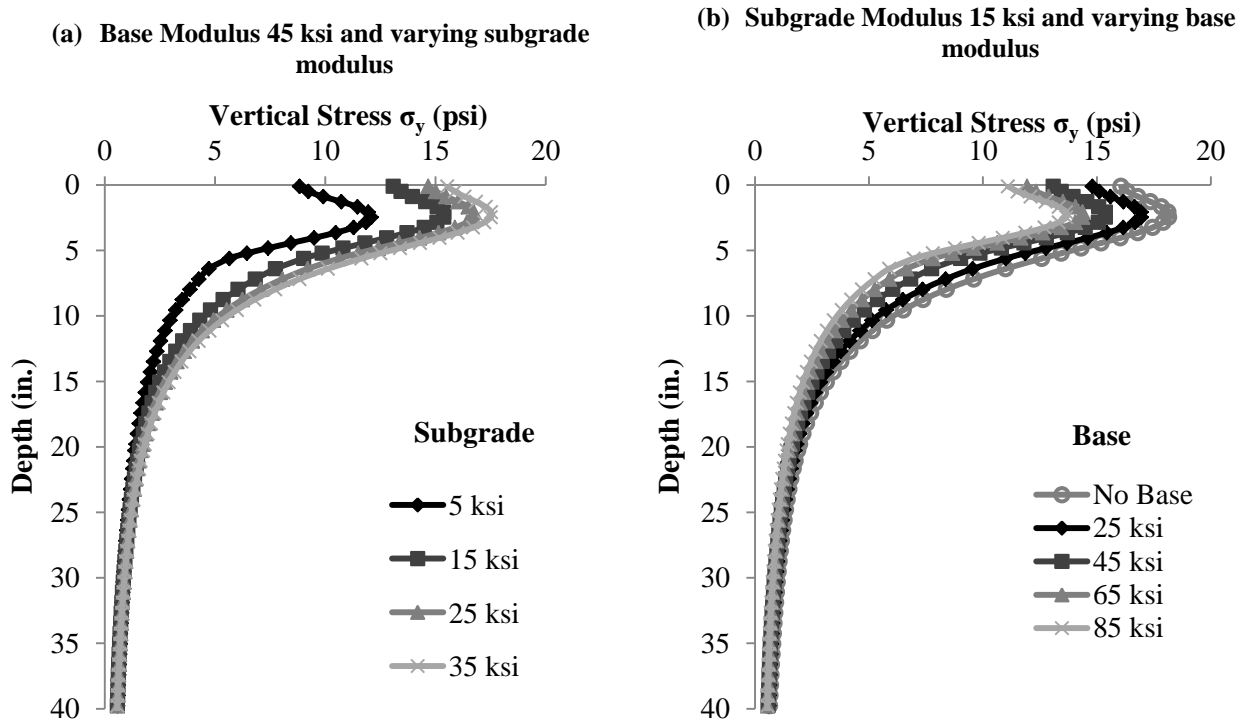


**Figure 3.12 – Vertical Stress Distributions of LWD Impact on a Section with a 6 in. Thick Base**

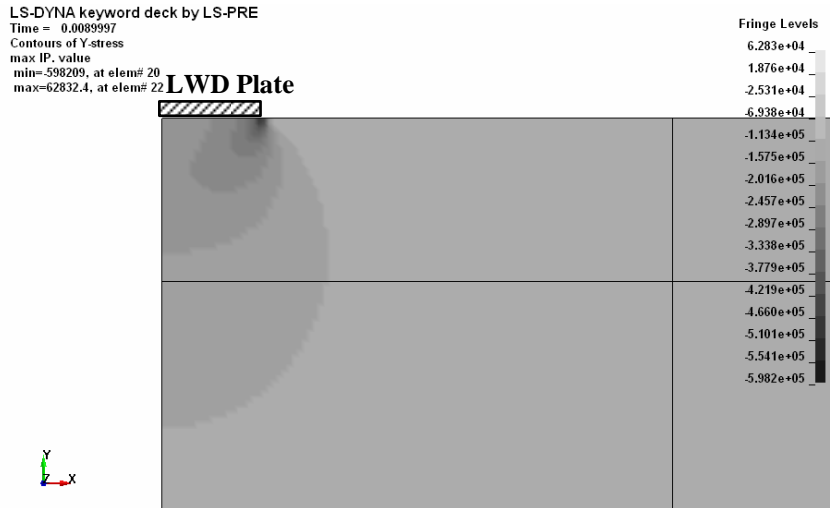
Though the depth of influence is calculated based on the peak surface vertical stress at the center of the plate, the maximum vertical stress occurs around the middle of the base layer. Moreover, maximum surface vertical stresses occur under the edge of the plate. Stresses from the edge of the plate propagate toward the center of the plate as shown in the stress contour plot provided in Figure 3.13a. A stress profile along the surface with respect to distance from the center of the LWD plate is provided in Figure 3.13b.

Profiles of peak vertical deformation are provided in Figure 3.14a for a 6 in. thick base layer with 45 ksi modulus and varying subgrade moduli, and Figure 3.14b for subgrade modulus of 15 ksi and varying base moduli. The one-layer system, i.e. subgrade only, is also included in Figure 3.14b. The vertical deflection increases as base modulus decreases at most until a depth of about 15 in. is reached. Vertical deformation increases even more for weaker subgrades through deeper depths, as shown in Figure 3.14a. The depth of influence in terms of stress and deformation was investigated for the cases studied. The depth of influence of soil was calculated using the base and subgrade responses in terms of stress and deflection. This depth was measured based on 10% and 5% of the magnitude of the peak surface responses.

Figure 3.15a shows the depth of influence in terms of vertical stress for a section with a 6 in. thick base for different subgrade moduli. The depth of influence for a 10% stress level decreases from 30 in. to 22 in. as subgrade modulus increases. When the stress level is further constrained to 5%, the depth of influence decreases from 48 in. to 33 in. as the subgrade modulus increases. As expected, the influence depths are shallower than the roller's depths.

The impact of base thickness on the influence depth is shown in Figure 3.15b for a stress level of 10% of the surface peak stress for sections with varying base moduli and subgrade modulus of 15 ksi. The influence depth is significantly affected by the base thickness, particularly as the base modulus increases. Base modulus does not impact significantly the depth of influence for the 6-in. thick base pavement, but the depth of influence decreases as base modulus increases to 12 in.

(a) Stress contour (Fringe levels in Pa)



(b) Stress profile along the soil surface

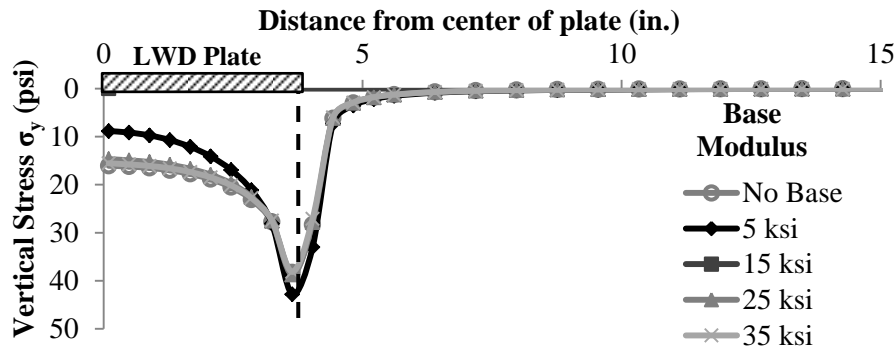


Figure 3.13 – Vertical Stress Contour Plots of LWD Impact under Different Layer Combinations

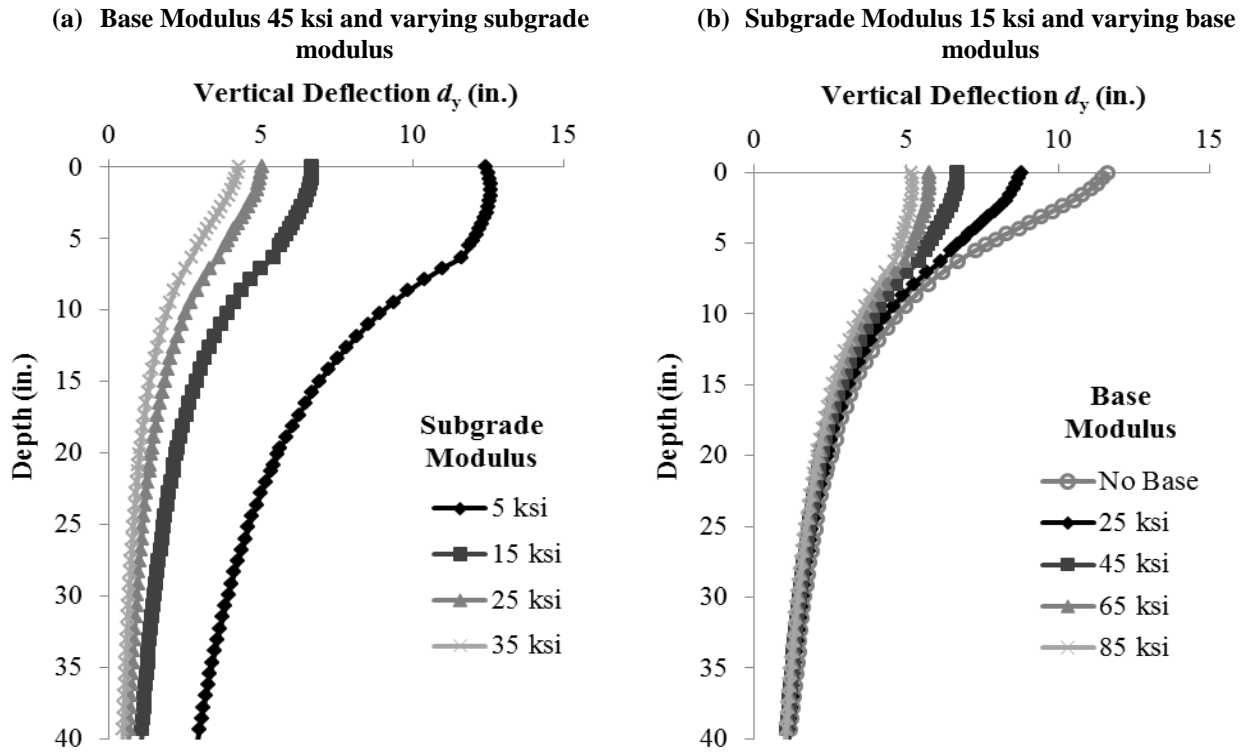


Figure 3.14 – Depth Profiles of Vertical Deformations for a Section with a 6 in. Thick Base

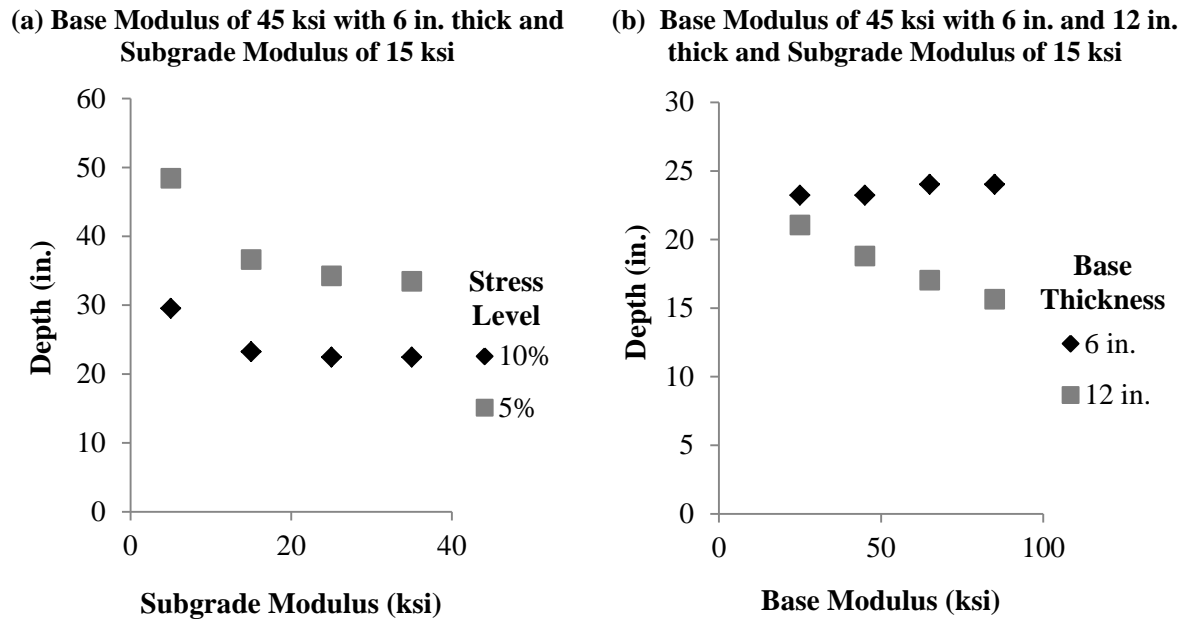


Figure 3.15 – Depth of Influence at a Stress Level of 10% of the Surface Peak Stress

The effects of variations in base and subgrade moduli were evaluated for all cases. Figure 3.16a shows the influence depth in terms of the vertical stress at a 10% peak vertical stress for all combinations of base and subgrade moduli, for a section with a base thickness of 6 in. The depth of influence remains fairly constant at around 23 in. as base and subgrade moduli increase. However, stresses penetrate deeper into

the soil when a weak subgrade of 5 ksi is present, increasing influence depth to a range of 28 in. to 33 in. depending on the base modulus. Comparing Figures 3.16a with 3.16b, the base thickness and base modulus contribute less significantly to the depth of influence. Once again, the depth of influence decreases significantly with base thickness when the base is laid on top of weak subgrade. Generally, the roller's depth of influence is about 10 in. deeper than LWD's depth of influence. In terms of vertical deflections, Figures 3.16c and 3.16d show that the depth of influence decreases significantly as subgrade modulus increases. Nonetheless, the depth of influence increases as the base modulus increases. This trend significantly increases in the stiffer subgrades. The base thickness had a minor effect on the influence depth. Similar to the roller's response, the depth of influence is lower when no base is present. This is due to the larger deformations occurring on the surface of the subgrade as compared to surface deformation of stiffer base layers present in two-layer systems, as shown in Figure 3.16b.

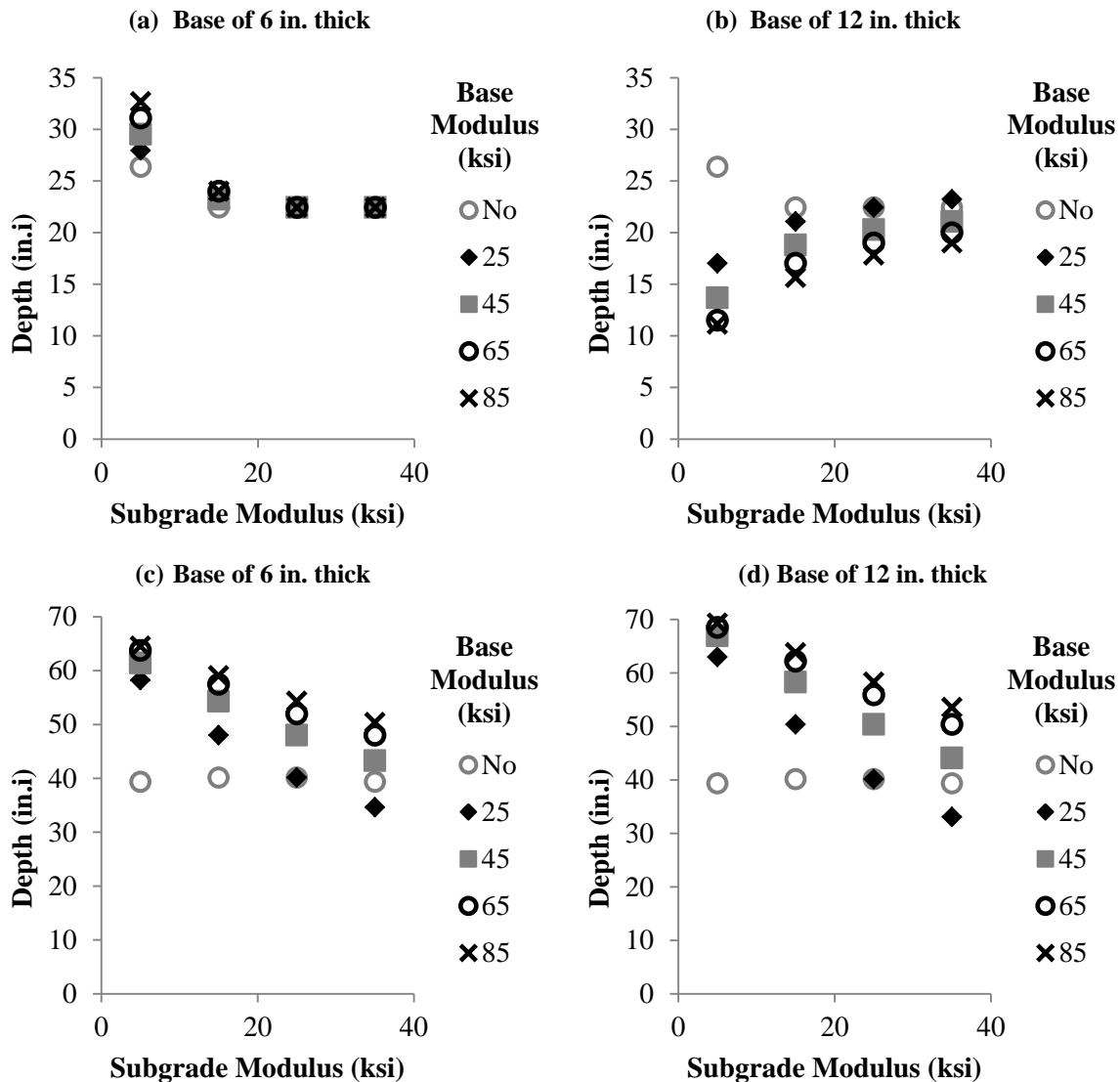


Figure 3.16 – Depth of Influence at a Level of 10% of the Surface Peak Stress for Deflection

### LWD Modulus

Surface deflection modulus,  $E_{LWD}$ , is calculated using Boussinesq's solution from

$$E_{LWD} = \frac{(1-\nu^2)\sigma_0 af}{d_0}, \quad (3.2)$$

where  $\nu$  is Poisson's ratio,  $\sigma_0$  is the uniformly distributed applied stress under the plate,  $a$  is the radius of the plate,  $d_0$  is measured settlement of soil at the center of plate, and  $f$  is the shape factor depending on stress distribution, assumed as  $\pi/2$  for a rigid type of plate that creates an inverse parabolic distribution shape (clay, subgrade and lime stabilized subgrade materials), 2 for flexible plates that creates a uniform distribution shape suitable (granular base underlain by clay subgrade), and  $8/3$  also for flexible plates that creates a parabolic shape (cohesionless sand) (Terzaghi and Peck, 1967; Fang, 1991). In this study, a value of  $\pi/2$  was assumed for the shape factor, suiting the inverse parabolic distribution shown in Figure 3.13.

Figure 3.17 shows the surface deflection modulus obtained from the finite element analysis for all cases. The modulus increases with the increase in the subgrade modulus and the base modulus. Comparing Figure 3.17a with 3.17b, the base thickness impacts  $E_{LWD}$ , especially at lower subgrade moduli. Figure 3.17c shows surface deflection modulus with respect to the base-to-subgrade modulus ratio.

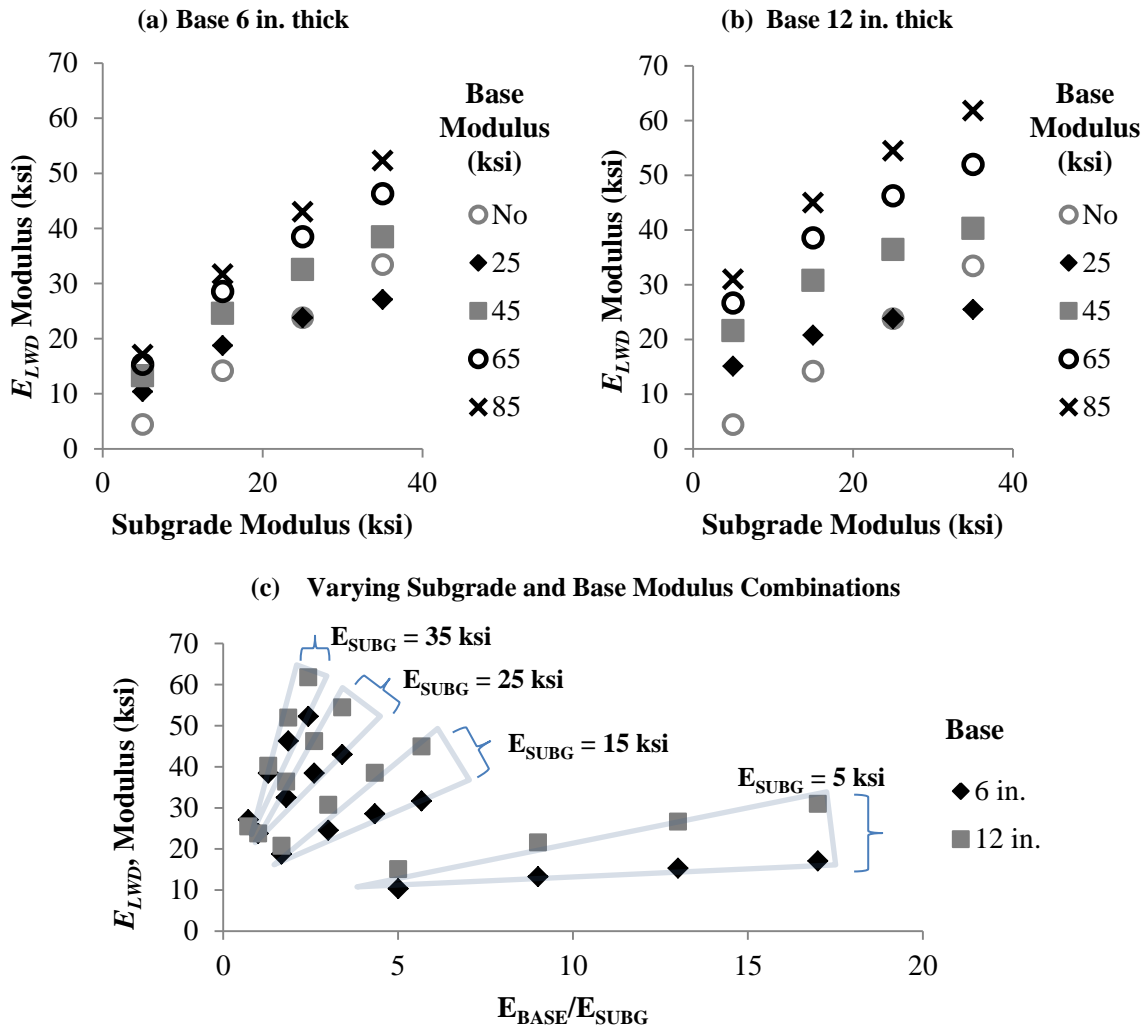
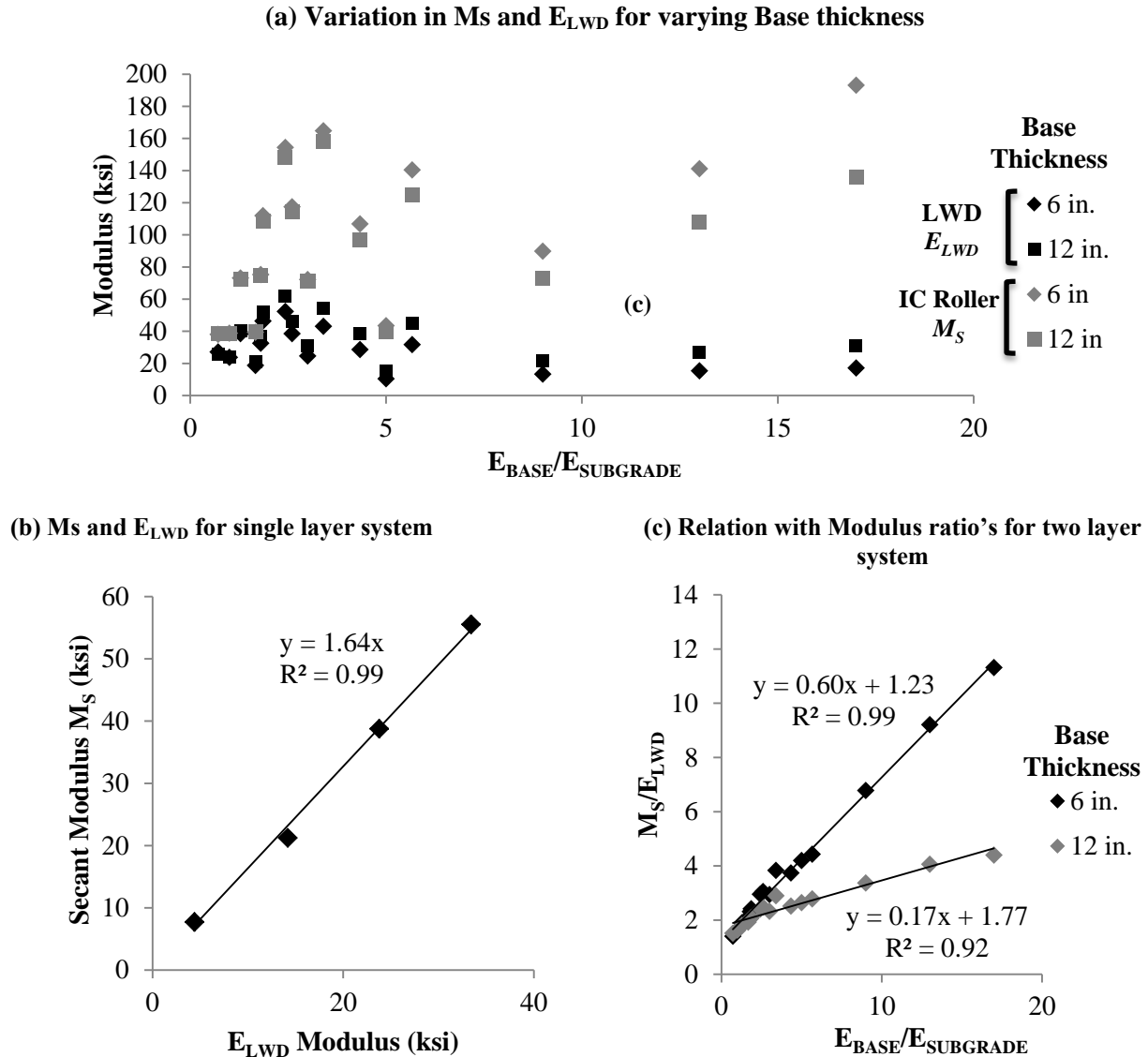


Figure 3.17 – Surface Deflection Moduli for Different Layer Combinations

The comparison of surface deflection modulus,  $E_{LWD}$ , to secant modulus,  $M_S$ , as obtained from the IC roller modeling is shown in Figure 3.18a. Since the trends are similar, a relationship was suggested by establishing an  $M_S$ -to- $E_{LWD}$  ratio with respect to base-to-subgrade modulus ratio as shown in Figure 3.18b.



**Figure 3.18 – Relationship of  $M_S$  and  $E_{LWD}$  under Different Layer Combinations**

Secant modulus can be estimated from the surface deflection modulus for a known base thickness from the following relationships:

$$M_S = \alpha E_{LWD}, \quad (3.3)$$

where  $\alpha = 1.64$  for subgrade only ( $R^2=0.996$ )

$\alpha = 0.60E_{BASE}/E_{SUBG} + 1.23$  for 6 in. base ( $R^2=0.994$ )

$\alpha = 0.17E_{BASE}/E_{SUBG} + 1.77$  for 12 in. base ( $R^2=0.920$ ).

A parametric study was carried out using 3-D finite element analysis to estimate the depth of influence based on the different type of responses, i.e. stress, strain and deflection, due to roller compaction. A one or two-layer pavement system consisting of a base course and subgrade was considered. Base and subgrade were modeled as linear elastic materials. Roller compaction model responses were compared to those of the LWD testing. Among the findings obtained from the analysis, the following stand out:

- Depth of influence in terms of stress due to roller compaction increases as the base becomes stiffer, while the contribution of subgrade modulus to the depth of influence is less significant. The influence depth for roller compaction based on 10% of the surface peak stress varies from 19 in. to 38 in. for two-layer systems; however, it can go up to 50 in. for weak subgrades as single layers. Base thickness impact on depth of influence is small except for a weak subgrade (5 ksi). The depth of influence for the LWD shows trends similar to the roller compaction with influence depths of about 12 in. shallower than the roller.
- Vertical compressive stresses decay slowly beyond a depth corresponding to 10% of surface stress. Thus, the 5% level of stress due to roller compaction occurs deeper than 100 in. which happens to be the model's depth.
- Depth of influence in terms of displacement using the surface vertical deformation at the center of the load occurs at depths of 73 in. to 85 in. for roller compaction. Base and subgrade moduli have a slight impact on the influence depth. The base thickness has no significant impact on influence depth. In single layer systems, the depth of influence decreases to 60 in. for a weak subgrade due to their larger surface deflection. The LWD modeling shows that the influence depth varies with the subgrade and base moduli, ranging from 35 in. to 65 in. in depth for two-layer systems, and is about 40 in. in depth for single layer systems. Trends between the roller and LWD are not comparable, at least for the two-layer systems.
- The secant and tangent stiffnesses and moduli are determined using hysteresis loops. Little difference is observed in magnitudes of the secant to tangent stiffness, and secant and tangent moduli. Thus, secant stiffness and modulus are evaluated with respect to the ratio of base-to-subgrade moduli.
- Both secant stiffness and secant modulus increase as the base modulus increases. In addition, base thickness affects the secant stiffness and secant modulus on base layers laid on weak subgrades. While the secant stiffness increases with the higher base thickness, the secant modulus increases with the lower base thickness. These responses are currently subject to further scrutiny since the case study is rather complex as it involves other variables.
- The LWD surface deflection modulus has a similar trend to the roller's compaction secant modulus. A linear regression relationship is developed to relate the  $E_{LWD}$  to secant modulus. No relationship could be established that relates  $E_{LWD}$  to the secant stiffness  $k_s$ .

## Chapter 4

# Experimental Study

### Introduction

The research team interacted with the Fort Worth District to identify two field demonstration sites. The field studies for the first site consisted of evaluating subgrade, base and lime-treated subgrade along SH 267 near Dublin, TX. In addition, the subgrade of a site north of Fort Worth as part of the reconstruction of IH 35W was evaluated. Appendices A and B present the comprehensive field and laboratory results and analyses of the roller and spot test data collected from these sites. This chapter gives a brief description of the project locations and the activities carried out to assess the compaction quality of these materials.

### Project Location

The first field evaluation was carried out at a construction site near Dublin at three locations as reflected in Figure 4.1a. Figures 4.2 depict the test sections. The first location was dedicated to evaluating the placement of a subgrade layer. The focus of the second location was the placement of a base layer, while the third section consisted of the placement of a lime-stabilized layer. The second field evaluation activity was carried out at a site in Tarrant County north of Fort Worth, Texas. Only the subgrade layer was evaluated in that study. This project was part of the reconstruction of the existing lanes and adding toll lanes along IH 35W (see Figure 4.1b). The project site was a part of the direct connection for IH 35W to US 81/287. Figure 4.3 depicts the embankment and subgrade layers during construction.

### Laboratory Test Results

The index properties of the SH 267 and IH 35W geomaterials are summarized in Table 4.1, and their gradation curves are presented in Figure 4.4. Two slightly different geomaterials (namely Subgrade A and Subgrade B) were used in SH 267. These subgrades were classified as low-plasticity clay as per Unified Soil Classification System (USCS), while the subgrade at IH 35W was a high-plasticity clay. The base was classified as well-graded gravel. The treated layer was primarily constructed with Subgrade A with nominally 6% lime. The optimum moisture contents and maximum dry unit weights of the geomaterials are also reported in Table 4.1. Based on previous tests of the IH 35W materials, the reported OMC was 16.3%. As such, the target OMC during field tests was 16.3% and not the 21.2% obtained from the actual material sampled.

Since the IC technology and modulus-based devices are based on measuring the stiffness of the layers, the resilient modulus (MR) and free-free resonant column (FFRC) tests were performed on laboratory specimens prepared at the OMC, dry of OMC and wet of OMC as summarized in Table 4.2. Figure 4.5 illustrates the variations of the laboratory FFRC moduli and representative MR values with moisture content. The two measured moduli decrease drastically when the specimens are prepared wet of OMC.



(a) SH 267 Site



(b) IH 35W Site

**Figure 4.1 – Locations of Field Evaluation Sites**

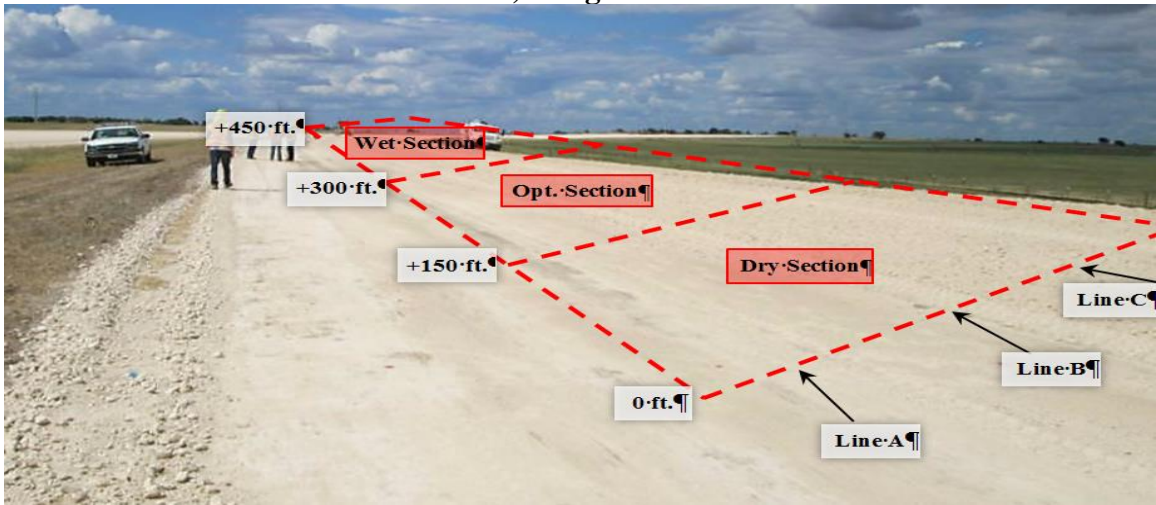
**Table 4.1 - Index Properties of Geomaterials**

| Site   | Soil Type       | Gradation % |             |           |       | USCS Class. | Specific Gravity | Atterberg Limits |    |    | Moisture/Density     |                          |
|--------|-----------------|-------------|-------------|-----------|-------|-------------|------------------|------------------|----|----|----------------------|--------------------------|
|        |                 | Gravel      | Coarse Sand | Fine Sand | Fines |             |                  | LL               | PL | PI | OMC <sup>*</sup> , % | MDUW <sup>**</sup> , pcf |
| SH 267 | Subgrade A      | 0           | 4.0         | 10.0      | 86.0  | CL          | 2.75             | 41               | 14 | 27 | 16.7                 | 107                      |
|        | Subgrade B      | 0           | 5.0         | 11.8      | 83.2  | CL          | 2.75             | 36               | 13 | 23 | 16.9                 | 109                      |
|        | Lime-Treated SG | 0           | 4.0         | 10.0      | 86.0  | CL          | 2.75             | 35               | 26 | 9  | 18.7                 | 95                       |
|        | Base            | 51.8        | 29.0        | 15.0      | 5.0   | GW          | 2.68             | 28               | 16 | 12 | 10.4                 | 120                      |
| IH 35W | Subgrade        | 0           | 8.0         | 2.5       | 89.4  | CH          | 2.76             | 55               | 15 | 40 | 21.2                 | 101.1                    |

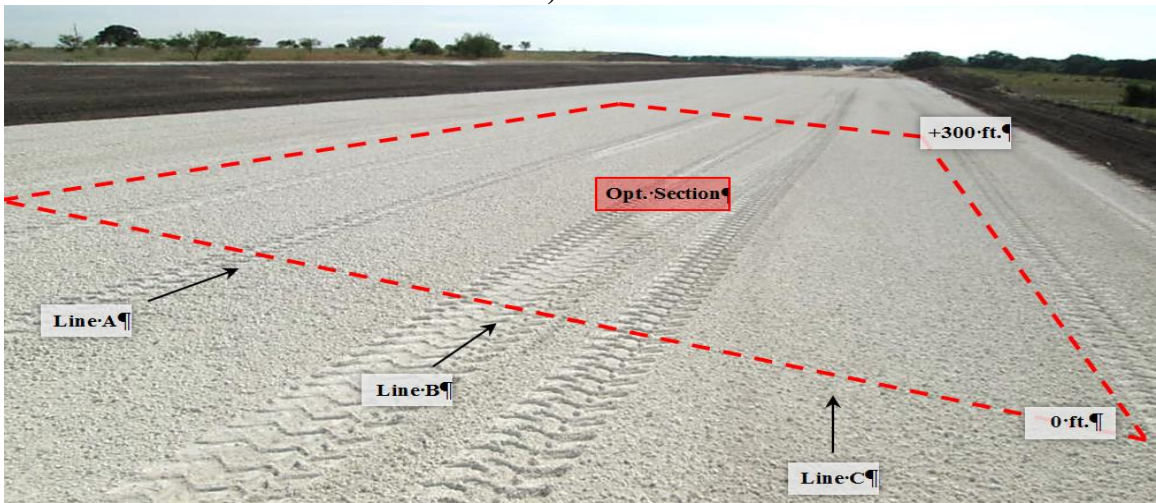
\*OMC = Optimum Moisture Content, \*\*MDUW = Maximum Dry Unit Weight



a) Subgrade



b) Base



c) Lime-Treated Subgrade

Figure 4.2 – Illustration of Test Sections in SH 267 Site

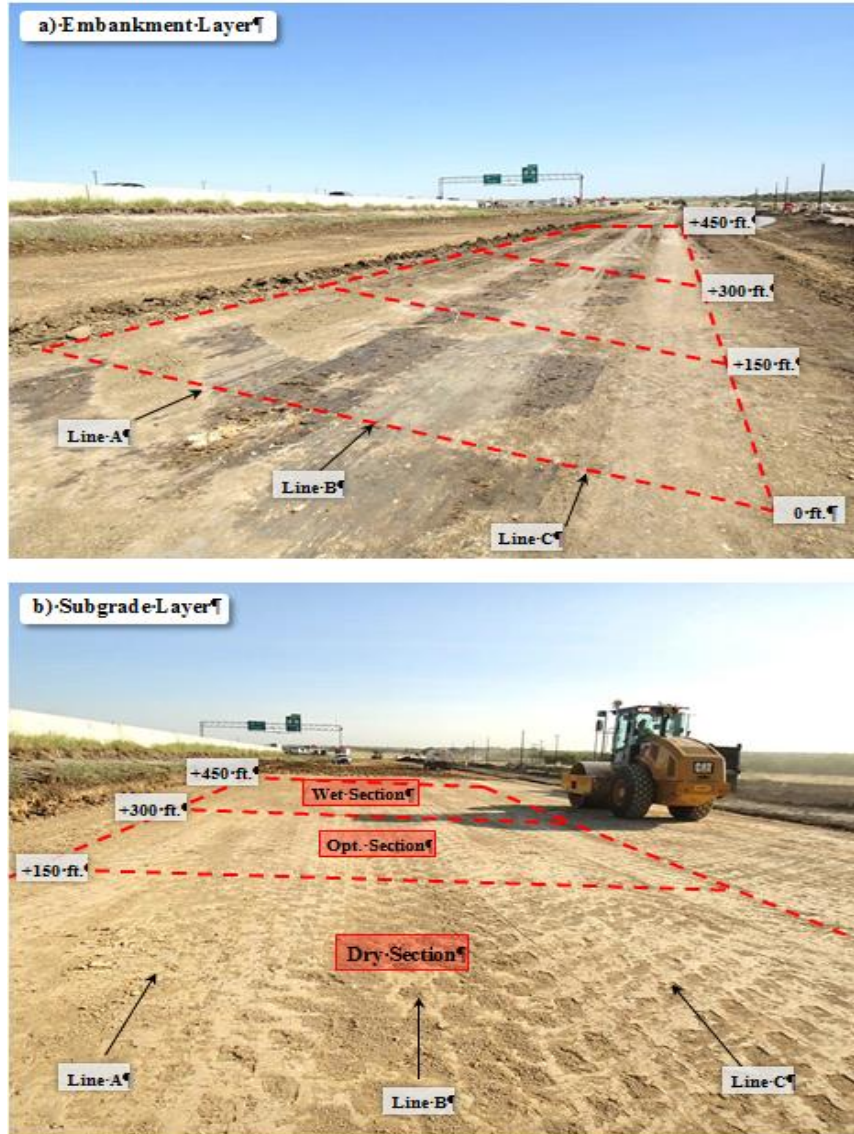


Figure 4.3 – Illustration of Test Sections along IH 35W Site

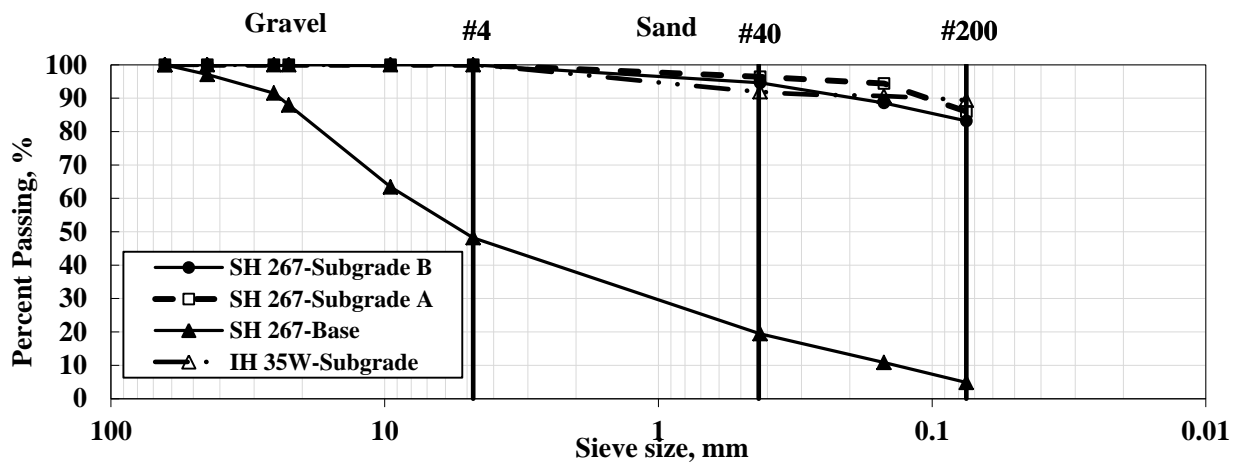
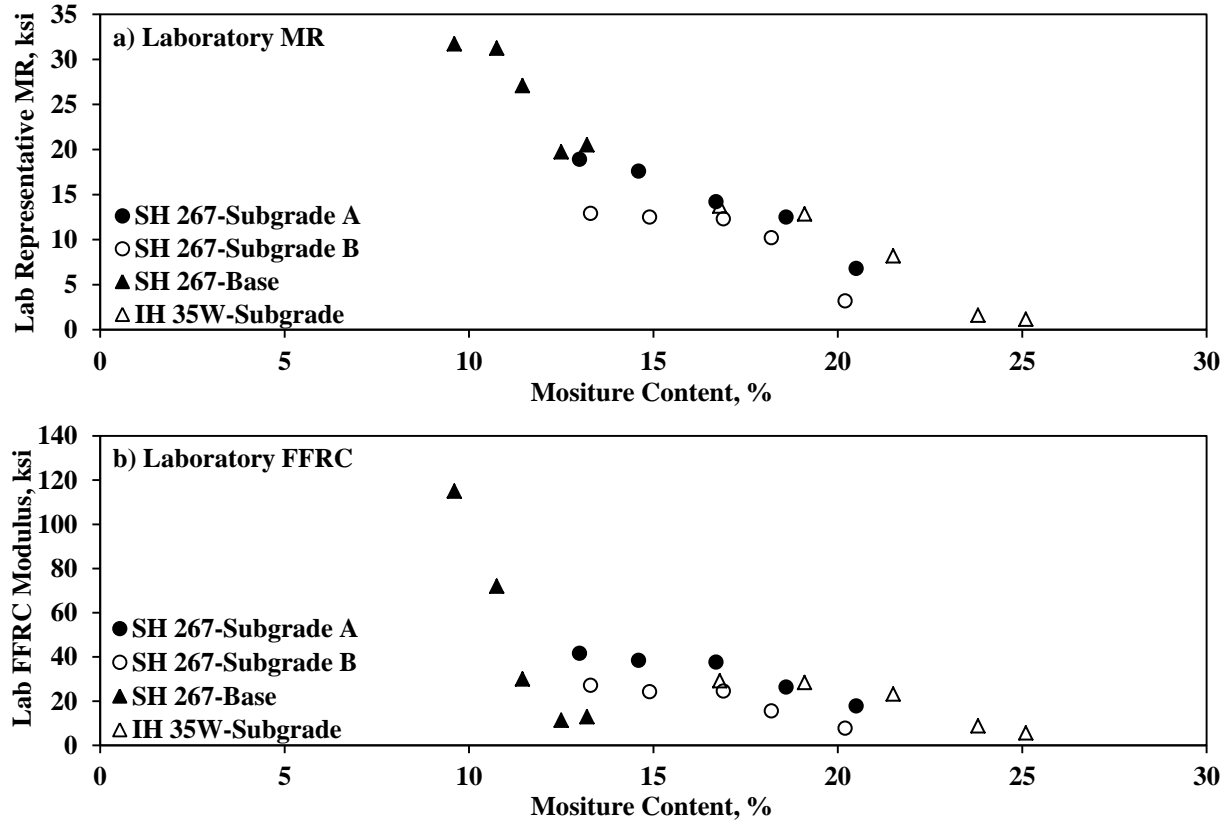


Figure 4.4 – Gradation Curves of Geomaterials

**Table 4.2 - Laboratory Results of MR and FFRC Tests of Geomaterials\***

| Site            | Type       | Target Moisture Content | Actual Moisture Content, % | Dry Density, pcf | FFRC Modulus, ksi | Resilient Modulus, ksi |
|-----------------|------------|-------------------------|----------------------------|------------------|-------------------|------------------------|
| SH 267          | Subgrade A | OMC-2                   | 13.0                       | 104.8            | 42                | 19                     |
|                 |            | OMC-1                   | 14.6                       | 106.3            | 38                | 18                     |
|                 |            | OMC                     | 16.7                       | 108.6            | 38                | 14                     |
|                 |            | OMC+1                   | 18.6                       | 105.7            | 26                | 13                     |
|                 |            | OMC+2                   | 20.5                       | 103.5            | 18                | 7                      |
|                 | Subgrade B | OMC-2                   | 13.3                       | 105.5            | 27                | 13                     |
|                 |            | OMC-1                   | 14.9                       | 107.0            | 24                | 13                     |
|                 |            | OMC                     | 16.9                       | 108.2            | 24                | 12                     |
|                 |            | OMC+1                   | 18.2                       | 106.4            | 16                | 10                     |
|                 |            | OMC+2                   | 20.2                       | 105.2            | 8                 | 3                      |
|                 | Base       | OMC-2                   | 9.6                        | 122.0            | 115               | 32                     |
|                 |            | OMC-1                   | 10.8                       | 123.4            | 72                | 32                     |
|                 |            | OMC                     | 11.5                       | 126.0            | 30                | 27                     |
|                 |            | OMC+1                   | 12.5                       | 125.1            | 11                | 20                     |
| Lime-Treated SG | OMC+2      | 13.2                    | 124.5                      | 13               | 21                |                        |
| IH 35W          | Subgrade   | OMC                     | 18.7                       | 94.7             | 30                | 27                     |
|                 |            | OMC-2                   | 16.8                       | 100.0            | 29                | 14                     |
|                 |            | OMC-1                   | 19.1                       | 101.9            | 28                | 13                     |
|                 |            | OMC                     | 21.5                       | 102.0            | 23                | 8                      |
|                 |            | OMC+1                   | 23.8                       | 101.0            | 9                 | 2                      |
| OMC+2           | 25.1       | 99.3                    | 6                          | 1                |                   |                        |

\* for more detail please see Appendices A and B



**Figure 4.5 – Variation of Laboratory MR and FFRC Modulus with Moisture Content**

## Test Program

Similar procedures were implemented for most sections. The procedure consisted of constructing and monitoring three experimental test beds at three different nominal moisture contents of 80% OMC to 1.2 OMC where OMC denotes the optimum moisture content. The goals of those activities were (1) to establish the variability of different test methods under field condition, and (2) to establish the effectiveness of using test strips for developing target values. The following activities were carried out at each test bed:

- Performed modulus-based nondestructive (NDT) tests with the LWD, DCP, portable seismic property analyzer (PSPA) and IC roller on the underlying layer to establish the variability of the foundation layer.
- Sampled materials for comparing gradations and moisture contents before compaction.
- Monitored the changes in density, modulus and IC roller values with the number of passes during construction.
- Tested a number of points with each NDT device, NDG and IC roller shortly after compaction.
- Test same points 16 to 24 hours after compaction with the NDT devices, NDG and IC roller.

When possible, similar activities were carried out on a one day of production at the site where the procedures were less controlled.

## Field Studies

Slightly different test programs were implemented at the different locations as discussed below.

**SH 267 Subgrade:** The field testing was carried out along three side-by-side sections, as illustrated in Figure 4.6. The embankment at the site had been prepared before the research team arrived at the site. The first activity was to map the embankment before the subgrade layer was placed using an IC roller. A reasonably old smooth drum roller that was retrofitted with a Trimble CCSFlex IC retrofit kit was used at this site. The roller operator was trained and competent. High accuracy survey grade GPS coordinates were collected for all spot test points. An LWD, a PSPA and an NDG were used to test the embankment layer of the three sections along Rows A and C.

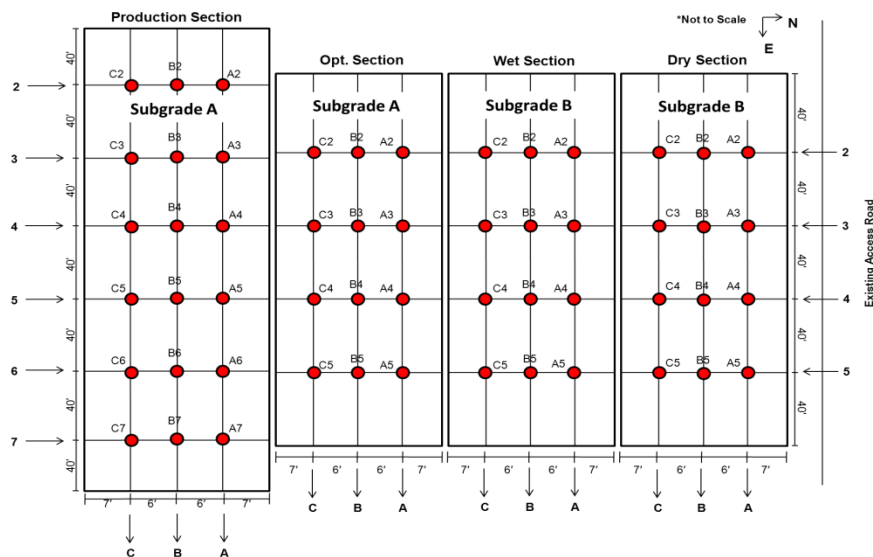


**Figure 4.6 – Test Locations on Embankment and Subgrade Layer of SH 267 Site**

A 12-in.-thick subgrade layer was then placed on top of each of the three sections. The first section was placed with Subgrade B dry of OMC, the second section was placed with Subgrade B wet of OMC, and the third section was placed with Subgrade A close to OMC.

Both a sheep foot roller and a vibratory IC roller were utilized in this project to compact the materials. One pass of the IC roller was used after every two passes of the sheep foot roller to measure the layer responses. At that time, spot tests with the LWD, PSPA and NDG were carried out at five points. A DCP was also used after the subgrade was compacted at all points along Rows A, B and C (see Figure 4.6). The same exercise was repeated after 16 to 24 hours of compaction. In addition, soil samples were extracted from the compacted subgrade layer at most points to estimate their oven-dried moisture contents.

A fourth section was selected as a "Production" section to evaluate the routine compaction process performed by the Contractor. The spot tests were carried out after the completion of the compaction and mapping with the IC roller.

**SH 267 Base:** As illustrated in Figure 4.7, the first section was placed at dry of OMC, the second section close to OMC, and the third section at wet of OMC. Prior to the placement of the base layer, the support condition of the subgrade was mapped with the IC roller and NDT devices. The 10-in.-thick base layer was compacted using the IC roller. The testing pattern was maintained the same as the subgrade.

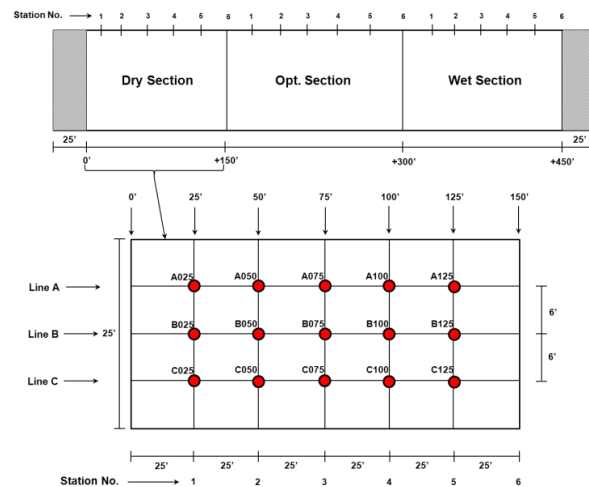


**Figure 4.7 – Test Locations on Base Layer of SH 267 Project**

**SH 267 Lime-Treated Subgrade:** A 300-ft-long and 50-ft-wide test section was selected to evaluate a 10-in.thick lime-treated subgrade soil (see Figure 4.8). Six percent (by weight) of quick lime was mixed with the compacted subgrade layer and sealed with a pass of a pneumatic roller. The sealed layer was milled after 48 hrs, mixed with water, and compacted with the combination of a pneumatic and the IC roller. The same test devices and testing routines were adopted and used for the compacted lime-treated subgrade layer.

**IH 35W Subgrade:** An 8-in. thick subgrade layer was placed, leveled and compacted at three sections. As illustrated in Figure 4.9, field testing was carried out on three sections. Each section was about 150 ft long and 25 ft wide. The first section was nominally placed at dry of OMC, the second section at OMC, and the third section at wet of OMC. The IC roller used on this project was new and equipped with the machine drive power (MDP) system. A Trimble CCSFlex unit was also retrofitted to the roller for simultaneous measurements of the MDP and CMV values for part of the project. The prepared embankment layer was tested before and after the placement of the subgrade layer following a protocol similar to the SH 267 subgrade sections.

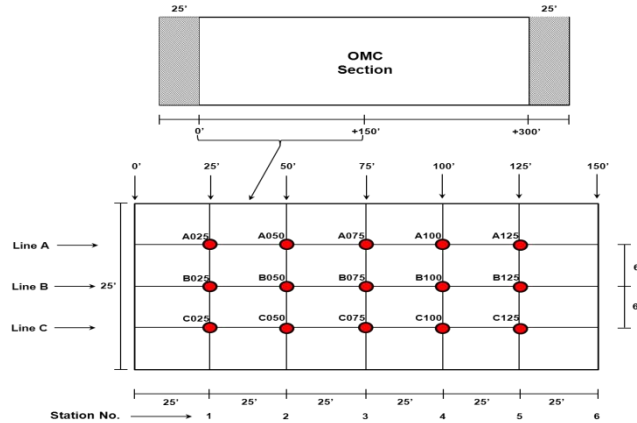


**Figure 4.8 – Test Locations on Lime-Treated Subgrade of SH 267 Project**

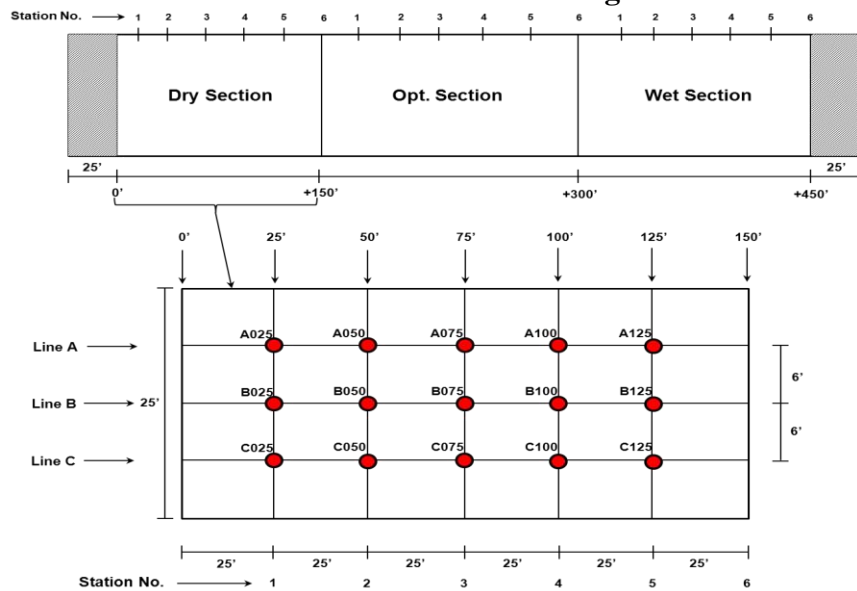


**Figure 4.9 – Test Locations on Embankment and Subgrade along IH 35W Section**

**Typical Results**

The subgrade layer from the SH 267 is used as an example. The results from other sections are provided in detail in the appendices. The variations of the moisture contents and dry densities of the embankment measured with the NDG before the placement of subgrade are depicted in Figure 4.10. The overall average moisture content of the embankment from the NDG was 9.4%, which was about 7% less than the OMC from the standard Proctor tests. The average dry density was 115.8 pcf. The embankment passed the density specification limit of 95% of MDD.

The average NDG moisture contents and dry densities (average of the three readings from lines A, B and C) measured on top of the subgrade are summarized in Figure 4.11 for all sections. The first and last rows of the compacted subgrade sections were not considered in the analysis to eliminate the effects of the construction boundaries. The average NDG moisture content of the dry section was 12.8% (3.9% dry of OMC), the wet section was 18.3% (1.6% wet of OMC) and the optimum section was 17.6% (0.7% wet of OMC). Based on the NDG results, moisture contents of the test sections were close to their nominal values (dry of OMC, wet of OMC and close to OMC).

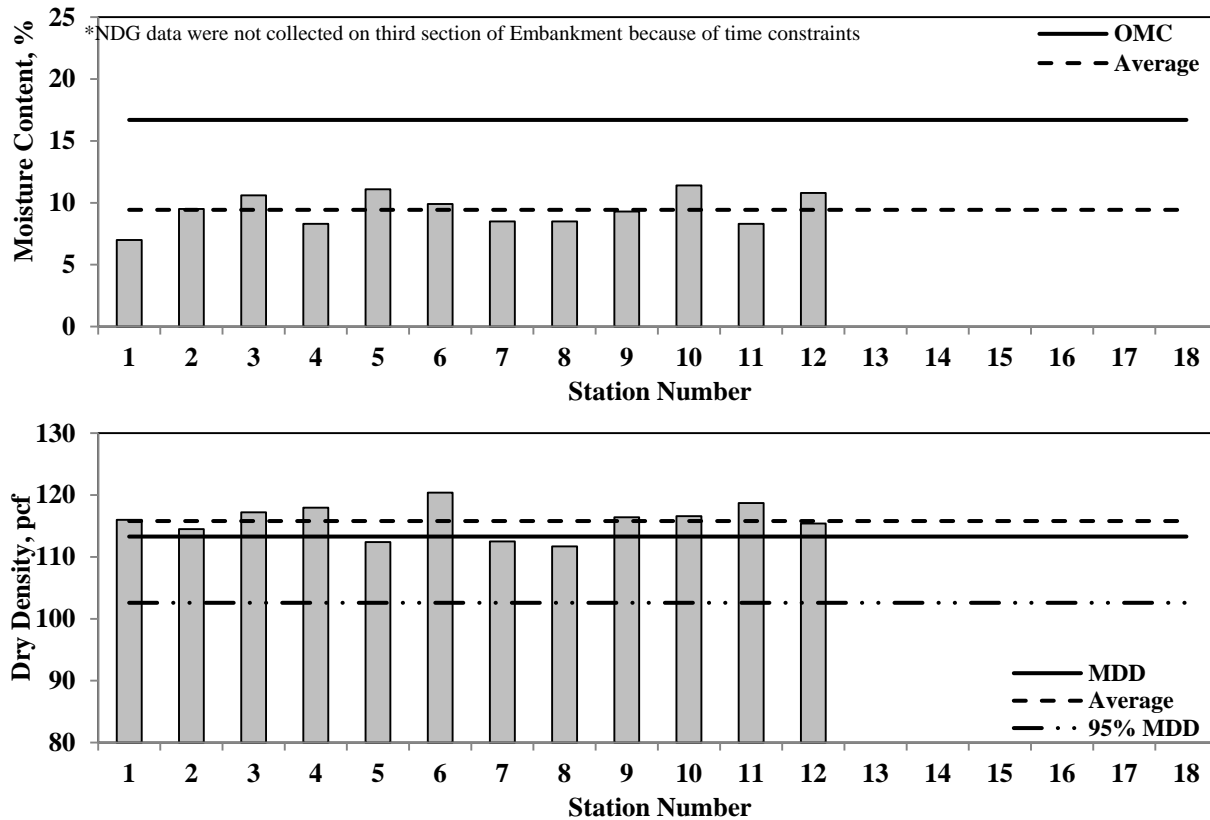


**Figure 4.10 – Spatial Variations of NDG Moisture Contents and Dry Densities of Embankment**

Dry densities measured by the NDG immediately after compaction of the subgrade layer are summarized in Figure 4.11. Almost all stations from the three sections passed the specification limit of 95% of MDD.

Soil samples were extracted to determine the oven moisture contents at the NDG test spots. Table 4.3 summarizes the average NDG and oven-dry moisture contents for all sections. The oven-dry moisture contents were about 2% less than those measured with the NDG.

The average NDG moisture contents and dry densities after different passes of the IC roller are summarized in Figure 4.12. Except for the wet section, the dry densities increased with more passes of the rollers. On the other hand, the moisture contents of the compacted layers decreased with passes of the roller. The rates of changes in dry density and moisture content are minimal for the wet section and more evident for the dry section. The gradient of density and moisture changes for the optimum section is intermediate.

An LWD and a PSPA were used on top of the embankment layer along Lines A and C shortly before the placement of the subgrade layer. The average moduli from lines A and C for each station are illustrated in Figure 4.13. The LWD modulus was  $15 \pm 8$  ksi (Figure 4.13a), and the average PSPA modulus was  $46 \pm 24$  ksi (Figure 4.13b).

Table 4.4 and Figure 4.14 contain the results of the measurements with the PSPA, LWD and DCP after the compaction of the subgrade layer. The variations of LWD and PSPA moduli between passes of IC roller during compaction of the subgrade layer are depicted in Figure 4.15. The modulus of the compacted layer increases for the most part with more passes of the roller.

**Table 4.3 - Comparisons of Average Moisture Contents of Subgrade with Different Devices**

| Section (Nominal MC, %) | Average Measured Moisture Content, % |      | Target Moisture Content, % |
|-------------------------|--------------------------------------|------|----------------------------|
|                         | NDG                                  | Oven |                            |
| Dry Section (OMC-2%)    | 12.8                                 | 11.4 | 14.7                       |
| Opt. Section (OMC)      | 17.6                                 | 15.3 | 16.7                       |
| Wet Section (OMC+2%)    | 18.3                                 | 16.2 | 18.7                       |

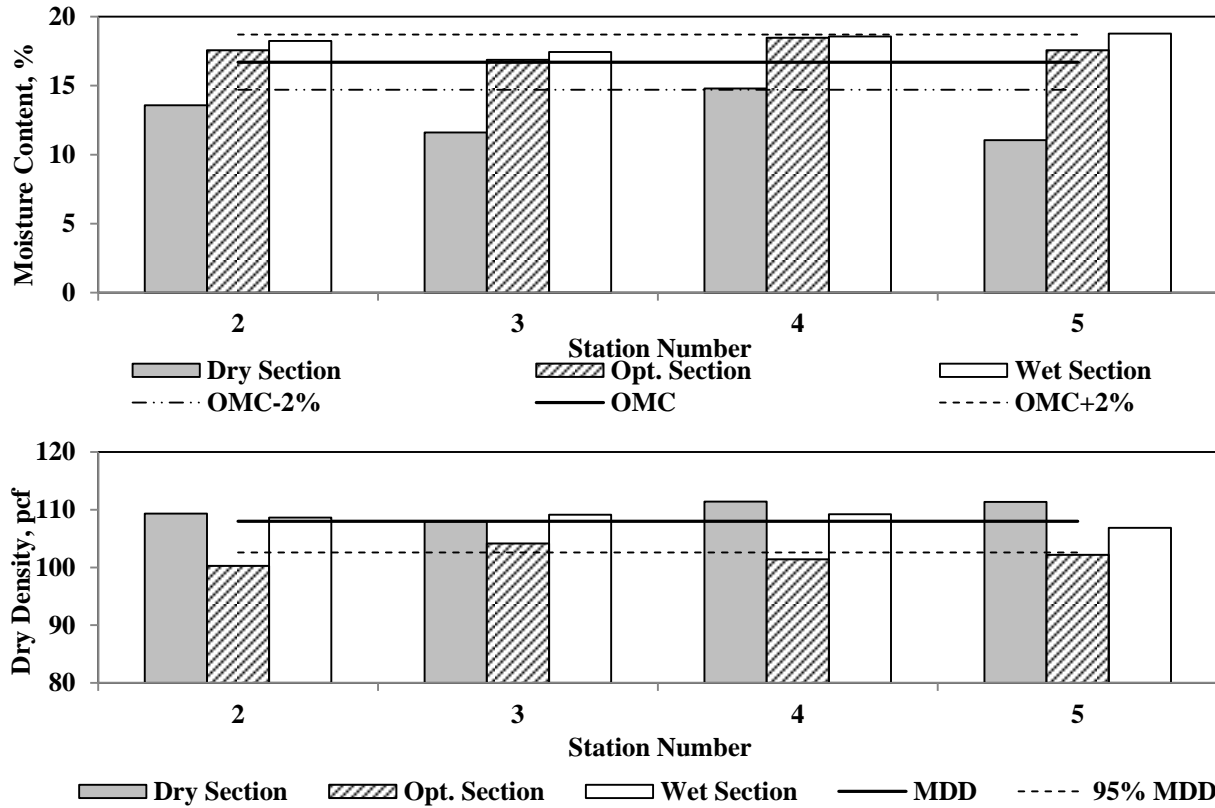


**Figure 4.11 – Spatial Variations of Moisture Content and Dry Density with NDG Immediately after Compaction of Subgrade Layer**

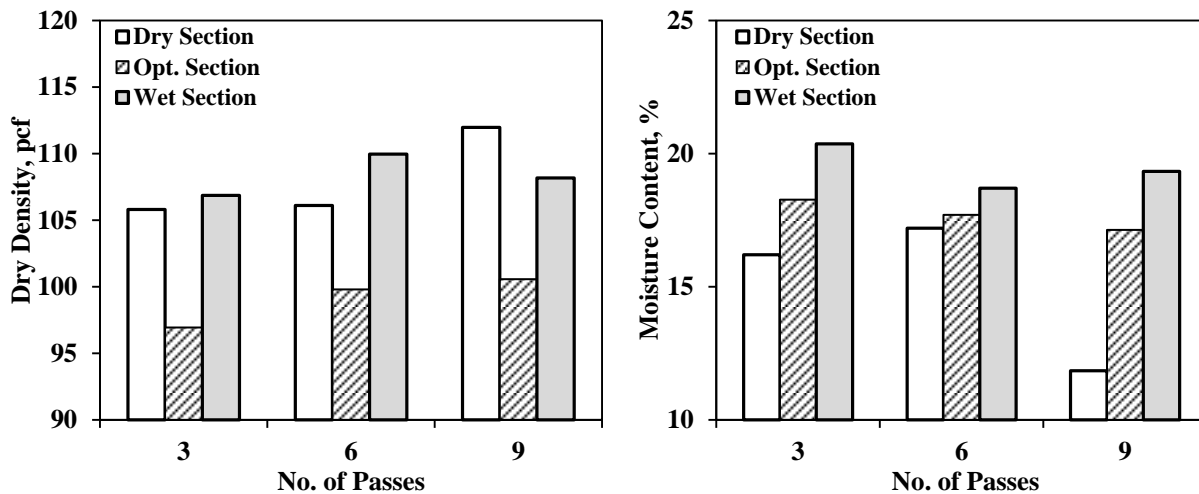


**Figure 4.12 – Variations of Average NDG Moisture Contents and Dry Densities with Number of Passes of Roller during Compaction of Subgrade Layer**

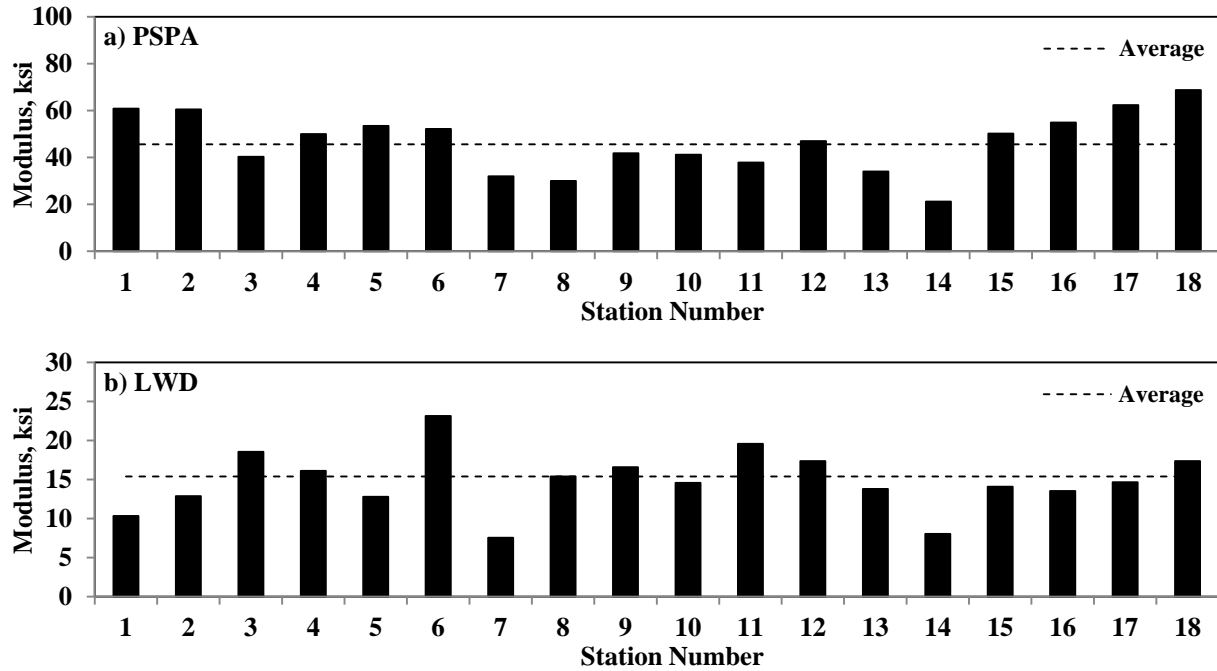


Figure 4.13 – Variations of Measured Moduli of Embankment Layer

Table 4.4 - Average Moduli from Different Sections

| Field Section | Average Modulus, ksi |            |          |            |          | Average Oven MC, % |
|---------------|----------------------|------------|----------|------------|----------|--------------------|
|               | PSPA                 |            | LWD      |            | DCP      |                    |
|               | Subgrade             | Embankment | Subgrade | Embankment | Subgrade |                    |
| Dry Section   | 38                   | 53         | 8.4      | 14.5       | 16.8     | 11.4               |
| Opt. Section  | 34                   | 40         | 9.3      | 12.4       | 13.0     | 14.9               |
| Wet Section   | 33                   | 36         | 4.6      | 13.5       | 7.6      | 16.2               |

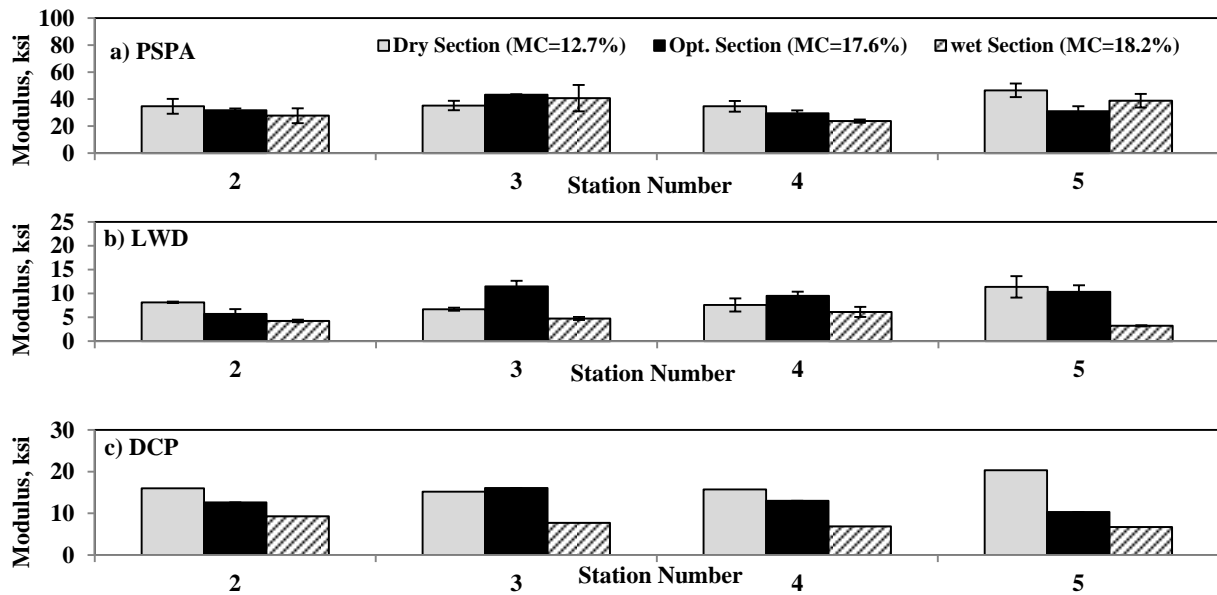
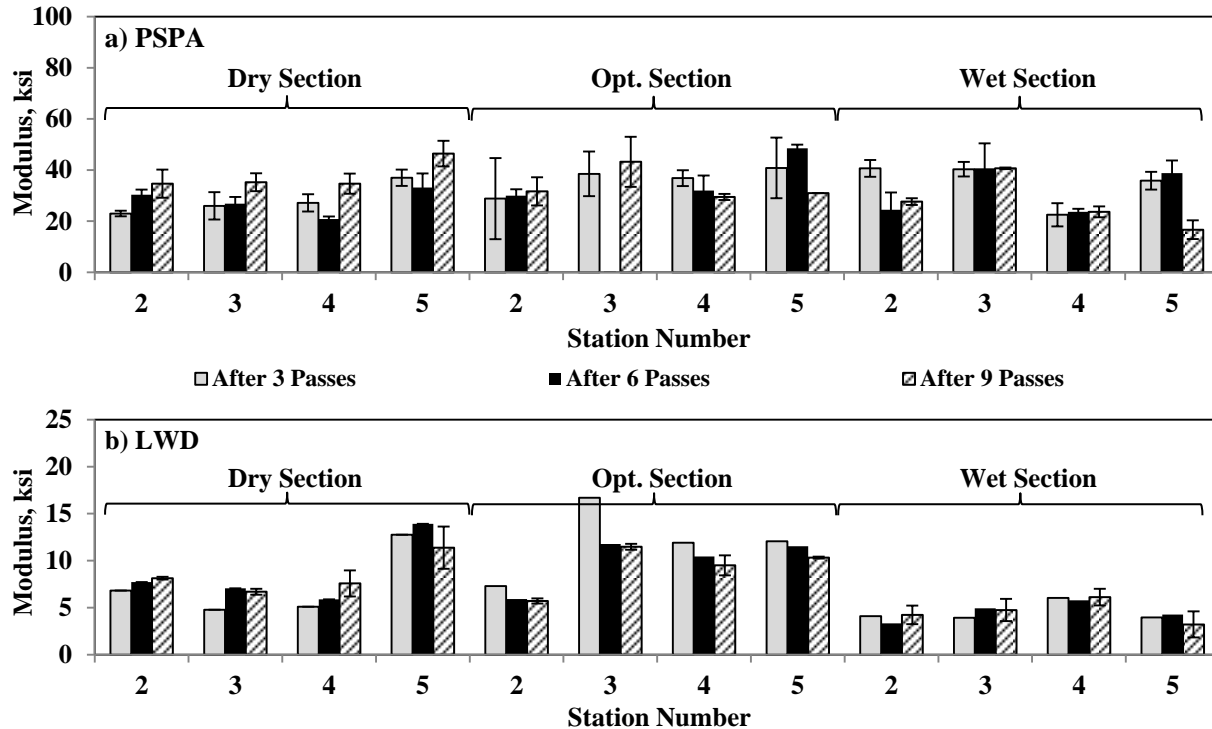


Figure 4.14 – Spatial Variations of Measured Moduli immediately after Compaction of Subgrade



**Figure 4.15 – Variations of Measured Moduli between Passes of IC Roller**

In this study, the roller drum and the soil interaction to compaction process were captured using two different proprietary technologies namely Compaction Meter Value (CMV) and the Machine Drive Power (MDP) as discussed in Table 2.1. The CMV technology uses the accelerometers to measure the roller drum accelerations in response to soil behavior during compaction and the MDP technology relates the roller drum rolling resistance to determine the energy required to overcome the resistance to motion (White and Thompson, 2008). The color maps of the distributions of the CMVs of the embankment and after the completion of compaction are presented in Figure 4.16. A more quantitative way of demonstrating the distributions of the CMVs is through their cumulative distribution curves. Figure 4.17 presents the distributions of the CMVs with the number of roller passes for the three subgrade sections. The CMV distribution for the dry section tends toward higher values with increase in compaction effort. The CMV distributions for the OMC section after six and nine roller passes are close, indicating that six passes of the roller were optimal. Eleven roller passes were required to achieve the optimal compaction for the wet section. The variations in the distribution of the CMVs of the wet section are comparable to the dry and OMC sections. However, the CMV measurements decrease with the increase in the number of passes for the wet section.

The contribution of subgrade layer placed on the embankment was explored by comparing the CMV distributions before and after the placement of the subgrade. From Figure 4.18, the CMV distributions before (labeled Mapping) and after the placement of the subgrade layer were similar. Since the embankment and subgrade materials were similar, one can conclude that the subgrade layer is placed properly. However, the CMV distribution for the embankment support of the wet section in Figure 4.18c is substantially greater than the CMV distribution after the subgrade placement. This signifies the influence of moisture control during compaction for more rigorous quality management.

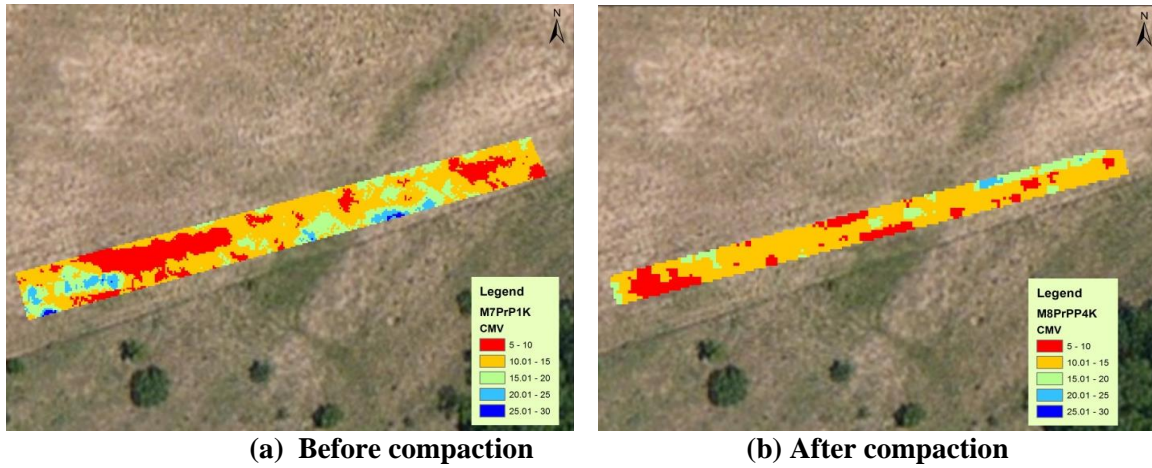


Figure 4.16 – Variations of CMV before and after Compaction of Subgrade

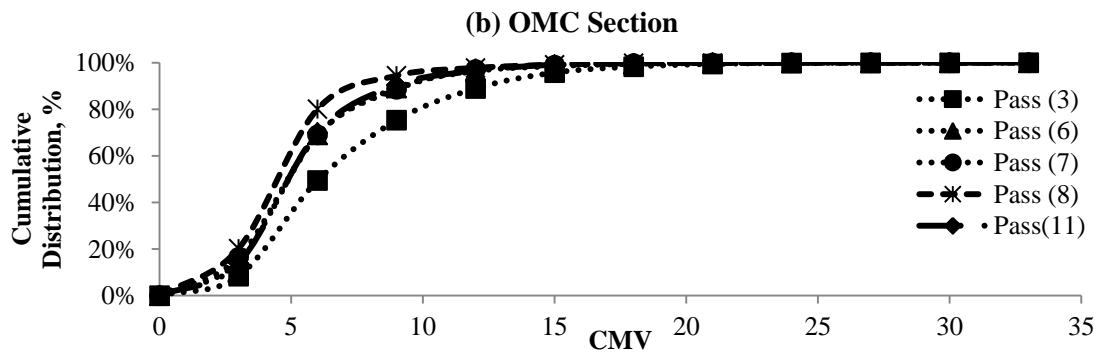
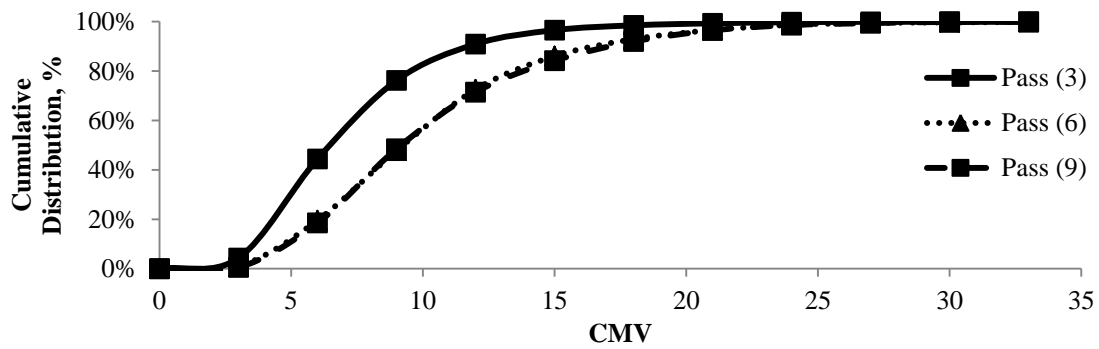
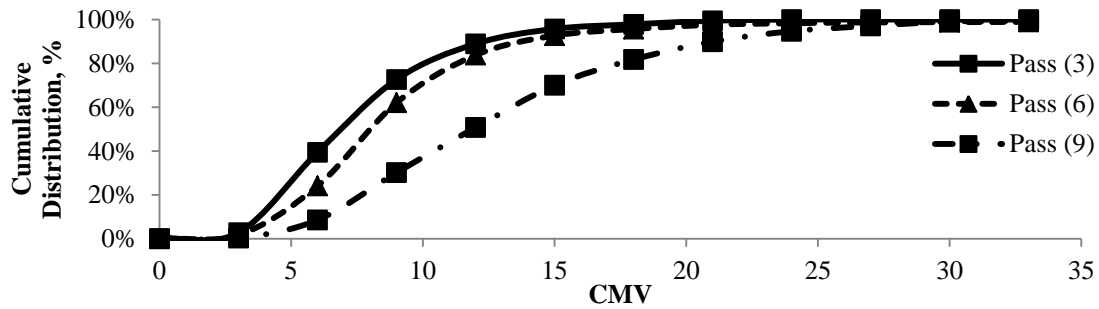
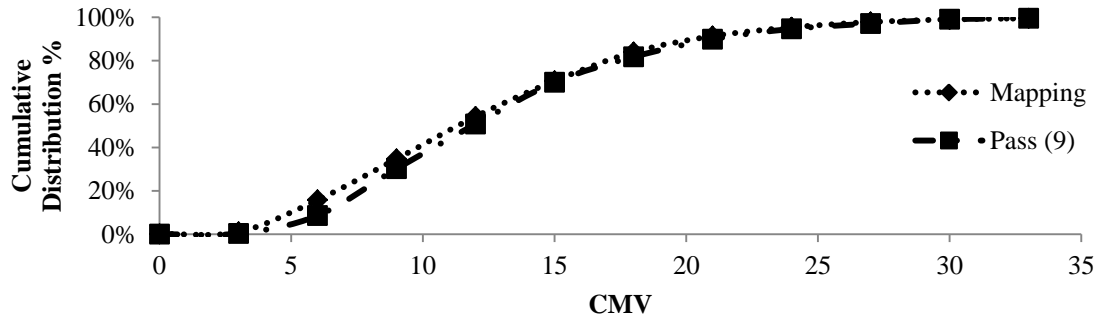
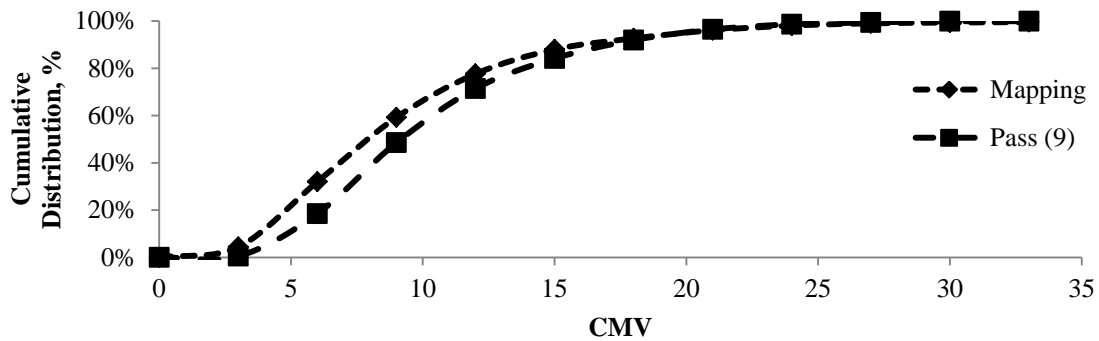


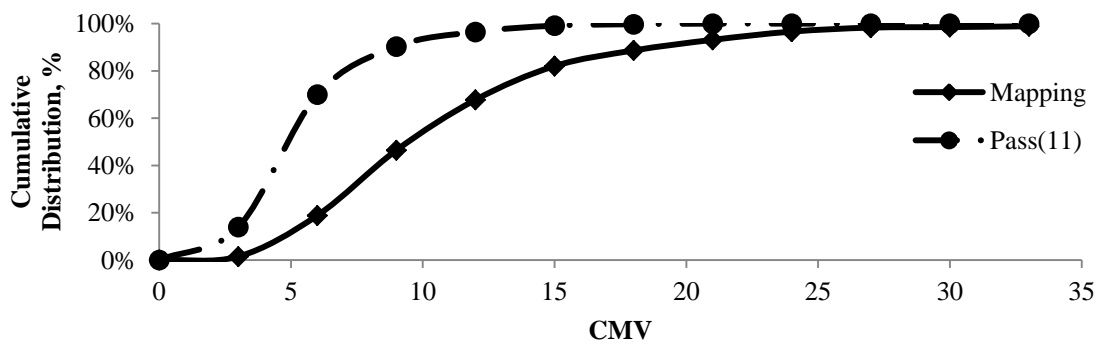
Figure 4.17 – Distributions of CMVs with Passes for Different SH 267 Subgrade Sections



(a) Dry Section



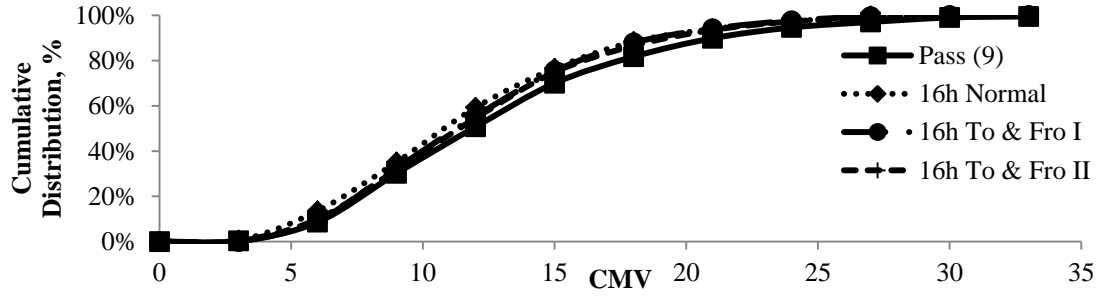
(b) OMC Section



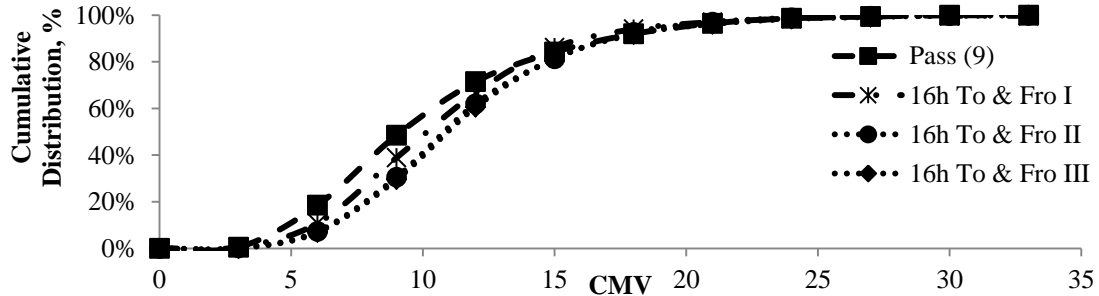
(c) Wet Section

**Figure 4.18 – Influence of Subgrade Lift Placement for Subgrade Sections**

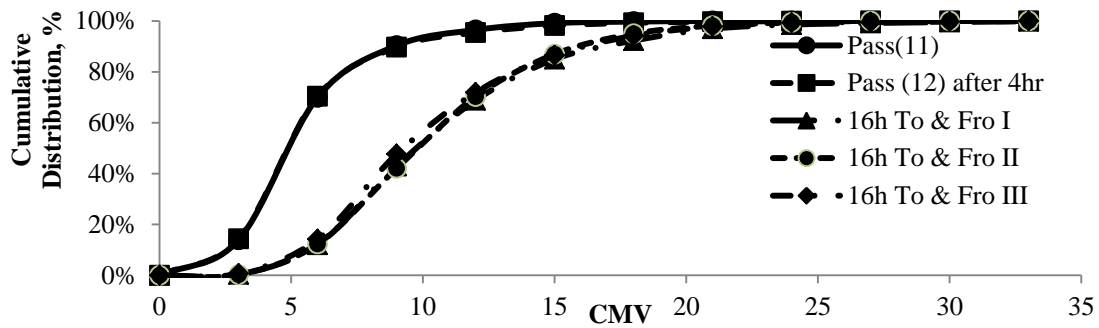
The influence of the rolling pattern and time of testing for quality assurance was assessed by studying the roller responses immediately after and 16 to 24 hrs after compaction. The rolling patterns were varied from the normal sequence of always forward sequence to forward and reverse sequence (To & Fro in the same path) at different times. Figure 4.19 presents the distributions of the CMV values for the final pass and 16 hrs later with normal and To & Fro patterns of rolling. For the dry and OMC sections, the CMV distributions remain comparable at different times and rolling sequences. However, for the wet section (Figure 4.19c), the distributions of the CMV values after 16 hrs are substantially greater as compared to the final pass. Figure 4.20 presents the distributions of the CMV values for the Production Section before and after subgrade compaction. The two CMV distributions are comparable since the embankment and the subgrade materials used are similar.



(a) Dry Section



(b) OMC Section



(c) Wet Section

Figure 4.19 – Influence of Time on Roller Measurement Values for Subgrade Sections

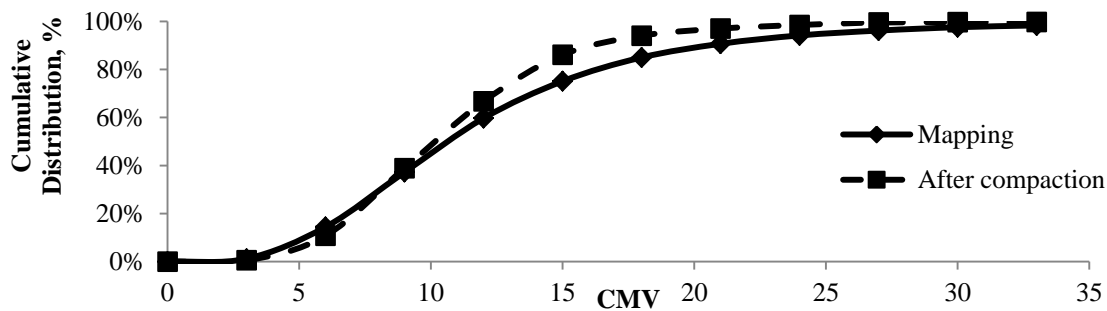


Figure 4.20 – Distributions of CMV with Passes for Production Section

## Summary of Results

Tables 4.5 and 4.6 summarize the descriptive statistics of the measurements on sections tested in this study. The dry densities from all sites demonstrate coefficients of variation (COVs) of 3% or less. However, the COVs associated with the moisture contents vary between 8% and 18%. Such moisture variations translate to high variability in the results from the NDT devices and the Roller Measurement Values (RMVs) from the IC rollers.

**Table 4.5 - Descriptive Statistics of NDT Devices on Different Sections of SH 267 Site**

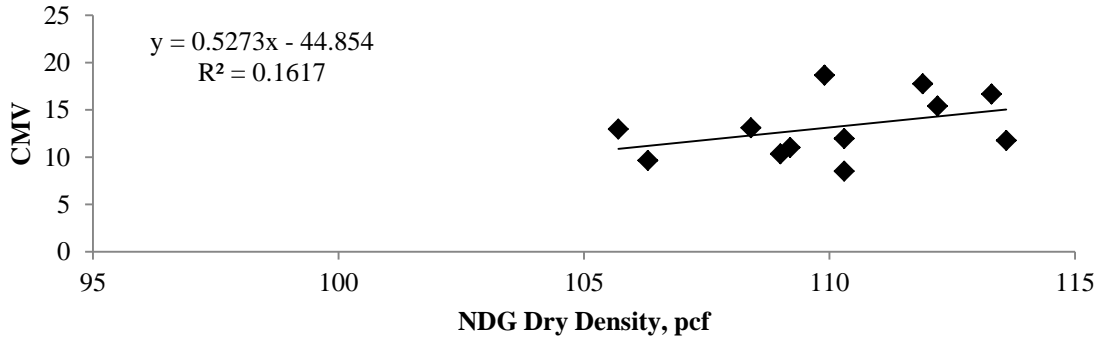
| Section                       |                     | Device              | Mean | STDEV | COV  | Sample Size | First Quartile | Third Quartile | Median |
|-------------------------------|---------------------|---------------------|------|-------|------|-------------|----------------|----------------|--------|
| Subgrade                      | Dry                 | Dry Density, pcf    | 110  | 3     | 2    | 12          | 109            | 112            | 110    |
|                               |                     | Moisture Content, % | 13   | 2     | 18   | 12          | 11             | 15             | 12     |
|                               |                     | CMV                 | 13   | 6     | 46   | 861         | 8              | 16             | 12     |
|                               |                     | LWD, ksi            | 9    | 3     | 32   | 12          | 7              | 10             | 8      |
|                               |                     | PSPA, ksi           | 42   | 8     | 19   | 12          | 37             | 46             | 41     |
|                               | OMC                 | Dry Density, pcf    | 102  | 4     | 4    | 12          | 99             | 104            | 102    |
|                               |                     | Moisture Content, % | 18   | 2     | 12   | 12          | 16             | 19             | 17     |
|                               |                     | CMV                 | 10   | 5     | 47   | 1156        | 7              | 13             | 9      |
|                               |                     | LWD, ksi            | 9    | 3     | 30   | 12          | 8              | 11             | 9      |
|                               |                     | PSPA, ksi           | 38   | 7     | 19   | 12          | 32             | 45             | 36     |
|                               | Wet                 | Dry Density, pcf    | 111  | 3     | 3    | 12          | 110            | 113            | 111    |
|                               |                     | Moisture Content, % | 17   | 2     | 11   | 12          | 15             | 18             | 17     |
|                               |                     | CMV                 | 5    | 3     | 51   | 1169        | 4              | 7              | 5      |
|                               |                     | LWD, ksi            | 5    | 2     | 48   | 12          | 3              | 6              | 4      |
|                               |                     | PSPA, ksi           | 30   | 4     | 13   | 12          | 28             | 31             | 29     |
|                               | Production          | Dry Density, pcf    | 107  | 3     | 3    | 24          | 105            | 109            | 107    |
|                               |                     | Moisture Content, % | 18   | 2     | 13   | 24          | 16             | 20             | 18     |
|                               |                     | CMV                 | 11   | 4     | 41   | 1270        | 8              | 13             | 10     |
|                               |                     | LWD, ksi            | 14   | 6     | 40   | 24          | 11             | 18             | 14     |
|                               |                     | PSPA, ksi           | 48   | 10    | 20   | 24          | 43             | 53             | 47     |
| Base                          | Dry                 | Dry Density, pcf    | 113  | 2     | 2    | 6           | 112            | 114            | 113    |
|                               |                     | Moisture Content, % | 8    | 1     | 14   | 6           | 7              | 8              | 8      |
|                               |                     | CMV                 | 32   | 9     | 27   | 489         | 25             | 39             | 31     |
|                               |                     | LWD, ksi            | 19   | 2     | 11   | 18          | 18             | 20             | 19     |
|                               |                     | PSPA, ksi           | 69   | 22    | 32   | 18          | 51             | 81             | 71     |
|                               | OMC                 | Dry Density, pcf    | 117  | 2     | 2    | 12          | 116            | 119            | 118    |
|                               |                     | Moisture Content, % | 9    | 1     | 9    | 12          | 9              | 10             | 9      |
|                               |                     | CMV                 | 29   | 9     | 29   | 479         | 23             | 34             | 27     |
|                               |                     | LWD, ksi            | 19   | 4     | 19   | 15          | 16             | 23             | 17     |
|                               |                     | PSPA, ksi           | 74   | 26    | 35   | 14          | 49             | 100            | 80     |
|                               | Wet                 | Dry Density, pcf    | 121  | 3     | 2    | 18          | 120            | 123            | 121    |
|                               |                     | Moisture Content, % | 11   | 1     | 12   | 18          | 10             | 12             | 12     |
|                               |                     | CMV                 | 54   | 22    | 40   | 1597        | 38             | 66             | 51     |
|                               |                     | LWD, ksi            | 12   | 5     | 42   | 15          | 8              | 17             | 14     |
|                               |                     | PSPA, ksi           | 56   | 15    | 26   | 15          | 46             | 64             | 55     |
| Lime Treated Subgrade Section | Dry Density, pcf    | 102                 | 4    | 4     | 5    | 100         | 101            | 100            |        |
|                               | Moisture Content, % | 21                  | 2    | 9     | 5    | 20          | 22             | 21             |        |
|                               | CMV                 | 28                  | 12   | 42    | 2020 | 20          | 33             | 26             |        |
|                               | LWD, ksi            | 16                  | 5    | 34    | 15   | 13          | 19             | 17             |        |
|                               | PSPA, ksi           | 61                  | 10   | 17    | 16   | 54          | 66             | 61             |        |

**Table 4.6 - Descriptive Statistics of NDT Devices on Different Sections of IH 35W Site**

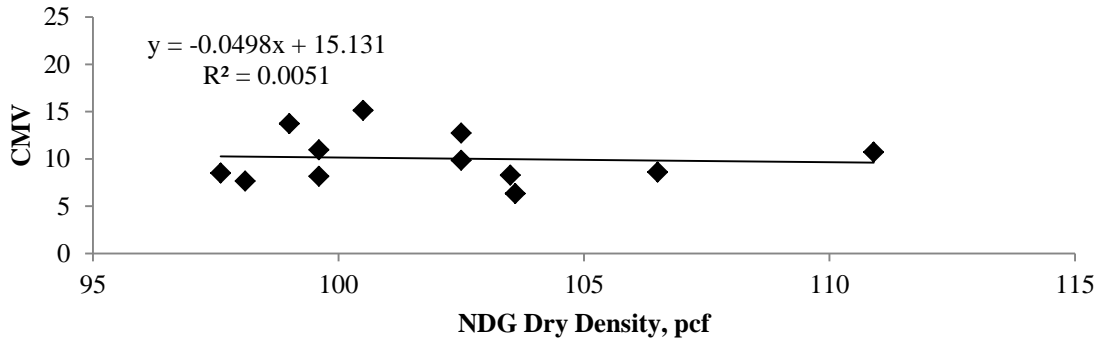
| Section | Device              | Mean | STDEV | COV | Sample Size | First Quartile | Third Quartile | Median |
|---------|---------------------|------|-------|-----|-------------|----------------|----------------|--------|
| Dry     | Dry Density, pcf    | 108  | 3     | 2   | 15          | 106            | 110            | 109    |
|         | Moisture Content, % | 17   | 1     | 8   | 15          | 16             | 18             | 17     |
|         | MDP                 | 148  | 2     | 1   | 3888        | 147            | 150            | 149    |
|         | LWD, ksi            | 5    | 2     | 44  | 15          | 3              | 6              | 4      |
|         | PSPA, ksi           | 30   | 10    | 32  | 15          | 21             | 37             | 30     |
| OMC     | Dry Density, pcf    | 110  | 3     | 3   | 15          | 108            | 112            | 111    |
|         | Moisture Content, % | 15   | 2     | 12  | 15          | 14             | 16             | 14     |
|         | MDP                 | 10   | 3     | 36  | 6448        | 8              | 12             | 10     |
|         | LWD, ksi            | 4    | 2     | 37  | 15          | 4              | 5              | 4      |
|         | PSPA, ksi           | 30   | 4     | 14  | 15          | 27             | 32             | 30     |
| Wet     | Dry Density, pcf    | 110  | 4     | 3   | 18          | 107            | 113            | 110    |
|         | Moisture Content, % | 14   | 2     | 15  | 18          | 12             | 15             | 13     |
|         | MDP                 | 146  | 5     | 3   | 5685        | 144            | 149            | 147    |
|         | CMV                 | 9    | 6     | 61  | 5685        | 5              | 13             | 9      |
|         | LWD, ksi            | 3    | 1     | 44  | 18          | 2              | 4              | 3      |
|         | PSPA, ksi           | 23   | 3     | 12  | 18          | 21             | 24             | 22     |

**Relations between Roller Measurements and NDT Devices**

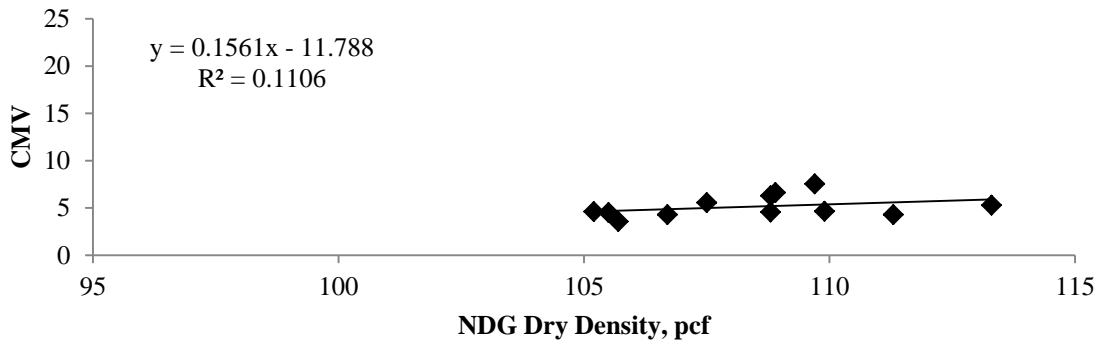
Figure 4.21 presents the relationships between the dry density from the NDG and the CMV measurements for all SH 267 subgrade sections. Similar results but for the base and lime-treated sections are included in Appendix A. The two parameters are not strongly correlated. As illustrated in Figures 4.22 and 4.23 (and in Appendix A), the relationships between the LWD or PSPA moduli and CMV measurements are also not very strong either. The same patterns were observed for the IH 35W sections as discussed in Appendix B. The main observation from that data is that the moduli from NDT devices or RMVs are not as sensitive to the density as it is to the moisture content of the layer being compacted since for any given test strip the variation in the density is less than 3%. The depth of penetration of the IC rollers and LWDs are greater than the thickness of the layer being compacted, the variability of the foundation layers also contribute to the variability of the moduli and RMVs measured. These sources of variability may impact the quality of the correlations between the spot test measurements and the RMVs. Therefore, it might be a good practice to implement a process control for the moisture content during the compaction process.



(a) Dry Section

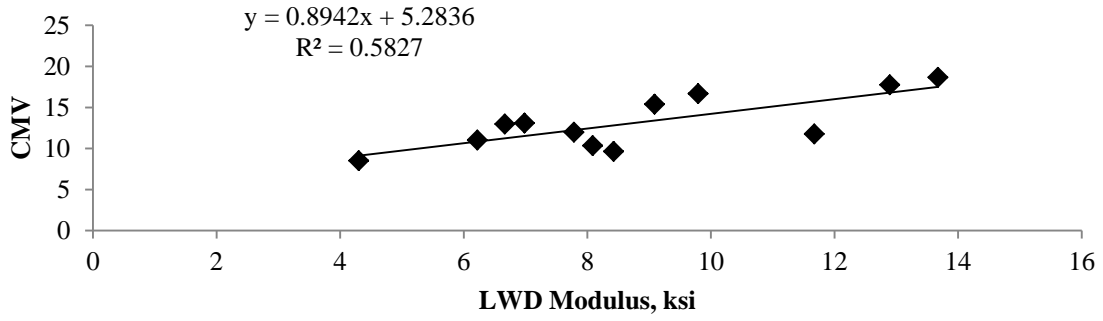


(b) OMC Section

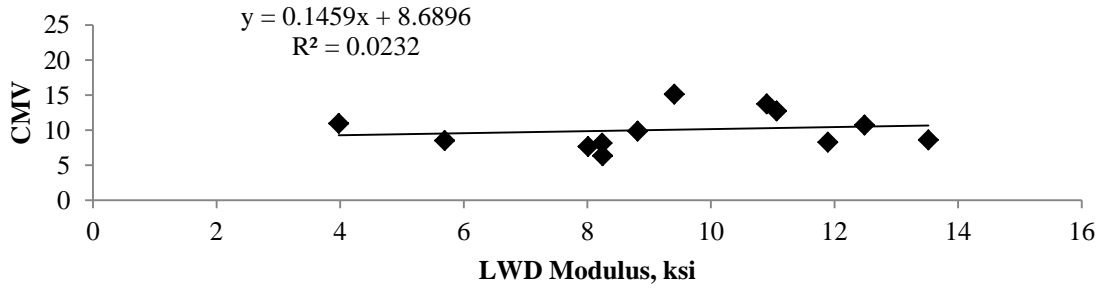


(c) Wet Section

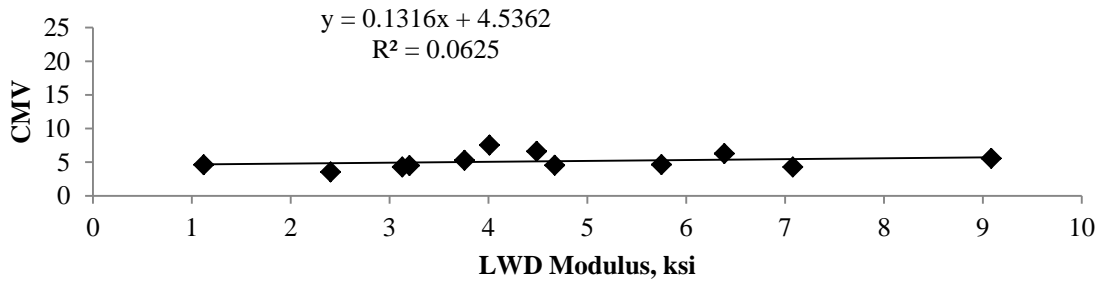
**Figure 4.21 – Relations between the NDG Dry Density and the CMV for Subgrade Sections of SH 267**



**(a) Dry Section**

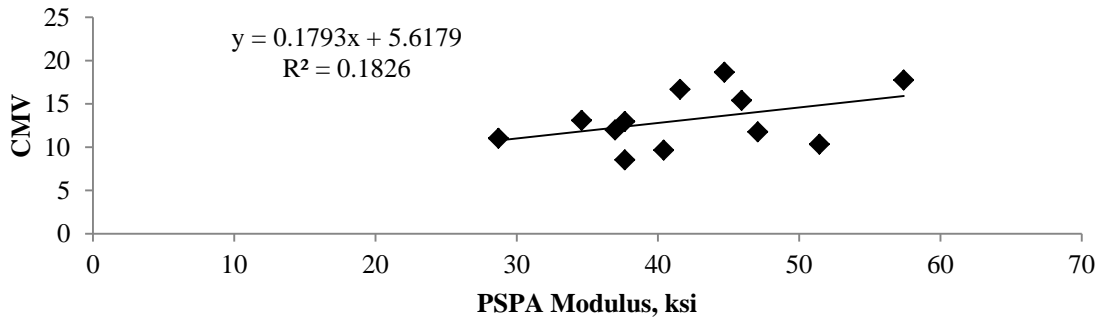


**(b) OMC Section**

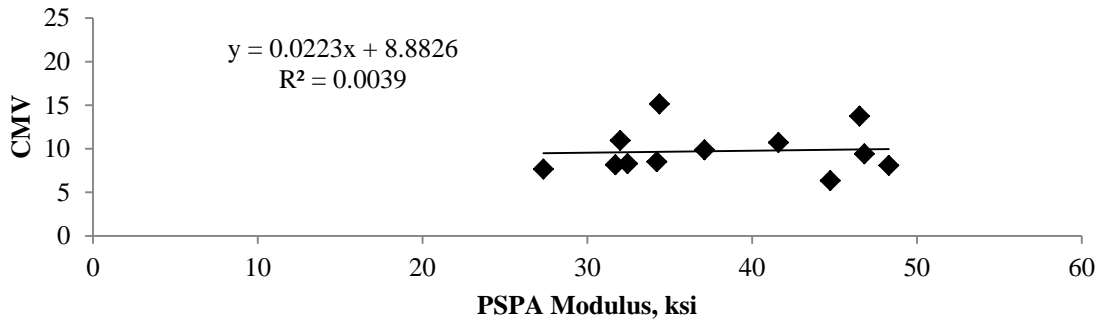


**(c) Wet Section**

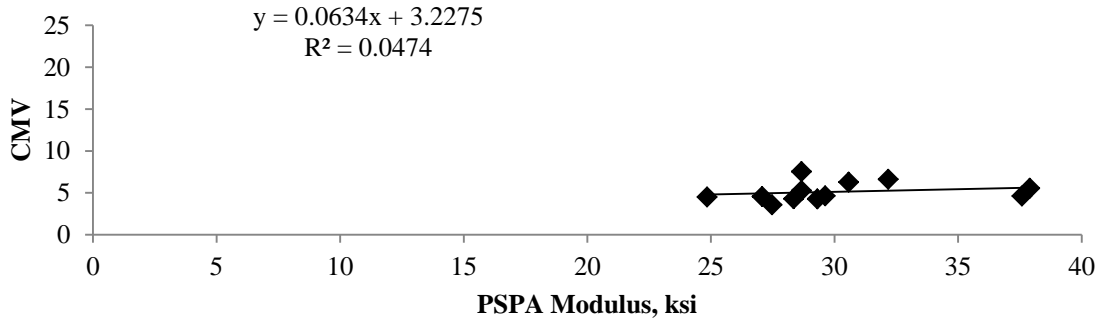
**Figure 4.22 – Relations between the LWD Modulus and the CMV for Different Sections of Subgrade**



(a) Dry Section



(b) OMC Section



(c) Wet Section

**Figure 4.23 – Relations between the PSPA Modulus and the CMV for Different Sections of Subgrade**

# Chapter 5

## Practical Observations

The practical lessons learned during the field studies and from the data analyses are discussed in this chapter.

### Roller Measurement Target Values

The approach to estimate the target values with different devices were explained in Chapter 2. Figure 5.1 describes the process adopted to estimate the target value for roller measurements. The target density for estimating the target RMV for subgrade was set at 95% of the MDD. Similarly 100% of the MDD was considered as the target density requirement to estimate the RMV for a base.

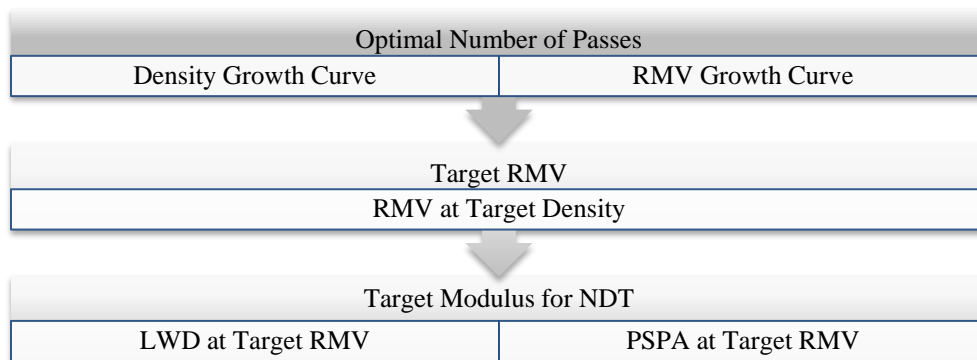
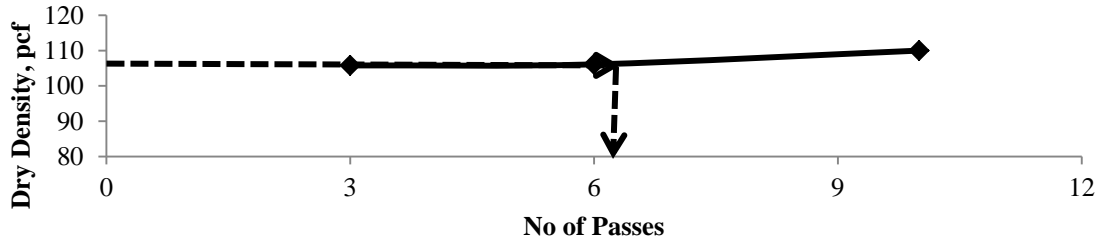
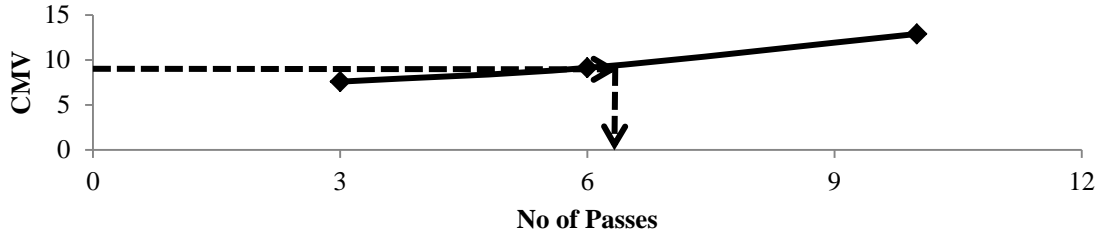


**Figure 5. 1 – Process of Estimating Optimal Passes and Target Roller Measurement Values**

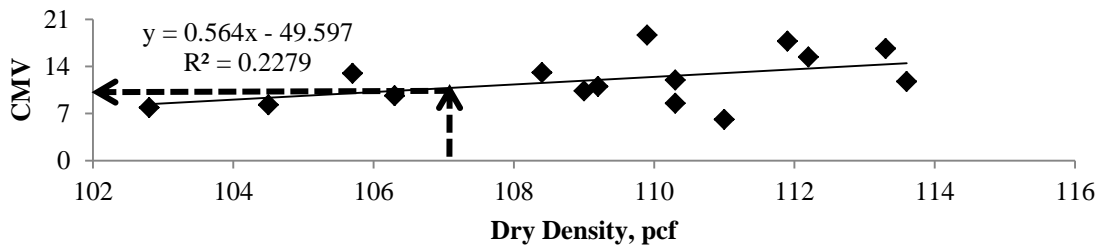
Figures 5.2 through 5.4 present the implementation of the above approach in estimating the target RMVs (in this case target CMVs) for the dry, optimum and wet subgrade sections of SH 267. Similar results for other sections are included in Appendix C. The determination of the target CMVs based on density or modulus requirements are sometimes difficult since the relevant parameters in some cases are not strongly correlated.



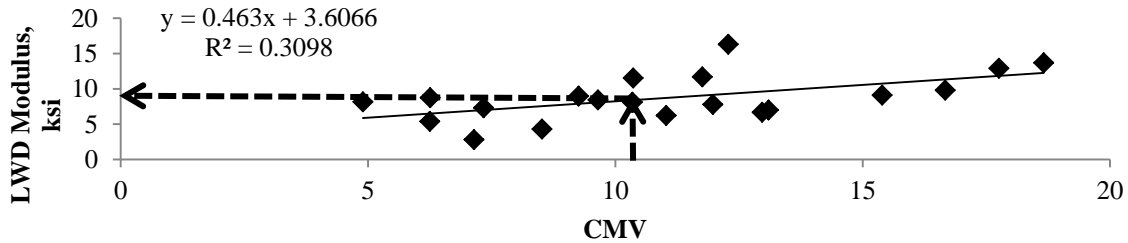
(a) Optimal Number of Passes based on Density Growth Curve



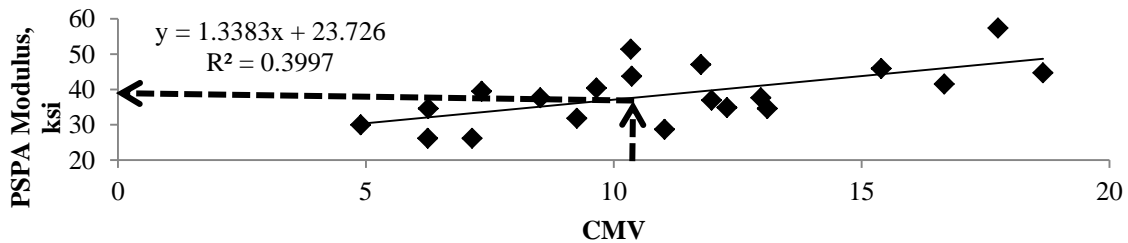
(b) Optimal Number of Passes based on CMV Growth Curve



(c) Target CMV based on Target Dry Density

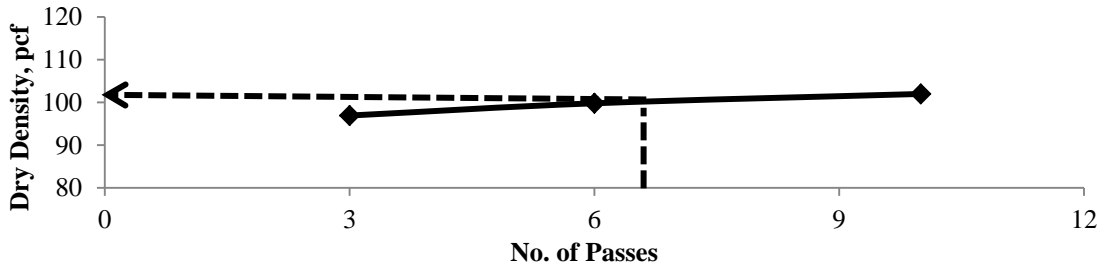


(d) Target LWD Modulus based on Target CMV

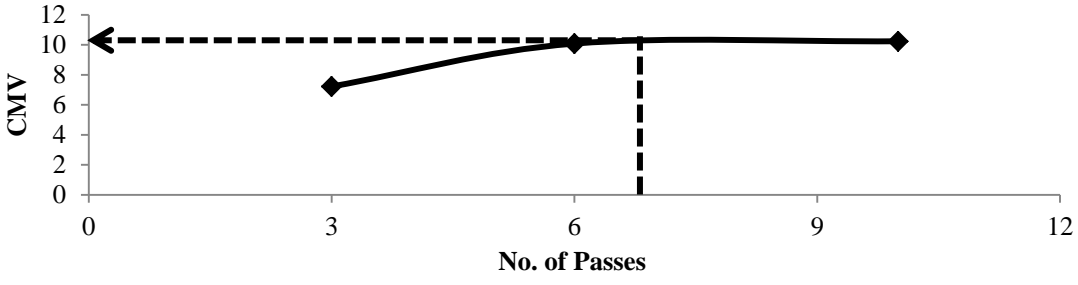


(e) Target PSPA values based on Target CMV

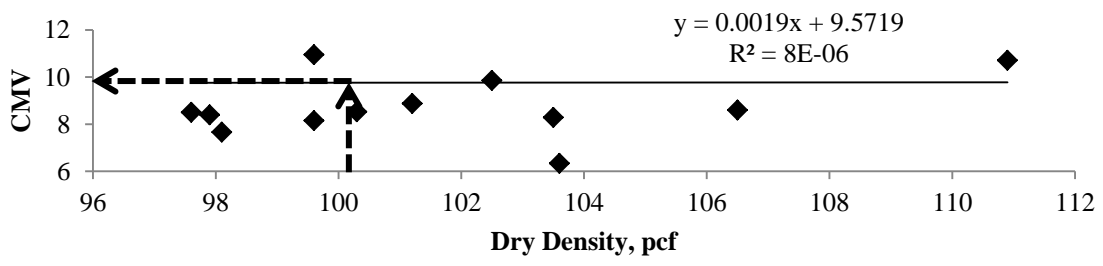
Figure 5.2 – Target RMV estimation Process for Dry Subgrade Section of SH 267 Site



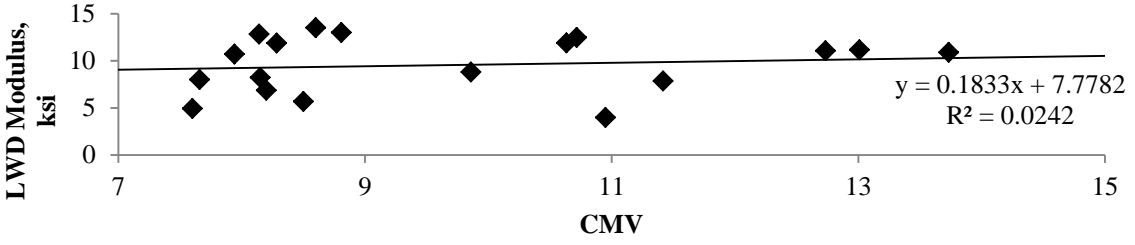
(a) Optimal Number of Passes based on Density Growth Curve



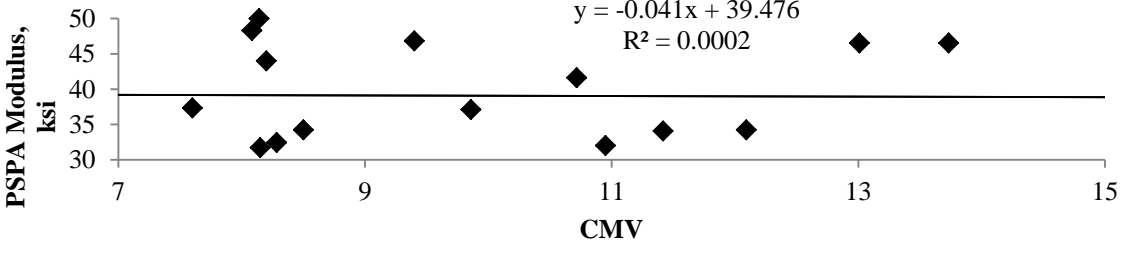
(b) Optimal Number of Passes based on CMV Growth Curve



(c) Target CMV based on Target Density

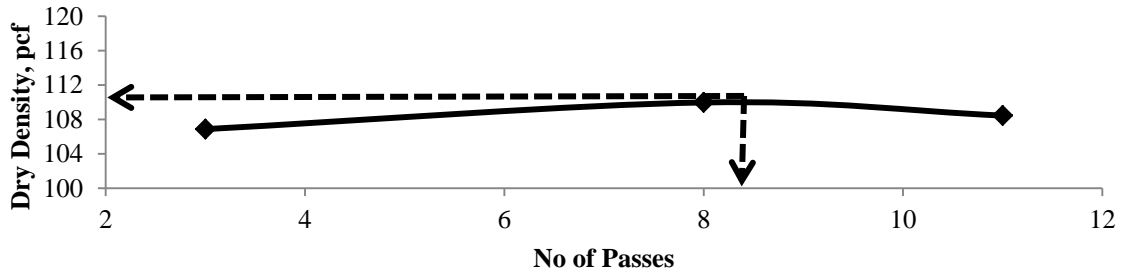


(d) Target LWD Value based on Target CMV

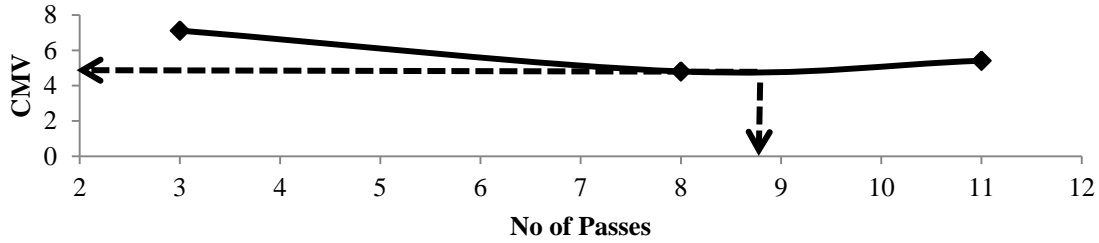


(e) Target PSPA Value based on Target CMV

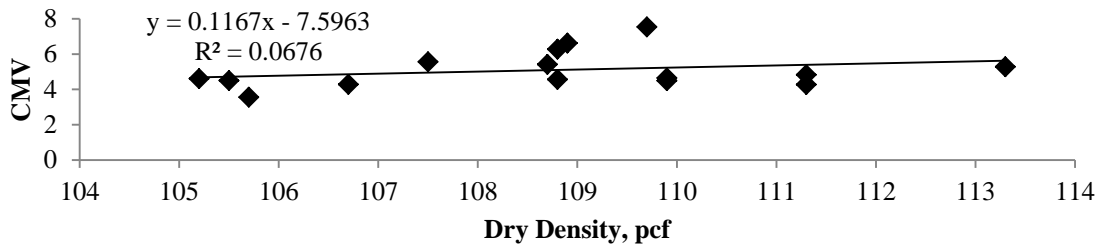
Figure 5.3 – Target RMV Estimation Process for OMC Subgrade Section of SH 267 Site



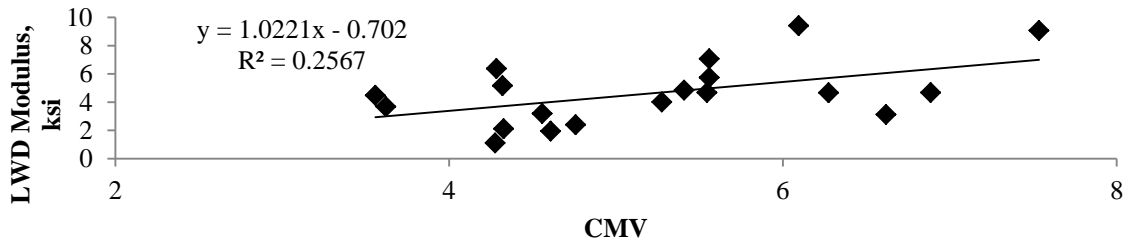
(a) Optimal Number of Passes based on Density Growth Curve



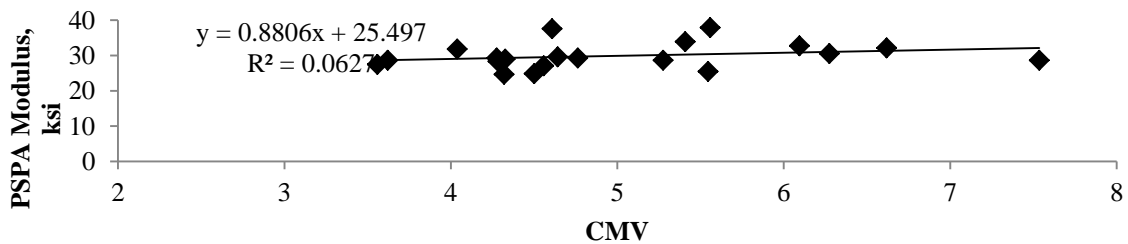
(b) Optimal Number of Passes based on CMV Growth Curve



(c) Target CMV based on Target Density



(d) Target LWD Value based on Target CMV



(e) Target PSPA Value based on Target CMV

Figure 5.4 – Target RMV estimation Process for Wet Subgrade Section of SH 267 Site

### Sensitivity of Roller Measurements to Compaction Process

Two different RMVs (i.e., MDP and CMV) were measured at the IH 35W project. Figure 5.5a compares the variations of the two RMVs measured simultaneously along the wet subgrade section of the IH 35W project. Even though the CMVs increase by a factor of 1.5 between the third and ninth passes, the MDP values are essentially constant. Figure 5.5b illustrates the variations in the MDP measurements with the number of passes. The distributions of the MDP values are not substantially different. This example indicates that either the roller is compacting the layers underneath the lift (instead of the lift newly placed to be compacted) or the MDP values are less sensitive to the compaction process.

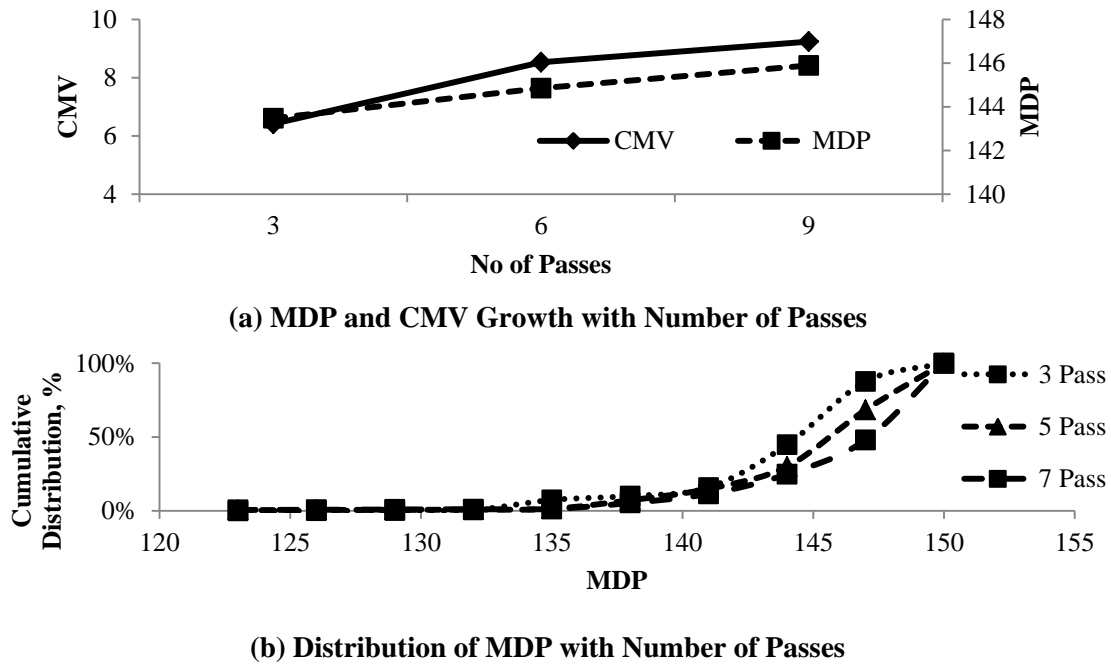


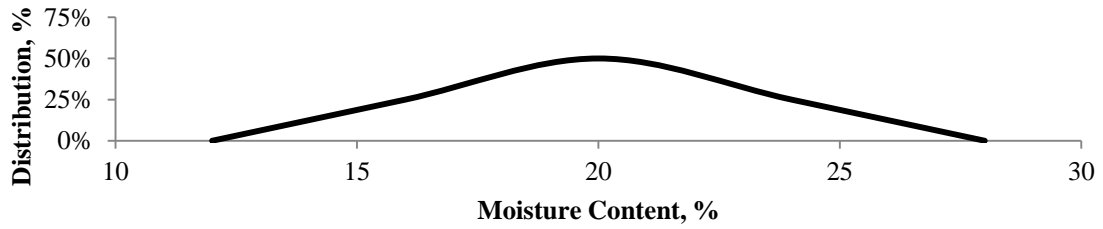
**Figure 5.5 – Variation in Roller Measurements with Compaction Process**

### Spatial Variability

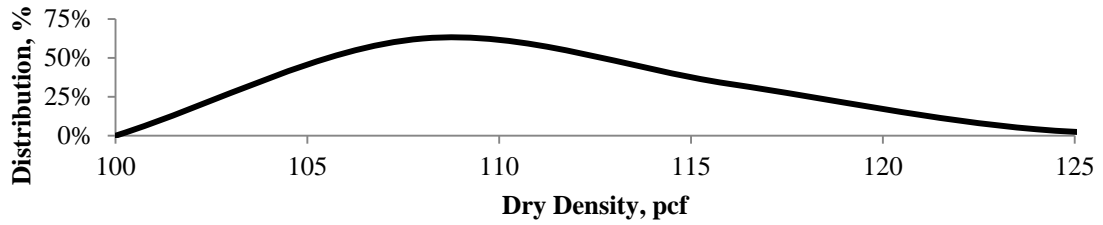
Figure 5.6 presents the distributions of the NDT tests and roller measurements from a typical site considered in this study. The moisture contents and densities are reasonably widely distributed. Such variations propagate to the measured IC values and test results with the NDT devices. These variations along with the small uncertainties in the GPS coordinates of the NDT tests and roller measurements may impact negatively the strength between different parameters. It seems that a more rigid process control may be required.

### Site Preparation

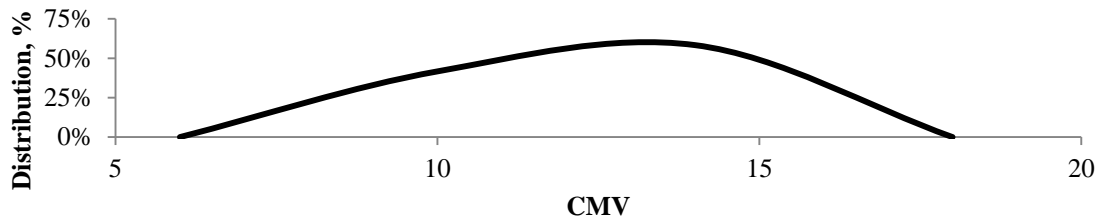
Sheep foot rollers are best suited for achieving the required compaction for clayey soils. However, based on the literature search provided in Chapter 2, the use of IC kits with the sheep foot rollers are discouraged. Not to impede the construction process, one pragmatic approach is to allow the compaction of the layer with a sheep foot roller and the IC mapping with a single wheel smooth drum IC roller. The compacted surface has to be bladed smooth before mapping the compacted section with the IC roller or before performing spot tests with the NDT devices. The utilization of two rollers and a grader may not be time efficient, especially that the IC mapping has to be performed at speeds on the order of 2 to 3 mph.



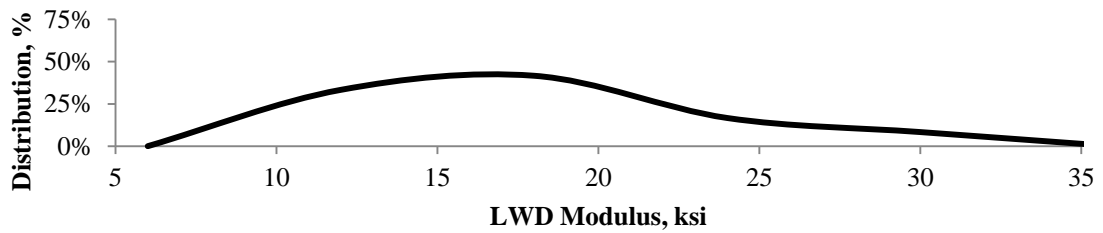
(a) Moisture Content



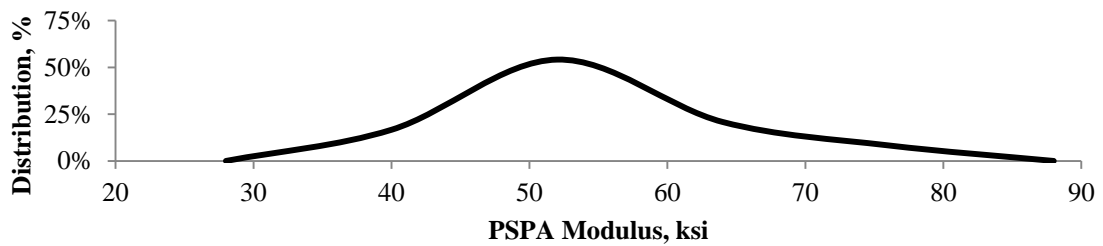
(b) Dry Density



(c) CMV



(d) LWD



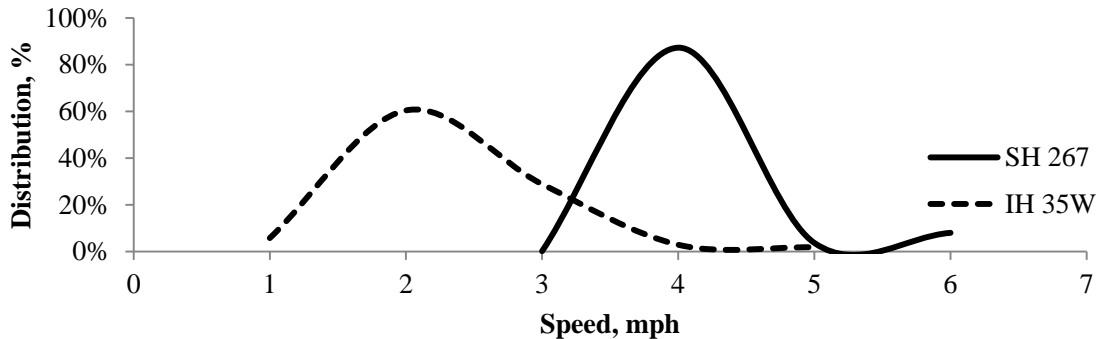
(e) PSPA

Figure 5.6 – Distributions of Measurements for a Production Section

### Variation in Roller Parameters

In both sites, single wheel smooth drum rollers were used. The one in the IH 35W site was a brand new roller with the factory-installed MDP measurement kit. The roller used in the SH 267 site was an older model equipped with the Trimble retrofit kit. Figure 5.7 presents the distributions of the mapping speed within typical sections at the two sites. Despite the best efforts by the operator, the speed of the roller used during the SH 267 studies was greater than the recommended limits (2-4 mph). That roller simply did not have the speed control mechanism that is provided on the new rollers. The older roller however maintained a narrower range of speed as compared to the new one. A higher speed reduces the sensitivity of roller measurements to the compaction process.

The frequency of 28 Hz and amplitude of 0.04 in. were maintained almost constant by the new roller used in the IH 35W project. However, the frequency varied between 27 and 32 Hz (recommended range 25-35 Hz) and the amplitude varied between 0.04 and 0.06 in. (recommended range of 0.02 to 0.04 in.) for the older roller with a less sophisticated control system. The variation in the above parameters may influence the roller measurements and hence the verification of the adequacy of these operational parameters of the rollers may be needed.



**Figure 5.7 – Distribution of Speed with Different Rollers**

### Analyses of Roller Measurements

Figure 5.8 depicts the three subgrade sites constructed at different moisture contents and the NDT test locations for the SH 267 site. The data recorded by the roller was exported and delivered as tag files. Using Site Vision Office (SVO) software, the tag files were converted to database files in a Comma Separated Values (CSV) format for each day. The data for all passes were exported together in a single file. SVO does not have the functionality to separate the data for each pass (according to Trimble the new software Vision Link will have such functionality).

The FHWA’s new software, VEDA, was sometimes successful in importing the output files from the SVO. Two of VEDA’s limitations for this study were that it does not separate the data from different passes and does not read any other sensor’s data other than CMV values. Therefore, other IC measurements such as MDP have to be copied to the CMV column in order for VEDA to read them.

Having to analyze each pass data separately, the data were imported into the ArcGIS software. Once in ArcMAP, the data was cleaned up by removing any data points with either NULL and zero CMV values or records that had no locational information. The IC roller data collection varied according to the speed of the roller but on average, a data point was collected every 1 ft and the values of CMV varied depending on the response of the material. As seen in Figure 5.9, the CMV values range from 2.2 to 36 as shown by the sizes of the circles.

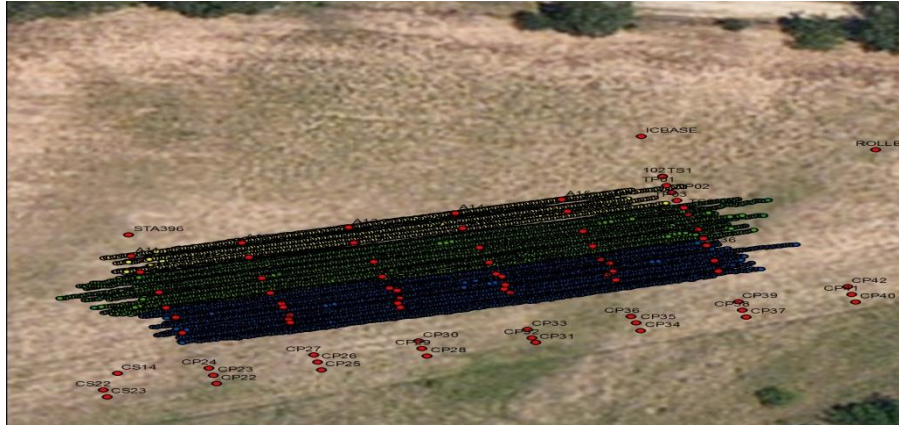


**Figure 5.8 – Subgrade Site at SH 267**

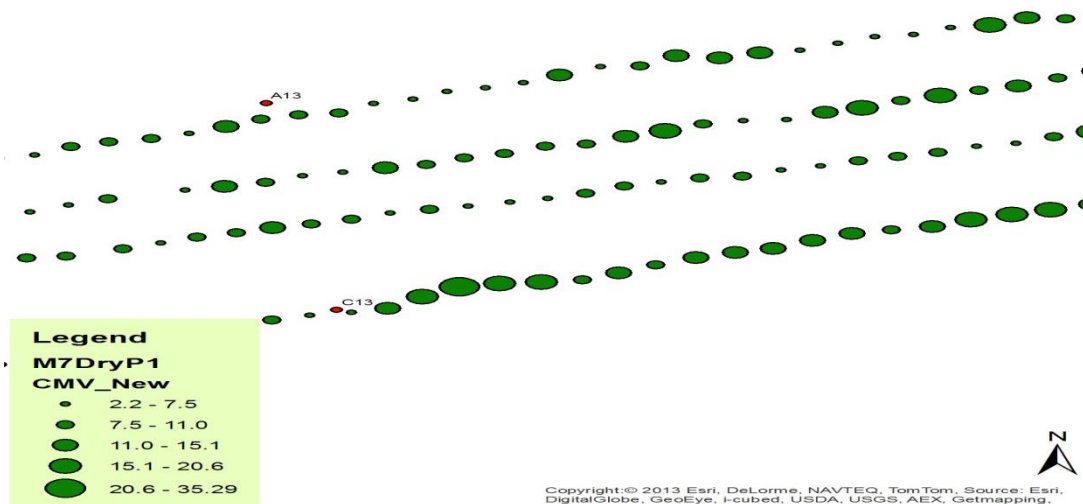
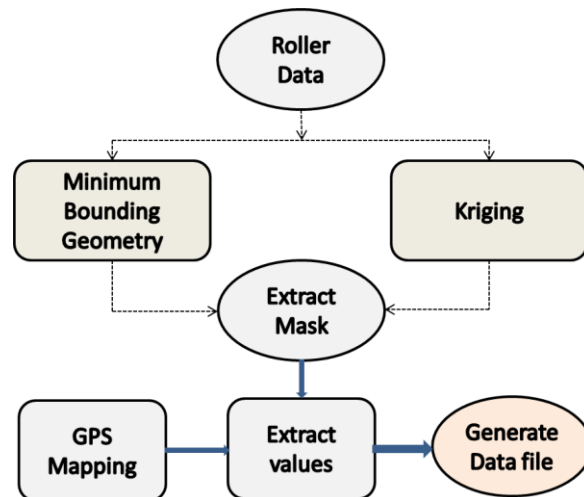


**Figure 5.9 – Distribution of Roller Measurements on the Dry Subgrade Section of SH 267**

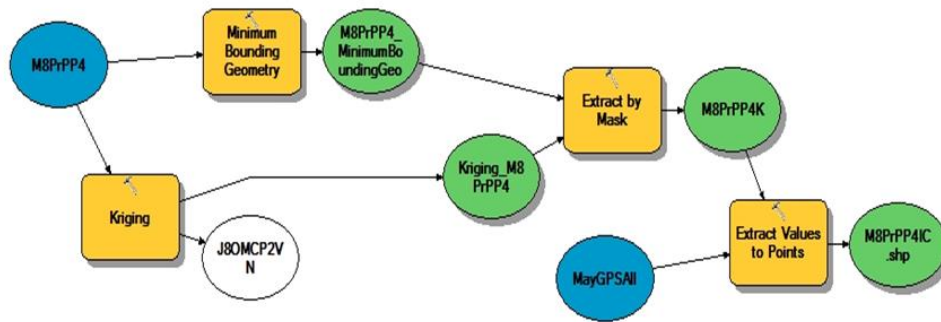
The workflow for analyzing the data starts by separating the passes using the IC recorded time that matched with the field notes for each section (dry, wet and OMC) for each day and for all three sites. This was done using selection by attribute and with some manual process.

A model created to automate part of the processing and analysis is shown in Figure 5.10. The data was gridded using “kriging”; at the same time, a “mask” was created using a minimum bounding geometry box. The two outputs are passed through an extraction by mask to get the raster data cut out around the data points.

Figure 5.11 shows the gridded CMV values for the OMC section after the first pass. The NDT test data were recorded for each section including the labels for each test point. These data were added to ArcMAP and a “join” was created between the GPS and the NDT data. Finally, to determine the roller measurement values where the NDT testing was done, the CMV values were extracted from the cell value by points and recorded in a new field to be used for the analyses.



a) General Flow Chart



b) ArcGIS Workflow

Figure 5.10 – Flow Chart Representation of Data Processing and Analysis using ArcGIS

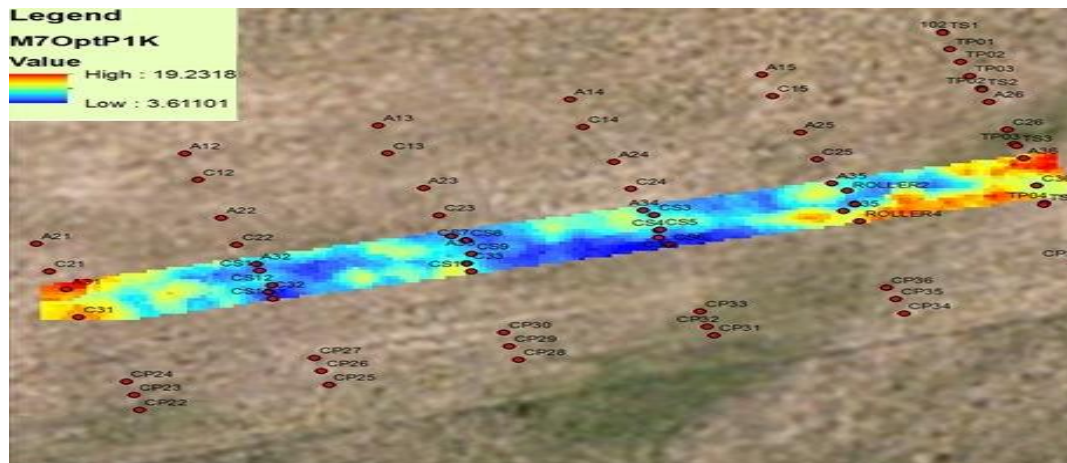


Figure 5.11 – Gridded Roller Measurement Values for Subgrade Section at SH 267

### GPS System Check and Calibration

An independent survey grade GPS instrument (Topcon GR-3) was used in all field testing to ensure the highest quality positions of all NDT tests and compared to the IC roller data collected for each section. The Topcon GR-3 base station was set up with post-processing recording. A rover was used to collect both the horizontal location and vertical elevation. These values were corrected in real time using real-time kinematics (RTK) for all sites.

The coordinate system selected was State Plane North Central Texas, unit feet and North American datum 1983. This system was also set for the IC roller according to the operators. The rover that was attached to the roller was receiving real time correction (RTK) from a base station.

The GPS system outfitted on the roller at SH 267 was tested before the data collection and the location of the roller was collected using the GPS system. Calibration of the roller position was taken using the GR-3 and the location data was copied from the Trimble system on the roller. It was noticed that there was a shift in the data collected by the IC roller in all three field experiments as compared to the GPS locations. The GPS locations were accurate and mapped at the correct positions on earth while the GPS data from the IC roller were consistently shifted to the North and East of the actual project locations.

Figure 5.12 shows the location of the IC Roller with the coordinates read from the Trimble device on the roller (red dot), while the GPS location collected for the roller by the GR-3 shows the true location (yellow dot). The possible shift could be related to the base station that the IC rover used and the parameters setup. There is no detailed information about the base stations used by the IC roller.

Future IC roller testing or projects should require detailed information about the base station, coordinate system and datum used.



**Figure 5.12 – IC Roller Calibration**

### Geospatial and Geostatistical Analyses

Geostatistical analyses are tools that help explore the data and look for patterns in the data. The CMV/MDP values collected are spatially related and have spatial dependency since they reflect the responses of the material beneath the roller. If there is data dependency, then the data contains information about the relationship between near values. This is important because the stronger the dependency, the better the interpolation. Kriging is an exact interpolation, but it also provides uncertainty that can be used for evaluation. To explore how the data behave, a histogram of the CMV values for a section after three passes is included in Figure 5.13. The data show that a wide range of CMV values, from 0.4 to 31 with a mean of 9.3, were collected. The CMVs between 6.6 and 9.7 occur with the highest frequency.

The semivariogram of the data (shown in Figure 5.14) allows an investigation of the spatial autocorrelation between the recorded CMV values. Points that are closer to each other will have similar

values. Spatial variation can be more effectively examined using a variogram and kriging. The results of the semivariogram show that the model fit had a y-intercept (nugget) of 2.8 with a partial sill of 40. The sill is the sum of both the nugget and the partial sill and it represents the asymptote when the model flattens out. The range was 59 indicating the value beyond which there are no correlations. The longer the range or the lower the sill, the more uniform and less variable the CMV values will be.

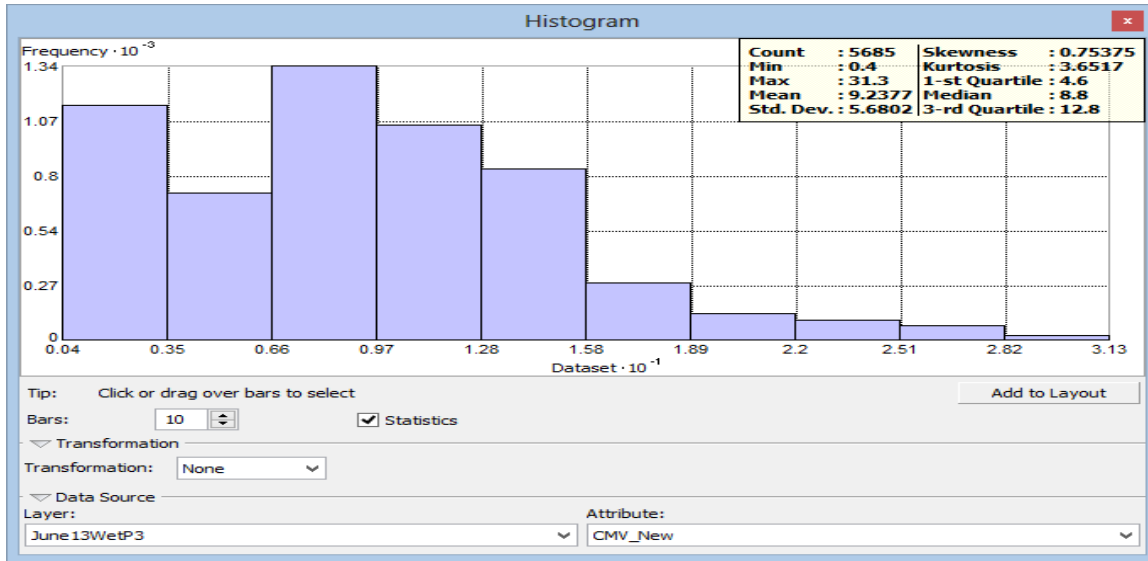


**Figure 5.13 – Histogram of Roller Measurements on IH 35W Subgrade**

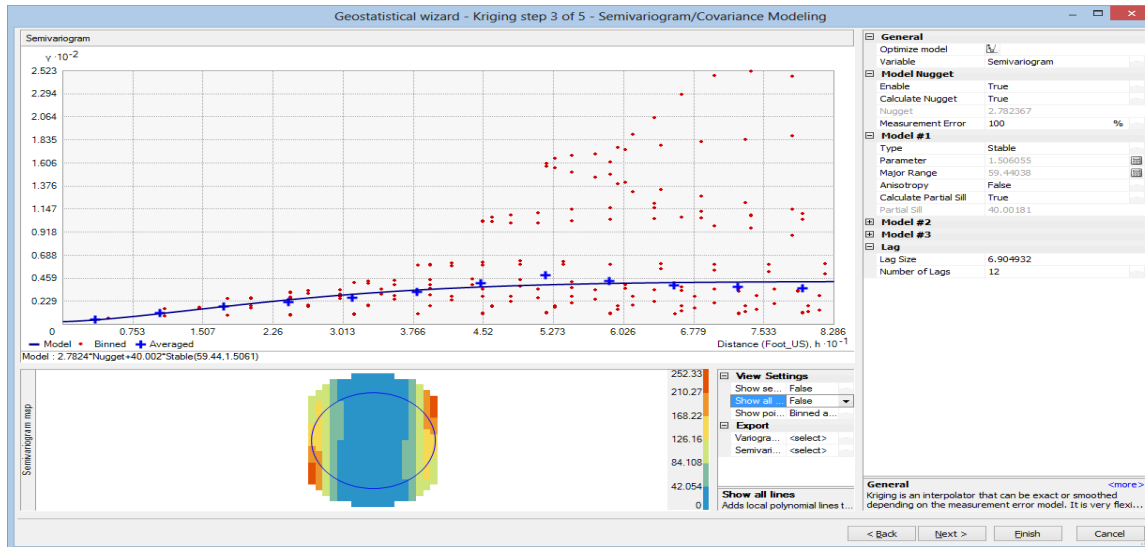


**Figure 5.14 – Semivariogram Constructed with Roller Measurement Values (CMV)**

The kriging predicts the CMV values well with a root mean square (RMS) error of 1.0 and an average standard error of 1.8 for the 3002 data points collected. The measured and the predicted CMVs fit well with a regression function of  $Y = 0.95X + 0.42$  (as seen in Figure 5.15).

The surface interpolation created from the kriging that employs the semivariogram model shows the spatial variation of the CMV which can be useful in determining under- or over-compacted areas

(Figure 5.16). Figure 5.17 is the hill shade relief illustrating 3D variation for the roller CMV values which is useful for visual inspection.

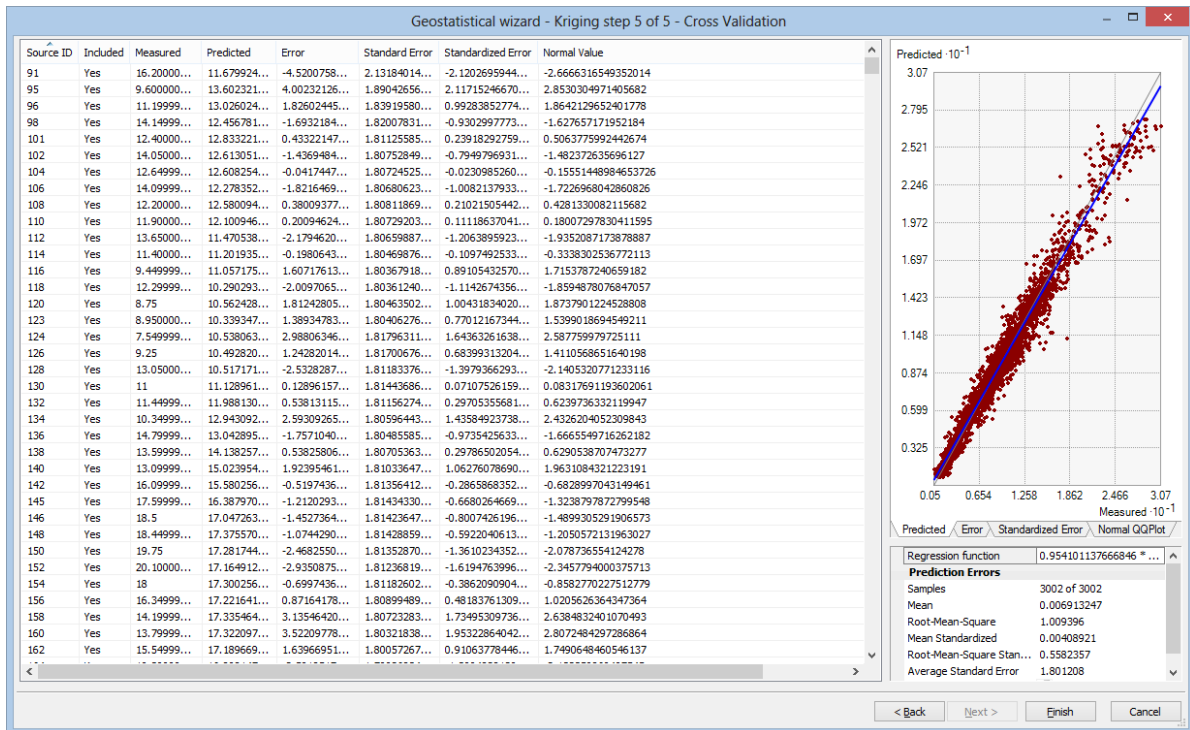


Figure 5.15 – Comparison of Data Predicted Using Kriging and Observed

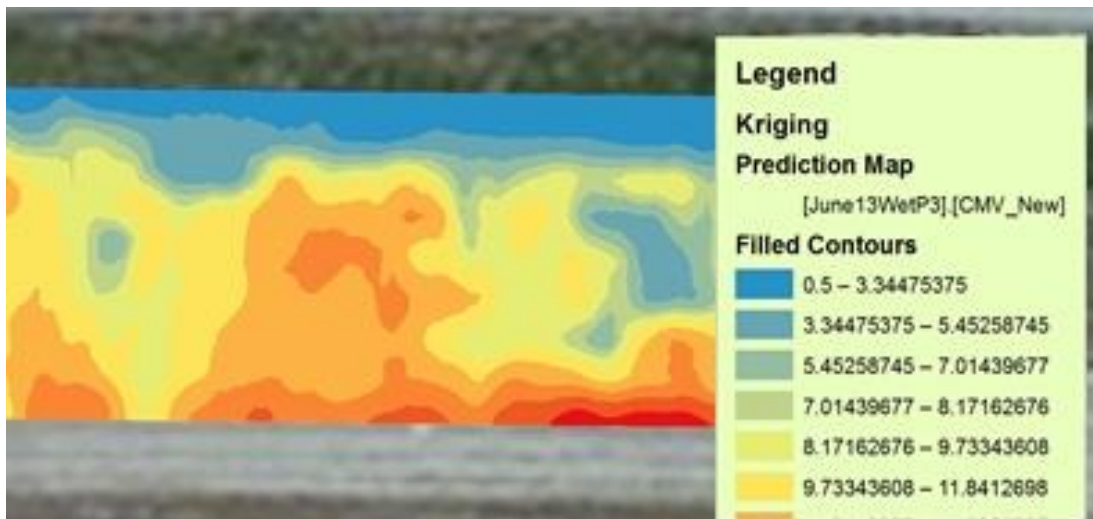
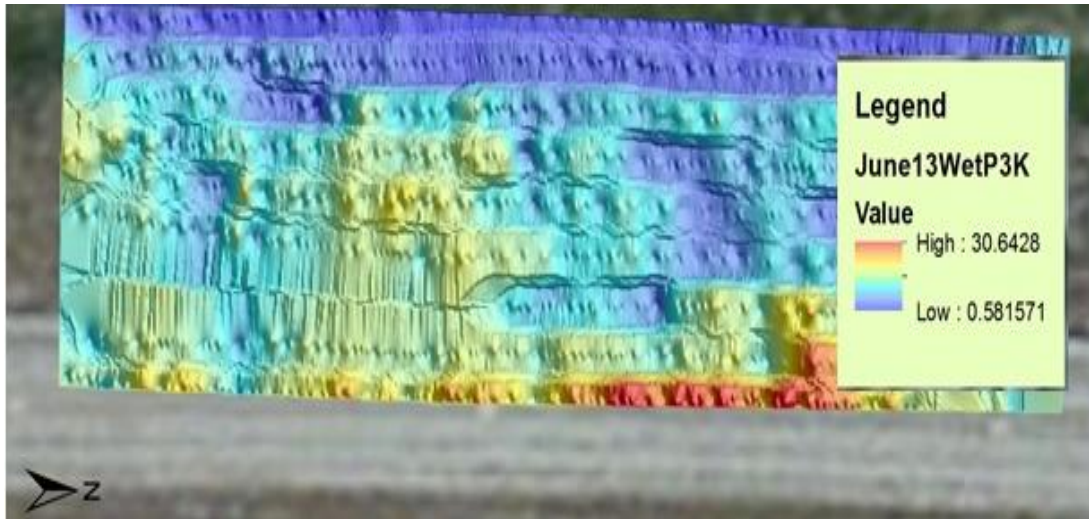
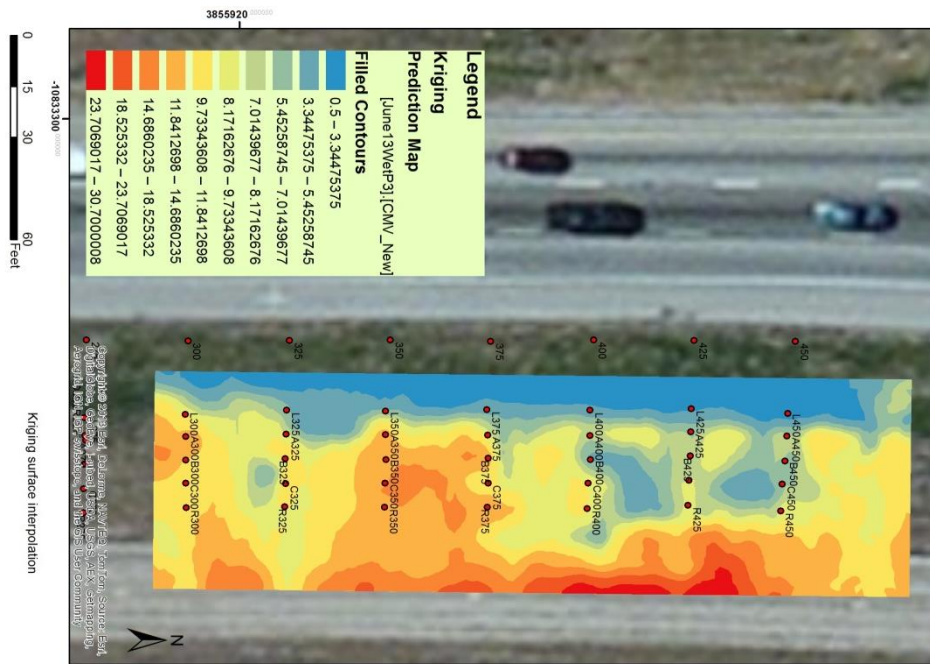


Figure 5.16 – Kriging Method to Identify the Weak Locations



**Figure 5.17 – Variation in Roller Measurements Using Kriging**

The kriged surface of the CMV data provides the means to determine the under-compacted areas that the traditional spot test can potentially miss. Figure 5.18 shows the distribution of the spot test points on the section. The blue colored under-compacted areas of the kriged surface in the center of the strip were not sampled. This indicates the importance of the almost real-time availability of such a map so that the inspector can conduct an informed testing of the section.



**Figure 5.18 – Kriged Surface with Spot Test Points**

### Training

The rolling pattern and roller parameters have significant influence on the roller measurements (as mentioned in Chapter 2). The variations in these parameters influence the correlation between the spot test and roller measurements. Training the roller operator and contractor to adopt the best practices will help to minimize the challenges of IC implementation.

## Chapter 6

# Modification of Prototype Specification

### Introduction

Chapters 4 and 5 documented the practical challenges, field studies and data analyses. Based on the field experience and documented literature, this chapter highlights the supporting information for the modification of the prototype specification as reported in Appendix C and D. Appendix E presents the proposed modified prototype specification.

### Traditional Tests and Sampling Frequencies

The selection of the NDT devices depends on the variability, sensitivity to construction anomalies and the levels of risk to the contractor and TxDOT. The variability analyses of different NDT measurements on different layers were reported in Chapter 4. Mazari et al. (2013) studied the precision and bias of several of the NDT devices used in this study. Table 6.1 summarizes the results of that study. Furthermore, Mazari et al. (2013) determined the sources of the variability in Table 6.1 for each device. As reflected in Table 6.2, aside from the repeatability and reproducibility, about 69 to 78% of estimated modulus variability is due to the variability in the specimens' moisture content and density.

**Table 6.1 - Analyses of Variability of Modulus-Based Devices**

| Measurement Device | Mean of Modulus Measurements, ksi | Equipment Variation, $\sigma$ due to Repeatability, ksi** | Operator Variation, $\sigma$ due to Reproducibility, ksi | Combined Device Variation, Gauge R&R, ksi | Specimen Variation, SV, ksi | Total Variation, TV, ksi | COV* of Total Variation, % |
|--------------------|-----------------------------------|---|--|---|-----------------------------|--------------------------|----------------------------|
| LWD                | 2.67                              | 0.08 (3%)   | 0.33 (12%)   | 0.34 (13%)                                | 0.65 (24%)                  | 0.73                     | 28                         |
| PSPA               | 22.33                             | 3.22 (14%)  | 1.09 (5%)  | 3.40 (15%)                                | 5.36 (24%)                  | 6.35                     | 29                         |
| Geogauge           | 6.21                              | 0.71 (11%)  | 0.44 (7%)  | 0.84 (14%)                                | 1.28 (21%)                  | 1.52                     | 24                         |

Confidence level = 95%, Study variation =  $\pm 6\sigma$ ,  $\sigma$  = standard deviation, No. of specimens = 18, No. of operators = 2, No. of measurement repetitions = 9, COV = Coefficient of Variation

**Table 6.2 - Contribution of each Variability Parameter to the Total Variability of the Modulus-Based Devices**

| Measurement Device | Equipment Variation (Repeatability) Proportion, % | Operator Variation (Reproducibility) Proportion, % | Combined R&R Proportion, % | Specimen Variation Proportion, % |
|--------------------|---|--|----------------------------|----------------------------------|
| LWD                | 1   | 20   | 22                         | 78                               |
| PSPA               | 26  | 3  | 29                         | 71                               |
| Geogauge           | 22  | 8  | 31                         | 69                               |

The following equation can be used to estimate the sample size, n (Burati et al., 2004):

$$n = \frac{(Z_\alpha + Z_\beta)^2 \sigma^2}{e^2} \quad (6.1)$$

where  $\alpha$  = Type I (contractor's) risk,  $\beta$  = Type II (owner's) risk,  $Z_\alpha$  = the  $(1 - \alpha)$ th percentile of the standard normal distribution,  $Z_\beta$  = the  $(1 - \beta)$ th percentile of the standard normal distribution,  $\sigma$  = standard deviation, and  $e$  = tolerable error. Typically,  $\sigma$  is an approximation of the variability of the modulus of the compacted geomaterials tested by each device. The overall pattern of the sample size based on different  $\alpha$  and  $\beta$ ,  $\sigma$  and  $e$  is presented in Figure 6.1. Parameter  $e$  is assumed to be equal to 1.5 times  $\sigma_t$  (i.e., total variation in Table 6.1) and  $\sigma$  is assumed to be equal to  $\sigma_{\text{Gauge}}$  (combined device variation). Based on the values reported in Table 6.1 for  $\sigma_t$  and  $\sigma_{\text{Gauge}}$  for each device, the number of samples necessary per lot for a given level of  $\alpha$  and  $\beta$  can be estimated. AASHTO (1984) categorizes projects into four groups (critical, major, minor and contractual) with corresponding  $\alpha$  and  $\beta$  values shown in Figure 6.1. Using  $\alpha=5.0\%$  and  $\beta=0.5\%$  (critical project), the sample sizes necessary are five for LWD, six for PSPA and seven for Geogauge. Such a study for the NDG was not carried out by Mazari et al. However, based on the known precision and bias of the NDG, this number of samples seems reasonable. The density of the measurement sampling with the IC rollers seems to be reasonable given the uncertainties in the geospatial information from the GPS.

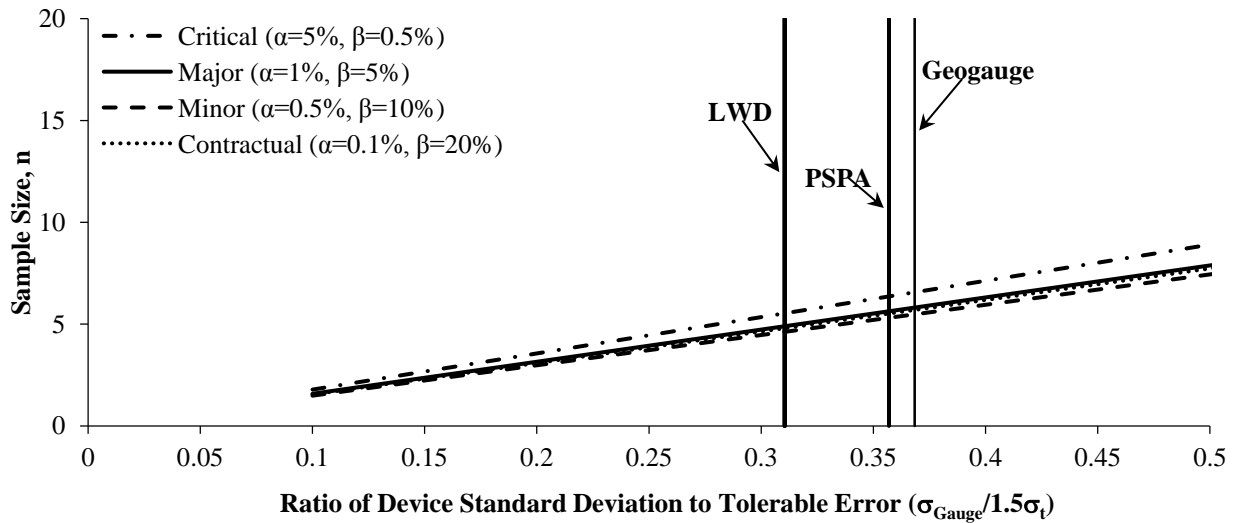


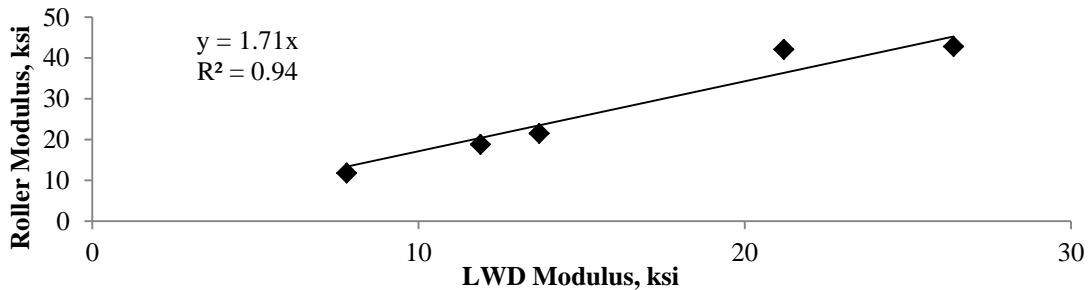
**Figure 6.1 - Suggested Sample Size for Different Devices**

### Means of Setting Target Values

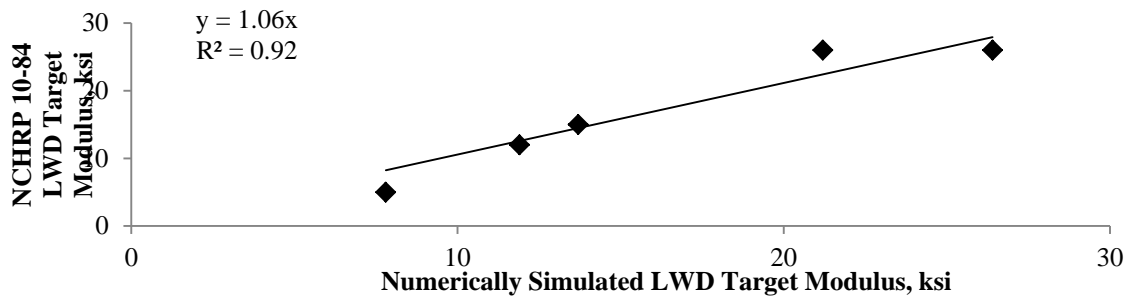
Nazarian et al. (2012), under NCHRP Project 10-84, proposed procedures for estimating the target values for the modulus-based devices such as LWD and PSPA (see Chapter 2). The estimated target values, assuming that the materials are placed at the OMC, are summarized in Table 6.3. Unfortunately, the estimation of the target CMV or MDP in that manner is not possible, since these parameters are estimated empirically. However, as discussed in Chapter 3, the target stiffness  $k$ , proposed by some IC roller manufactures can be estimated using the soil-roller interaction. As shown in Table 6.3 and Figure 6.2, the roller target moduli are about 1.7 times greater than the corresponding target moduli estimated for the LWD device. This can be attributed to the interaction of the devices with the soil, the methods of analysis and the depths of influence of different devices. As seen in Figure 6.3, a strong relation ( $R^2 = 0.9$ ) exists between the numerically-simulated LWD modulus and the modulus estimated using the process developed by Nazarian et al. (2012) for the LWD.

**Table 6.3 - Estimated Target Moduli of the Different Devices**

| Material                     | Device      | Estimated Target Modulus, ksi |                               |
|------------------------------|-------------|-------------------------------|-------------------------------|
|                              |             | Based on NCHRP 10-84          | Based on Numerical Simulation |
| SH 267 Subgrade A            | PSPA, ksi   | 81                            | N/A                           |
|                              | LWD, ksi    | 15                            | 14                            |
|                              | Roller, ksi | N/A                           | 21                            |
| SH 267 Subgrade B            | PSPA, ksi   | 53                            | N/A                           |
|                              | LWD, ksi    | 12                            | 12                            |
|                              | Roller, ksi | N/A                           | 19                            |
| SH 267 Base                  | PSPA, ksi   | 116                           | N/A                           |
|                              | LWD, ksi    | 26                            | 21                            |
|                              | Roller, ksi | N/A                           | 42                            |
| SH 267 Lime-Treated Subgrade | PSPA, ksi   | 154                           | N/A                           |
|                              | LWD, ksi    | 26                            | 26                            |
|                              | Roller, ksi | N/A                           | 43                            |
| IH 35W Subgrade              | PSPA, ksi   | 50                            | N/A                           |
|                              | LWD, ksi    | 5                             | 8                             |
|                              | Roller, ksi | N/A                           | 12                            |



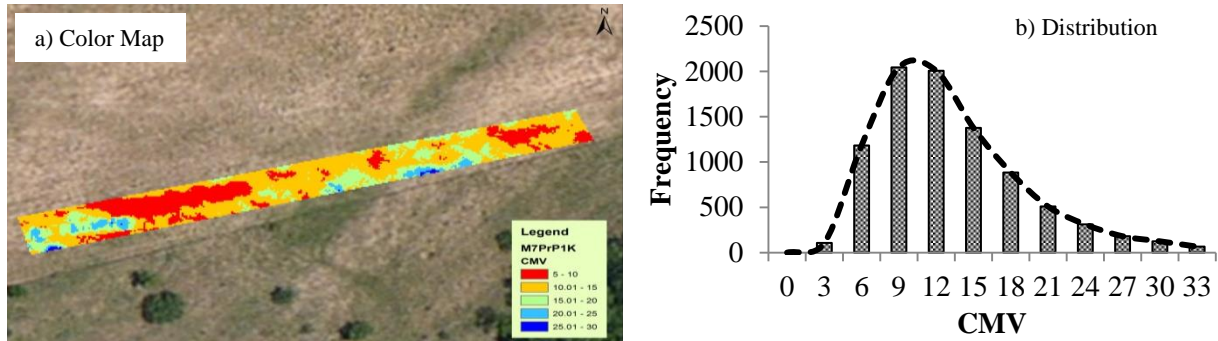
**Figure 6.2 -Relation of Simulated Roller and LWD Moduli**



**Figure 6.3 -Relation of the Simulated and NCHRP 10-84 Estimated LWD Moduli**

Two alternative means of setting target values for the IC rollers can be considered. The first approach is to set the target values based on test beds as discussed in Chapters 4 and 5. The concern with that process is the time necessary to construct the test beds. This matter becomes more critical when the source of the material varies reasonably frequently. In addition, the test strip process cannot account for the natural spatial variability of the underlying layers.

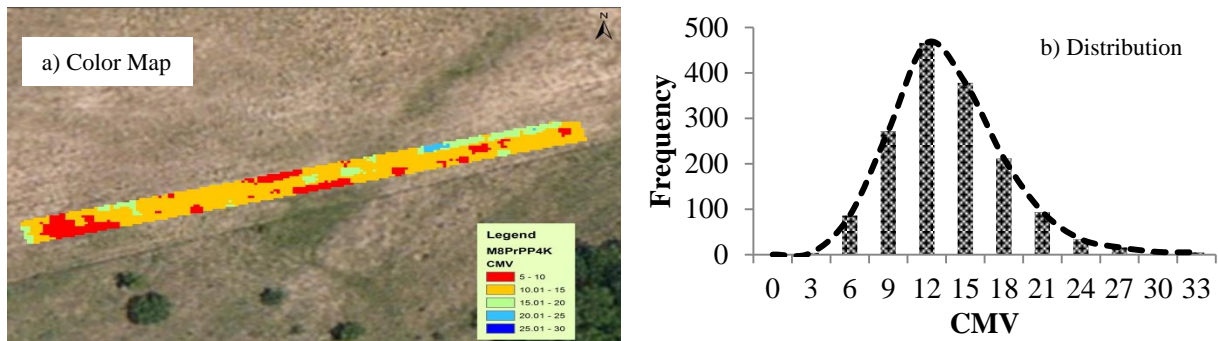
An alternative approach is to map the existing layer before compacting any new layer and then to estimate the contribution of the new layer to the stiffness of the section. This method is described through an example. Figure 6.4a shows the CMV color map of the production section from the SH 267 site before the next subgrade layer was placed. The statistical distributions of the CMVs are shown in Figure 6.4b. The average CMV is about 12 with a standard deviation of 7. With a coefficient of variation of 57%, the section cannot be strictly considered uniform.



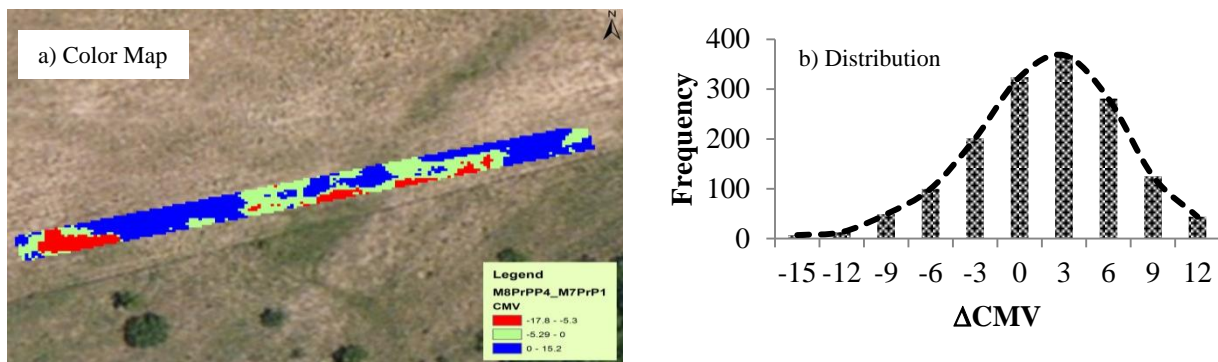
**Figure 6.4 - Variation of the CMV before Lift Placement**

Figure 6.5 contains the CMV color map and statistical distribution of the CMV for the same section after the placement and compaction of a 12-in. thick layer of subgrade with similar soil. The average CMV in this case is about 12 with a standard deviation of 4 (COV of 36%). The following two desirable aspects of proper compaction can be observed in these statistics:

- The average CMVs before and after compaction are similar. Since the foundation and new layers were constructed from similar materials, one can assume that for the most part the optimal compaction of the new lift was carried out.
- The COV of CMVs of the new lift is less than the COV of the foundation, indicating that a more uniform pavement system was achieved.



**Figure 6.5 - Variation of the CMV after Placement and Compaction of the Next Lift**



**Figure 6.6 - Variation of the Differences in CMVs ( $\Delta$ CMV) After Placement and Compaction of the Next Lift and Foundation Layer**

The color map and statistical variation of point-by-point differences between the CMVs,  $\Delta$ CMVs, of the foundation layer and the compacted lift are included in Figure 6.6. A positive  $\Delta$ CMV indicates that the stiffness has improved, which can be translated to an effective compactive effort. One can surmise that an area with negative  $\Delta$ CMV has not been compacted as effectively. To accommodate the uncertainty in the GPS information and CMV measurements, a marginal point is defined as a point with a  $\Delta$ CMV between zero and minus one standard deviation ( $-\sigma$ ) of  $\Delta$ CMVs. With these criteria, the contractor can rework the (red color) areas and the inspector can focus the acceptance tests in the areas that are less stiff than anticipated. To quantify the percentage of areas with acceptable and marginal compaction, the distribution shown in Figure 6b can be translated to cumulative distribution as shown in Figure 6.7. As marked in the figure, about 55% of the section passes and about 82% is acceptable or better.

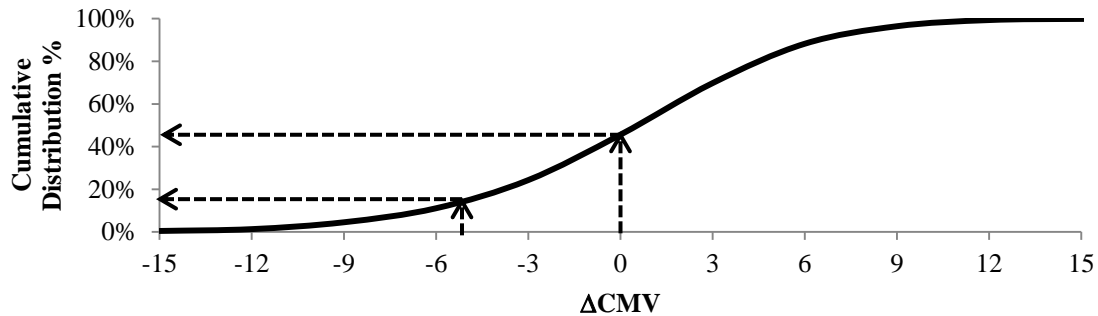


**Figure 6.7 - Variation of the Differences in the CMVs ( $\Delta$ CMV) After Placement and Compaction of the Next Lift and Foundation Layer**

An ideal acceptable compacted section not only has to achieve adequate compaction but has to be uniform as well. It is recommended that for embankment construction the target CMV for each subsequent lift to be set as the average CMV of the corresponding layer. With this target value, color maps similar to Figure 6.5a will be available to the inspector to make sure that the target is met or exceeded. Color maps similar to Figure 6.6a can be used by the contractor to control the quality of the compaction process and the inspector to make a decision about the acceptance of the compaction. The best option is to further compact the red-colored areas in Figure 6.6a for a more uniform section or conduct the acceptance tests within those areas to ensure that the desired quality is achieved.

Different approaches were evaluated to assess the compaction quality with the NDT devices and roller measurement values. The different approaches adopted are as follows:

- Assess the quality of compaction of the foundation layer based on either target density or target modulus, and
- Establish the percent passing based on the lift contribution (i.e.,  $\Delta$ CMV) as discussed above.

The results from the above approaches for different sections and material types studied are presented in Tables 6.4 and 6.5.

**Density Criteria:** Due to the lack of availability of an NDG, densities were not measured on the foundation layers of the subgrade OMC and production sections of the SH 267 site. The foundation/supporting layers for all other subgrade and base sections before the placement of the next lift achieved the required density. The dry and wet subgrade sections achieved 100% compaction. In the case of the OMC and production subgrade sections, the percentage points that strictly achieved the target densities are 42% and 90%, respectively. However, most of the points marginally failed the 95% relative density as judged by their COVs of 3% and less in Table 6.2. For the SH 267 base sections, while 80% of the points tested along the wet sections achieved 100% relative compaction, 10% or less of the points on the dry and optimum sections achieved 100% relative compaction. However, in most cases in all three

**Table 6.4 - Descriptive Statistics of the NDT Devices on the Different Sections of SH 267 Site**

| Section               |            | Device           | NDT Test Approach on Support layer (Embankment/ Subgrade) | NDT Test Approach on Layer of Interest |                         | Roller Measurement Difference Approach, $\Delta$ CMV/ $\Delta$ MDP |                 |
|-----------------------|------------|------------------|---|--|-------------------------|--|-----------------|
|                       |            |                  | Percent Passing   | Percent Passing                        | Equivalent Roller Value | Percent Marginal   | Percent Passing |
| Subgrade              | Dry        | Dry Density, pcf | 100   | 100                                    | N/A                     | 32   | 50              |
|                       |            | LWD, ksi         | 67  | 38                                     | 14                      |  |                 |
|                       |            | PSPA, ksi        | 100   | 90                                     | 6                       |  |                 |
|                       | OMC        | Dry Density, pcf | N/T   | 42                                     | 11                      | 31   | 58              |
|                       |            | LWD, ksi         | 83  | 17                                     | 14                      |  |                 |
|                       |            | PSPA, ksi        | 43  | 18                                     | 14                      |  |                 |
|                       | Wet        | Dry Density, pcf | 100   | 100                                    | N/A                     | 37   | 5               |
|                       |            | LWD, ksi         | 83  | 5                                      | 12                      |  |                 |
|                       |            | PSPA, ksi        | 100   | 42                                     | 7                       |  |                 |
|                       | Production | Dry Density, pcf | N/T   | 90                                     | 7                       | 27   | 55              |
|                       |            | LWD, ksi         | N/T   | 65                                     | 8                       |  |                 |
|                       |            | PSPA, ksi        | N/T   | 42                                     | 13                      |  |                 |
| Base                  | Dry        | Dry Density, pcf | 100   | 0                                      | N/A                     | 20   | 70              |
|                       |            | LWD, ksi         | 60  | 35                                     | 35                      |  |                 |
|                       |            | PSPA, ksi        | 85  | 42                                     | 35                      |  |                 |
|                       | OMC        | Dry Density, pcf | 100   | 10                                     | 45                      | 25   | 45              |
|                       |            | LWD, ksi         | 83  | 29                                     | 34                      |  |                 |
|                       |            | PSPA, ksi        | 50  | 52                                     | 27                      |  |                 |
|                       | Wet        | Dry Density, pcf | 100   | 80                                     | 35                      | 12   | 80              |
|                       |            | LWD, ksi         | 100   | 10                                     | 90                      |  |                 |
|                       |            | PSPA, ksi        | 62  | 16                                     | 80                      |  |                 |
| Lime Treated Subgrade |            | Dry Density, pcf | N/T   | 100                                    | N/A                     | 16   | 4               |
|                       |            | LWD, ksi         | 72  | 11                                     | 11                      |  |                 |
|                       |            | PSPA, ksi        | 57  | 100                                    | N/A                     |  |                 |

\* N/T = Not tested

**Table 6.5 - Descriptive Statistics of the NDT Devices on the Different Sections of IH 35W Site**

| Section | Device           | NDT Test Approach on Support layer (Embankment /Subgrade) | NDT Test Approach |                         | Roller Measurement Difference Approach |                 |
|---------|------------------|---|-------------------|-------------------------|--|-----------------|
|         |                  | Percent Passing   | Percent Passing   | Equivalent Roller Value | Percent Marginal                       | Percent Passing |
| Dry     | Dry Density, pcf | 100   | 100               | N/A                     | 20                                     | 62              |
|         | LWD, ksi         | 70  | 43                | 147                     |  |                 |
|         | PSPA, ksi        | 42  | 45                | 147                     |  |                 |
| OMC     | Dry Density, pcf | 100   | 100               | N/A                     | N/A                                    | N/A             |
|         | LWD, ksi         | 59  | 45                | 12                      |  |                 |
|         | PSPA, ksi        | 60  | 23                | 14                      |  |                 |
| Wet     | Dry Density, pcf | 100   | 100               | N/A                     | N/A                                    | N/A             |
|         | LWD, ksi         | 34  | 20                | 13                      |  |                 |
|         | PSPA, ksi        | 30  | 5                 | 20                      |  |                 |

sections, the densities exceeded 95% relative compaction. As reflected in Table 6.5, the densities measured after the completion of the compaction at all points exceeded the target density for the IH 35W site.

**LWD Criteria:** The LWD, similar to the IC roller but to a lesser depth, measures the stiffness of the lift of interest as well as the underlying foundation layer. About 67% to 83% of the points tested on the foundation layer at the SH 267 site before placing the subgrade lift exceeded the target modulus established for the LWD testing. After the compaction of the subgrade, 38%, 17% and 5% (for the dry, OMC, and wet sections, respectively) of the points tested exceeded the target modulus (see Table 6.4). This pattern signifies the importance of moisture control during compaction. About 65% of the points tested on the production section at the SH 267 site exceeded the target modulus. Based on field observation at the time of testing, the heavy construction traffic running on this area during and shortly after compaction could have contributed to a stiffer section relative to the three test sections.

As reflected in Table 6.5, the foundation layer under the three test sections on the IH 35W project varied significantly. The foundation layer under the dry section was the stiffest where 70% of the LWD measurements exceeded the target modulus while the foundation under the wet section was the least stiff with 34% of the test points' moduli exceeding the target modulus. After the placement and compaction of the subgrade layers, the percentage of the points with moduli above the target modulus for the dry, optimum and wet sections were 43, 45 and 20, respectively. Based on the LWD moduli, in addition to the importance of process control during compaction, the importance of improving the stiffness and uniformity of the foundation layer before placing the next lift is apparent.

**PSPA Criteria:** The PSPA measurements supplement the LWD moduli by providing lift-specific moduli. For the SH 267 site, as presented in Table 6.4, moduli of the top 12-in. of at least 43% of the test points on the foundation layer exceed the PSPA target modulus. After the placement and compaction of the subgrade lift, the moduli of the top 12-in. of the dry section are close to the target modulus. Similar to the results from other in-situ tests, the OMC section yields the lowest quality with only 18% of the points achieving the target modulus. For the SH 267 base sections, the moduli of 62% to 85% of the points tested before the placement of the base exceeded the target modulus. However, after the placement and compaction, only 42% (on the dry section) and 16% (on the wet section) of the test points exhibited moduli that met the target value. For the IH 35W project, only 30% (on the wet section) and 60% (on the OMC section) of the foundation spots tested met the target modulus (see Table 6.5). Only 16% (on the wet section) and 45% (on the OMC section) of the points tested after the compaction of the subgrade met the target modulus.

**$\Delta$ CMV Criteria:** The outcomes of the acceptance based on the differences in the roller measurements before and after lift placement and compaction are also reported in Tables 6.4 and 6.5. For the SH 267 subgrade, the percentages of the areas in the acceptable range (marginal plus passing in Tables 6.4 and 6.5) are 82%, 89%, 42% and 82% percent for the dry, OMC, wet and production sections. For the SH 267 base sections, the acceptable areas are 70% to 92% to the areas compacted. For the IH 35W subgrade sections, only the information from the dry section is available as discussed in Chapter 4. In that case, 82% of the compacted area is acceptable.

The results from the different acceptance scenarios are summarized in Figure 6.8. Three out of the seven cases that pass density will not pass the  $\Delta$ CMV criteria (see Figure 6.8a). Since the roller IC values are more an indication of the mechanical properties of the material, it may be more appropriate to compare the results from the  $\Delta$ CMV criteria with the LWD and PSPA criteria. Based on the LWD results, a greater percentage of the area of each section will be acceptable under the  $\Delta$ CMV criteria than the LWD criteria (see Figure 6.8b). The same pattern is observed for the PSPA results in Figure 6.8c. Based on this discussion, it seems that the  $\Delta$ CMV criteria may be a reasonable yet practical means of controlling the

compaction quality. As more experience is gained by the contractors and TxDOT personnel, the acceptance criteria using this method can be tightened.

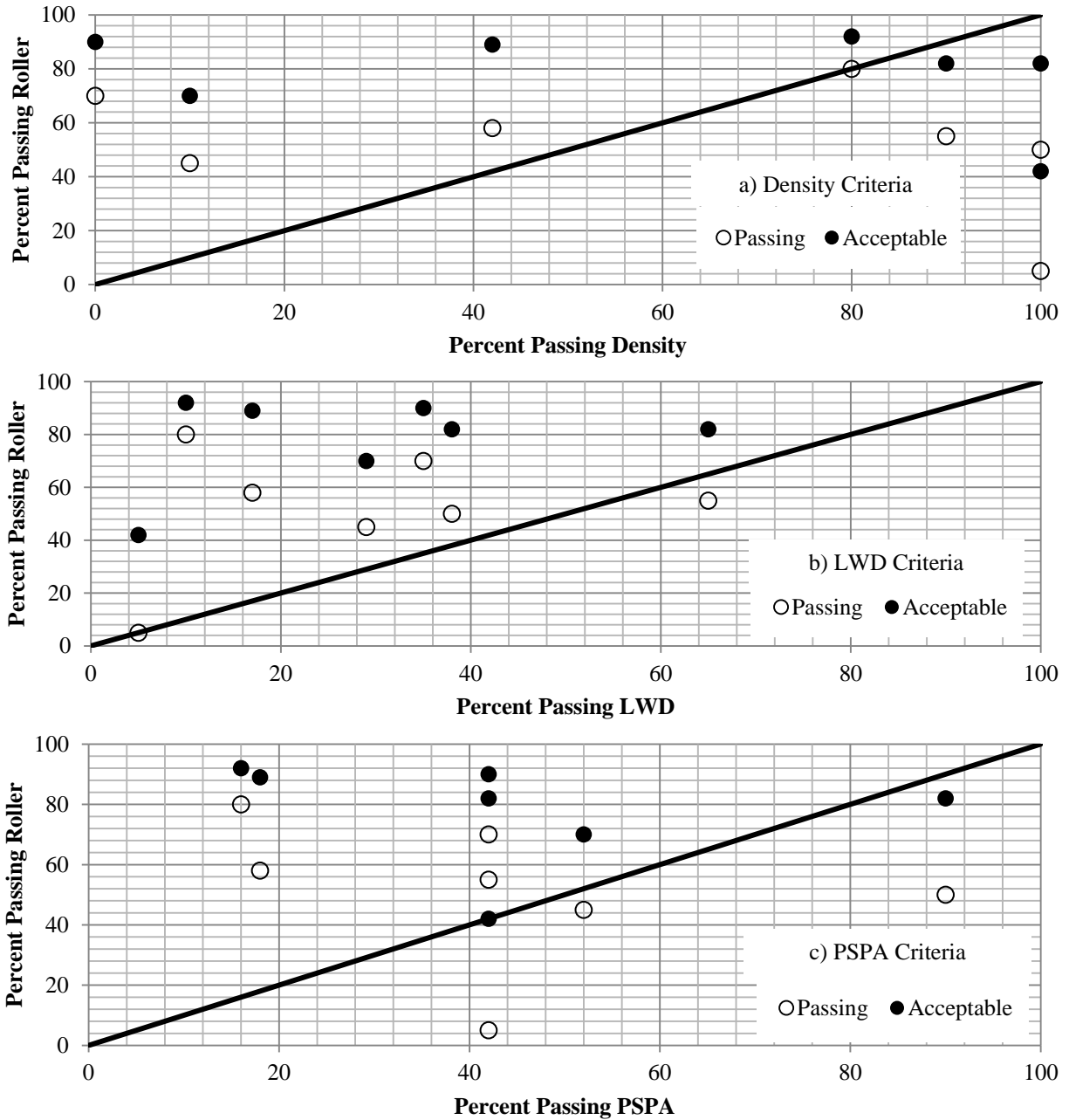


**Figure 6.8 – Comparison of the Different Acceptance Scenarios**

## Chapter 7

### Conclusions and Recommendations

The use of intelligent compaction is aimed to achieve uniformity in compaction of pavement layers, to improve the quality of construction, and to enhance the performance of pavements with reduced cost of construction. In this research project, the use of intelligent compaction was evaluated at two sites on three different materials. The compaction characteristics of three types of subgrade soils, base material and a lime treated subgrade layer were studied at varying moisture levels. Two different types of roller measurement values and five density and modulus-based NDT devices were used to study the compaction properties of different soils and base materials. Numerical analysis was carried out to understand the soil roller interaction and measurement depth with different layers.

Based on the knowledge gained so far, the following observations were made and conclusions were drawn:

- From the laboratory investigations, it is observed that irrespective of the soil types, the modulus decreases drastically when tested towards the wet side of the OMC.
- Based on numerical analyses, depth of influence in terms of stress due to roller compaction increases as the base becomes stiffer, while the contribution of subgrade modulus to the depth of influence is less significant. The influence depth for roller compaction based on 10% of the surface peak stress varies from 19 in. to 38 in. for two-layer systems; however, it can be as deep as 50 in. for weak subgrades as single layers. Base thickness impact on depth of influence is small except for a weak subgrade (5 ksi). The depth of influence for the LWD shows trends similar to the roller compaction with influence depths of about 12 in. shallower than the roller.
- Depth of influence in terms of displacement using the surface vertical deformation at the center of the load occurs at depths of 73 in. to 85 in. for roller compaction. Base and subgrade moduli have a slight impact on the influence depth. The base thickness has no significant impact on influence depth. In single layer systems, the depth of influence decreases to 60 in. for a weak subgrade due to the large surface deflections. The LWD modeling shows that the influence depth varies with the subgrade and base moduli, ranging from 35 in. to 65 in. in depth for two-layer systems, and is about 40 in. in depth for single layer systems. Trends from numerical analyses between the roller and LWD are not comparable, at least for the two-layer systems.
- The LWD surface deflection modulus,  $E_{LWD}$  has a similar trend to the roller's compaction secant modulus. A linear regression relationship was developed to relate the  $E_{LWD}$  to the secant modulus. No relationship could be established that relates  $E_{LWD}$  to the secant stiffness  $k_s$ .
- Both density- and modulus-based NDT devices exhibited significant spatial variations. The NDG measurements were not sensitive to changes in moisture and compaction as compared to the LWD and PSPA measurements.
- Roller measurement values and NDT measurements were observed to be significantly influenced by the moisture content of the lift being compacted.

- Among the two roller measurement values studied, the machine drive power was observed to be not sensitive to the compaction process as compared to the compaction meter value.
- Estimation of roller target values based on the NDT measurements may pose significant challenge for the implementation of intelligent compaction technology for quality control due to the spatial variability in the ground support conditions, variation in moisture contents and with different measurement depths.
- Calibration of the GPS system and roller measurement sensitivity needs to be checked periodically. The use of the kriging method to interpolate the roller measurement values provides useful information to evaluate the uniformity of the compaction process.
- The alternate method proposed in this study to map the ground condition before and to fix the target values based on the statistics may eliminate the need for the construction of control strips. Also, the difference roller measurement value will help to identify uniformity level and the weak areas for reworking.

## REFERENCES

- AASHTO (1984). "Acceptance Sampling Plans for Highway Construction, AASHTO Materials, Part 43 I Specifications: R-9." American Association of State Highway and Transportation Officials.
- Anderegg, R., and Kaufmann, K. (2004). "Intelligent compaction with vibratory rollers feedback control systems in automatic compaction and compaction control." *Transportation Research Record, Journal of the Transportation Research Board*, 1898, 124-134.
- Anderegg, R., Dominik A. von Felten., and Kaufmann, K. (2006). "Compaction monitoring using intelligent soil compactors." *Geo Congress 2006*, American Society of Civil Engineers, 1-6.
- Briaud, J.L and Seo, J., (2003) "Intelligent compaction: Overview and research needs", Research Report, Texas A&M University, College Station Texas.
- Burati, J. L., Weed, R. M., Hughes, C.S., Hill, H.S. (2003), "Optimal Procedures for Quality Assurance Specifications," Report No. FHWA-RD-02-095, Federal Highway Administration (FHWA), pp. 57-59.
- Cary, C. E., and Zapata, C. E. (2010). "Enhanced model for resilient response of soils resulting from seasonal changes as implemented in mechanistic-empirical pavement design guide." *Journal of the Transportation Research Board, Transportation Research Record*, 2170, pp. 36-44.
- Chang, G., Xu, Q., Rutledge, J., Horan, B., Michael, L., White, D. J., and Vennapusa, P. (2012). "Accelerated implementation of intelligent compaction technology for embankment subgrade soils, aggregate base, and asphalt pavement materials." *Federal Highway Administration, U.S. Department of Transportation*, FHWA-IF-12-002.
- Chiroux, R. C., Foster, W. A., Johnson, C. E., Shoop, S. A., and Raper, R. L. (2005). "Three-Dimensional Finite Element Analysis of Soil Interaction with a Rigid Wheel." *Applied Mathematics and Computation*, 162(2), 707-722.
- Fang, H. (1991). *Foundation engineering handbook*, 2<sup>nd</sup> Ed., Van Nostrand Reinhold, NY, 170-171.
- Gallivan, V. L., Chang, G. K., and Horan, D. R. (2011). "Intelligent compaction for improving roadway construction." *Geotechnical special publication*, American Society of Civil Engineers, 218, 117-124.
- Guler, M., Bosscher, P. J., and Plesha, M. E. (2002). "A Porous Elastoplastic Compaction Model for Asphalt Mixtures with Parameter Estimation Algorithm." *15th ASCE Engineering Mechanics Conference*, Columbia University, New York, NY.
- Hossain, M., Mulandi, J., Keach, L., Hunt, M., and Romanoschi, S. (2006). "Intelligent compaction control." *Airfield and Highway Pavements*, American Society of Civil Engineers, 304-316.
- Hügel, H. M., Henke, S., and Kinzler, S. (2008). "High-Performance Abaqus Simulations in Soil Mechanics." *2008 ABAQUS Users' Conference*, Newport, RI, 1-15.
- Kelm, M. (2003). "Numerische Simulation der Verdichtung kohäsionsloser Böden mit Vibrationswalzen." TU Hamburg-Harburg.
- Khoury, N. N., and Zaman, M. M. (2004). "Correlation between resilient modulus, moisture variation, and soil suction for subgrade soils." *Journal of Transportation Research Board, Transportation Research Record*, 1874, National Research Council, Washington, D.C., pp. 99-107.
- Kim, K. (2010). "Numerical simulation of impact rollers for estimating the influence depth of soil compaction." Texas A&M University.

- Mazari, M., Garcia, G., Garibay, J., Abdallah, I and Nazarian, S. (2013). "Impact of Modulus Based Device Variability on Quality Control Of Compacted Geomaterials Using Measurement System Analysis." 92<sup>nd</sup> Annual Meeting, Transportation Research Board, Washington DC, <http://trid.trb.org/view/2013/C/1241890>.
- Mooney, A. M., and Rinehart, R. V. (2007). "Field monitoring of roller vibration during compaction of subgrade soil." *Journal of Geotechnical and Geoenvironmental Engineering*, American Society of Civil Engineers, 133(3), 257-265.
- Mooney, M. A., Rinehart, R. V., Facas, N. W., Musimbi, O. M., White, D. J., Vennapusa, P. K. R. (2010). "Intelligent soil compaction systems." *National Cooperative Highway Research Program (NCHRP)*, 676, Transportation Research Board.
- Mooney, M., and Adam, D. (2007). "Vibratory roller integrated measurement of earthwork compaction: An overview." *Seventh International Symposium on Field Measurements in Geomechanics (FMGM 2007)*, American Society of Civil Engineers, 1-12.
- Mooney, M., Rinehart, R. V., and Susante, P. (2006). "The influence of heterogeneity on vibratory roller compactor response." *Geo Congress 2006*, American Society of Civil Engineers, 1-6.
- Morrow, M. (2013). "Quality compaction using intelligent compaction rollers." *Special specification*, Texas Department of Transportation, CSJ: 0353-03-059.
- Nazarian, S., Mazari, M., Abdallah, I. N., Puppala, A. J., Mohammad, L. N. (2011). "Modulus-based construction specification for compaction of earthwork and unbound aggregate." NCHRP 10-84 Phase-I Report, Transportation Research Board, Washington, DC.
- Nazarian, S., Mazari, M., Abdallah, I. N., Puppala, A. J., Mohammad, L. N. (2012). "Modulus-based construction specification for compaction of earthwork and unbound aggregate." NCHRP 10-84 Phase-II Report, Transportation Research Board, Washington, DC.
- Pacheco, L.G., and Nazarian, S. (2011). "Impact of moisture content and density on stiffness-based acceptance of geomaterials." In *Journal of Transportation Research Board 90th Annual Meeting session 514*, No. 11-0667. Transportation Research Board, Washington, DC.
- Patrick, J., and Werkmeister, S. (2010). *Compaction of Thick Granular Layers, NZ Transport Agency Research Report No. 411*. New Zealand Transport Agency, Wellington, New Zealand, 40.
- Petersen, D. L., and Peterson, R. (2006). "Intelligent compaction and in-situ testing at MnDOT TH53." *Minnesota Department of Transportation*, MN/RC – 2006-13.
- Petersen, D. L., Erickson, M. L., Roberson, R., and Siekmeier, J. (2007). "Intelligent soil compaction: geostatistical data analysis and construction specifications." *86<sup>th</sup> Annual Meeting of the Transportation Research Board*, Annual Meeting CD-ROM.
- Petersen, D. L., Siekmeier, J., Nelson, C. R., and Peterson, R. L. (2006). "Intelligent soil compaction technology results and a roadmap toward widespread use." *Transportation Research Record, Journal of the Transportation Research Board*, 1975, 81-88.
- Puppala, A.J., (2008), "Estimating Stiffness of Subgrade and Unbound Materials for Pavement Design," NCHRP Synthesis 382, Transportation Research Board, Washington, DC.
- Rahman, F., Hossain, M., Hunt, M. M., and Romanoschi, S. A. (2007). "Intelligent compaction control of highway embankment soil." *86<sup>th</sup> Annual Meeting of the Transportation Research Board*, Annual Meeting CD-ROM.
- Rahman, F., Hossain, M., Romanoschi, S. A., and Brennan, J. (2012). "Kansas experience with stiffness-based quality control/quality assurance specifications for compaction of highway embankments." *Geo Congress 2012*, American Society of Civil Engineers, 1522-1561.

- Richter, C., (2006). "Seasonal variations in the moduli of unbound pavement layers." Publication No. FHWA-HRT-04-079, Turner – Fairbanks Highway Research Center, McLean, Va.
- Rinehart, R. V. and Mooney, M. A. (2009). "Measurement depth of vibratory roller-measured soil stiffness." *Geotechnique*, 8, 101-111.
- Rinehart, R. V., Mooney, M. A., Facas, N. F., and Musimbi, O. (2012). "Examination of roller-integrated continuous compaction control on a Colorado test site." *91<sup>st</sup> Annual Meeting of the Transportation Research Board*, Annual Meeting CD-ROM.
- Sebesta, S. D., Scullion, T., Taylor, R. J., and Frazier, J. T. (2012) "Alternative methods of flexible base compaction acceptance." Texas Transportation Institute, Research report No. 0-6587-1, The Texas A&M University System, College Station, TX.
- Siekmeier, J. A. (2011). "Unsaturated soil mechanics implementation during pavement construction quality assurance." proceedings of *59<sup>th</sup> Annual Geotechnical Engineering Conference*, St. Paul, MN.
- Ter Huerne, H. L. (2004). "Compaction of Asphalt Road Pavements Using Finite Elements and Critical State Theory." University of Twente, Enschede, the Netherlands.
- Terzaghi, K., and Peck, R. B. (1967). *Soil Mechanics in Engineering Practice*, 2<sup>nd</sup> Ed., John Wiley & Sons, Inc., NY, 281–283.
- Vennapusa, K. R. P., White, D.J., and Morris, M. D. (2010). "Geostatistical analysis for spatially referenced roller-integrated compaction measurements." *Journal of Geotechnical and Geoenvironmental Engineering*, American Society of Civil Engineers, 136(6), 813-822.
- Von Quintus, H. L., Rao, C., Bhattacharya, B., Titi, H., and English, R. (2010). "Evaluation of intelligent compaction technology for densification of roadway subgrades and structural layers." Submitted to the Wisconsin Highway Research Program (WHRP), Draft Final Report.
- Wang, L., Zhang, B., Wang, D., and Yue, Z. (2007). "Fundamental Mechanics of Asphalt Compaction through FEM and DEM Modeling." *Analysis of Asphalt Pavement Materials and Systems Analysis: Engineering Methods, GSP 176*, L. Wang and E. Masad, eds., American Society of Civil Engineers, Boulder, CO, 45–63.
- White, D. J., and Thompson, M. J. (2008). "Relationships between in situ and roller-integrated compaction measurements for granular soils." *Journal of Geotechnical and Geoenvironmental Engineering*, American Society of Civil Engineers, 134(12), 1763-1770.
- White, D. J., Jaselskis, E. J., Schaefer, V. R., and Cackler, E. T. (2005). "Real-time compaction monitoring in cohesive soils from machine response." *Transportation Research Record, Journal of the Transportation Research Board*, 1936, 173-180.
- White, D. J., Morris, M., and Thompson, M. J. (2006). "Power-based compaction monitoring using vibratory pad foot roller." *Geo Congress 2006*, American Society of Civil Engineers, 1-6.
- White, D. J., Thompson, M. J., Vennapusa, P., and Siekmeier, J. (2008). "Implementing intelligent compaction specification on Minnesota TH-64 synopsis of measurement values, data management, and geostatistical analysis." *Transportation Research Record, Journal of the Transportation Research Board*, 2045, 1–9.
- White, D. J., Vennapusa, P., and Gieselman, H. (2011). "Field assessment and specification review for roller-integrated compaction monitoring technologies." *Advances in Civil Engineering*, 2011,1-15.
- White, D. J., Vennapusa, P., Zhang, J., Gieselman, H., and Morris, M. (2009). "Implementation of intelligent compaction performance based specifications in Minnesota." *Minnesota Department of Transportation, MN/RC – 2009-14*.

- Xia, K. (2011). "Finite element modeling of tire/terrain interaction: Application to predicting soil compaction and tire mobility." *Journal of Terramechanics*, ISTVS, 48(2), 113–123.
- Xia, K., and Pan, T. (2010). "Understanding Vibratory Asphalt Compaction by Numerical Simulation." *International Journal of Pavement Research and Technology*, 4(3), 185–194.
- Xu, Q., Chang, G. K., Gallivan, V. L., and Horan, R. D. (2012). "Influences of intelligent compaction uniformity on pavement performances of hot mix asphalt." *Construction and Building Materials*, Elsevier Ltd, 30, 746–752.

## **Appendix A**

### **FIELD EVALUATION CASE STUDY (SH 267)**

# FIELD EVALUATION CASE STUDY: SH 267

## A.1 Introduction

This Appendix presents the comprehensive data analysis carried out from the field studies on SH 267 for subgrade, base and lime treated layers.

## A.2 Evaluation of Moisture-Density Devices

**Embarkment:** The variations of the average moisture contents of the embankment measured with the SDG and NDG before the placement of subgrade are depicted in Figure A.2.1. The averages of the device readings from Lines A and C are shown for all three sections. The NDG data were not collected along the third section because of time constraints between construction phases. The overall average moisture content of the embankment from the SDG was 9.3% and from the NDG was 9.4%, which was about 7% less than the OMC from the standard Proctor tests.

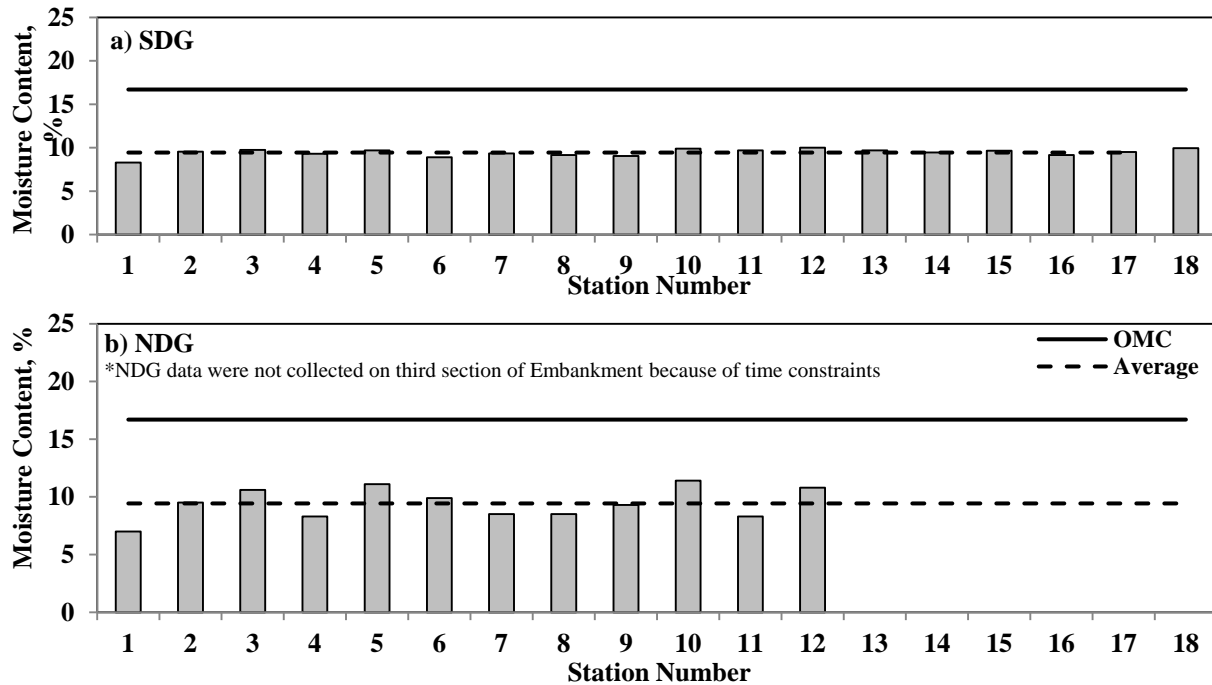


**Figure A.2.1 – Spatial Variations of SDG and NDG Moisture Contents of Embankment**

Figure A.2.2 summarizes the dry densities measured with the SDG and NDG. The average dry density from the SDG was 88.7 pcf, while the average dry density estimated with the NDG was 115.8 pcf. The SDG results seem low based on the condition of the site. The embankment passed the density specification limit of 95% of MDD based on the NDG results.

**Subgrade Layer:** The average SDG and NDG moisture contents (average of the three readings from lines A, B and C) measured on top of the subgrade are summarized in Figure A.2.3 for all sections. The first and last rows of the compacted subgrade sections were not considered in the analysis to eliminate the effects of the construction boundaries. The SDG results do not reflect the changes in the moisture contents among the three sections (see Figure A.2.3a). As illustrated in Figure A.2.3b, the NDG results reflect the variations in moisture contents among different sections. The average NDG moisture content of the dry section was 12.8% (3.9% dry of OMC), the wet section was 18.3% (1.6% wet of OMC) and the optimum section was 17.6% (0.7% wet of OMC). Based on the NDG results, moisture contents of the test sections are close to their nominal values (dry of OMC, wet of OMC and close to OMC).

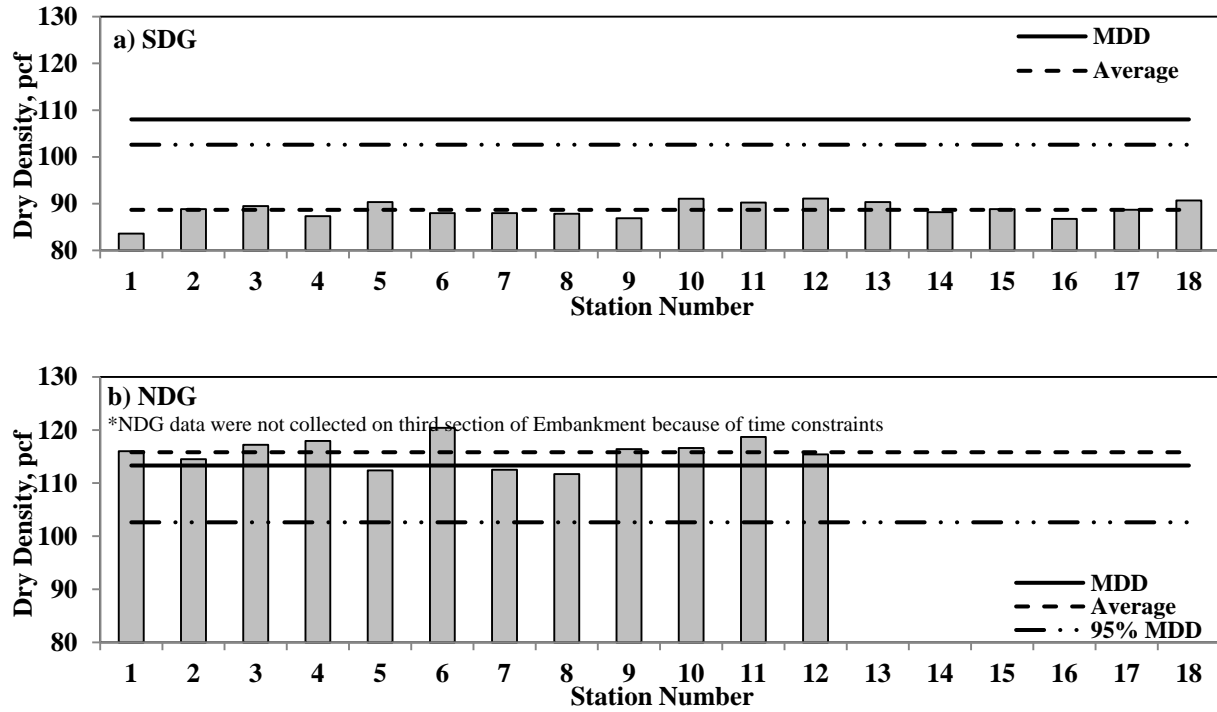


Figure A.2.2 – Spatial Variations of SDG and NDG Dry Densities of Embankment Layer

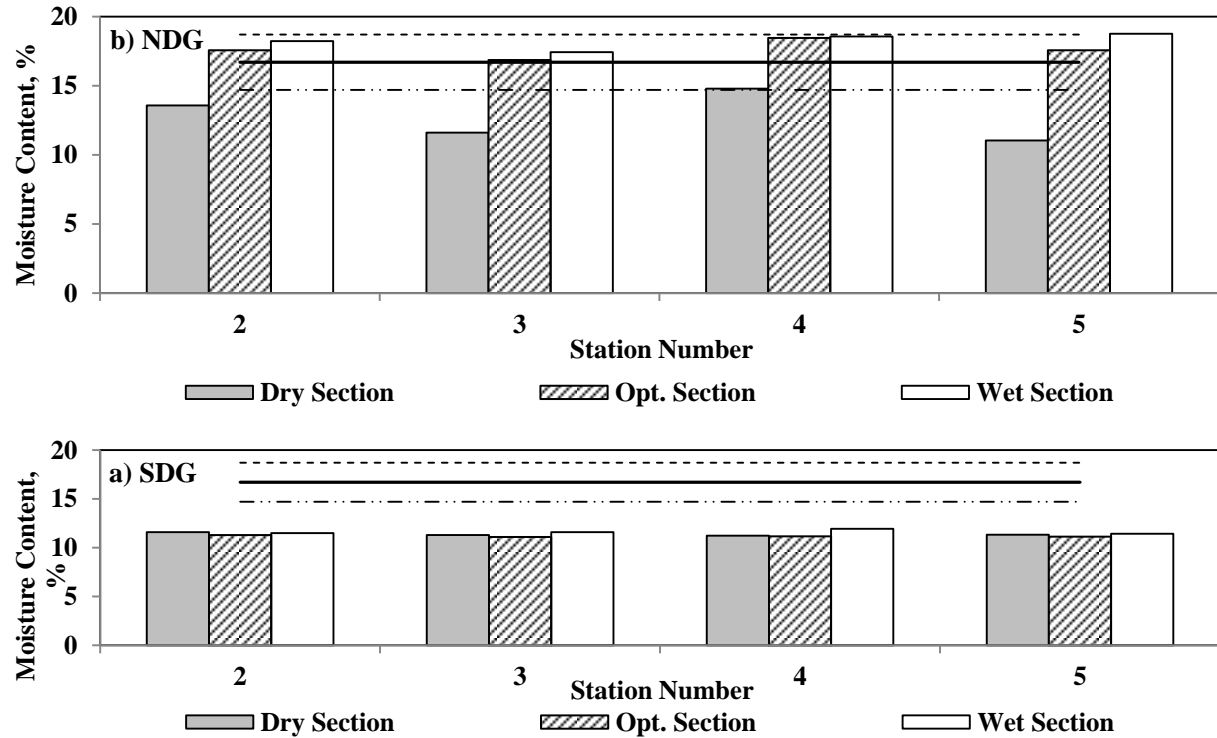


Figure A.2.3 – Spatial Variations of SDG and NDG Moisture Contents Immediately after Compaction of Subgrade

Soil samples were extracted to determine the oven moisture contents at the SDG and NDG test spots. Table A.2.1 summarizes the average SDG, NDG and oven-dry moisture contents for all sections. The oven-dry moisture contents were about 2% less than those measured with the NDG. Again, the SDG moisture readings do not reflect the variation in actual field conditions.

**Table A.2.1 – Comparisons of Average Moisture Contents of Subgrade with Different Devices**

| Section (Nominal MC, %) | Average Measured Moisture Content, % |      |      | Target Moisture Content, % |
|-------------------------|--------------------------------------|------|------|----------------------------|
|                         | SDG                                  | NDG  | Oven |                            |
| Dry Section (OMC-2%)    | 11.4                                 | 12.8 | 11.4 | 14.7                       |
| Opt. Section (OMC)      | 11.2                                 | 17.6 | 15.3 | 16.7                       |
| Wet Section (OMC+2%)    | 11.6                                 | 18.3 | 16.2 | 18.7                       |

Dry densities measured by the SDG and NDG immediately after compaction of the subgrade layer are summarized in Figure A.2.4. The SDG results do not show the variation in dry density for the different sections. According to the NDG results, almost all stations from the three sections passed the specification limit of 95% of MDD.

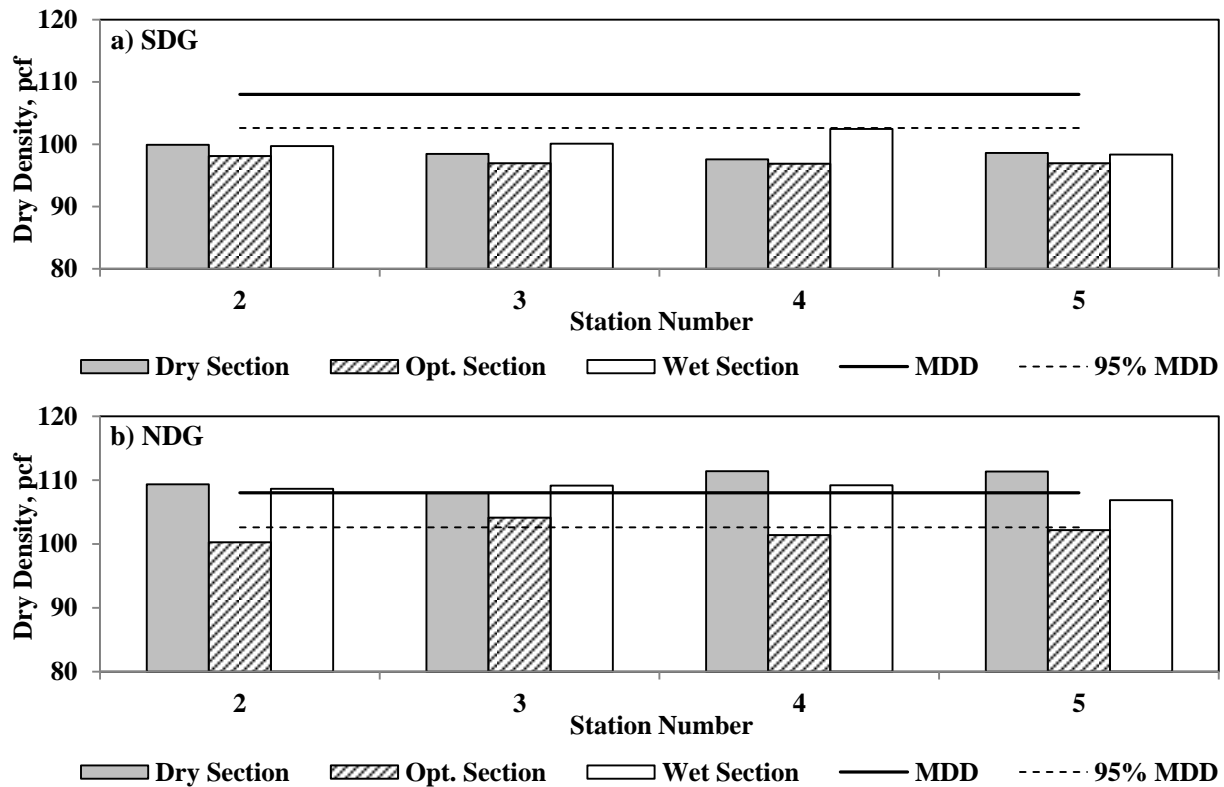


**Figure A.2.4 – Spatial Variations of SDG and NDG Dry Densities Immediately after Compaction of Subgrade Layer**

The variations in the NDG dry density and moisture content of the subgrade layer for different passes of the IC roller are illustrated in Figure A.2.5. With a few exceptions, the dry densities increased with the increase in the number of roller passes. Considering the uncertainties in the NDG readings, the changes in the moisture contents between the passes are for the most part small.

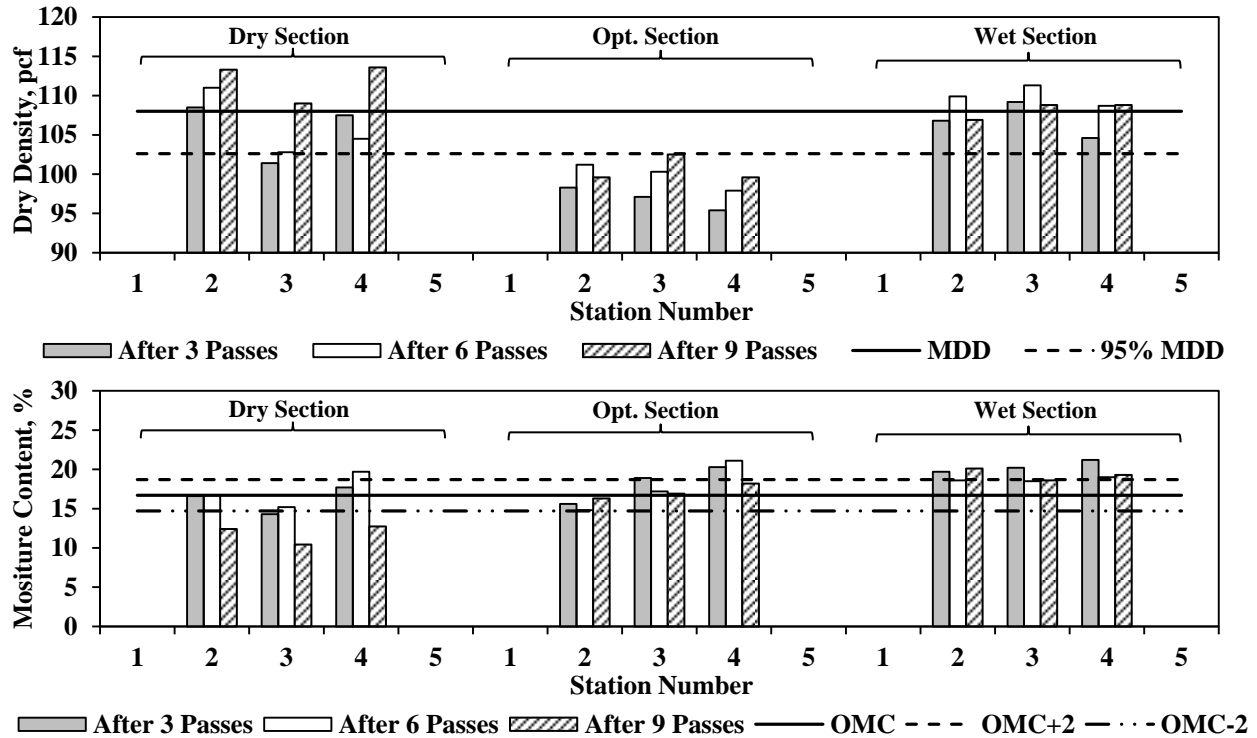


**Figure A.2.5 –Variations of NDG Readings with Number of Passes of Roller during Compaction of Subgrade Layer**

The average NDG moisture contents and dry densities after different passes of the IC roller are summarized in Figure A.2.6. Except for the wet section, the dry densities of the sections increased with more passes of the roller. On the other hand, the moisture contents of the compacted layers decreased after each pass of the roller. The rates of changes in dry density and moisture content are minimal for the wet section and more evident for the dry section. The gradient of density and moisture changes for the optimum section is intermediate.

The results from the SDG device are presented in Figure A.2.7. As discussed earlier, the SDG results do not reflect the changes in neither moisture content nor dry density of the compacted layer between the passes of the IC roller. The average SDG readings on the three sections (dry, wet and optimum) are depicted in Figure A.2.8. Even the average of dry densities and moisture contents do not reflect any changes between passes of the roller and even between the three sections.

**Production Section:** A 280-ft-long production section was also tested. Figure A.2.9 summarizes the SDG and NDG moisture contents from the production section. The average NDG moisture content is 18.1% (as compared to the OMC of 16.9%) while the average SDG moisture content is 9.8% (about 7% less than OMC). Figure A.2.10 depicts the dry densities measured on the production section with the SDG and NDG. Based on the NDG results, all test stations are in the range of acceptance limit for density of 95% of MDD. The SDG dry densities are high (with the average of 143 pcf) which is not reasonable when compared to the maximum dry density of 108 pcf from the laboratory Proctor tests.

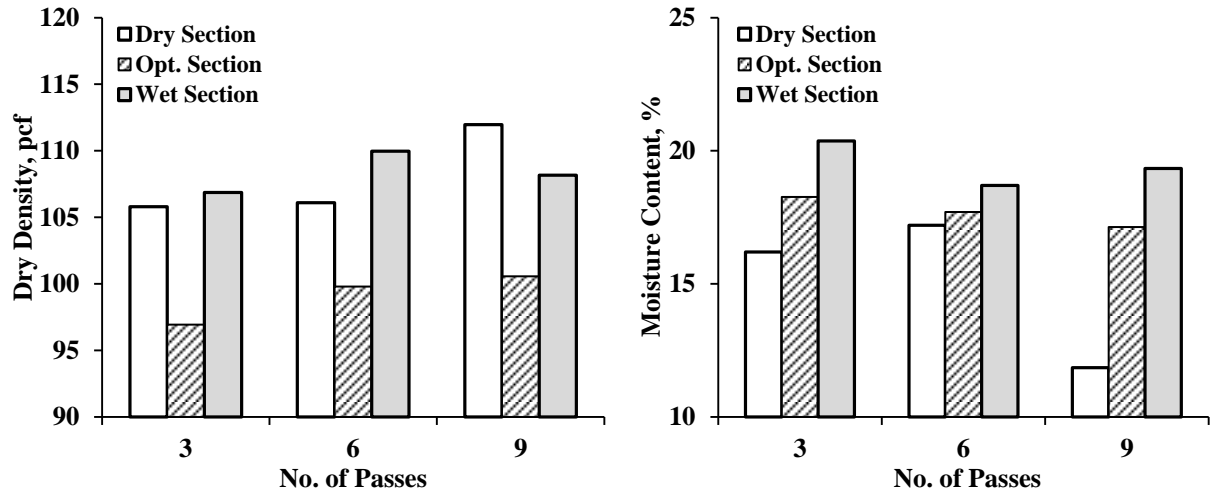


Figure A.2.6 – Variations of Average NDG Moisture Contents and Dry Densities with Number of Passes of Roller during Compaction of Subgrade Layer

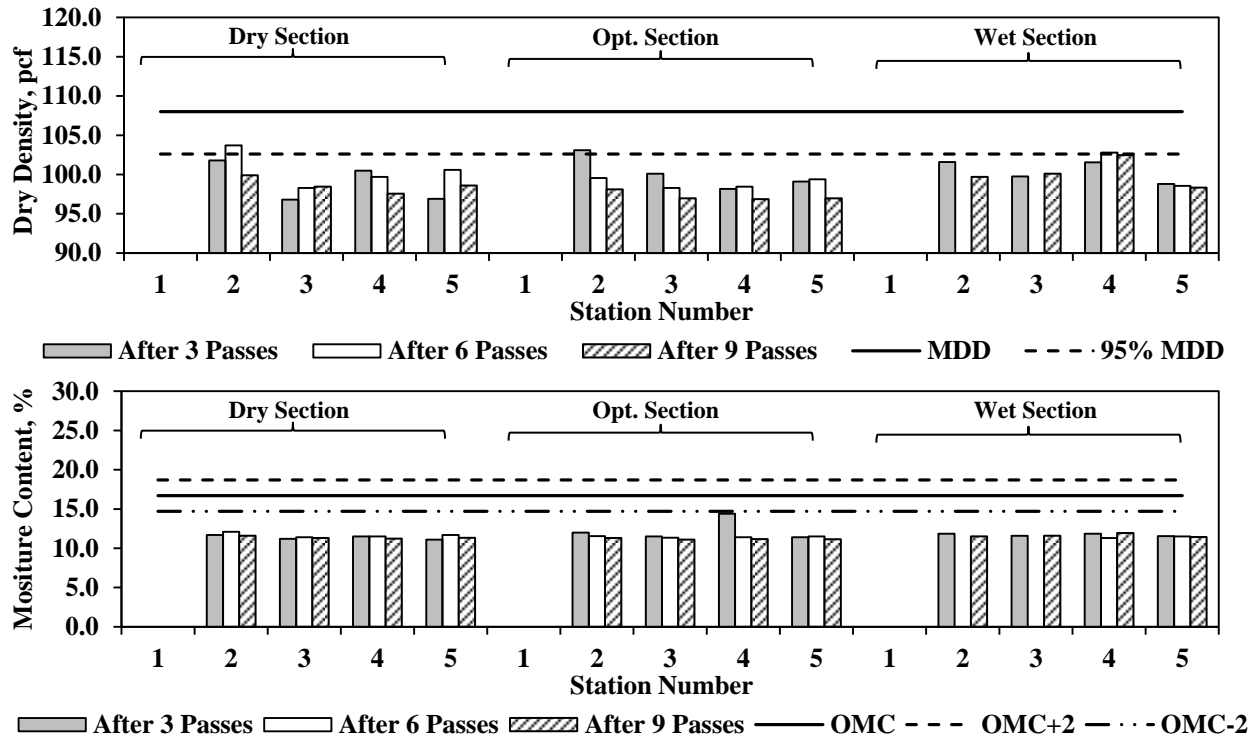


Figure A.2.7 – Variations of SDG Dry Densities and Moisture Contents with Number of Passes of Roller during Compaction of Subgrade Layer

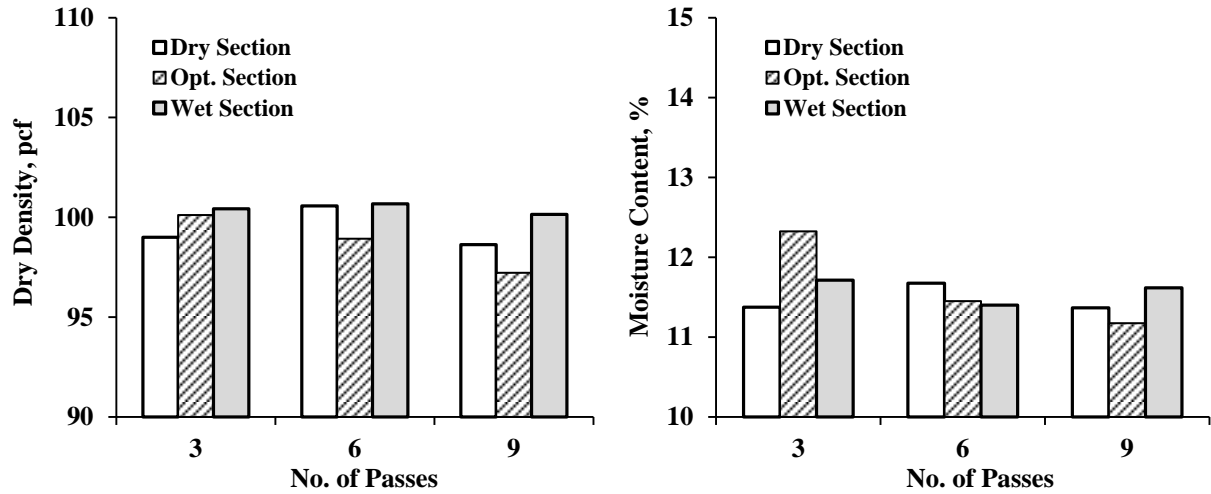


Figure A.2.8 – Variations of Average SDG Moisture Contents and Dry Densities with Number of Passes of Roller during Compaction of Subgrade

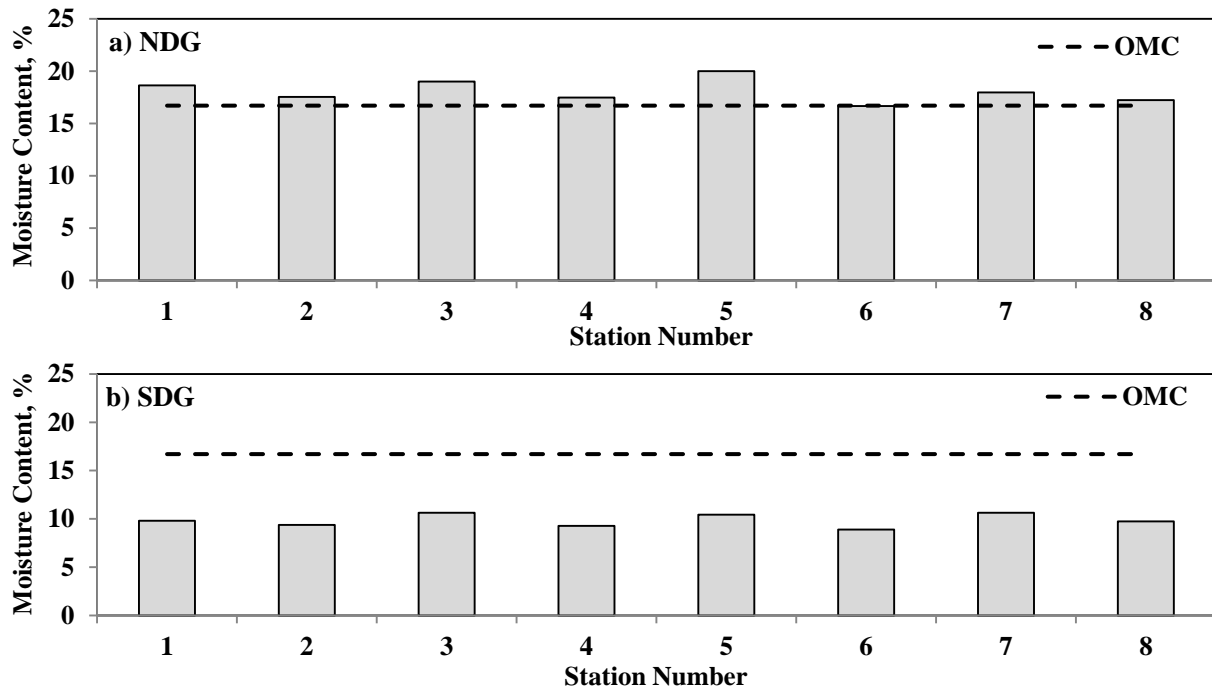
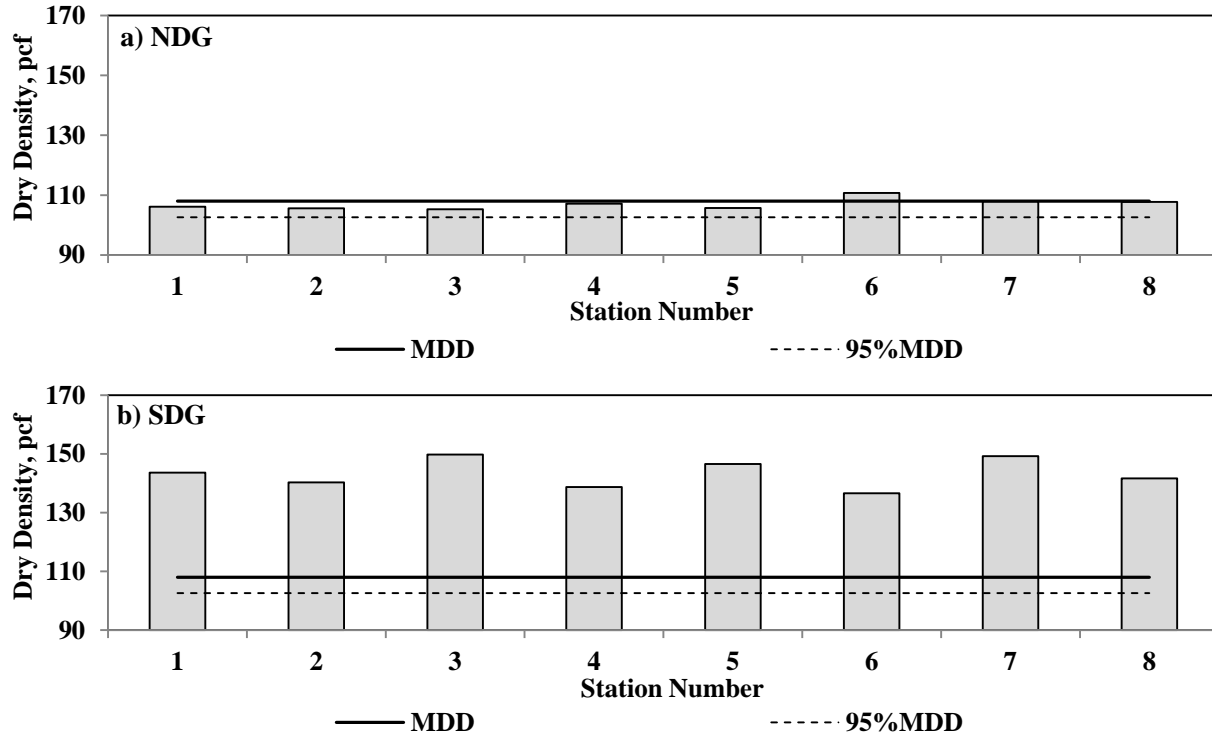
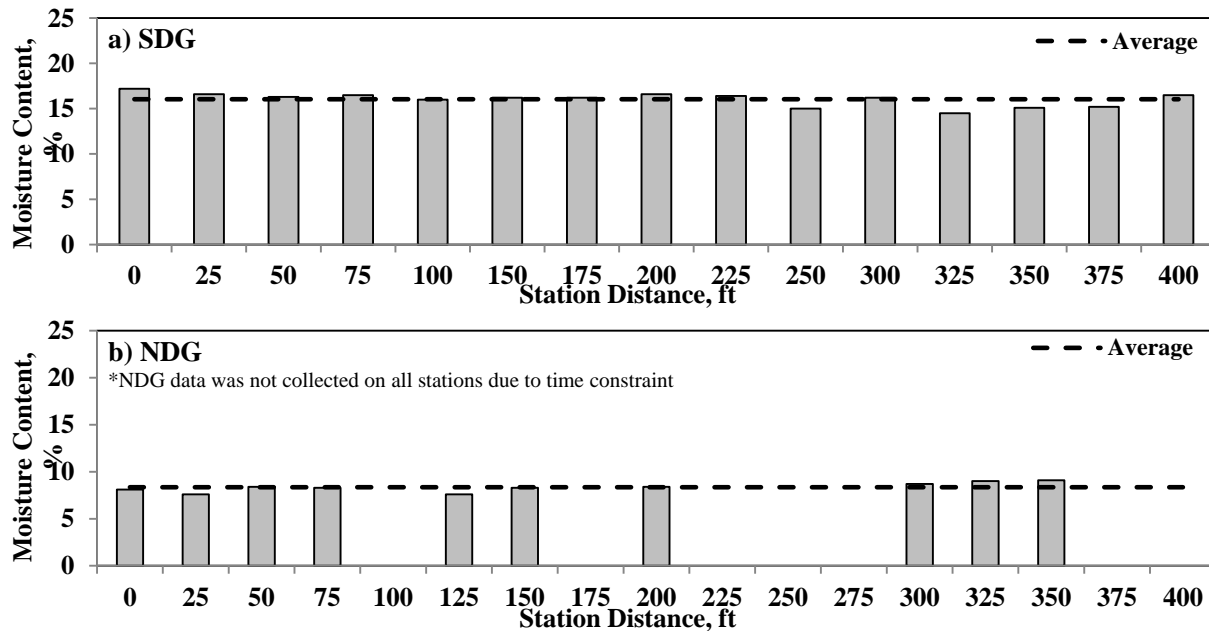


Figure A.2.9 – Variation of Average NDG and SDG Moisture Content of Production Section of Subgrade Layer



**Figure A.2.10 – Variations of Average NDG and SDG Dry Densities of Production Section of Subgrade Layer**

**Base Layer:** Variations in the SDG and NDG moisture contents of the foundation layer before the placement of the base are presented in Figure A.2.11. The average moisture content of the foundation layer was 16.0% with the SDG and the more realistic value of 8.4% with the NDG. The NDG tests were not carried out on some stations due to time constraints.



**Figure A.2.11 – Spatial Variations of SDG and NDG Moisture Contents on Foundation Layer before Placement of Base**

Dry density readings from the SDG and NDG on the foundation layer before the placement of the base are summarized in Figure A.2.12. The average SDG dry density was 123.8 pcf and that of the NDG was 124.4 pcf.

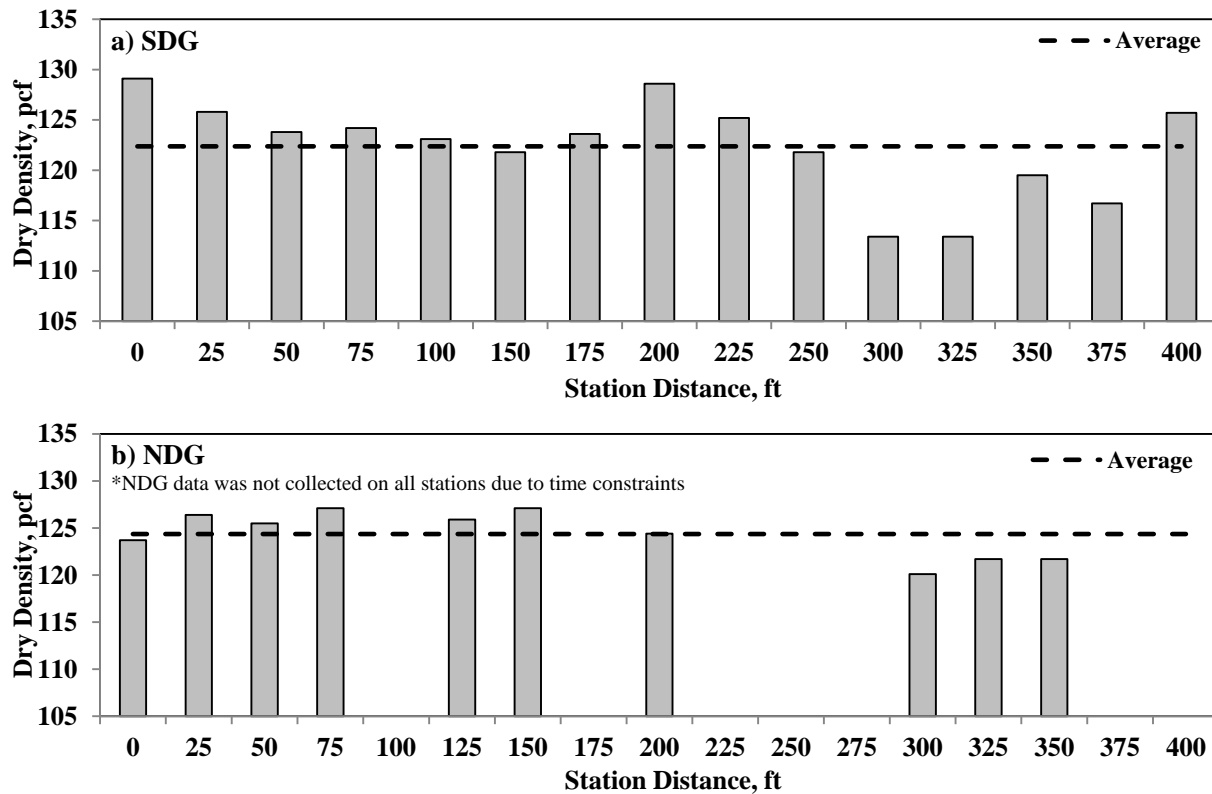


**Figure A.2.12 – Spatial Variations of SDG and NDG Dry Densities on Foundation Layer before Placement of Base**

The SDG and NDG were utilized immediately after the compaction of the base layer to determine the moisture contents and dry densities. The results of those tests are summarized in Figures A.2.13 and A.2.14. Based on the SDG results (Figure A.2.13a), the average moisture content of the dry section was 11.4%, the optimum section was 11.7% and the wet section was 15.3%. The optimum moisture content from the laboratory modified Proctor tests was 10.4% (see Table 5.1). According to the NDG results (Figure A.2.13b), the average moisture content of the dry section was 7.0%, the optimum section was 9.0% and the wet section was 11.3%. Some of the stations were not tested due to time constraints. Table A.2.2 summarizes the average SDG and NDG moisture contents compared to the oven dry moisture data.

**Table A.2.2 – Comparisons of Average Moisture Contents of Base with Different Devices**

| Section (Nominal MC, %) | Average Measured Moisture Content, % |      |      | Target Moisture Content, % |
|-------------------------|--------------------------------------|------|------|----------------------------|
|                         | SDG                                  | NDG  | Oven |                            |
| Dry Section (OMC-2%)    | 11.4                                 | 7.0  | 6.6  | 8.4                        |
| Opt. Section (OMC)      | 11.7                                 | 9.0  | 8.8  | 10.4                       |
| Wet Section (OMC+2%)    | 15.3                                 | 11.3 | 11.0 | 12.4                       |

Dry densities from the SDG and NDG of the compacted base layer are presented in Figure A.2.14. The SDG dry densities were less than 95% of the MDD except for the wet section. The NDG results show that all test stations were for the most part between 95% and 100% of the MDD. The SDG and NDG data were not collected at some stations due to the malfunction of the SDG and unavailability of the NDG.

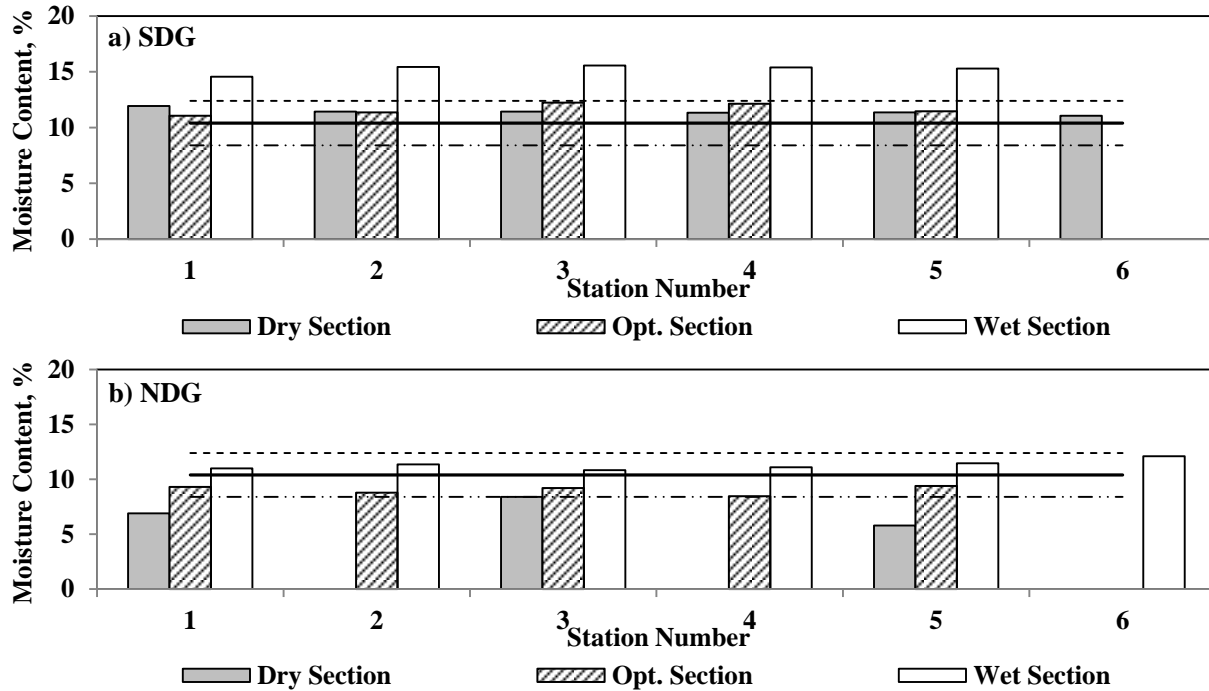


Figure A.2.13 – Spatial Variations of SDG and NDG Moisture Contents Immediately after Compaction of Base Layer

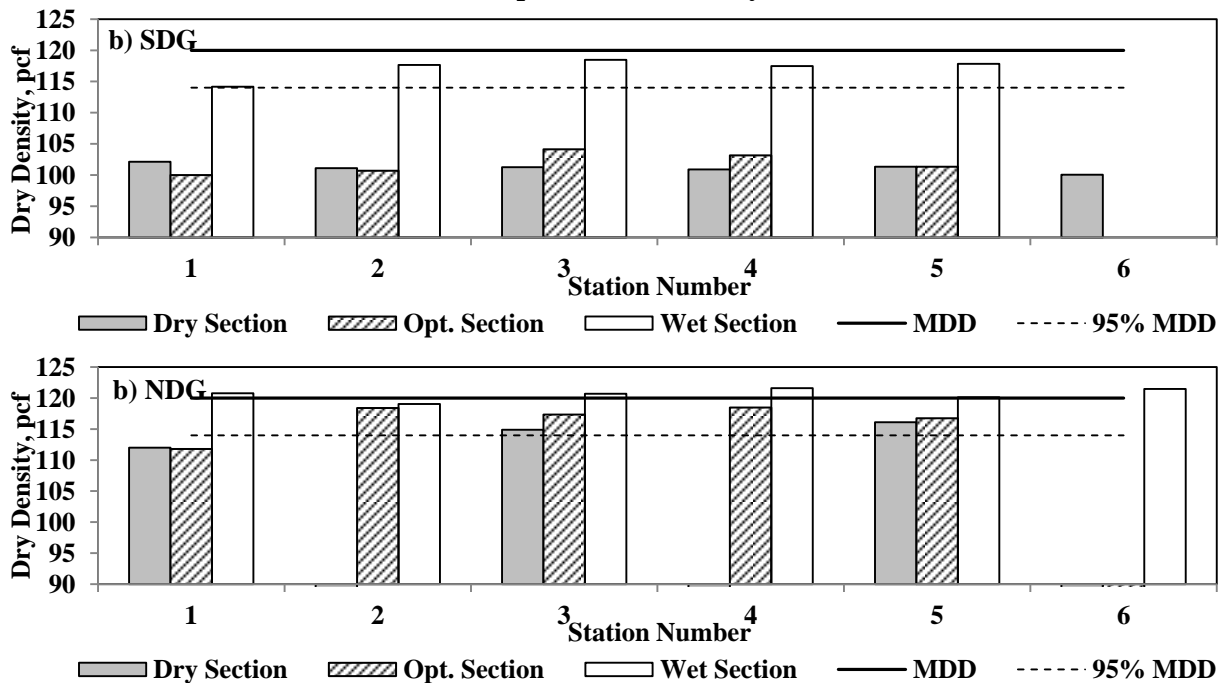
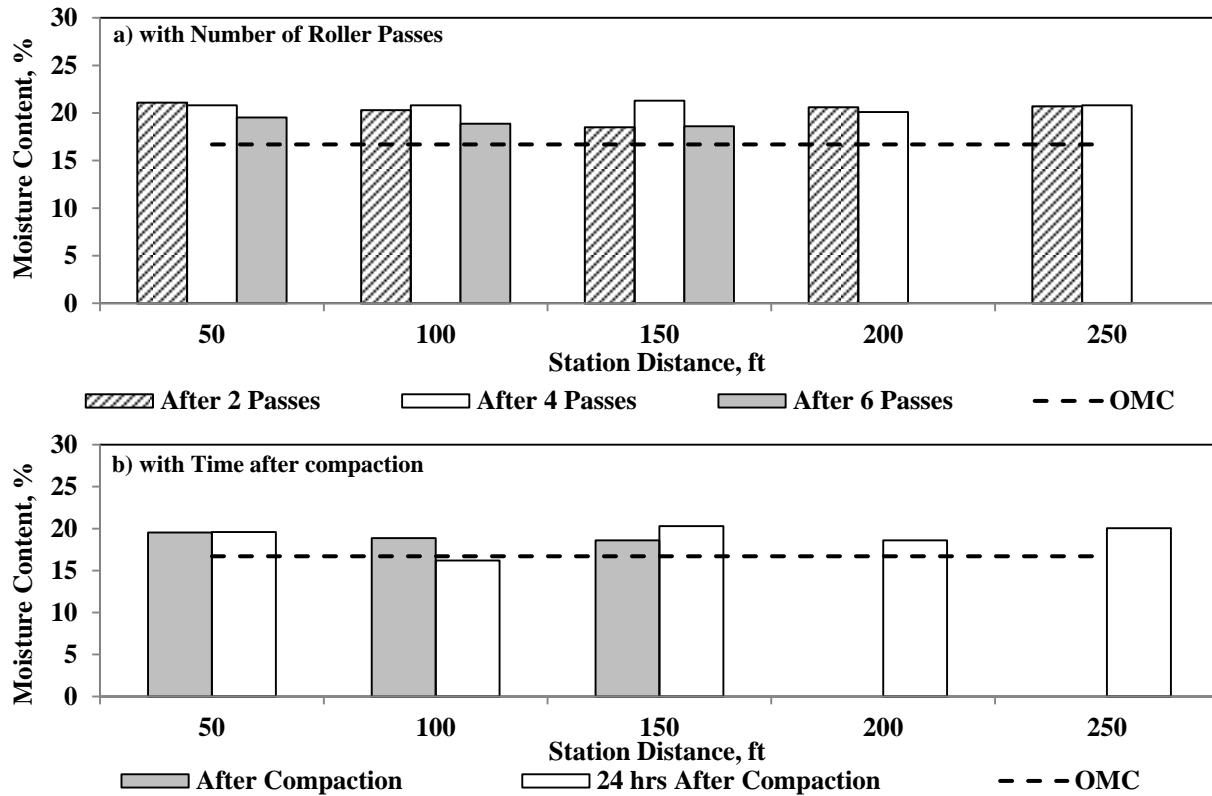


Figure A.2.14 – Spatial Variations of SDG and NDG Dry Densities Immediately after Compaction of Base Layer

**Lime-Treated Subgrade Layer:** Moisture contents and dry densities of the compacted lime-treated subgrade as a function of the passes of the roller and after completing the compaction process are summarized in Figures A.2.15 and A.2.16. Figure A.2.15a illustrates the variations of the SDG moisture

contents between the passes of the IC roller. A clear pattern is not apparent in the data. The changes in the SDG moisture contents immediately after compaction and 24 hours after compaction are small (see Figure A.2.15b). Figure A.2.16 summarizes the SDG density readings during and after the compaction process. Again, a significant pattern is not observed (see Figure A.2.16a).



**Figure A.2.15 – Spatial Variations of SDG Moisture Contents for Lime-Treated Subgrade**

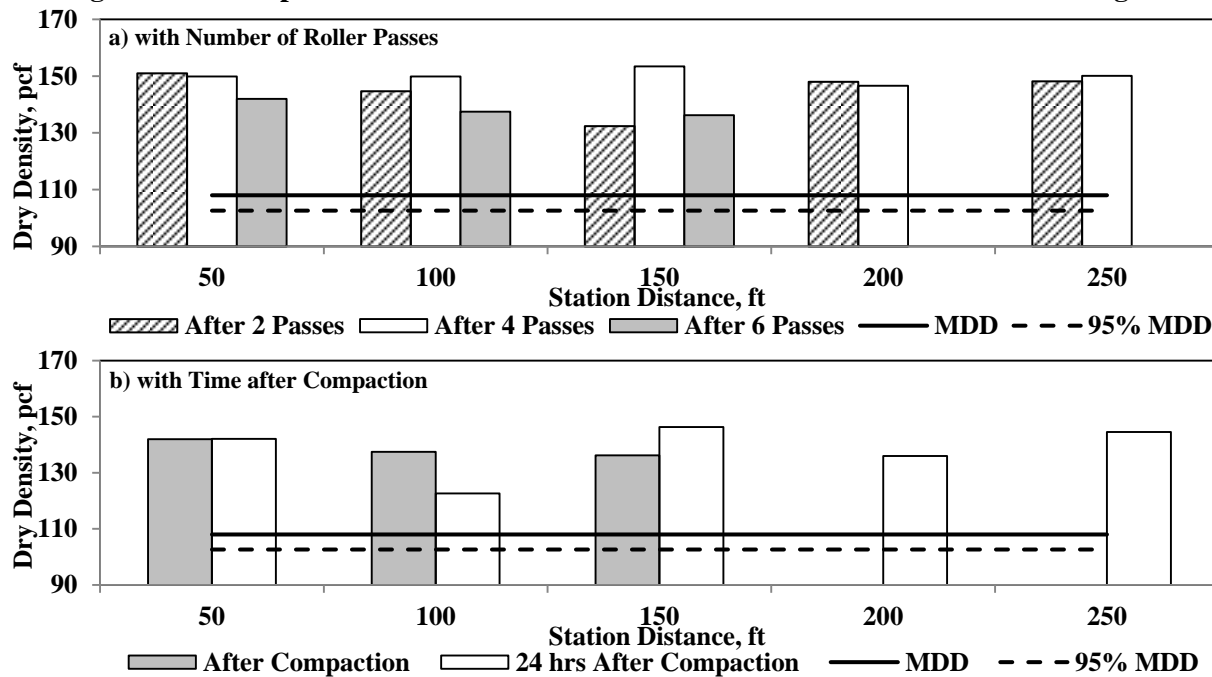


**Figure A.2.16 – Spatial Variations of SDG Dry Densities for Lime-Treated Subgrade**

NDG readings at the same stations of the compacted lime-treated subgrade are presented in Figure A.2.17. The NDG data were collected only after the compaction process was completed. Furthermore, due to functional problems of the device and construction time constraints, it was not possible to collect all the required data. On average, the moisture content was 2% greater than the OMC and the dry density was close to 95% of the MDD.

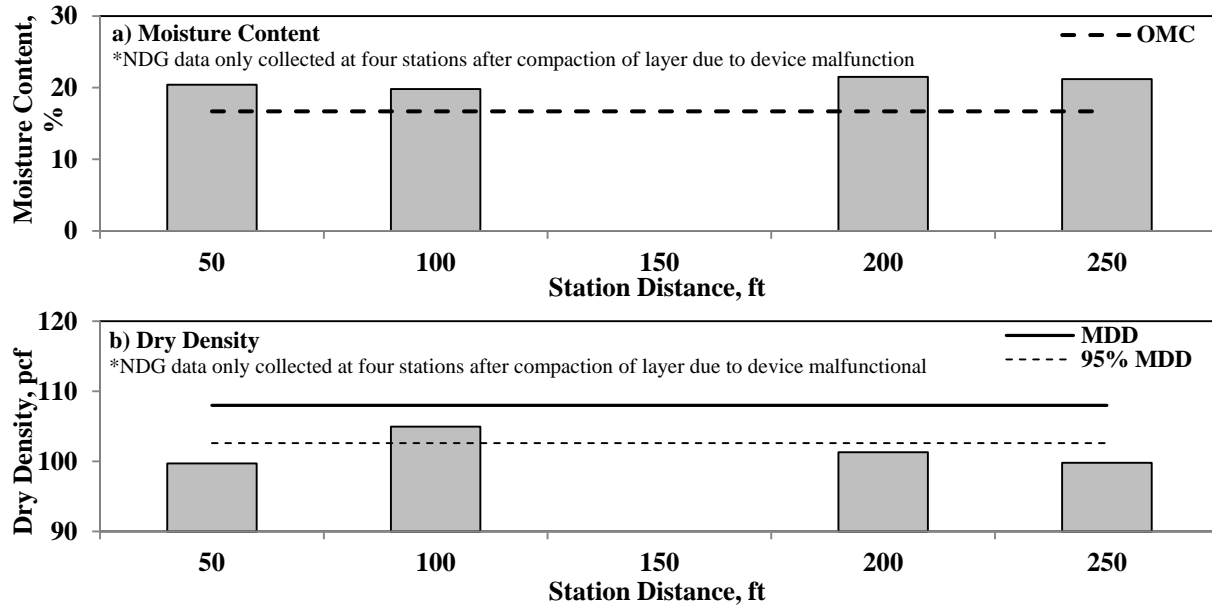


**Figure A.2.17 – Spatial Variations of NDG Moisture Contents and Dry Densities after Compaction of Lime-Treated Subgrade**

### A.3 Evaluation of Modulus-Based Devices

**Subgrade Layer:** A Zorn LWD and a PSPA were used on top of the embankment layer along Lines A and C shortly before the placement of the subgrade layer. The average moduli from lines A and C for each station are illustrated in Figure A.3.1. The Zorn LWD modulus was  $15.4 \pm 7.8$  ksi (Figure A.3.1a), and the average PSPA modulus was  $45.6 \pm 24.4$  ksi (Figure A.3.1b).

Table A.3.1 and Figure A.3.2 contain the results of the measurements with the PSPA, Geogauge, Zorn LWD and DCP after the compaction of the subgrade layer. The variations in the average modulus among the three sections with the PSPA is rather small as supported by the laboratory modulus test results presented in Table A.3.2 for the range of moisture contents varying from 13% to 17% for subgrade layer.

**Table A.3.1 – Average Moduli from Different Sections**

| Field Section | Average Modulus, ksi |            |          |          |            |          | Average Oven MC, % |
|---------------|----------------------|------------|----------|----------|------------|----------|--------------------|
|               | PSPA                 |            | Geogauge | Zorn     |            | DCP      |                    |
|               | Subgrade             | Embankment | Subgrade | Subgrade | Embankment | Subgrade |                    |
| Dry Section   | 38                   | 53         | 48       | 8.4      | 14.5       | 16.8     | 11.4               |
| Opt. Section  | 34                   | 40         | 61       | 9.3      | 12.4       | 13.0     | 14.9               |
| Wet Section   | 33                   | 36         | 47       | 4.6      | 13.5       | 7.6      | 16.2               |

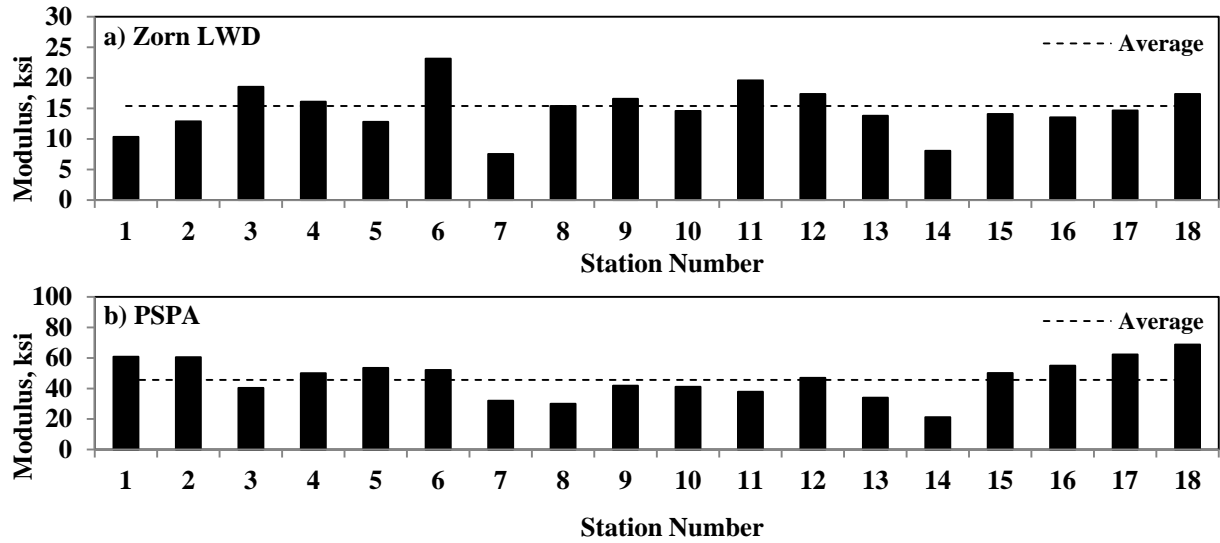


**Figure A.3.1 – Variations of Measured Moduli of Embankment Layer**

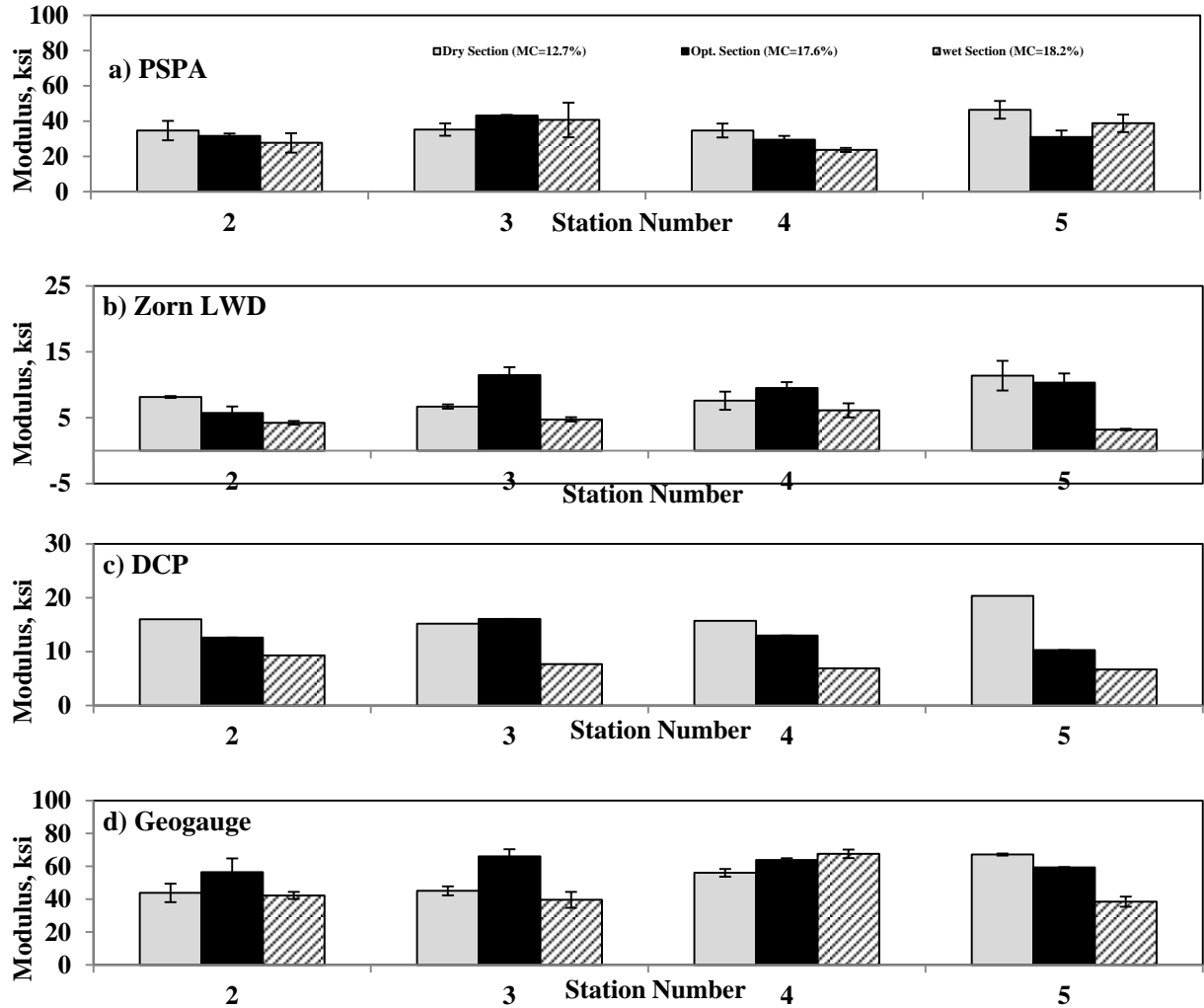


**Figure A.3.2 – Spatial Variations of Measured Moduli immediately after Compaction of Subgrade (Average of Lines A, B, and C)**

The variations of the Zorn LWD and PSPA moduli between passes of the IC roller during compaction of the subgrade layer are depicted in Figure A.3.3. The modulus of the compacted layer increases for the most part with more passes of the roller (except for some stations).

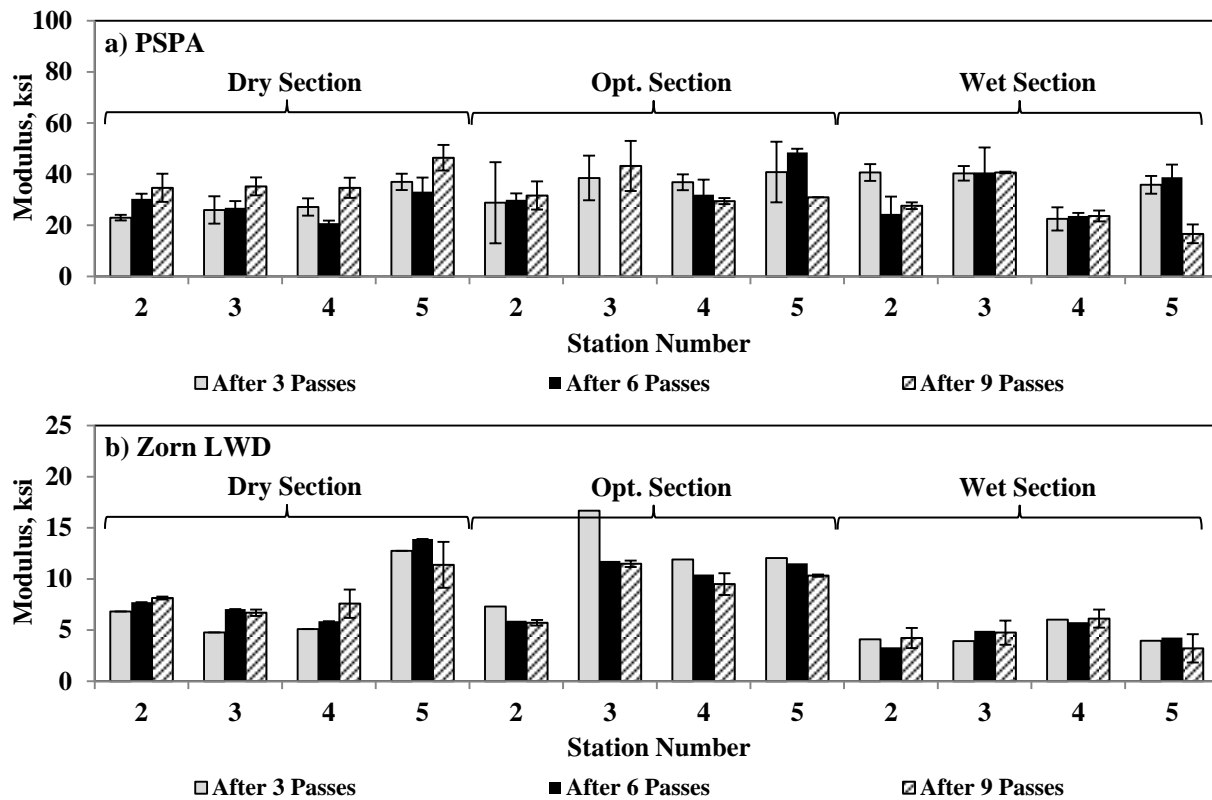


**Figure A.3.3 –Variations of Measured Moduli between Passes of IC Roller during Compaction of Subgrade Layer**

The results of the modulus-based devices on the compacted subgrade layer from the production section are summarized in Figure A.3.4. The moduli of the compacted section from the different devices are mostly consistent. The average of the PSPA modulus is 41.6 ksi, the Zorn LWD is 14 ksi, the DCP is 17 ksi and the Geogauge is 70 ksi. The production section is stiffer than the other subgrade sections. This can be attributed to numerous passing of reclaimers and water tanks in addition to the compactors over that section. Such construction traffic was avoided for the other three sections. The standard deviations of replicate tests on the same stations are illustrated as error bars in Figure A.3.4. DCP data was not collected at all testing stations due to time constraints.

**Base Layer:** The results from the PSPA, Zorn LWD and DCP tests on subgrade before the placement of the base layer are summarized in Figure A.3.5. The average PSPA modulus is 58 ksi while the average LWD modulus is 15 ksi. The average DCP modulus is 33 ksi. The variations in moduli from all three devices follow almost the same pattern. Stations 0, 200, 250, 300 and 450 ft are less stiff as compared to the other ones.

The results from the modulus testing of the three base sections are summarized in Figure A.3.5. Based on LWD results (see Figure A.3.6b), the average modulus for the dry section is 19 ksi, the optimum section is 19 ksi and the wet section is 12 ksi. Such results for the PSPA are 76 ksi, 75 ksi, and 50 ksi, respectively (see Figure A.3.6a). There is not much difference between the moduli of the dry and optimum sections from both the LWD and PSPA. For both devices, the modulus of the wet section decreased by about 35%. Such a pattern was not recognized from the DCP data in which the average

moduli of dry, optimum and wet sections were 24, 26 and 26 ksi, respectively. There is not a significant change in modulus with respect to moisture content according to the DCP results. Comparing the representative laboratory MR values (reported in Table 4.2), the lab modulus increases by about 15% for the dry samples and decreases by about 24% for the wet samples, respectively. As compared to the sample tested at OMC, the laboratory FFRC moduli increased by 74% and decreased by 57% for the dry and wet samples, respectively.

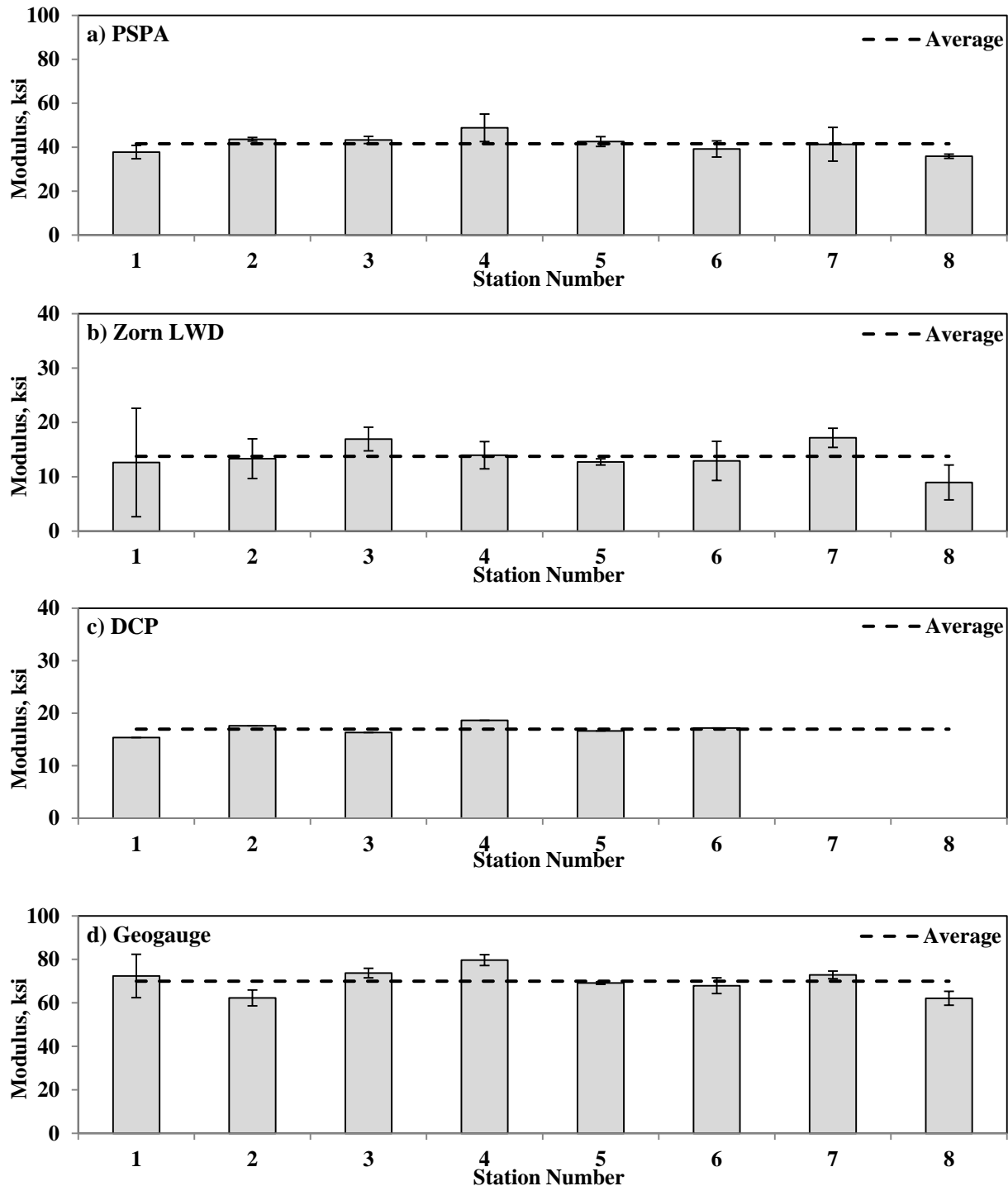


Figure A.3.4 – Spatial Variations of Measured Moduli immediately after Compaction of Subgrade at Production Section

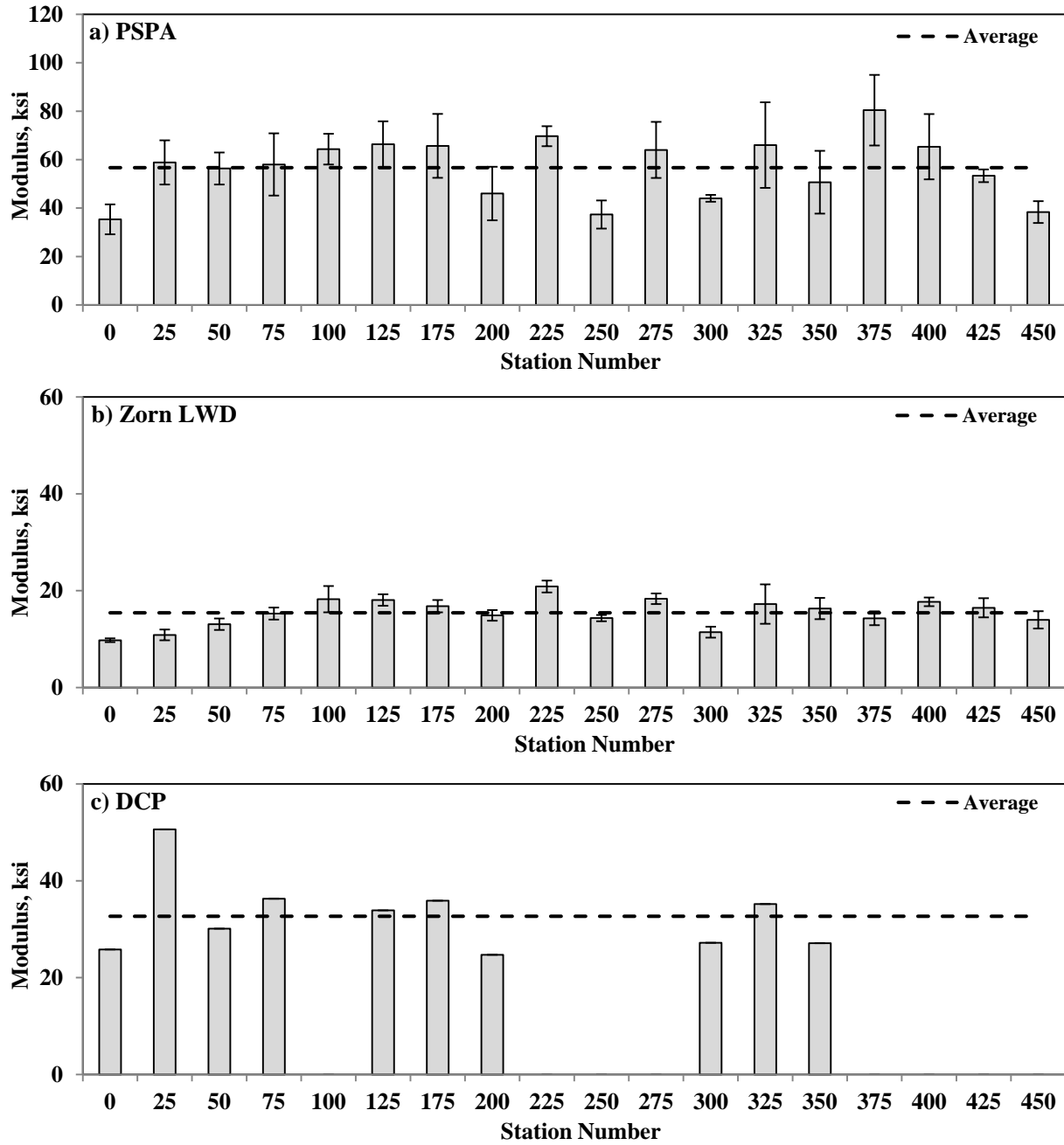
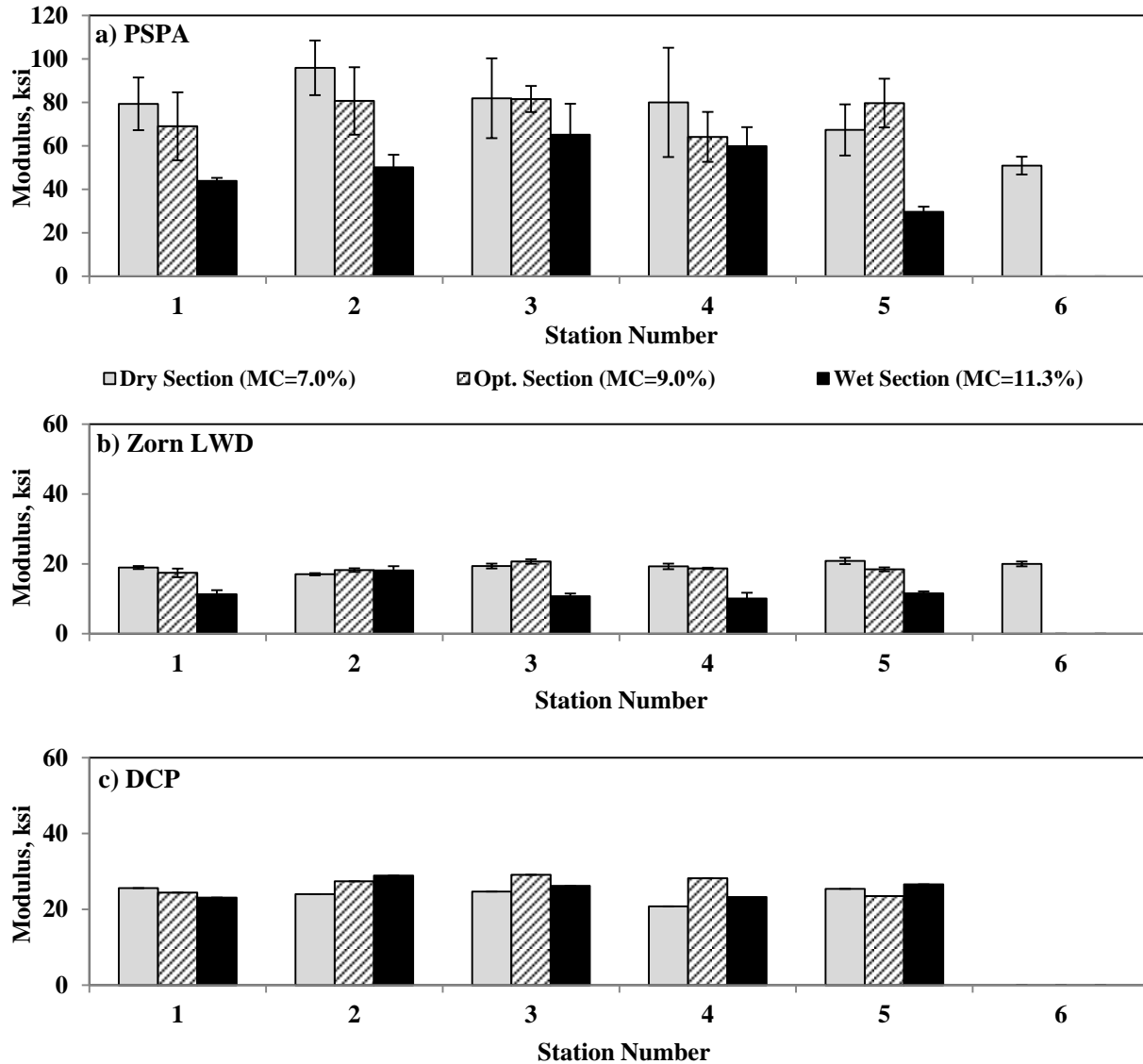


Figure A.3.5 – Spatial Variations of Measured Modulus of Subgrade before Placement of Base



**Figure A.3.6 – Spatial Variations of Measured Modulus immediately after Compaction of Base**

**Lime-Treated Subgrade Layer:** Figure A.3.7 illustrates the results of the modulus measurements on the prepared subgrade layer before the treatment process. The modulus variations among the testing stations are similar with Stations 100 and 150 and having slightly higher moduli as compared to the other stations. The average of the LWD modulus was 12 ksi and that of the PSPA was 51 ksi.

The modulus measurements between the passes of the IC roller on the lime-treated subgrade and after completion of the compaction process (6 passes of IC roller) for the different devices are presented in Figure A.3.8. The DCP data were collected only after the final pass of the roller due to time constraints. Figure A.3.9 depicts the changes in the measured moduli with the different devices with respect to the passes of the IC roller. The stiffness of the compacted layer (from both LWD and PSPA) increases with more passes of the roller.

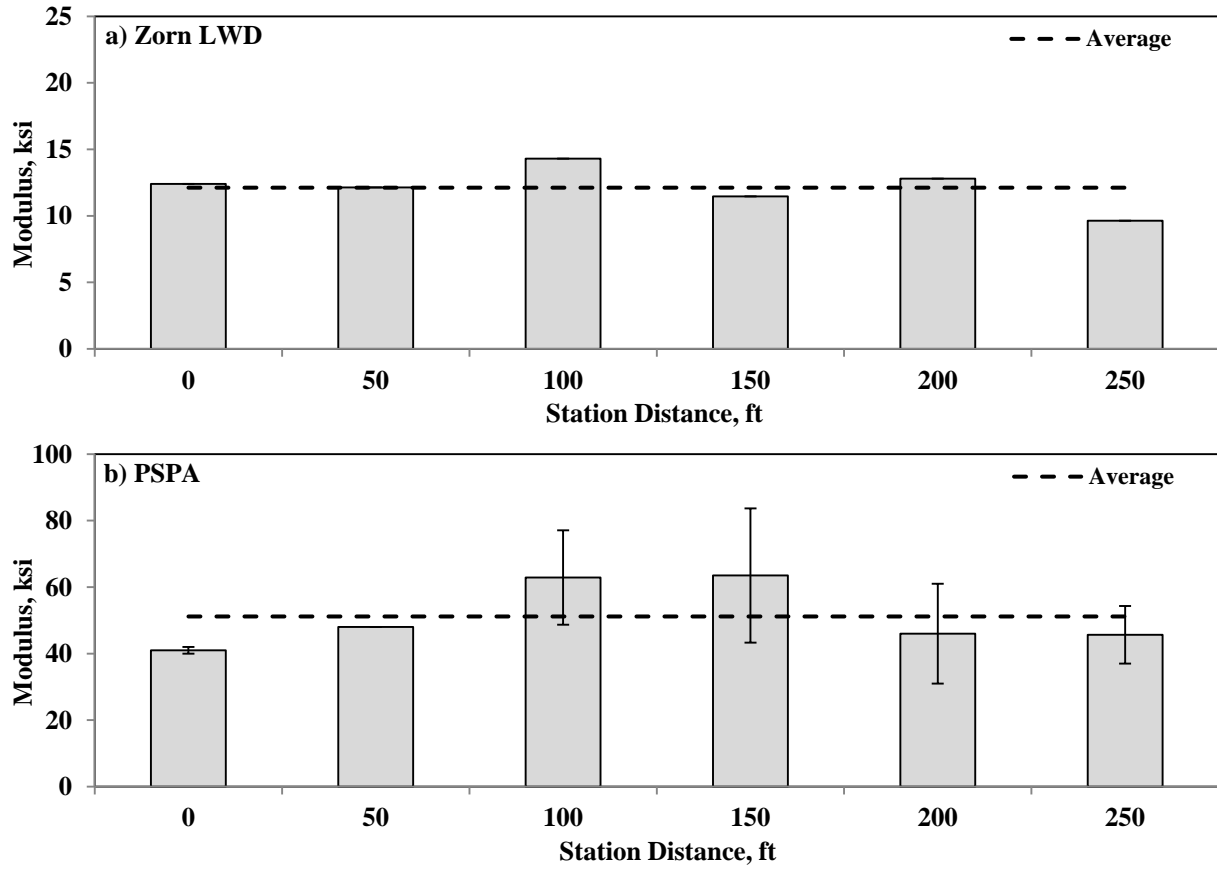


**Figure A.3.7 – Spatial Variations of Measured Modulus before Lime-Treatment of Subgrade Layer**

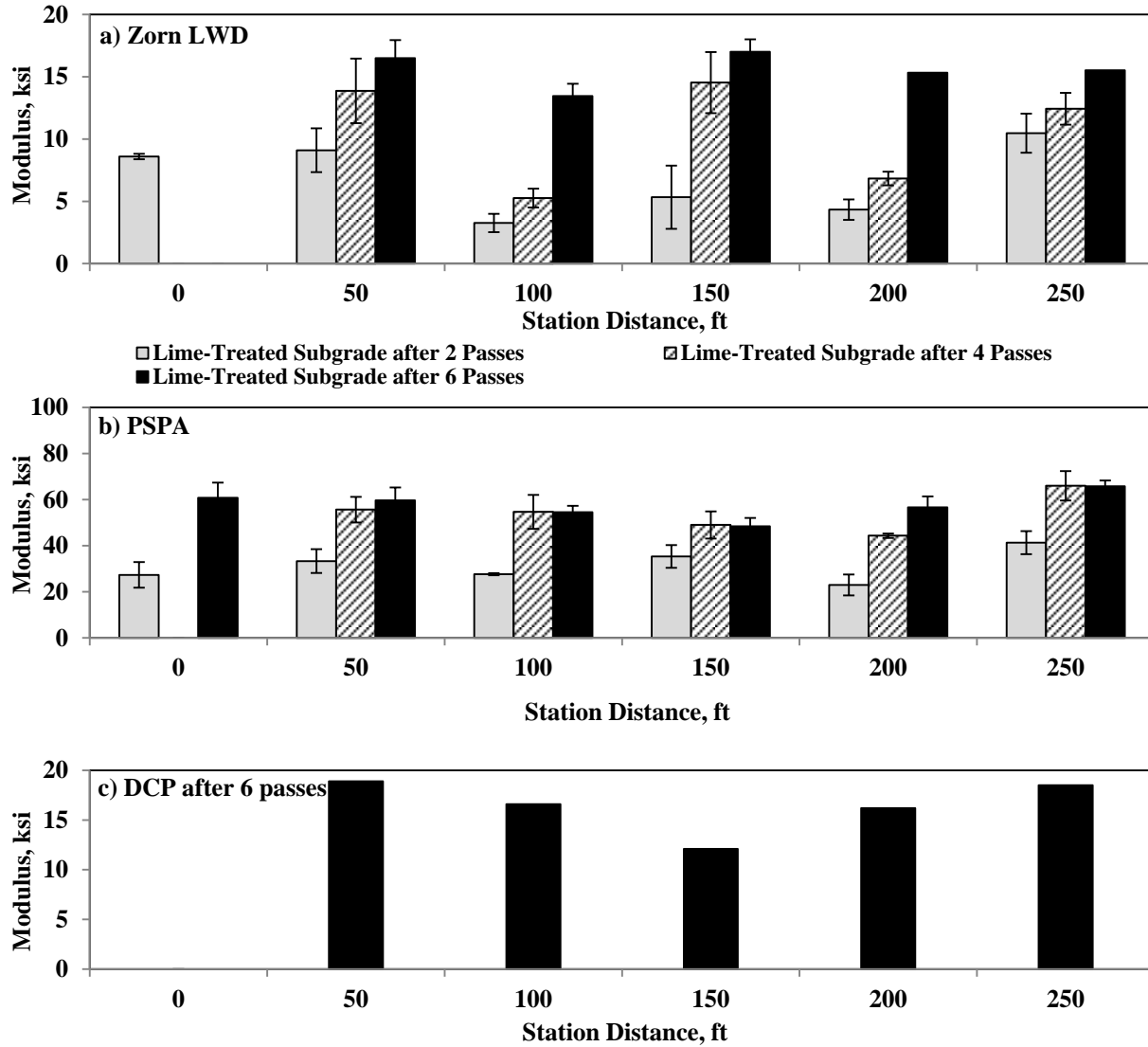


Figure A.3.8 – Spatial Variations of Measured Moduli between Passes of IC Roller and Immediately after Compaction of Lime-Treated Subgrade Layer

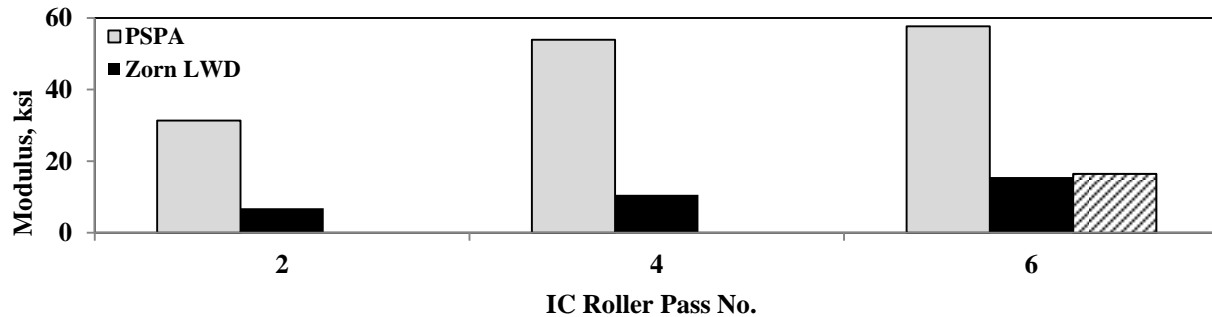


Figure A.3.9 – Variations of Moduli between Passes of IC Roller from Different Devices

#### A.4 Variability of Modulus-Based Devices

**Subgrade Layer:** In order to investigate the variability of the modulus-based devices for the in-situ modulus estimation, the coefficient of variation (COV) of the replicate tests at each testing spot was calculated after the final pass of the IC roller. The distribution of the COV with the measured field moduli for the PSPA, LWD and Geogauge are summarized in Figure A.4.1. A clear trend between the average measured modulus and the COV cannot be observed for any of the devices. The maximum COVs for the PSPA and Geogauge were 49%, while the value for the LWD was 38%. The relatively high COVs might be due to the compaction nonuniformity among the test locations at each station as shown in Figure A.4.2.

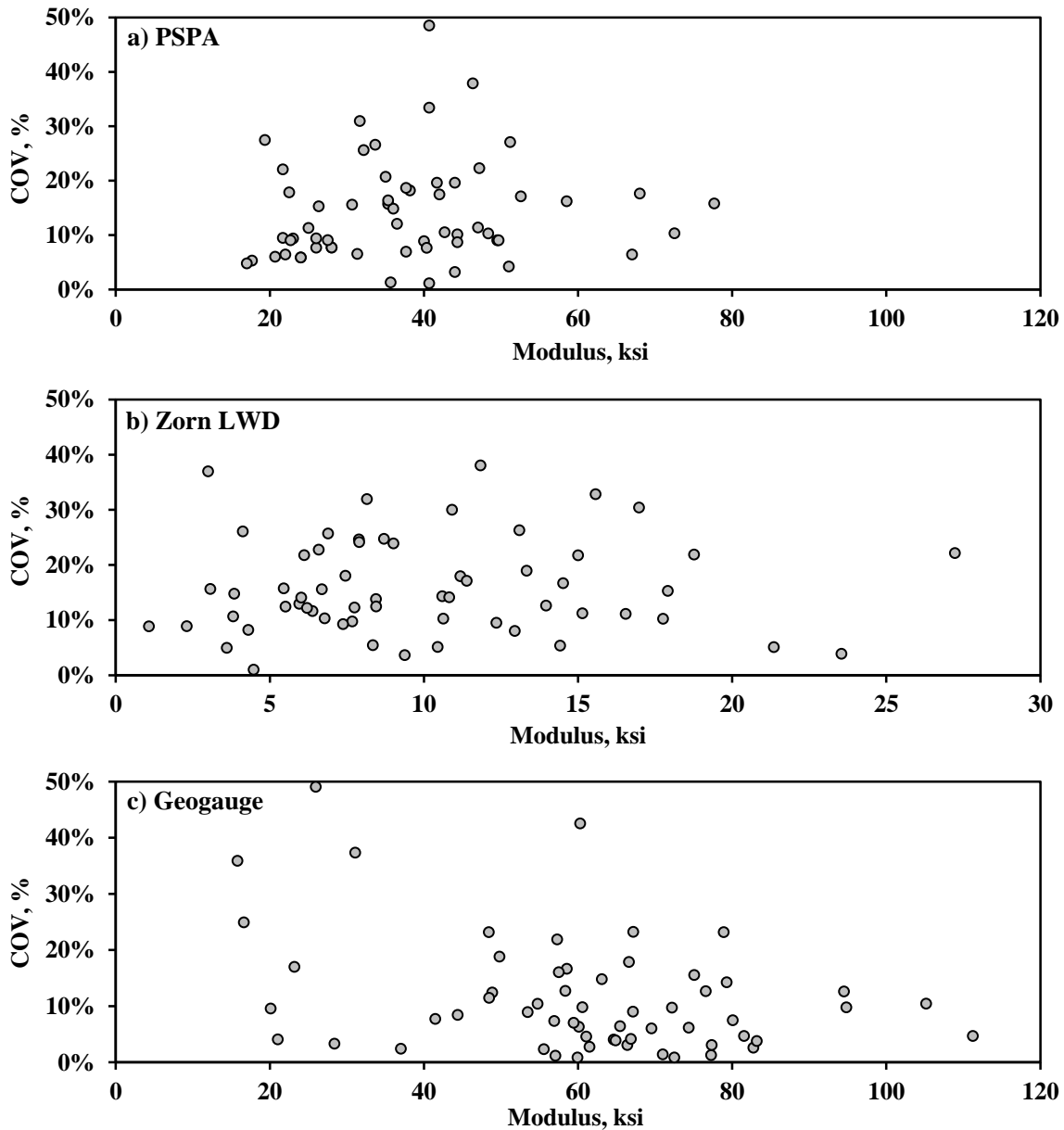
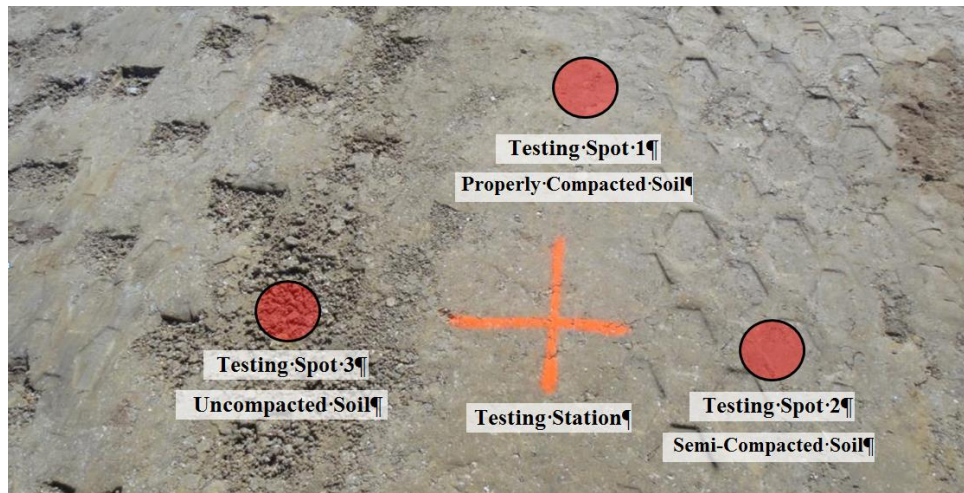
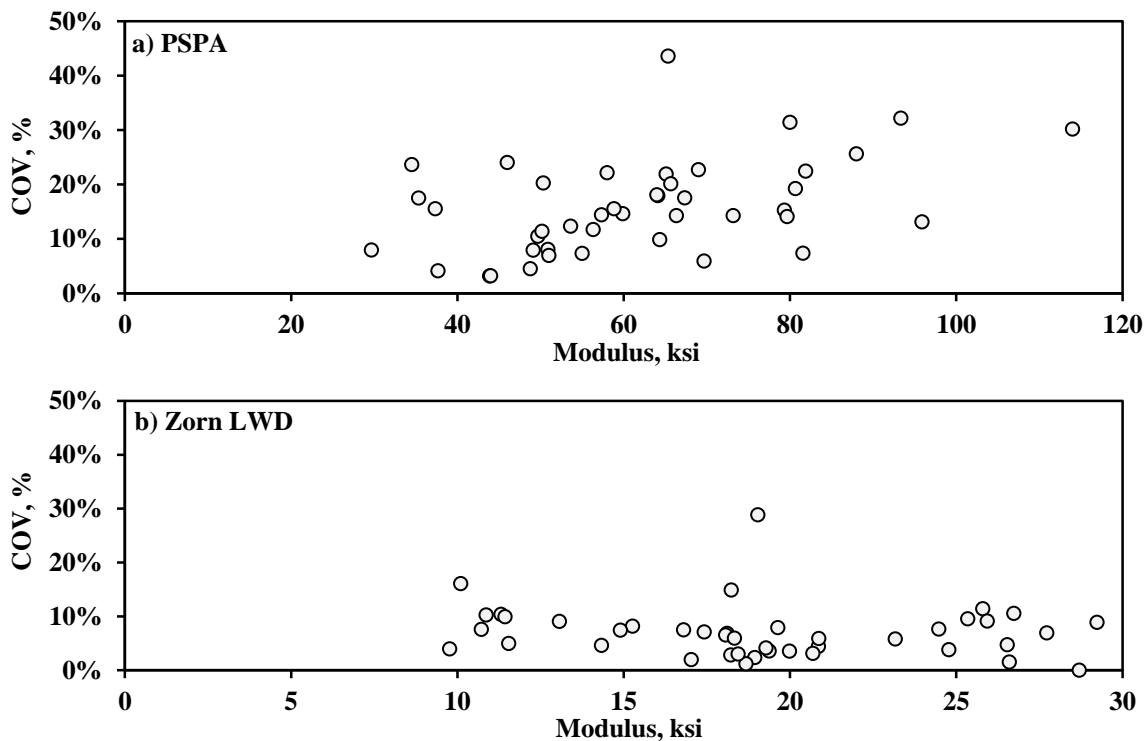


Figure A.4.1 – Variations in Coefficient of Variation (COV) of Modulus-based Devices with Average Measured Modulus of Subgrade Layer



**Figure A.4.2 – Compaction Discrepancy among Testing Spots around a Sample Station**

**Base Layer:** The distributions of the COVs for the corresponding measured moduli with the LWD and the PSPA are presented in Figure A.4.3. The average COV value for the LWD measurements is 7% with the maximum COV of 29%. The maximum COV for the PSPA readings is 44% with an average of 16%. The differences in the COVs can be partially attributed to the fact that the LWD measures a composite modulus of the base and subgrade while the PSPA directly measures the modulus of the base layer.



**Figure A.4.3 – Variations in Coefficient of Variation (COV) of Modulus-based Devices with Average Measured Modulus of Base Layer**

**Lime-Treated Subgrade:** The distributions of the COVs for the measured moduli of the lime-treated subgrade are summarized in Figure A.4.4 for the LWD and the PSPA. The average PSPA COV is 13% with a maximum of 33% while the values for the LWD are 11% with a maximum of 23%.

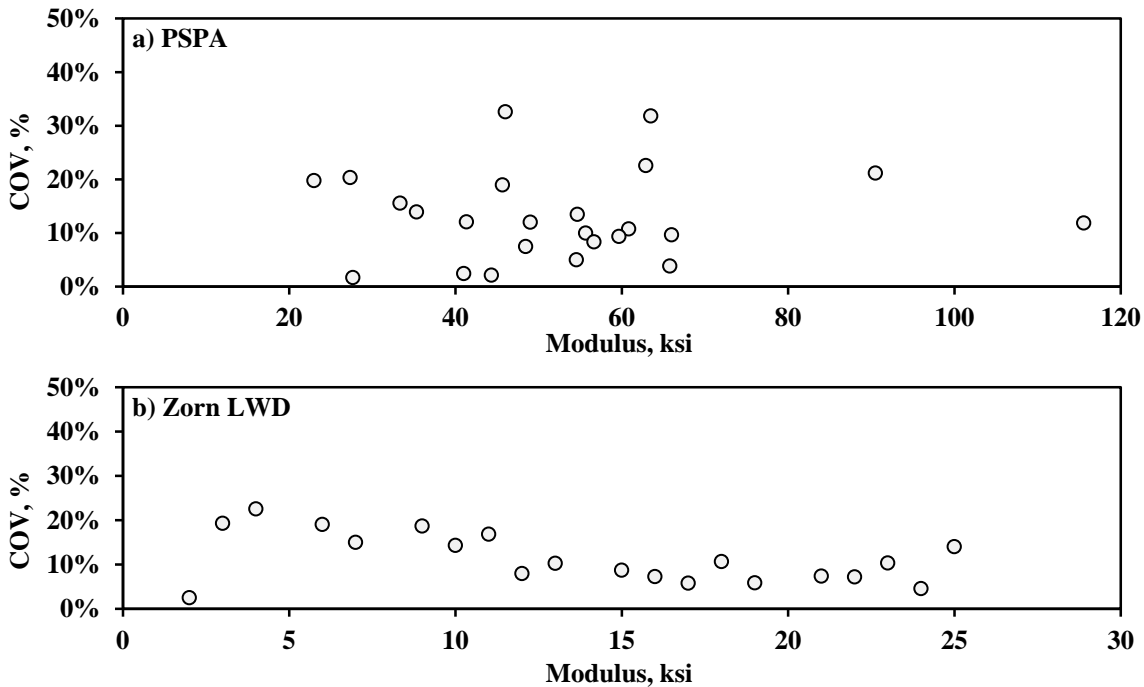
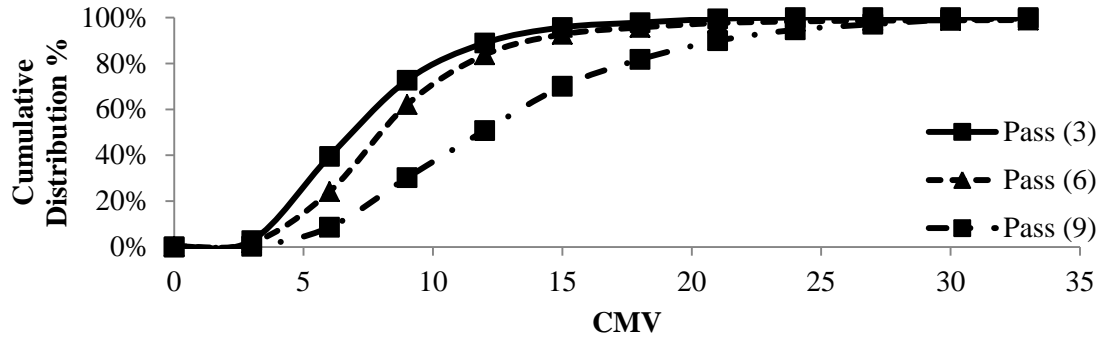


**Figure A.4.4 – Variations in Coefficient of Variation (COV) of Modulus-based Devices with Average Measured Modulus of Lime Treated Subgrade Layer**

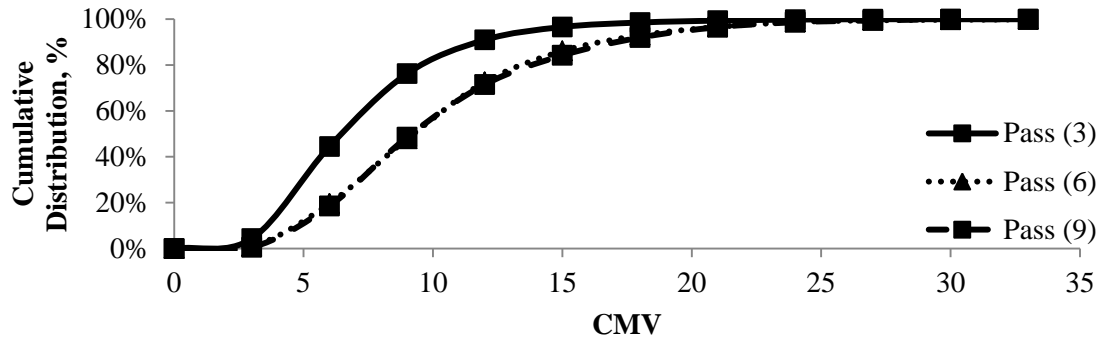
### A.5 Roller Integrated Compaction Monitoring

**Subgrade Layer:** This section presents the analysis and interpretation of the roller measurement values collected during the subgrade construction as explained in Chapters 4 and 5. The rolling pattern and data collection sequences during the subgrade construction are described in Chapter 4. For example, Pass 3 in Figure A.5.1a means two passes of the sheep foot roller and one pass of the IC roller. Figure A.5.1 presents the distributions of the roller compaction measurement values (CMV) with the number of roller passes for the three subgrade sections. From Figure A.5.1a, the CMV distribution for the dry section tends toward higher values with an increase in the compaction effort. From Figure A.5.1b, the CMV distributions for the OMC section after six and nine roller passes are close, indicating that six passes of the roller were optimal. Eleven roller passes were required to achieve the optimal compaction for the wet section. From Figure A.5.1c, the variations in the distribution of the CMV measurements of the wet section are comparable to the dry and OMC sections. However, the CMV measurements decrease with the increase in the number of passes for the wet section.

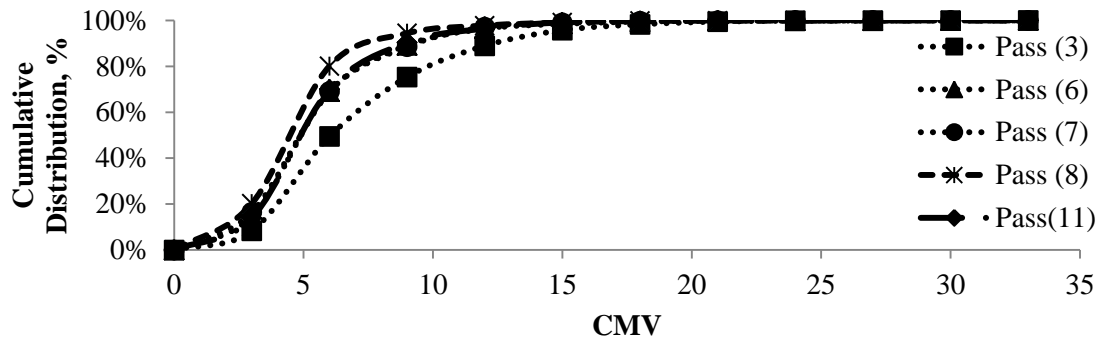
The contribution of the subgrade layer placed on the embankment was explored by comparing the CMV distributions before and after the placement of the subgrade. From Figures A.5.2a and A.5.2b, the CMV distributions before (labeled Mapping) and after the placement of the subgrade layer were similar. Since the embankment and subgrade materials were similar, one can conclude that the subgrade layer was placed properly. However, the CMV distribution for the embankment support of the wet section in Figure A.5.2c is substantially greater than the CMV distribution after the subgrade placement. This signifies the influence of moisture control during compaction for quality management.



(a) Dry Section SH 267 Subgrade (B)

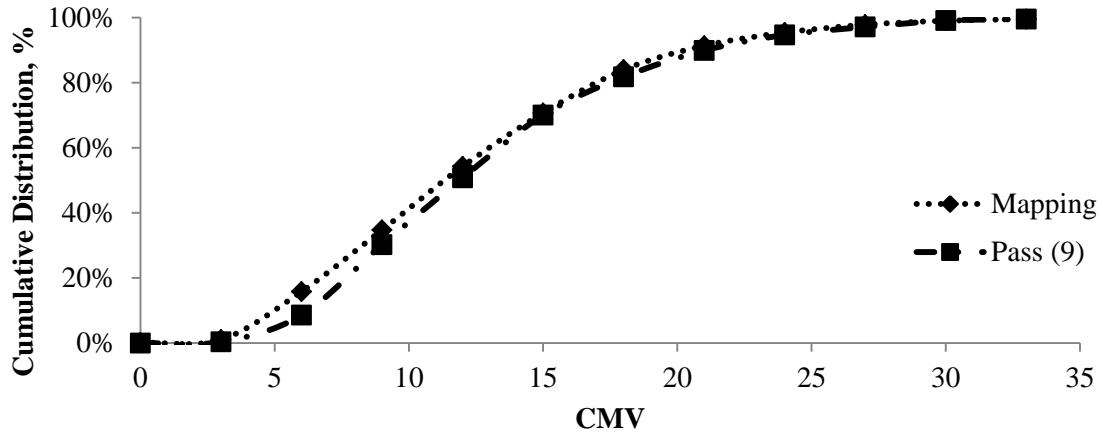


(b) OMC Section SH 267 Subgrade (A)

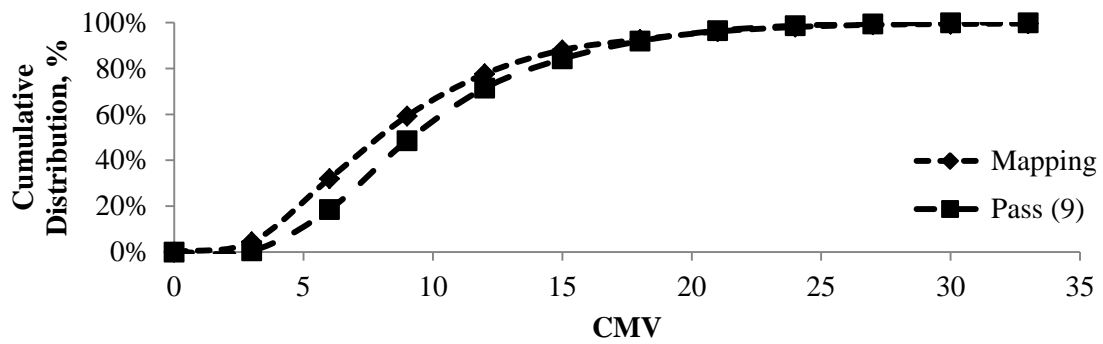


(c) Wet Section SH 267 Subgrade (B)

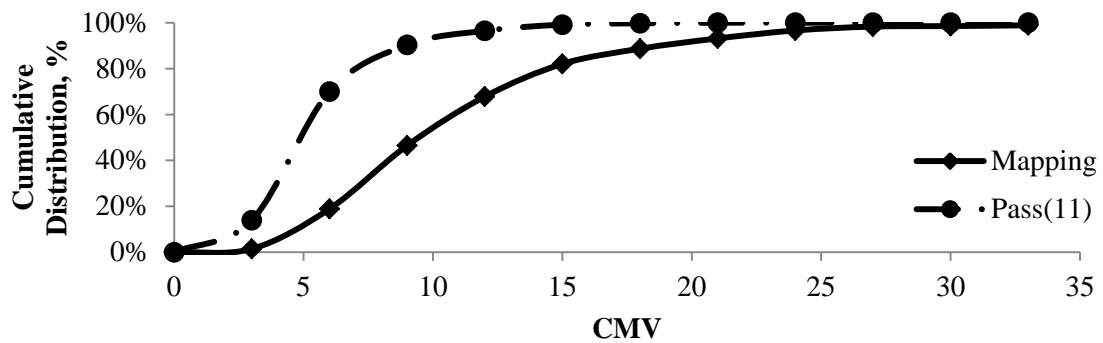
Figure A.5.1 - Distributions of CMV with Passes for different Subgrade Sections



(a) Dry Section SH 267 Subgrade (B)



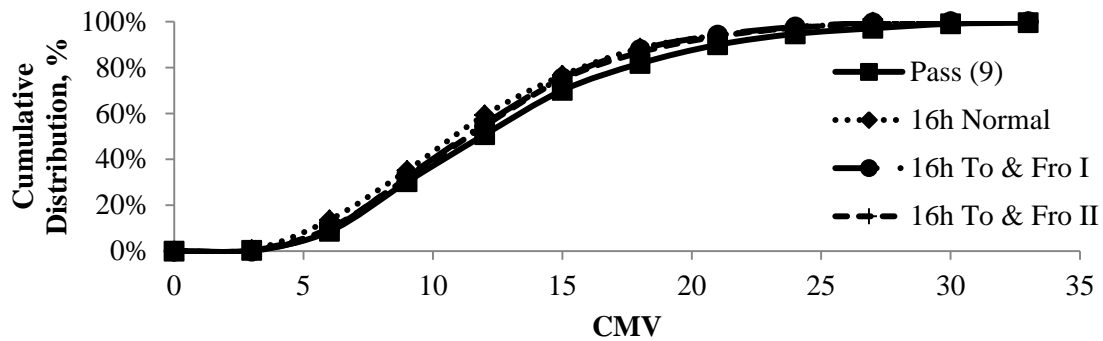
(b) OMC Section SH 267 Subgrade (A)



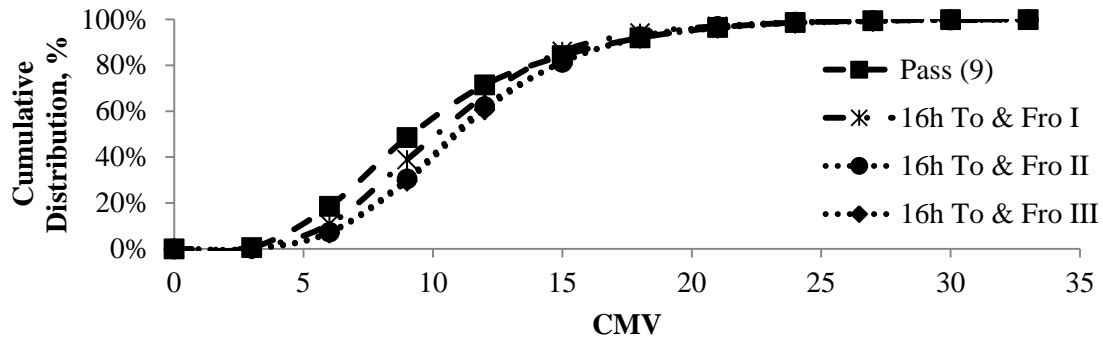
(c) Wet Section SH 267 Subgrade (B)

Figure A.5.2 - Influence of Subgrade Lift Placement for Subgrade Sections

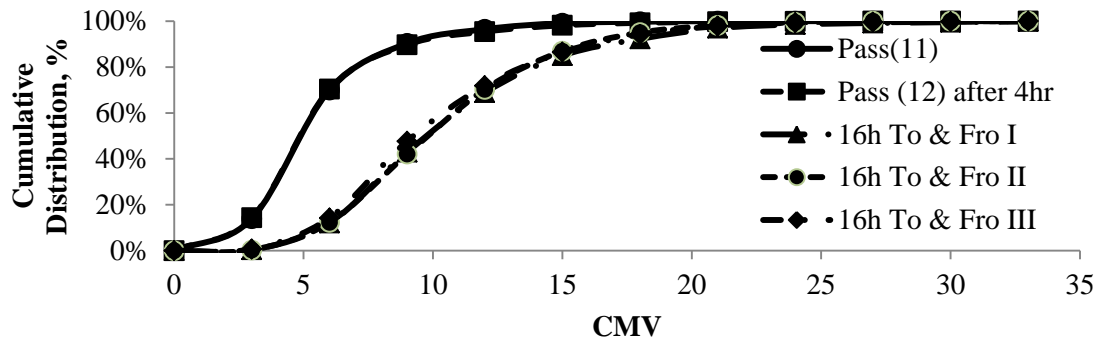
The influence of the rolling pattern and time of testing for quality assurance was assessed by studying the roller responses immediately after and 16 to 24 hrs after compaction. The rolling patterns were varied from the normal sequence to a forward and reverse sequence (To-and-Fro) at different times. Figures A.5.3a and A.5.3b present the distributions of the CMV values for the final pass and 16 hrs later with regular and to-and-fro patterns of rolling. For the dry and OMC sections, the CMV distributions remain comparable at different times and rolling sequences. However, for the wet section (Figure A.5.3c), the distributions of the CMV values after 16 hrs are substantially greater as compared to 4 hrs later and to the final pass. Figure A.5.4 presents the distributions of the CMV values for the production section before and after subgrade compaction. The two CMV distributions are comparable since the embankment and the subgrade material used were similar.



(a) Dry Section SH 267 Subgrade (B)



(d) (b) OMC Section SH 267 Subgrade (A)



(e) (c) Wet Section SH 267 Subgrade (B)

**Figure A.5.3 - Influence of Time on Roller Measurement Values for Subgrade Sections**

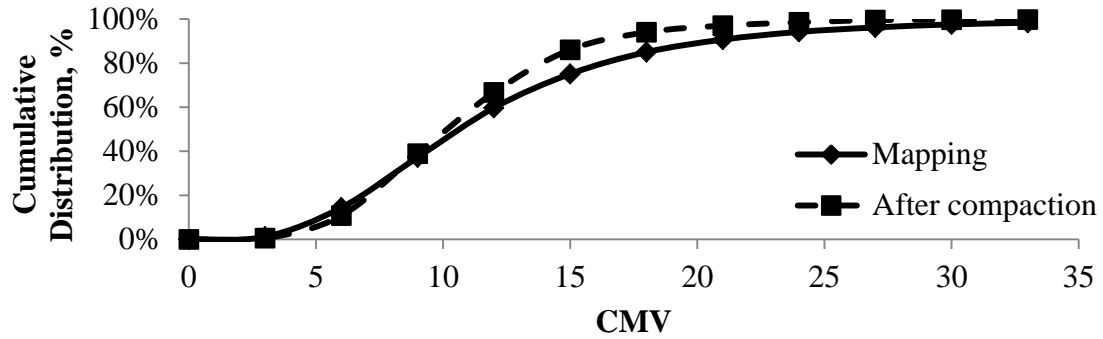


**Figure A.5.4 - Distributions of CMV with Passes for Production Section**

**Lime-Treated Subgrade:** The CMV distributions with the number of passes for the lime-treated subgrade section are illustrated in Figure A.5.5. Even though the CMV values increased with the number of passes, the variability of the CMV values also increased with the number of passes (as judged by the shapes of the distributions. Figure A.5.6 illustrates the effect of the lime treatment of the subgrade. The CMV measurements of the mapping (before lime treatment) are greater than after lime treatment. It is anticipated that the CMV values from the treated section will increase with time. This indicates that the timing of the proof mapping with the IC roller is important.

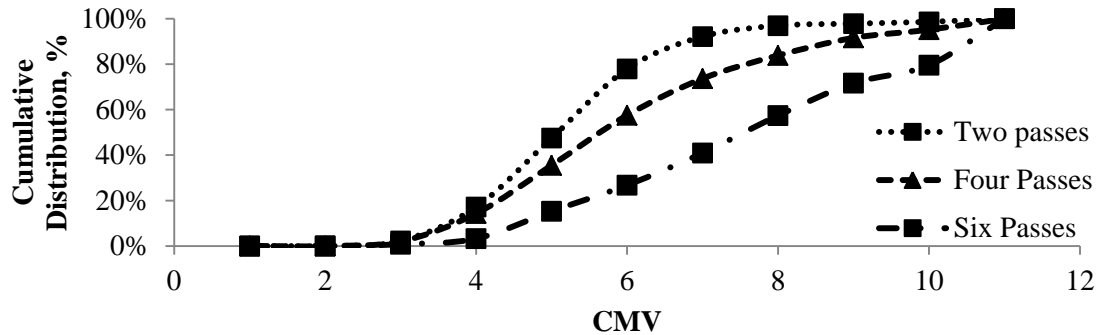


**Figure A.5.5 - Distributions of CMV with Number of Passes for Lime Treated Section**

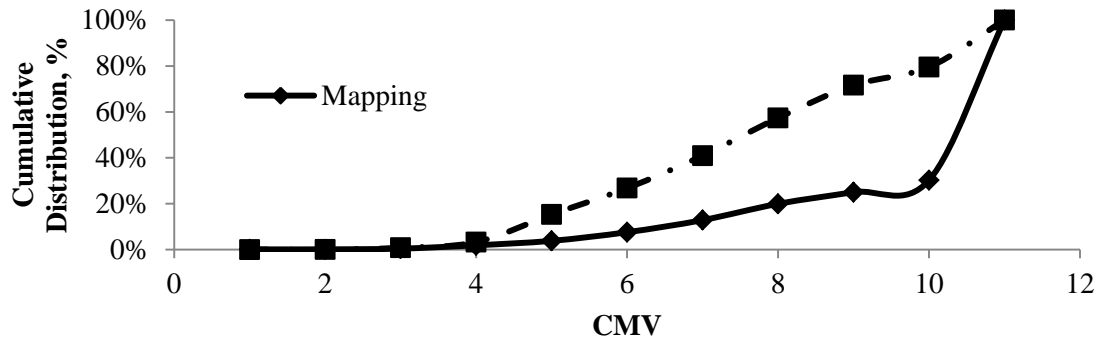
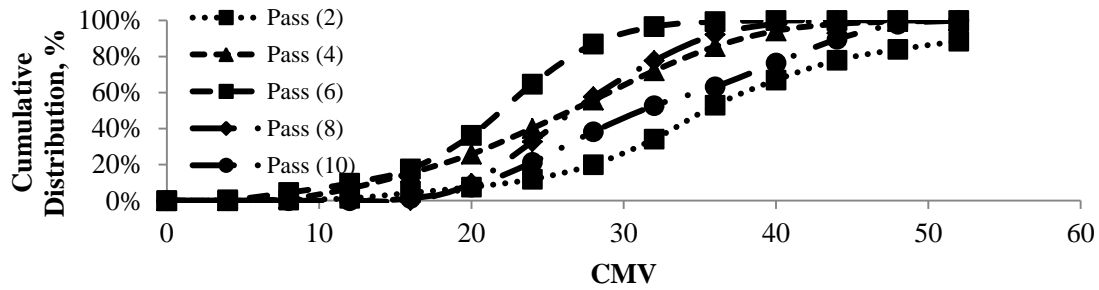


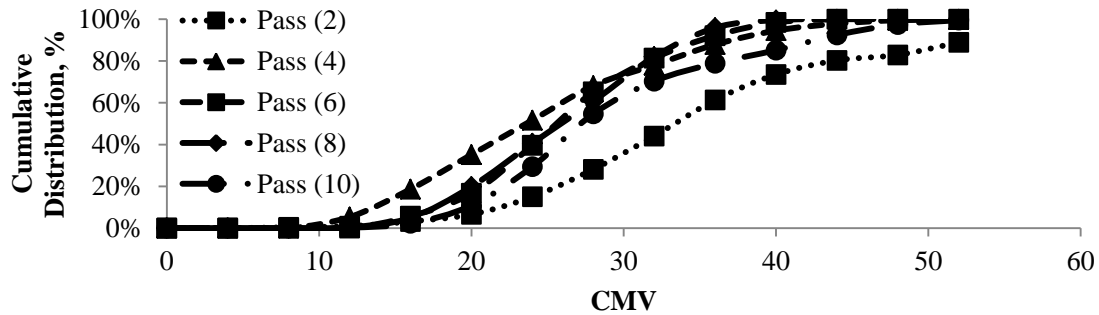
**Figure A.5.6 - Influence of Lime Stabilization**

**Base:** The construction sequence of the base layer was quite different as compared to the subgrade layers. The 10 in. thick layer of base material was compacted by placing 2 to 2 ½ in. thick successive lifts of base material. Each lift was graded and watered before rolling. Figure A.5.7 presents the distributions of the CMV measurements with the number of passes for the sections placed at different moisture contents. For the base layer constructed towards the dry side of the OMC in Figure A.5.7a, the increase in the roller passes (up to 8 passes) reduces the variability in the CMV distributions (i.e., a more uniform section). For both the dry and OMC sections, the CMV measurements are more uniformly distributed for Pass 6 and Pass 8 when compared to the lower and higher number of passes.

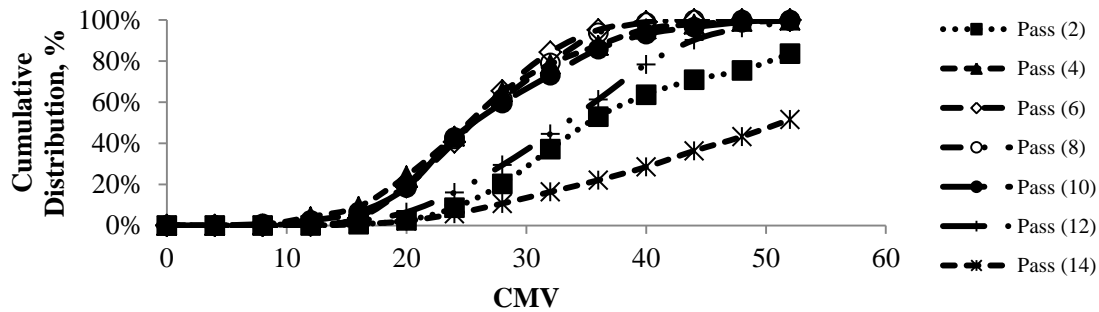
The wet section was reworked after 10 passes to achieve the required moisture content. Hence, four additional roller passes were required to meet the quality requirements similar in the dry and OMC sections. From Figure A.5.7c, the distributions of the CMV values remain similar until the 10th roller pass. Substantial differences in the CMV distributions can be observed after the 12th and 14th passes. The differences in the CMV distributions can be attributed to the rework carried out and the base layer being compacted as a single lift. Hence, the CMV values are also substantially higher than Passes 2 to 10.



(a) Dry Section SH 267 Base



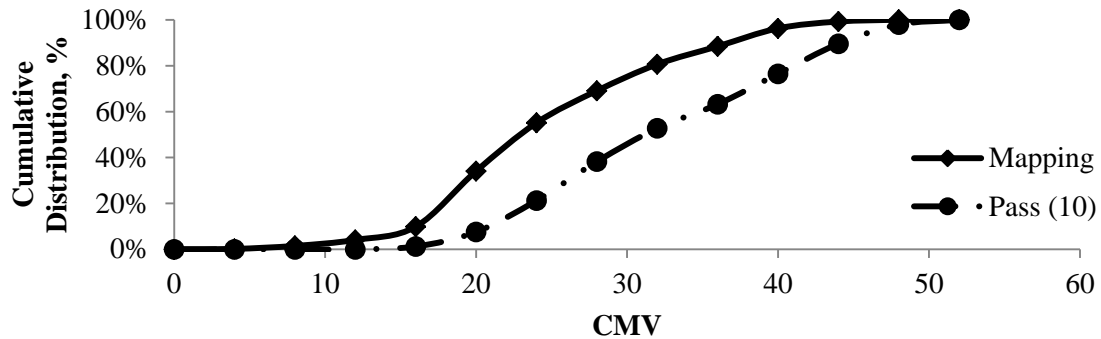
(b) OMC Section SH 267 Base



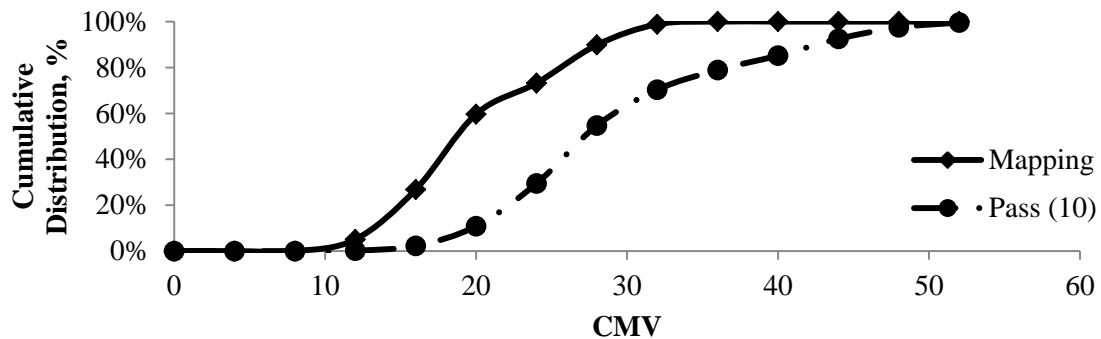
(c) Wet Section SH 267 Base

Figure A.5.7 - Distributions of CMV with Passes for different Base Sections

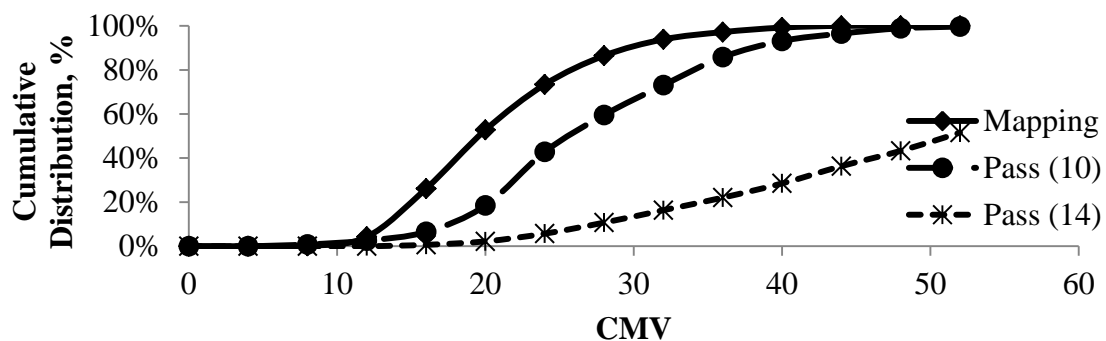
The structural contribution of the base layer to the pavement structure was assessed by mapping the ground support conditions before and after the base layer placement. Figure A.5.8 demonstrates the variations in the roller measurements for the three sections before and after the base layer placement. For the dry and OMC sections, the CMV values are substantially higher than the ground support conditions. The CMV values for the dry section (Figure A.5.8a) are greater than those for the OMC section (Figure A.5.8b). The CMV values for the wet section (Figure A.5.8c) are substantially greater than the ground support conditions and even higher than the dry and OMC sections. This pattern can be due to the rework of the wet base and collecting the roller data for the entire lift at the time of compaction.



(a) Dry Section SH 267 Base



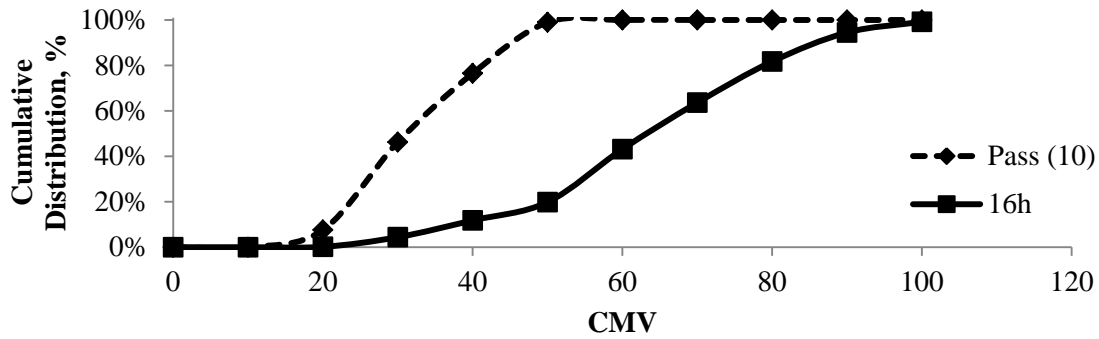
(b) OMC Section SH 267 Base



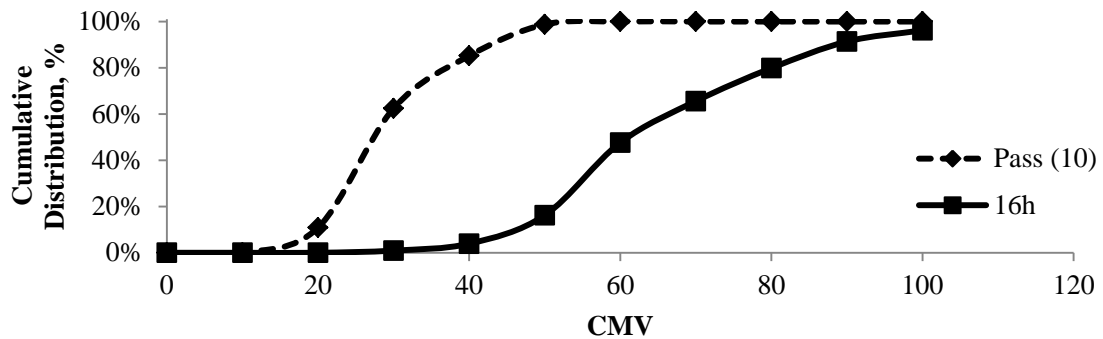
(c) Wet Section SH 267 Base

Figure A.5.8 - Influence of Base Lift Placement for different Test Sections

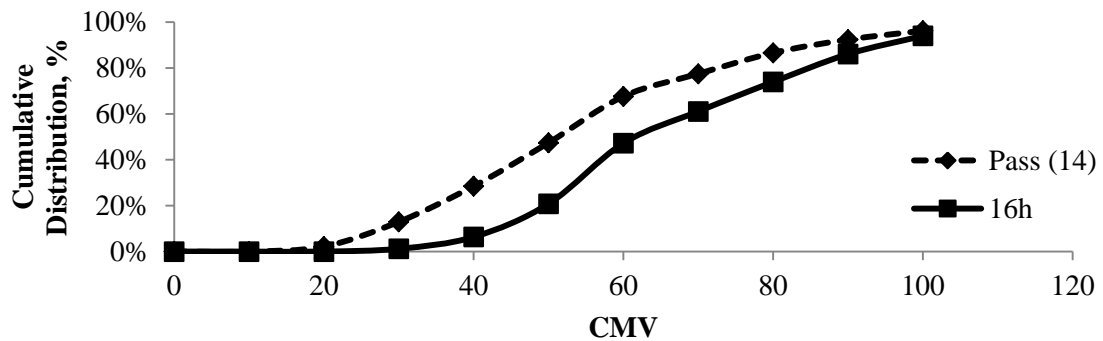
The influence at the time of testing on the CMV measurements was assessed by comparing the roller data collected at the end of compaction and 16 hrs after compaction as reflected in Figure A.5.9. The dry (Figure A.5.9a) and OMC (Figure A.5.9b) sections demonstrate similar trends. The CMV measurements after compaction were significantly less than those measured after 16 hrs. The difference in the CMV measurements after compaction and 16 hrs after compaction are not as different as for the cases of the dry and OMC sections. It seems that the production process and moisture variation highly influenced the roller measurements.



(a) Dry Section SH 267 Base



(b) OMC Section SH 267 Base



(c) Wet Section SH 267 Base

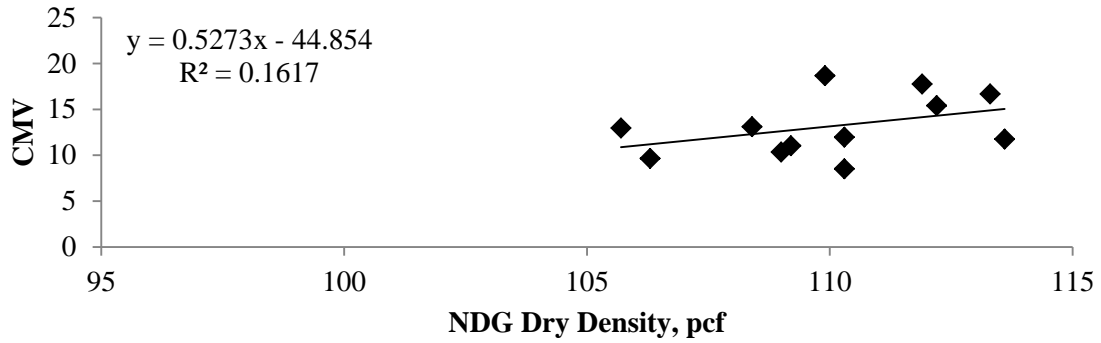
Figure A.5.9 - Influence of Time of Testing on Roller Measurement Values for Base Sections

## **A.6 Relations between Roller Measurements and NDT Devices**

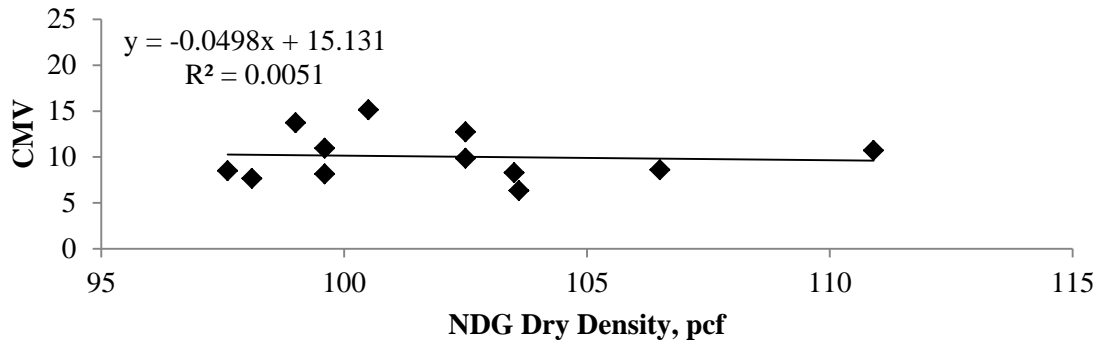
**NDG Density:** Figures A.6.1 through A.6.3 present the relationships between the dry density from the NDG and the CMV measurements for all sections tested. The two parameters are not strongly correlated.

**LWD Modulus:** Figures A.6.4 through A.6.6 illustrate the relationships developed between the CMV and the LWD moduli taken at different locations. The correlations between the LWD and CMV measurements are also not very strong.

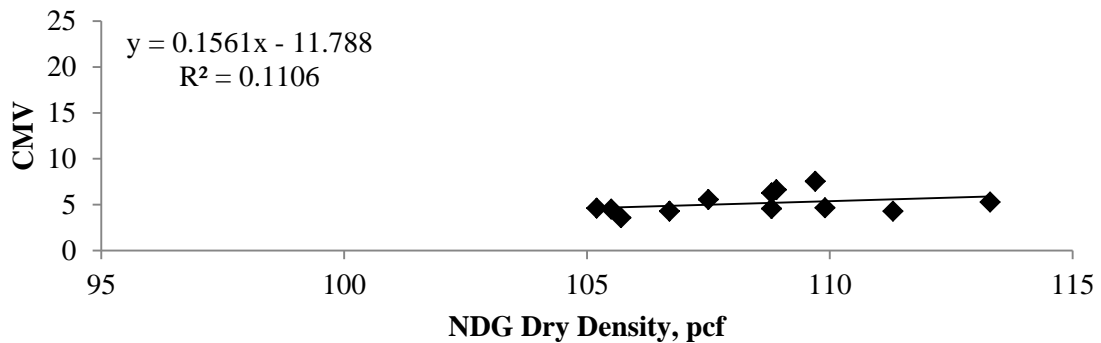
**PSPA Modulus:** As reflected in Figure A.6.7 through A.6.9, the relationships between the CMV measurements and PSPA moduli are not very strong either.



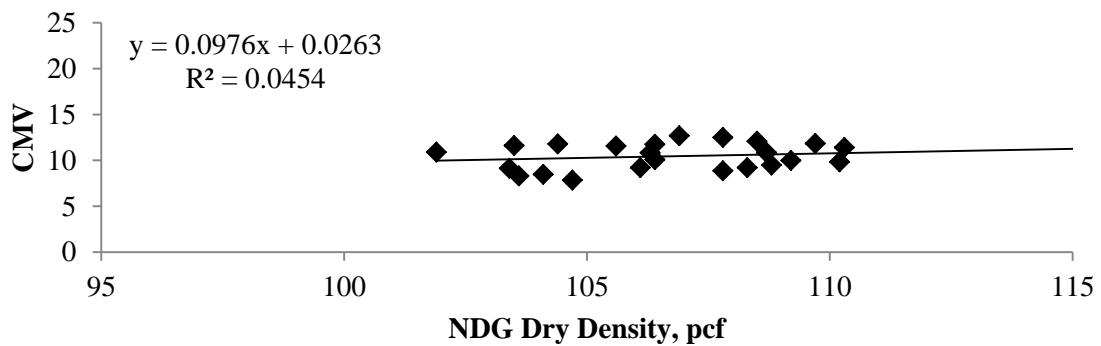
(a) Dry Section (Subgrade B)



(b) OMC Section (Subgrade A)

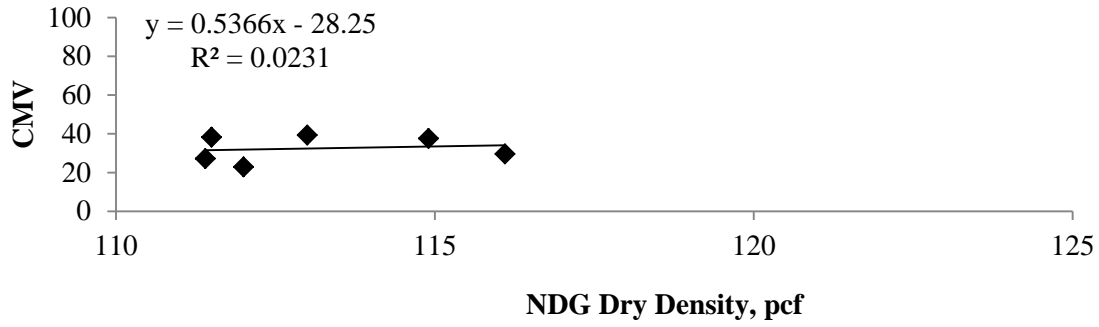


(c) Wet Section (Subgrade B)

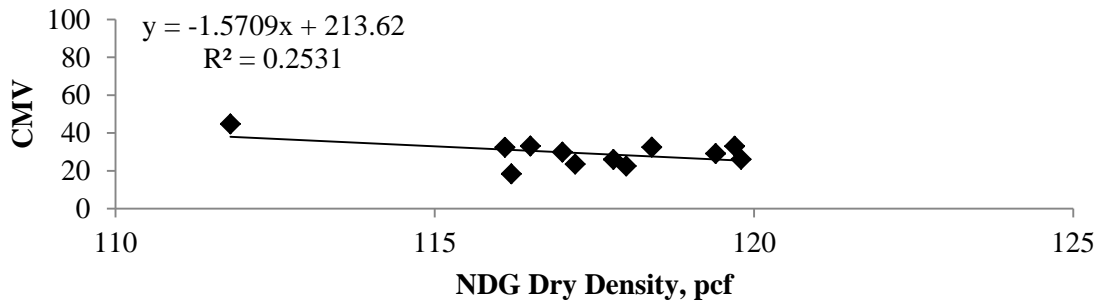


(d) Production Section (Subgrade A)

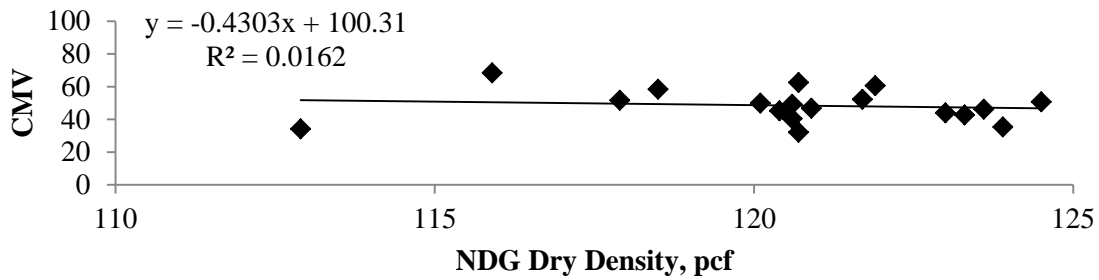
Figure A.6.1 - Relations between the NDG Dry Density and the CMV for Subgrade Sections



(a) Dry Section



(b) OMC Section



(c) Wet Section

Figure A.6.2 - Relations between the NDG Dry Density and the CMV for Base Sections

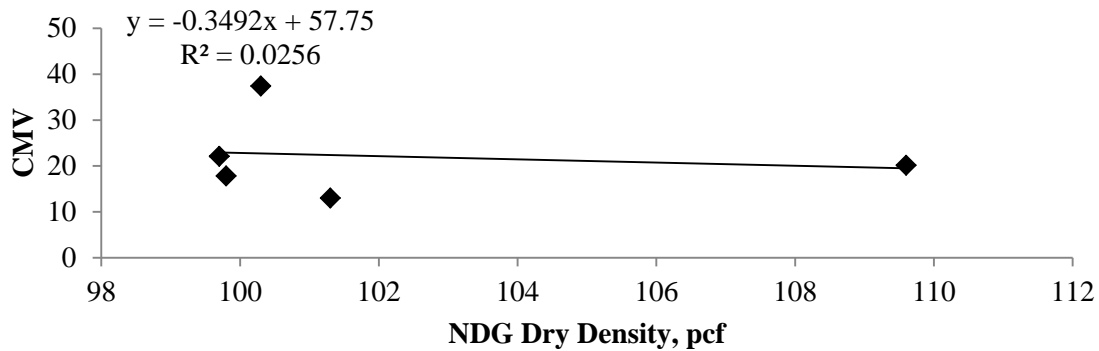
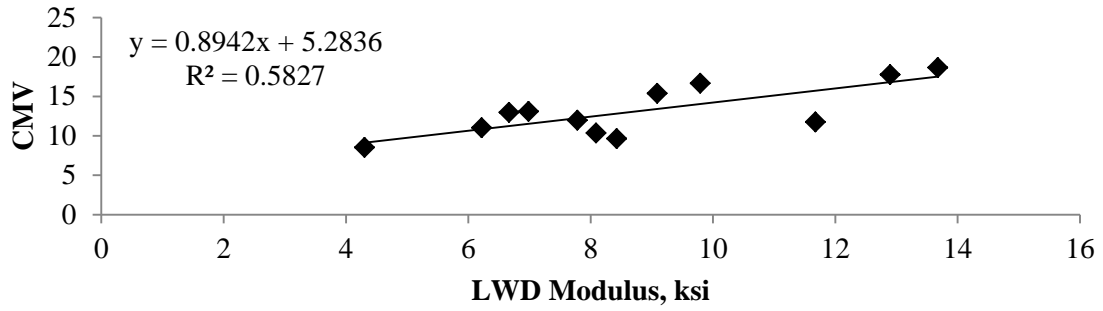
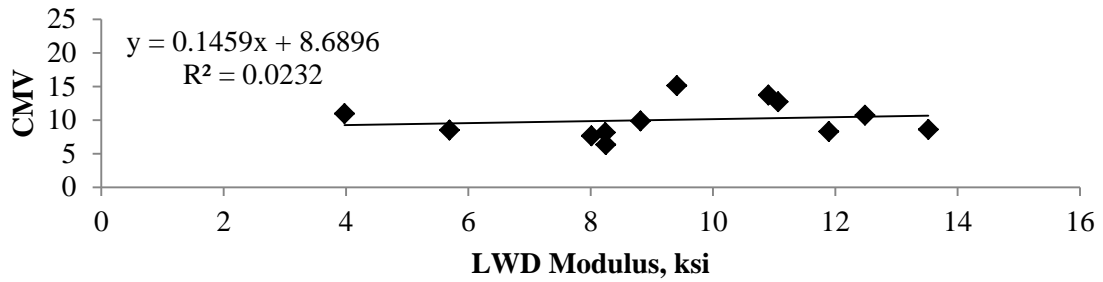


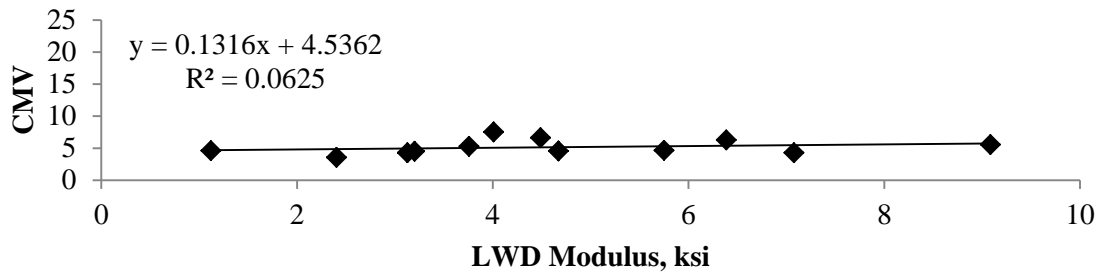
Figure A.6.3 - Relation between the NDG Dry Density and the CMV for Lime Treated Subgrade



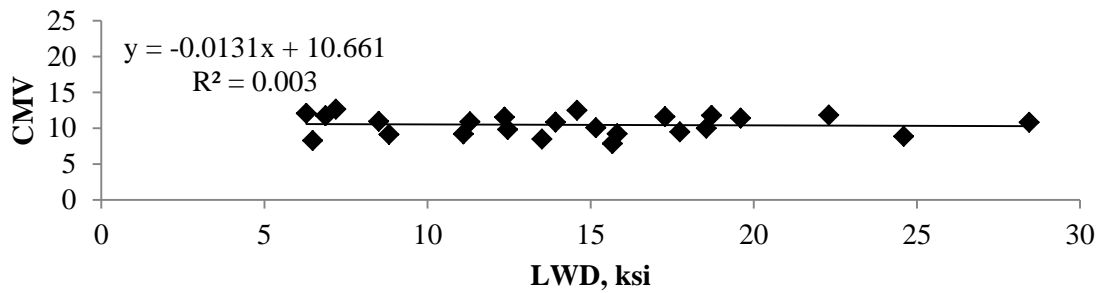
(a) Dry Section



(b) OMC Section

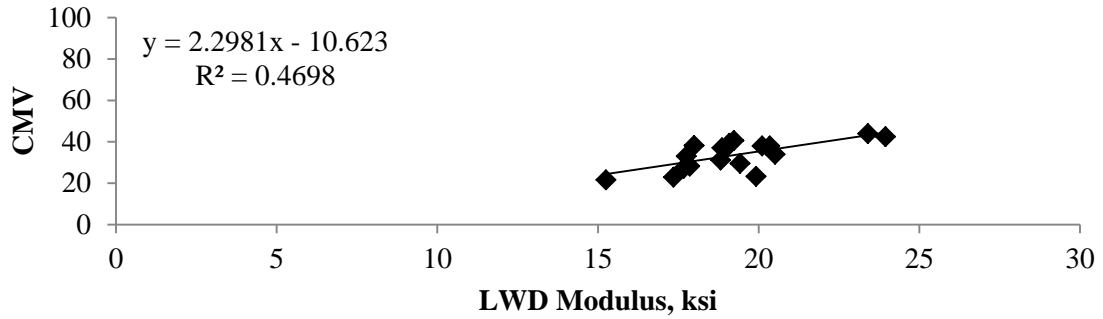


(c) Wet Section

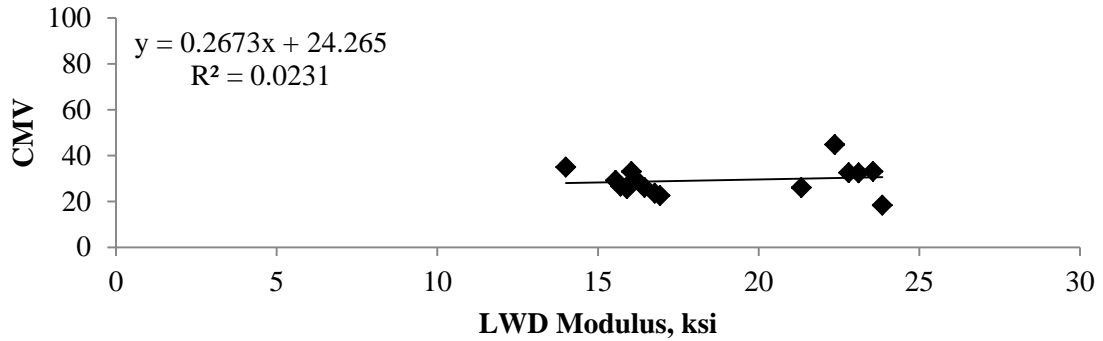


(d) Production Section

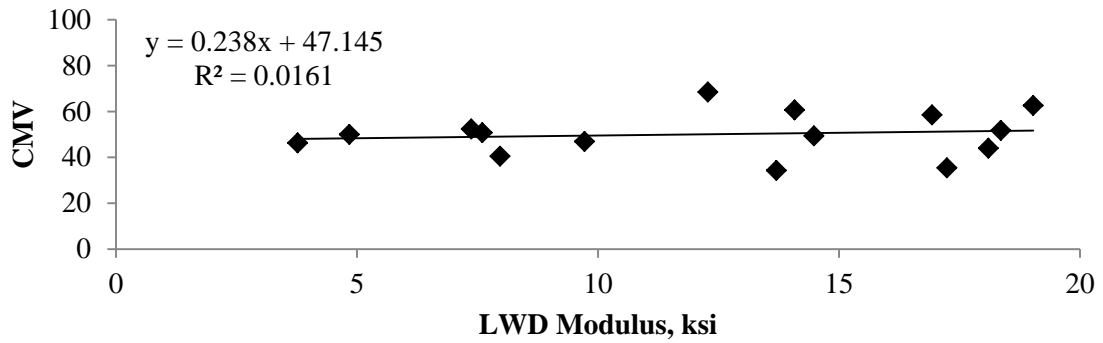
Figure A.6.4- Relations between the LWD Modulus and the CMV for Different Sections of Subgrade



(a) Dry Section



(b) OMC Section



(c) Wet Section

Figure A.6.5- Relations between the LWD Modulus and the CMV for Base Sections

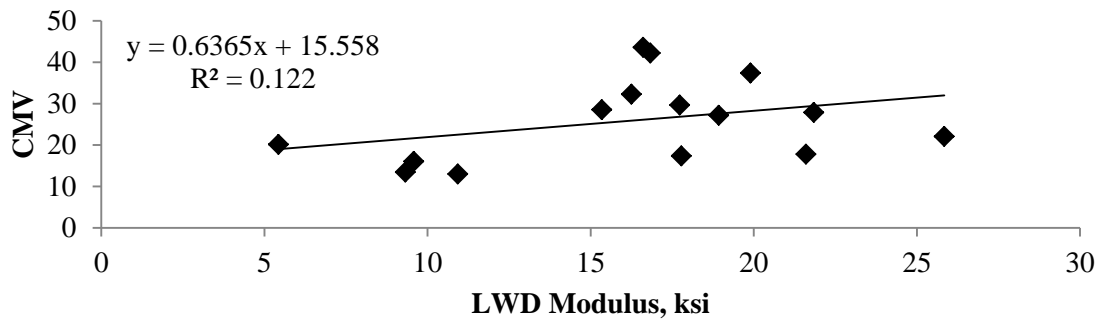
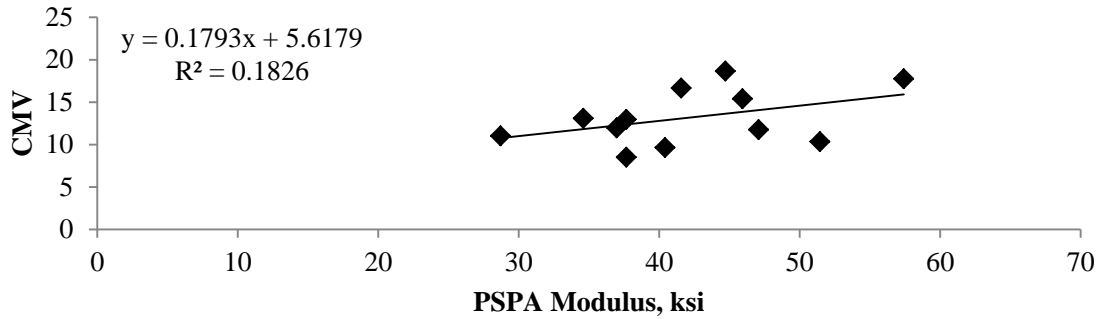
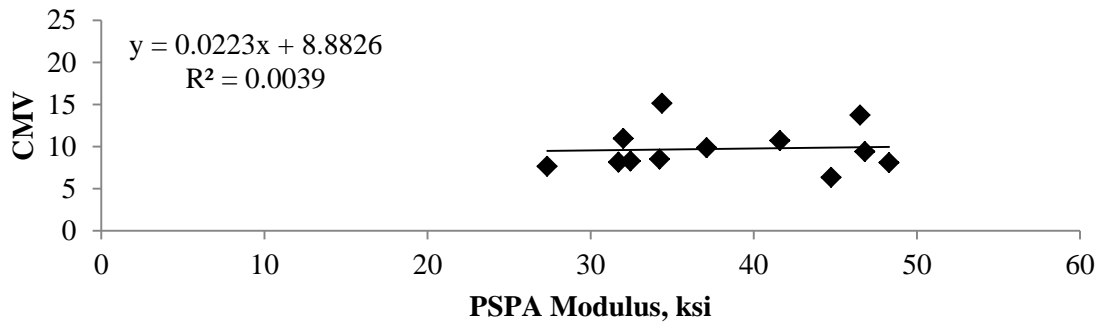


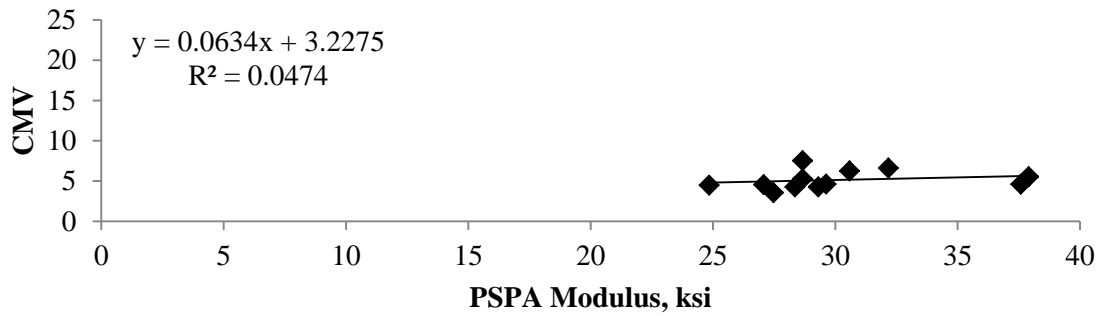
Figure A.6.6- Relations between the LWD Modulus and the CMV for Lime Treated Subgrade Section



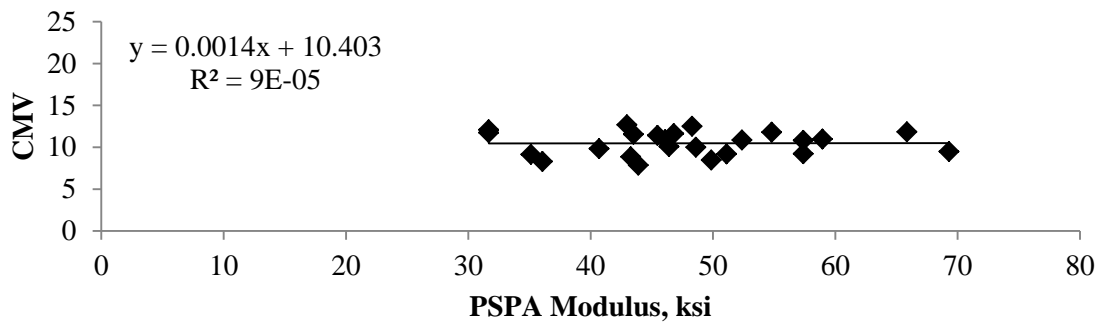
(a) Dry Section



(b) OMC Section

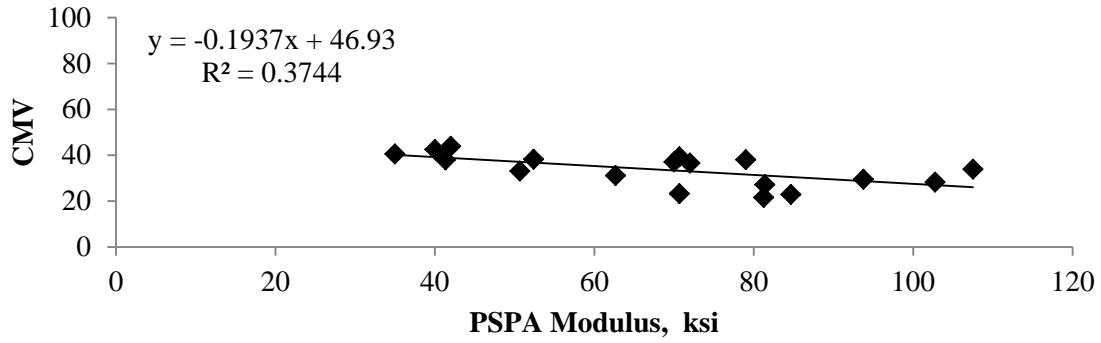


(c) Wet Section

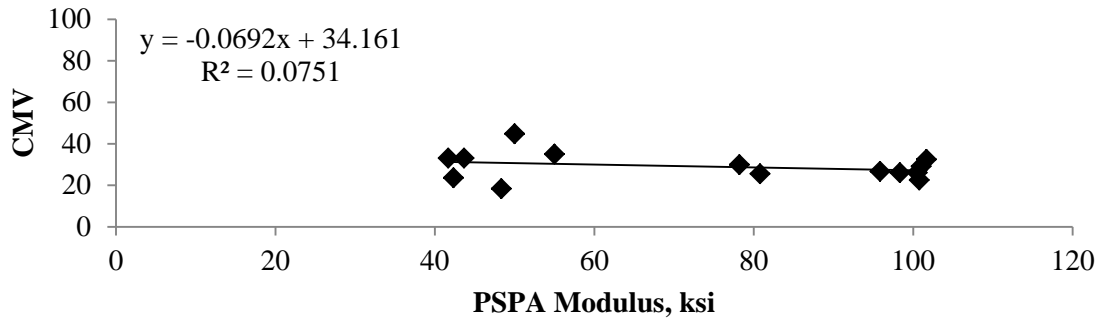


(d) Production Section

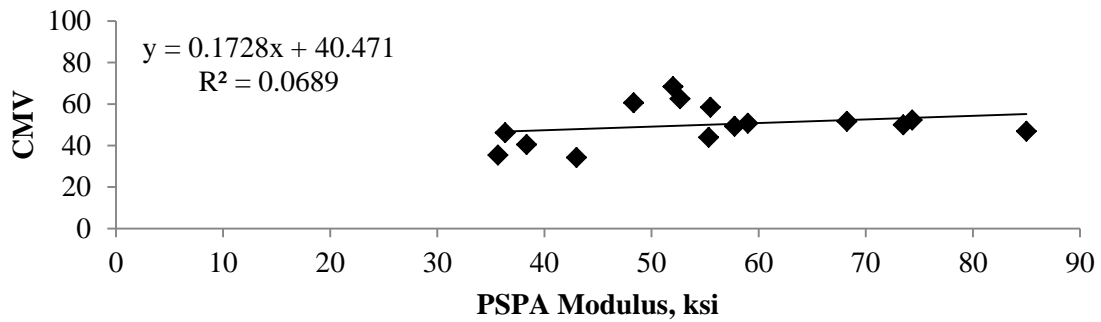
Figure A.6.7- Relations between the PSPA Modulus and the CMV for different Sections of Subgrade



(a) Dry Section



(b) OMC Section



(c) Wet Section

Figure A.6.8- Relations between the PSPA Modulus and the CMV for Base Sections

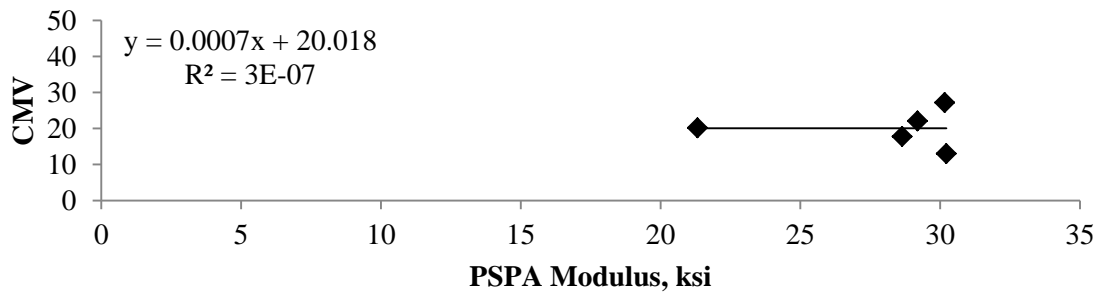


Figure A.6.9- Relations between the PSPA Modulus and the CMV for Lime Treated Subgrade Section

## **Appendix B**

### **FIELD EVALUATION CASE STUDY (IH 35W)**

## FIELD EVALUATION CASE STUDY: IH 35W

### B.1 Introduction

This Appendix presents the detailed analysis of the data collected from a second field evaluation activity on IH 35W in Tarrant County north of Fort Worth, Texas. This project was part of the reconstruction of the existing lanes and adding toll lanes on IH 35W.

### B.2 Evaluating Moisture-Density Devices' Results

**Embankment Layer** - The NDG test results on top of the prepared embankment layer are shown in Figure B.2.1. The average NDG moisture content was 17.6%, which was about 3.6% less than the actual OMC and 1.3% above the nominal OMC. The average dry density was 106.8 pcf, which was 5.7 pcf greater than the MDD.

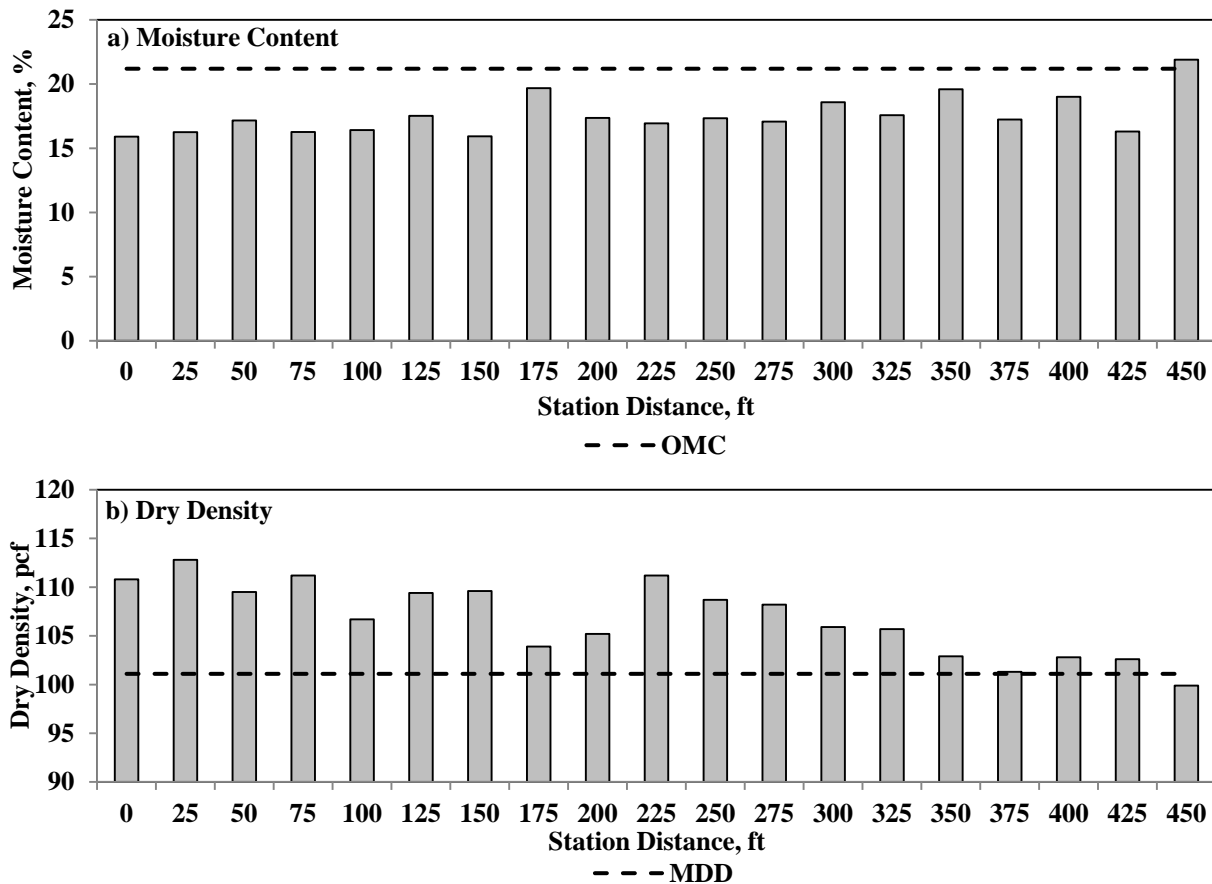


**Figure B.2.1 – Spatial Variations of the NDG Moisture Content and Dry Density of Embankment Layer**

**Subgrade Layer** - The subgrade was prepared at three different moisture contents (wet of OMC, OMC, and dry of OMC) and compacted with a sheep foot compactor and a smooth drum IC roller. Figure B.2.2 depicts the SDG and NDG moisture contents immediately after the final pass of the IC roller. Based on the NDG results, the three sections were placed dry of OMC as compared to the actual Proctor tests and around the contractor's target OMC. The SDG results show more dispersion from the target moisture contents. The oven dry moisture contents from the field specimens exhibit nonuniform variation in moisture contents at the site.

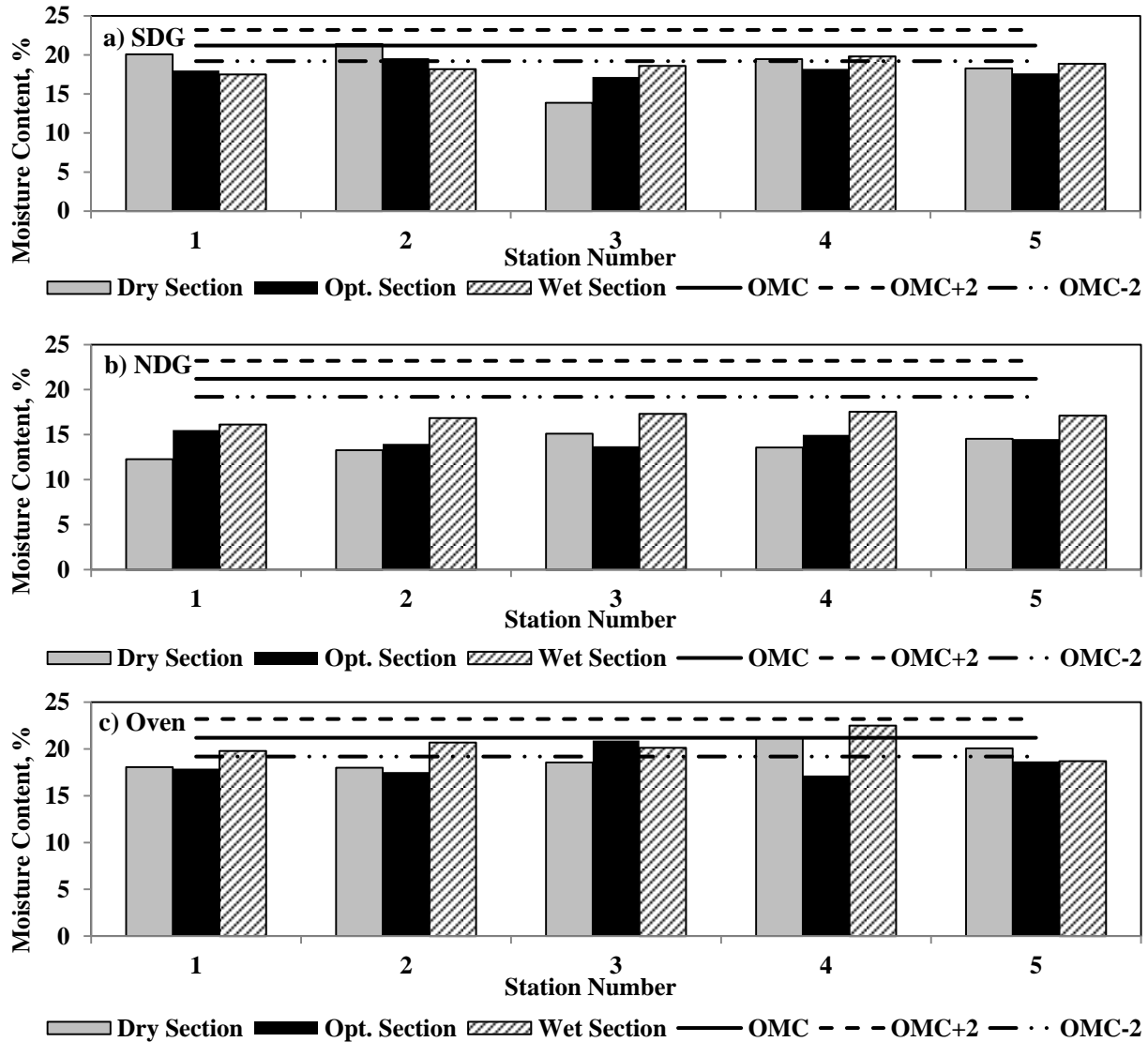


**Figure B.2.2 – Spatial Variations of Moisture Contents Immediately after Compaction of Subgrade**

Figure B.2.3 summarizes the SDG and NDG dry densities after the compaction of the subgrade layer. All test sections yielded dry densities that exceeded the acceptance limit of 95% of MDD. The average SDG dry densities were about 132 pcf, which is much greater than the NDG average dry density of 109.5 pcf.

Figure B.2.4 summarizes the NDG moisture contents during the passes of the IC roller. Considering typical uncertainties associated with the NDG, the moisture contents do not change appreciably between passes. The same process was repeated for the measured NDG densities in Figure B.2.5. It seems that the optimum number of passes is perhaps four.

The SDG and NDG moisture contents are compared with the oven moisture contents in Figures B.2.6 and B.2.7. Since the SDG data were collected only after the final pass of the IC roller, the number of data points illustrated in Figure B.2.6a is less than in Figure B.2.6b. Overall, the NDG readings are less than the oven moisture contents, while the SDG moisture contents are scattered about the oven moisture contents.

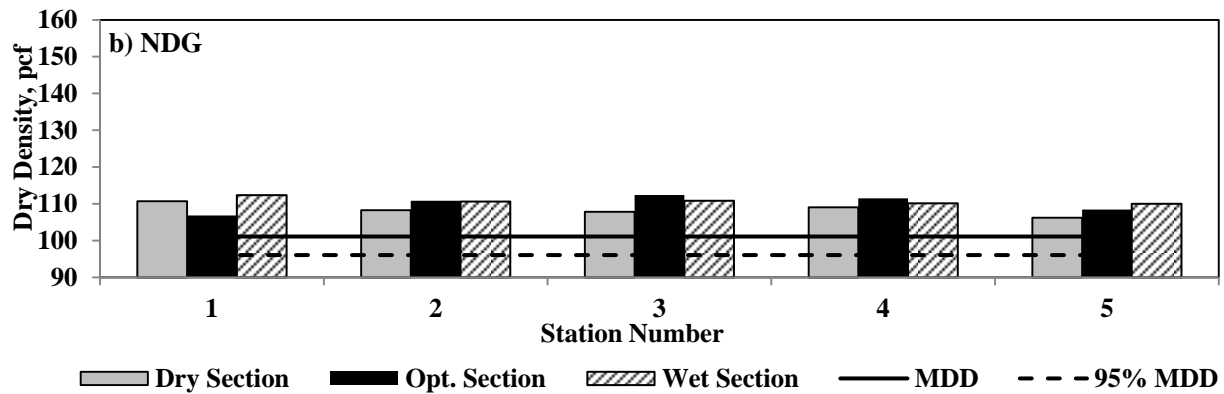
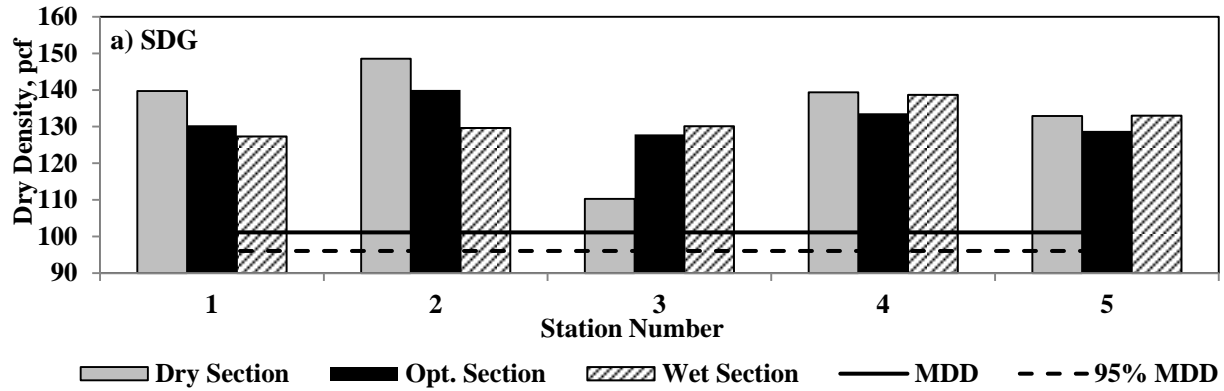


Figure B.2.3 – Spatial Variations of Dry Densities Immediately after Compaction of Subgrade

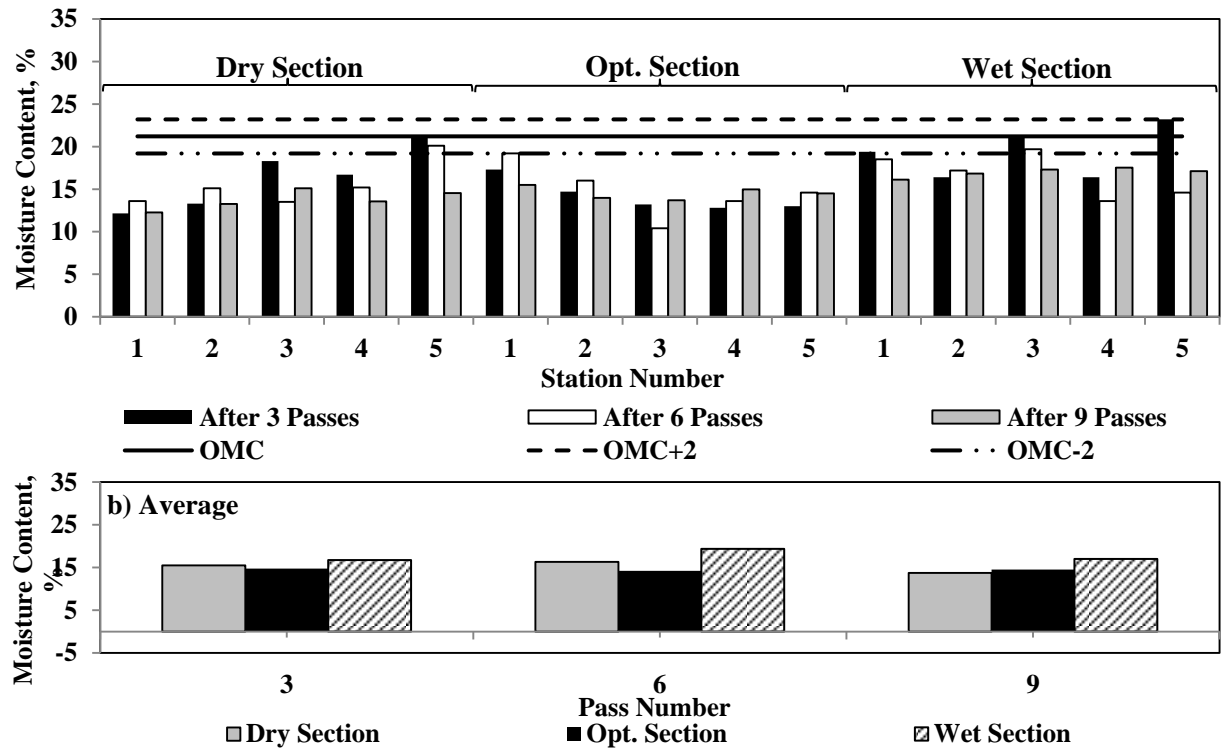


Figure B.2.4 – Variations of the NDG Moisture Contents during Compaction of Subgrade Layer

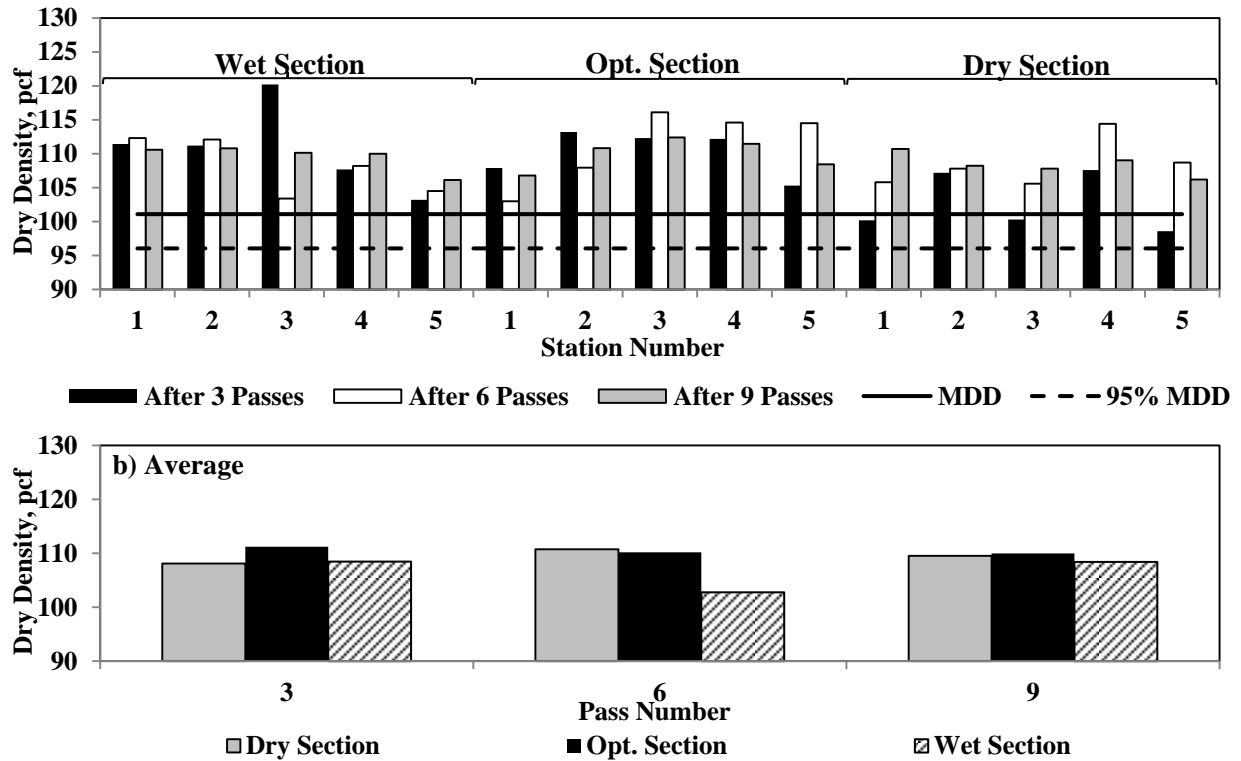


Figure B.2.5 – Variations of the NDG Dry Density during Compaction of Subgrade Layer

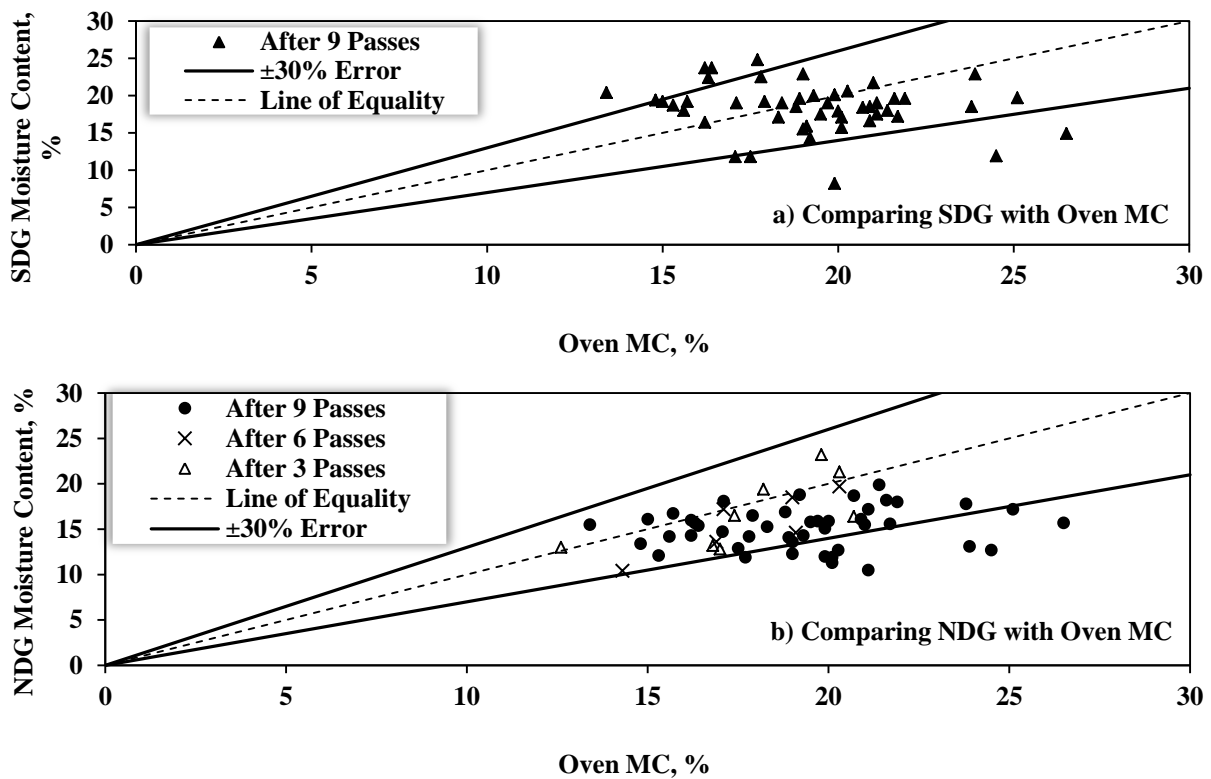


Figure B.2.6 – Comparisons of the SDG and the NDG Moisture Contents with Oven Moisture Contents for Subgrade Layer

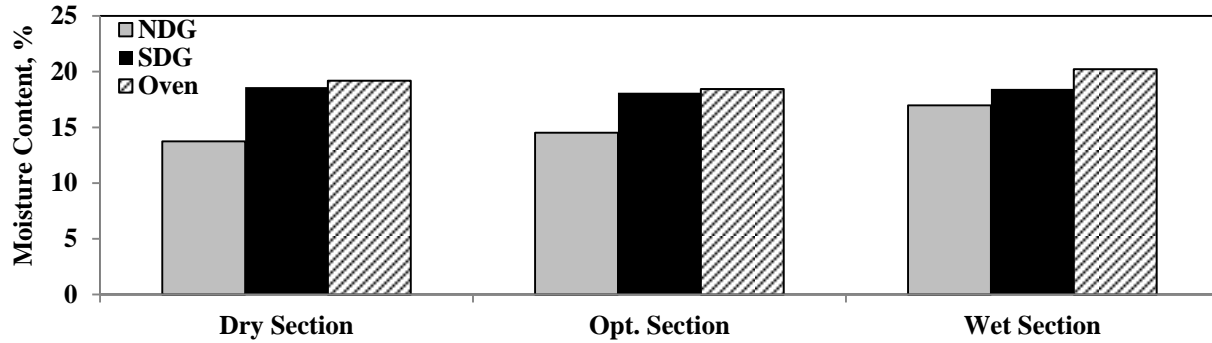


Figure B.2.7 – Average Moisture Contents after Compaction of Subgrade Layer from Different Methods

### B.3 Evaluating Variability of Layer Properties with Modulus-Based Devices

**Embankment Layer** - Figure B.3.1 summarizes the results of the modulus-based devices used on the embankment layer. The PSPA and LWD devices depict the same general patterns of modulus variation throughout the test section. The average PSPA modulus is 30 ksi and the average LWD moduli is 6 ksi.

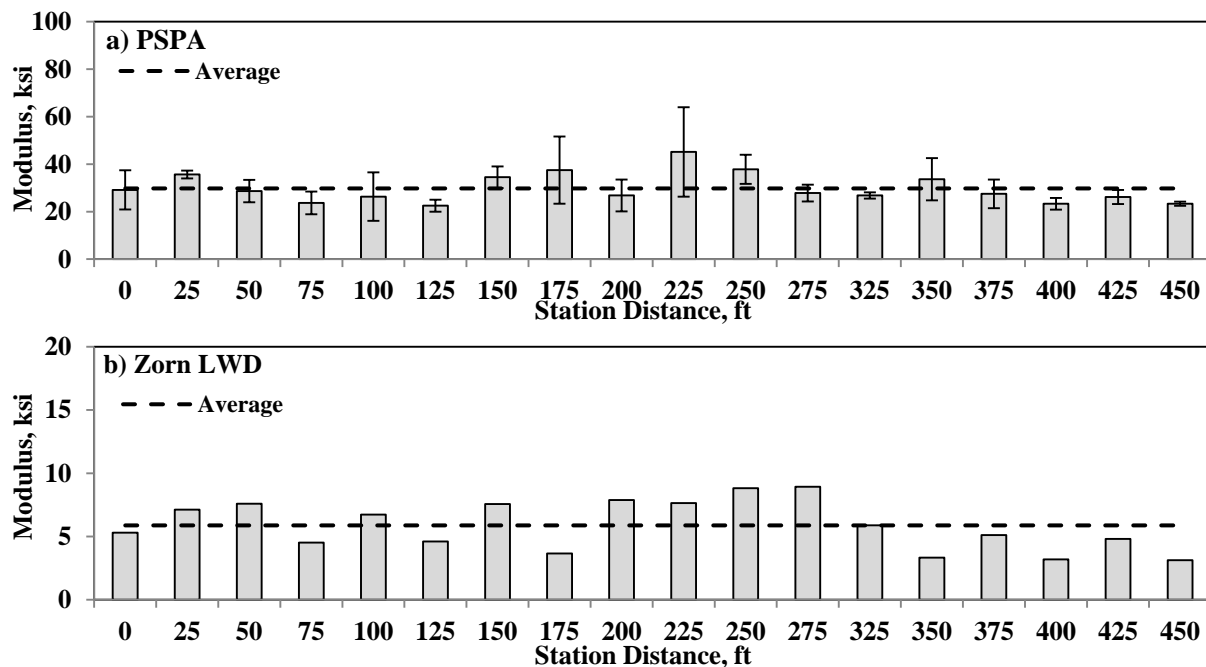
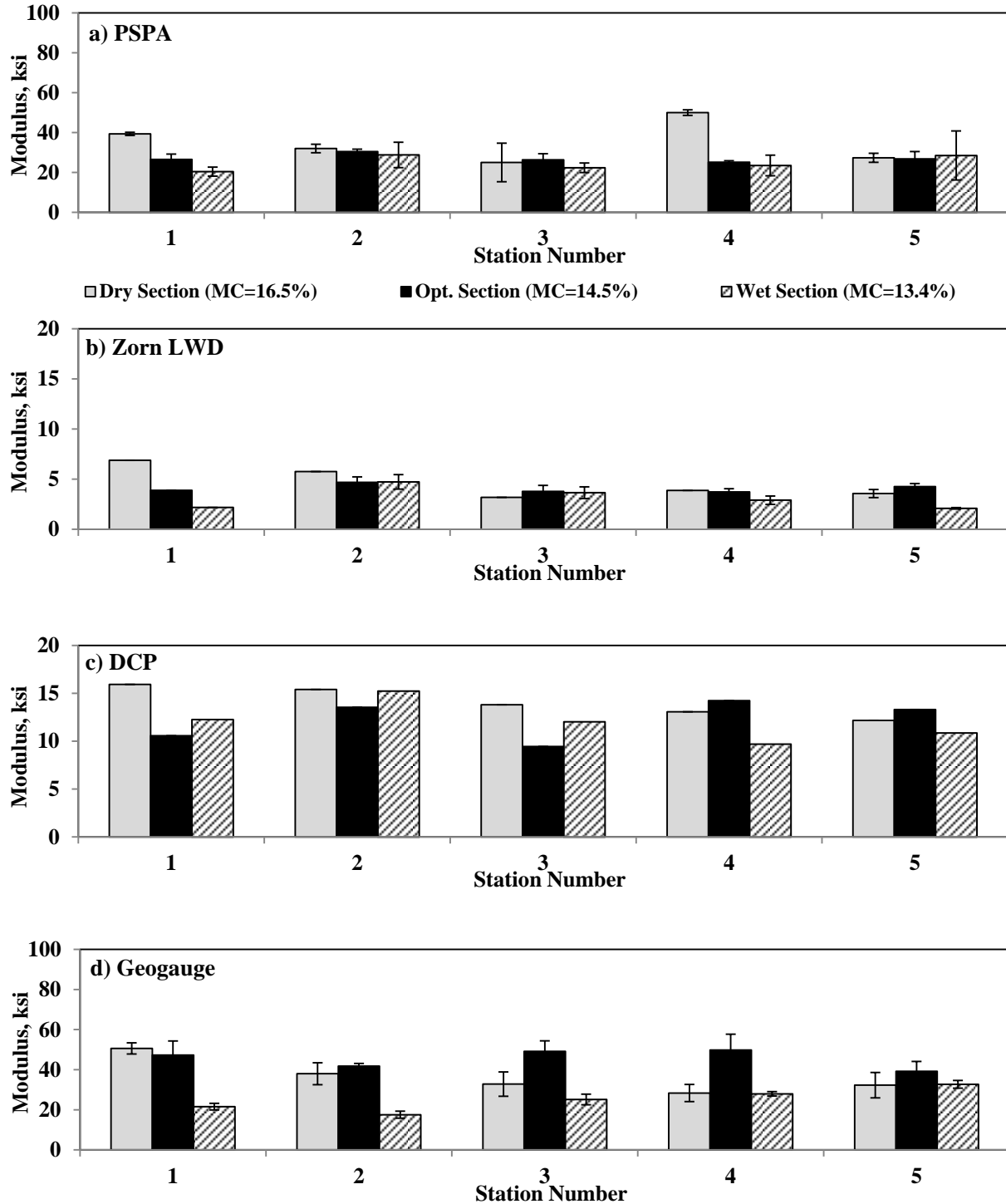


Figure B.3.1 – Spatial Variations of Measured Modulus of Embankment Layer before Placement of Subgrade Materials

**Subgrade Layer** - The measured moduli on top of the subgrade layer immediately after compaction are shown in Figure B.3.2. The standard deviation of replicate tests at each test point is depicted as error bars in the Figure. According to the PSPA measurements, the average moduli of the dry, optimum and wet sections are 35 ksi, 27 ksi and 25 ksi, respectively. The average LWD moduli are 5 ksi, 4 ksi and 3 ksi, respectively. The average DCP moduli are 14 ksi, 12 ksi and 12 ksi for the dry, optimum and wet sections, respectively. The DCP shows a similar trend to the PSPA and LWD. Based on the Geogauge readings, the average moduli are 36 ksi, 45 ksi and 25 ksi, respectively. The high average Geogauge modulus of the second section could be due to the high variability of the measurements.



**Figure B.3.2 – Variations of Measured Moduli of Subgrade Layer with Different Devices**

Figures B.3.3 and B.3.4 depict the variations of the PSPA and LWD moduli during the compaction process, and after the 2<sup>nd</sup>, 4<sup>th</sup> and 6<sup>th</sup> passes of the sheep foot roller. Some of the LWD data points from the second pass are missing due to device malfunction. The variations in the moduli after the second pass

are small with both devices. Slight degradation or increase in modulus with the increase in the number of passes is observed.

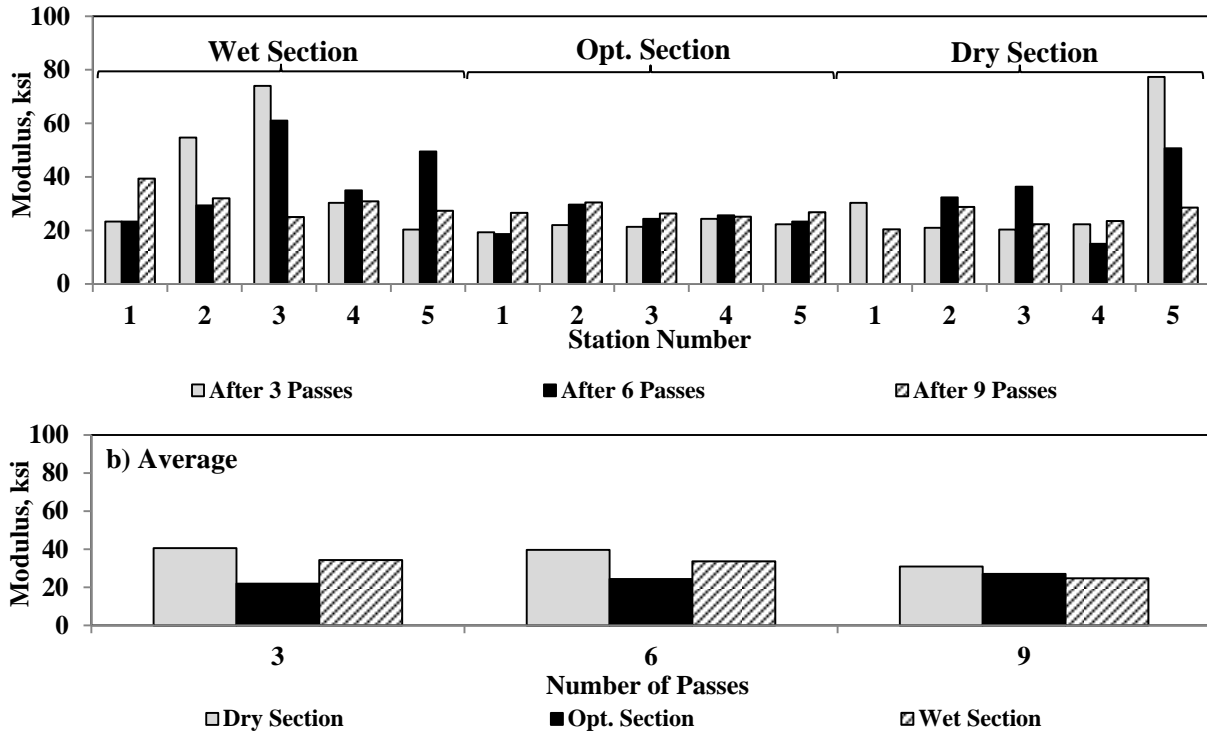


**Figure B.3.3 – Measured PSPA Moduli between Passes of IC Roller during Compaction of Subgrade Layer**

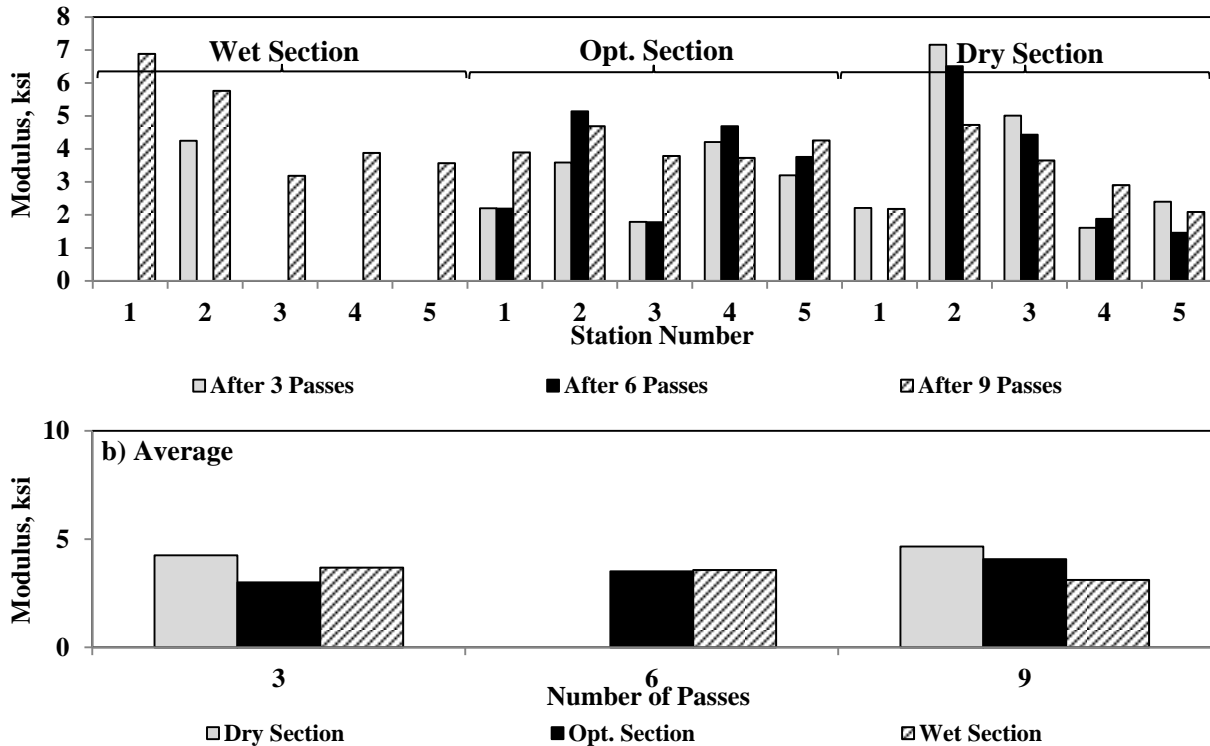


**Figure B.3.4 – Measured Zorn LWD Moduli between Passes of IC Roller during Compaction of Subgrade Layer**

#### **B.4 Roller Integrated Compaction Monitoring**

The new Caterpillar roller available at the site came with the factory installed MDP data kit. In addition to the existing MDP kit, a Trimble accelerometer kit collecting CMV was also installed on the same roller on the second day of the field study. Due to the delay in installation of the Trimble kit, only the MDP measurements were recorded on the existing embankment on all the three test sections. Due to a malfunction, the MDP measurements from the 3<sup>rd</sup> pass on the dry and OMC sections were not recorded. Both the MDP and CMV data were recorded successfully for all passes of the wet section. IC measurements 16 hrs after compaction on the wet section were not carried out due to roller break down.

Figure B.4.1 presents the cumulative distributions of the MDP and/or CMV measurements during the compaction process of the three subgrade sections. The MDP measurements for the dry section (Figure B.4.1a) increased with an increase in the number of roller passes despite the theoretical concept of the reduction in the MDP with an increase in the compactive effort. The CMV measurements for the OMC section (Figure B.4.1b) increased and the section became more uniform with the number of passes. As observed in the case of the dry section, the MDP distributions of the wet section (Figure B.4.1c) tend toward higher values with the increase in the number of roller passes. The CMV measurements carried out simultaneously with the MDP measurements for the wet section are depicted in Figure B.4.1d. The distributions of the CMV measurements tend toward higher values with an increase in the compactive effort.

To evaluate the influence of the subgrade lift placement on the IC measurements, the distributions of the roller measurements before and after the placement of the lift for the dry and wet sections are compared in Figure B.4.2. Since the embankment and the subgrade were constructed with similar soils, the roller measurements from the before and after placement of the lift vary marginally.

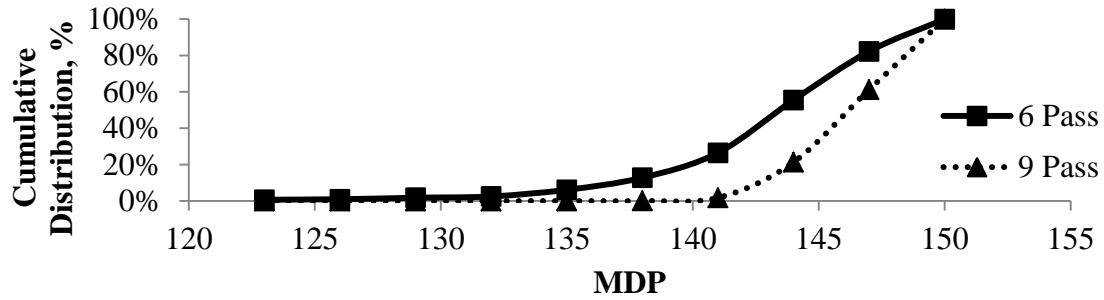
The influence of testing time can be visualized in Figure B.4.3. As indicated above, such data are only available for the dry section. The MDP measurements after 16 hrs are slightly greater than those just after the completion of compaction.

#### **B.5 Relations between Roller Measurements and NDT Devices**

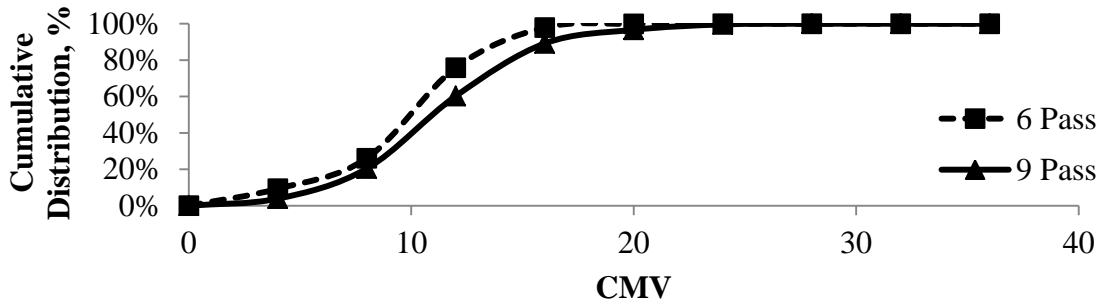
**NDG Density:** Figures B.5.1 and B.5.2 present the relationships between the dry density from the NDG and the CMV or MDP measurements for all sections tested. The two parameters are not strongly correlated.

**LWD Modulus:** Figures B.5.3 and B.5.4 illustrate the relationships developed between the CMV or MDP and the LWD moduli taken at different locations. The correlations between the LWD and CMV or MDP measurements are also not very strong.

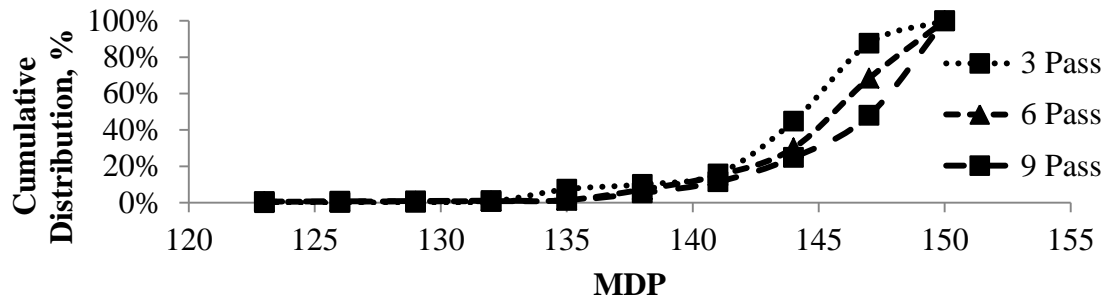
**PSPA Modulus:** As reflected in Figure B.5.5 and B.5.6, the relationships between the CMV or MDP measurements and PSPA moduli are not very strong either.



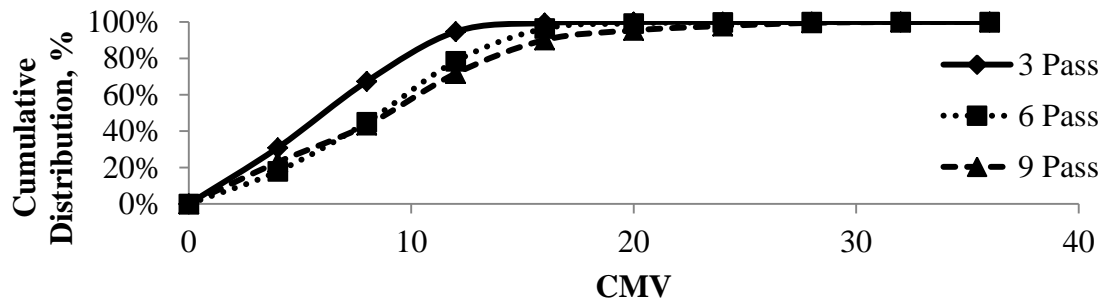
(a) Dry Section



(b) OMC Section

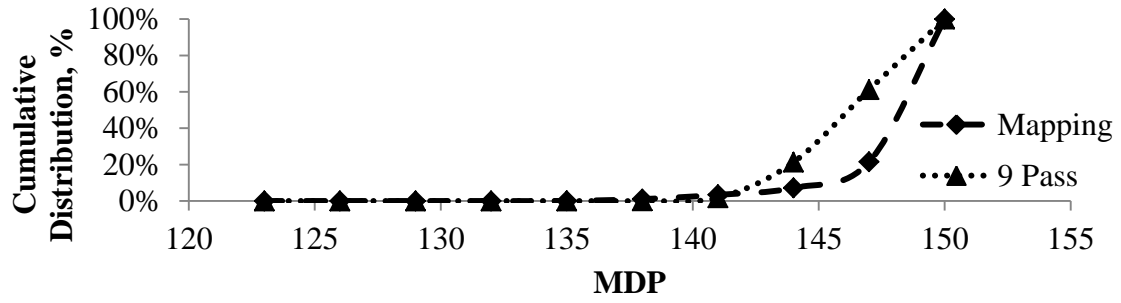


(c) Wet Section (MDP)

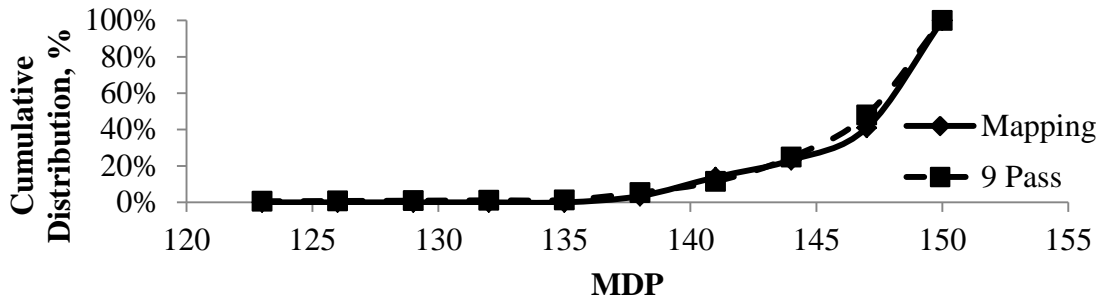


(d) Wet Section (CMV)

Figure B.4.1 - Distributions of the MDP and the CMV with Passes for Different Sections



(a) Dry Section



(b) Wet Section

Figure B.4.2 - Influence of the Subgrade Lift Placement for different Test Sections

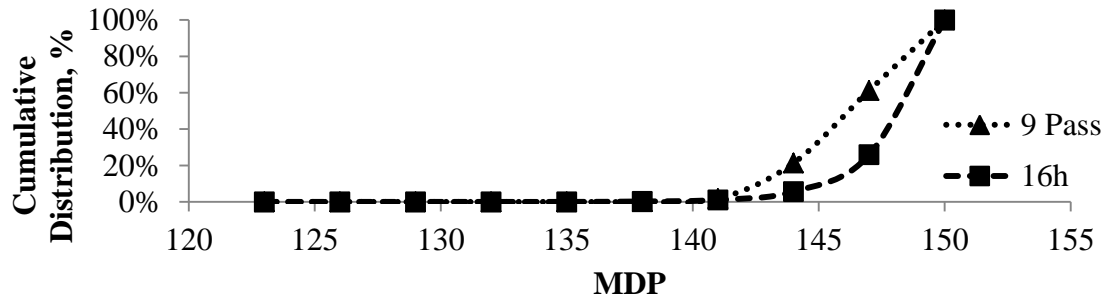


Figure B.4.3 Influence of the Time of Testing on the Roller Measurement Values for Dry Section

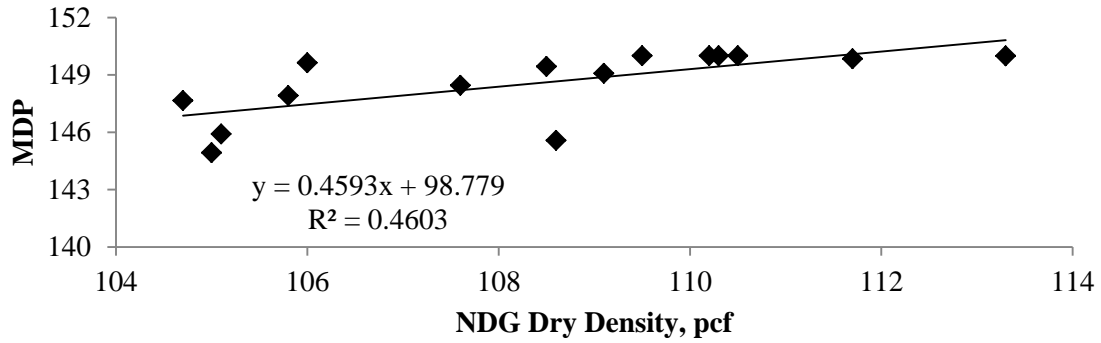
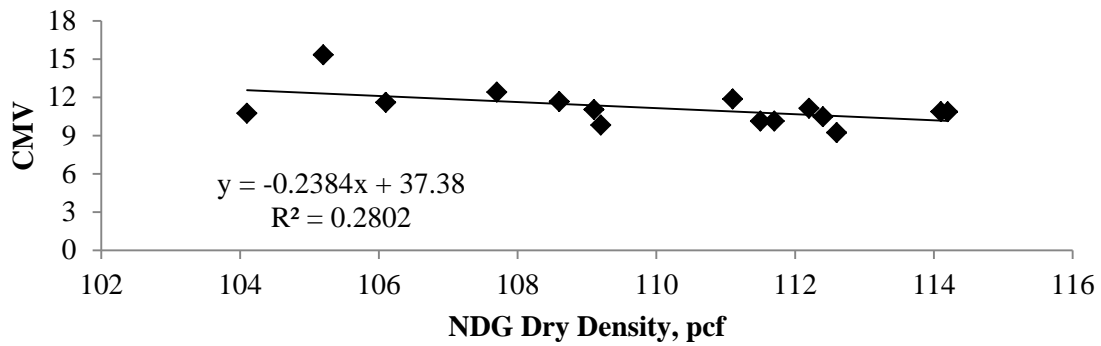
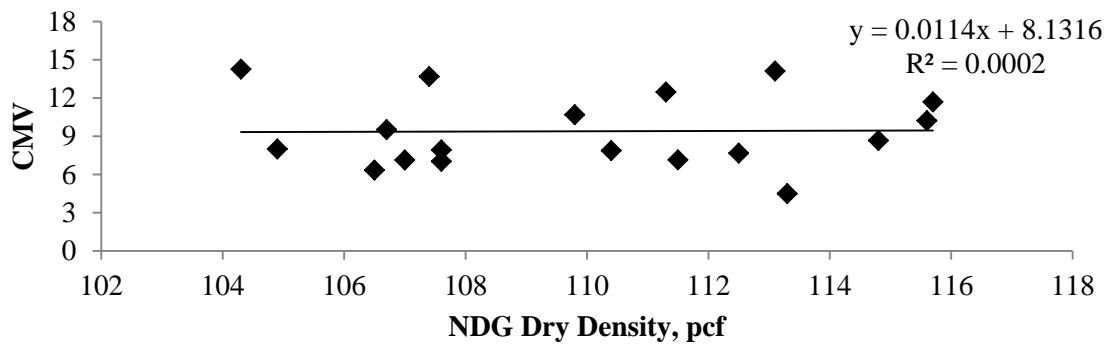


Figure B.5.1- Relation between the NDG Density and the MDP for Dry Section



(a) OMC Section



(b) Wet Section

Figure B.5.2- Relation between the NDG Density and the CMV for OMC and Wet Sections

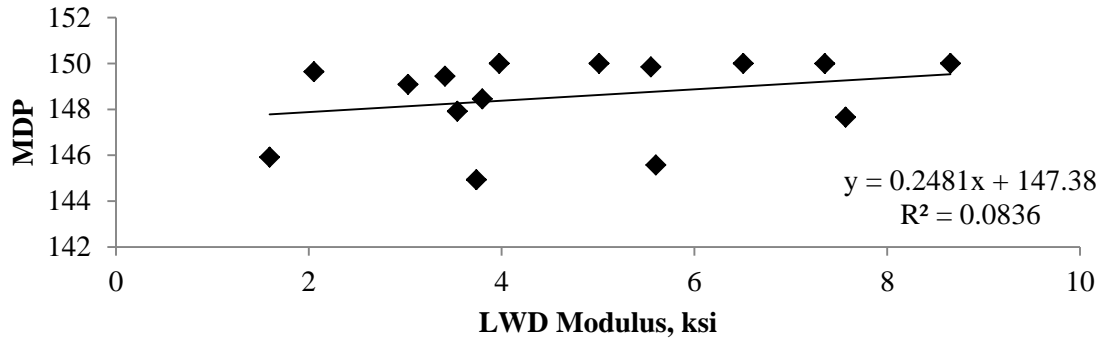
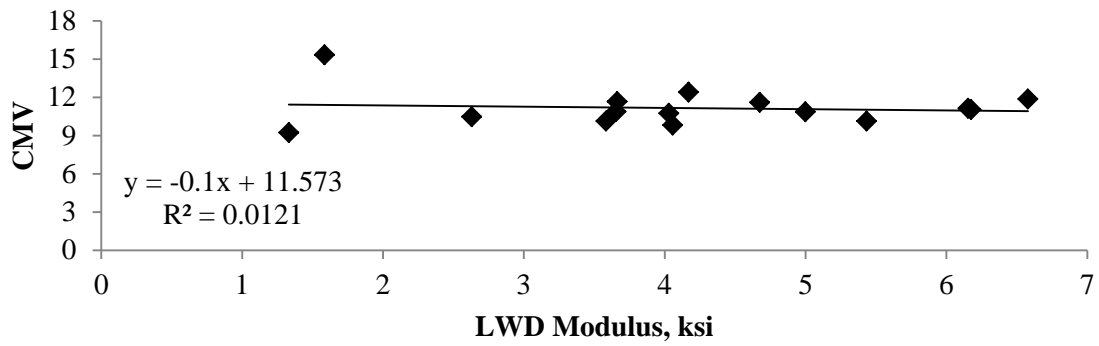
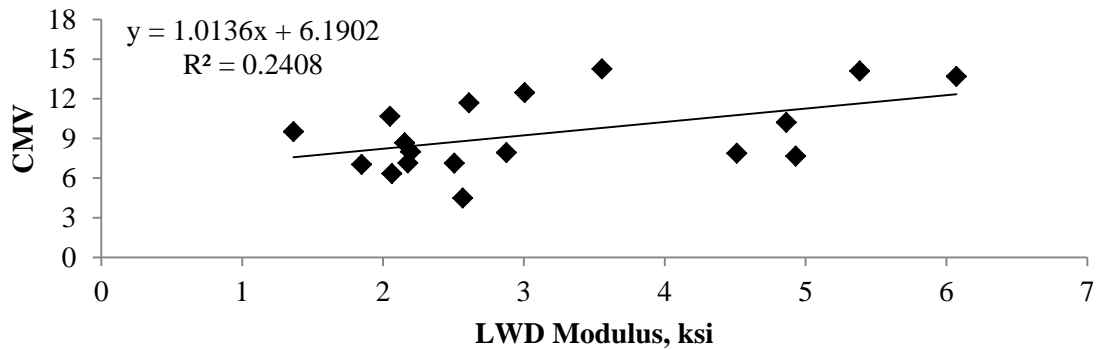


Figure B.5.3- Relation between the LWD Modulus and the MDP for Dry Section



(a) OMC Section



(b) Wet Section

Figure B.5.4-Relation between the LWD Modulus and the CMV for OMC and Wet Sections

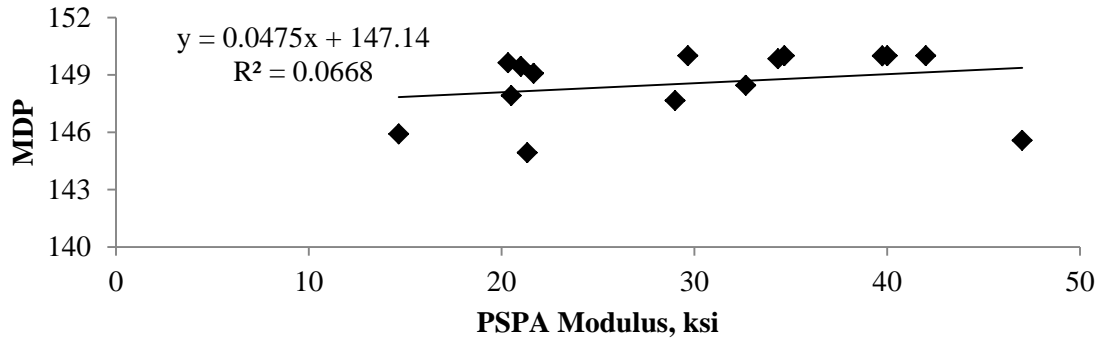
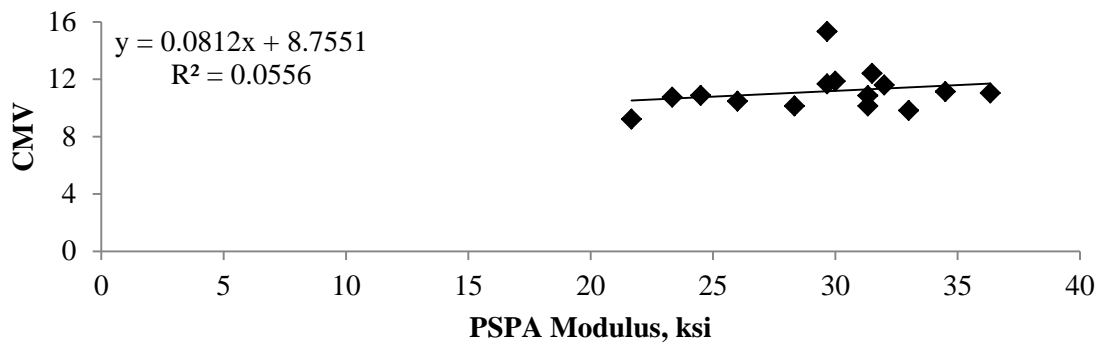
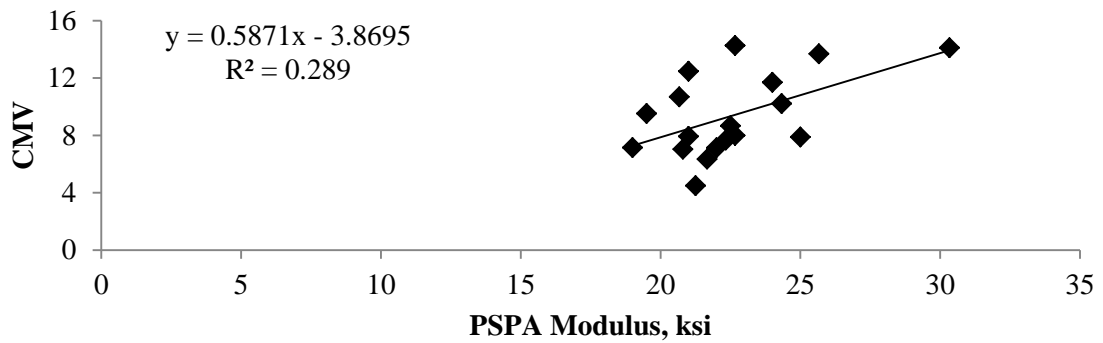


**Figure B.5.5 Relation between the PSPA Modulus and the MDP for Dry Section**



**(a) OMC Section**



**(b) Wet Section**

**Figure B.5.6- Relation between the PSPA Modulus and the CMV for Different Sections**

## **Appendix C**

### **ESTIMATION OF TARGET ROLLER MEASUREMENT VALUES**

## Estimation of Target Roller Measurement Values

### C.1 Introduction

This Appendix presents the detailed analysis of the data collected from the field evaluation to estimate the target values based on the approach presented in Chapter 5.

### C.2 Estimation of Roller Target Value: SH 267 Lime-Treated Subgrade

The target value estimation process discussed in Chapter 5 was adopted to find the relation between the roller measurement values and the spot test results. There are no strong relations and the growth trend is observed in Figure C.2.1.

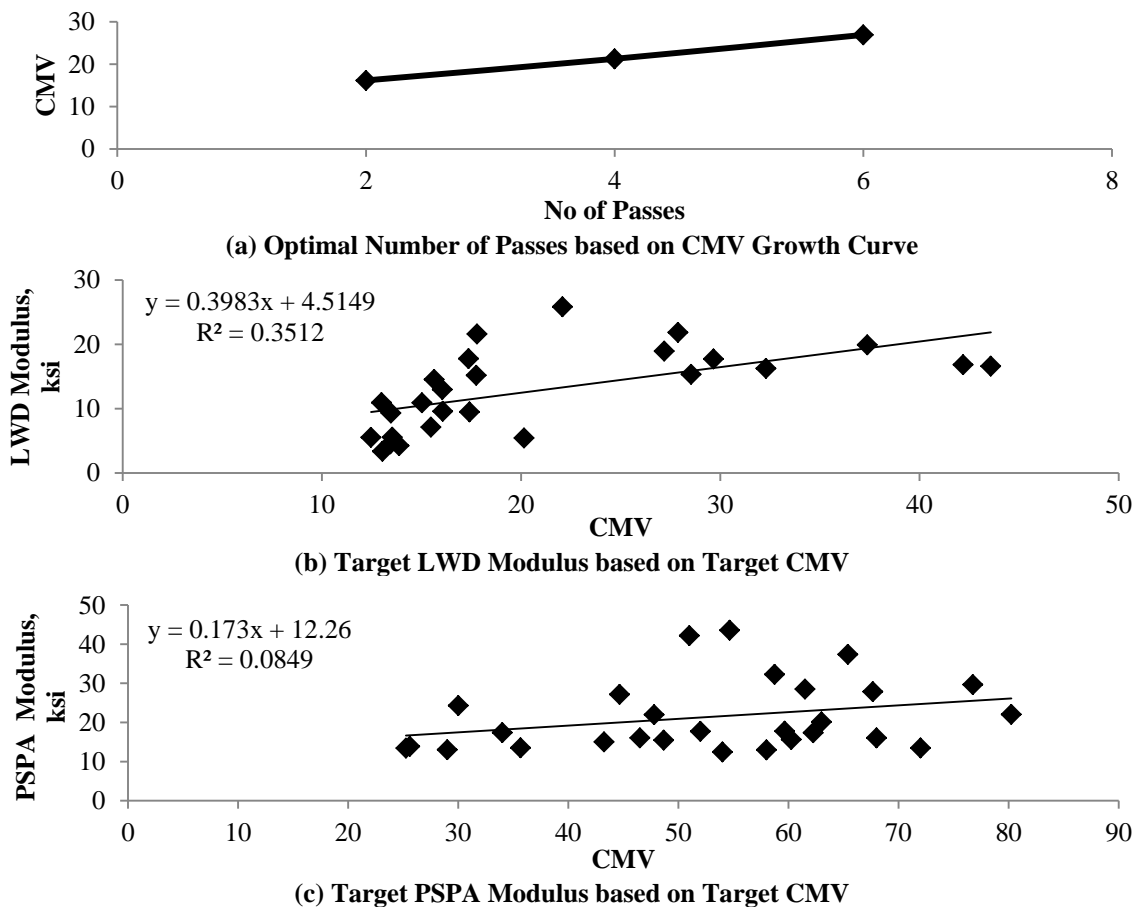


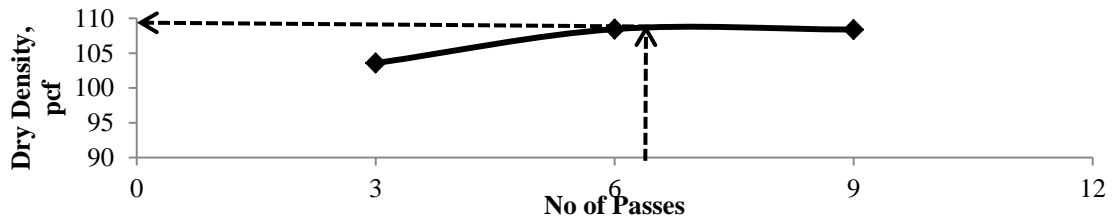
Figure C.2.1- Target RMV Estimation Process for OMC Lime-Treated Subgrade Section of SH 267 Site

### C.3 Estimation of Roller Target Value: SH 267 - Base

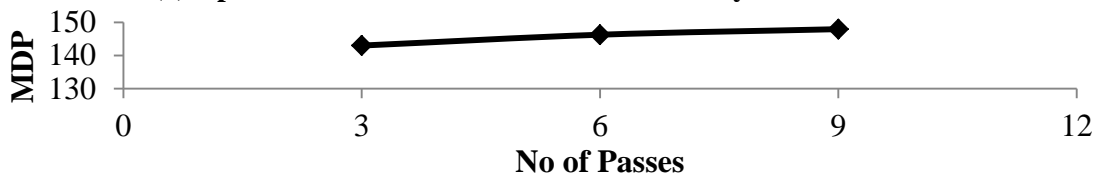
As discussed in Chapter 4, the construction process was carried out with compacting thin lifts of 2 in.; hence, spot tests were not carried out between the passes. In such situations, the target value estimation could be based on the target values of the spot test results as discussed in Chapter 5.

### C.4 Estimation of Roller Target Value: IH 35W - Subgrade

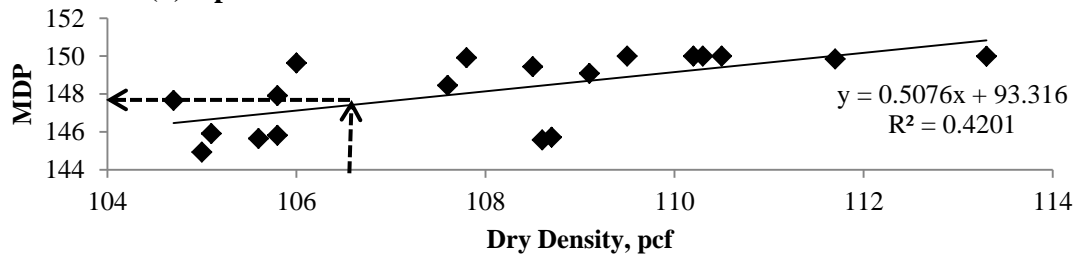
The target value estimation process discussed in Chapter 5 was adopted to find the relation between the roller measurement values and the spot test results. There are no strong relations and the growth trend is observed in Figures C.4.1 to C.4.3.



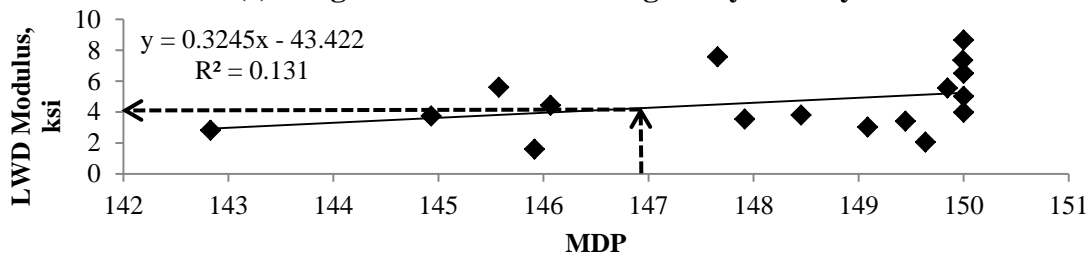
(a) Optimal Number of Passes based on Density Growth Curve



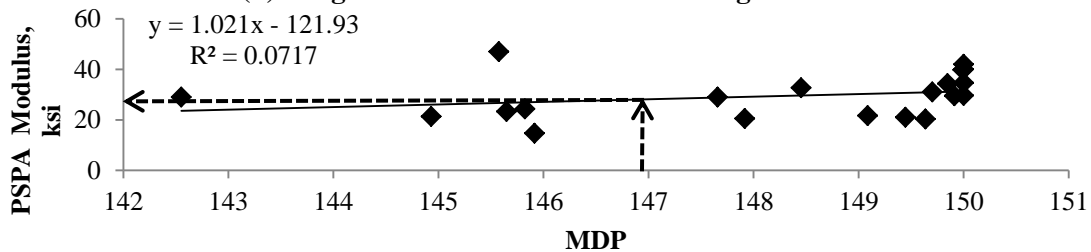
(b) Optimal Number of Passes based on CMV Growth Curve



(c) Target CMV based on Target Dry Density

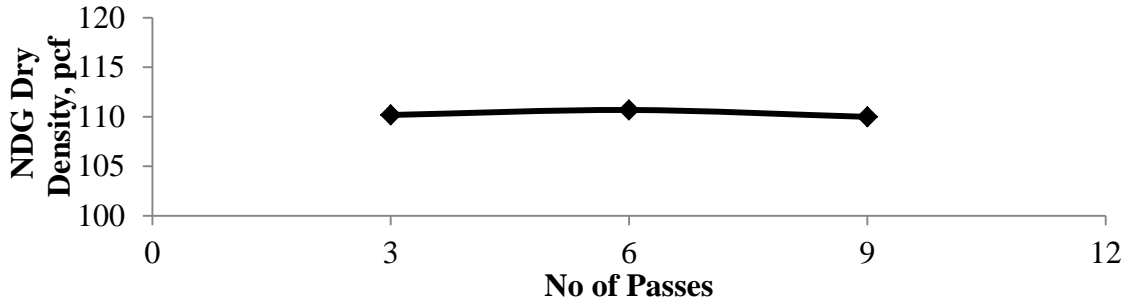


(d) Target LWD Modulus based on Target CMV

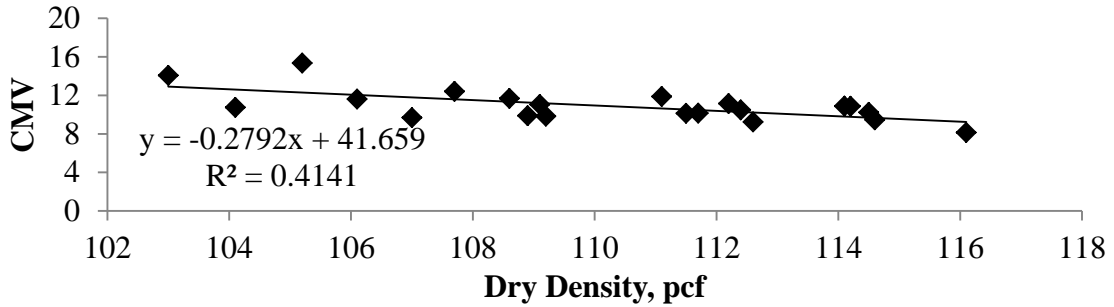


(e) Target PSPA values based on Target CMV

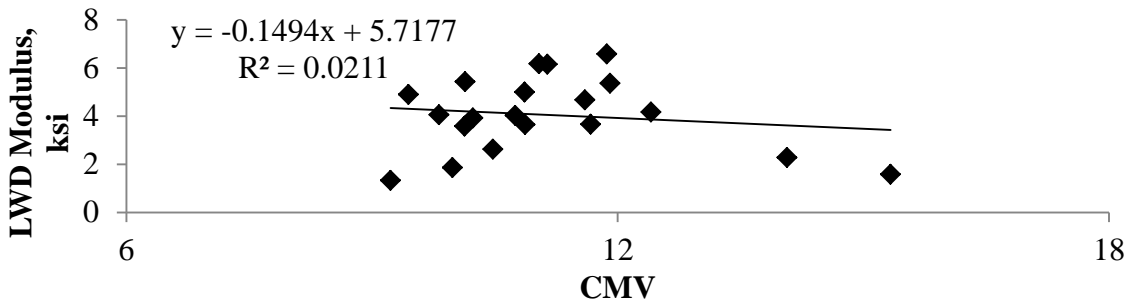
Figure C.4.1- Target RMV Estimation Process for Dry Subgrade Section of IH 35W Site



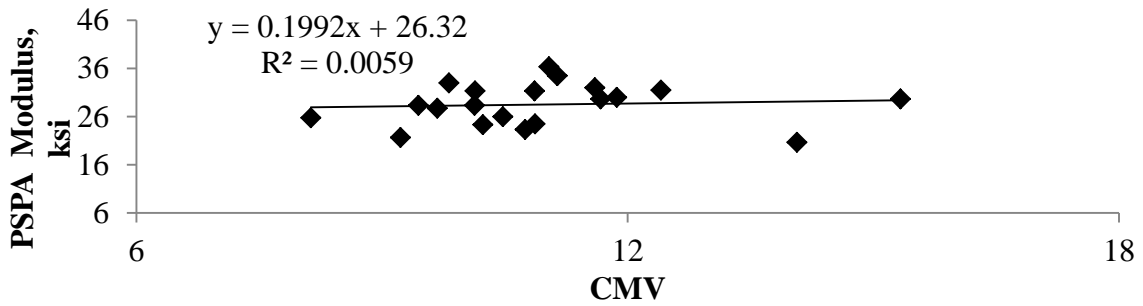
(a) Optimal Number of Passes based on Density Growth Curve



(b) Target CMV based on Target Dry Density

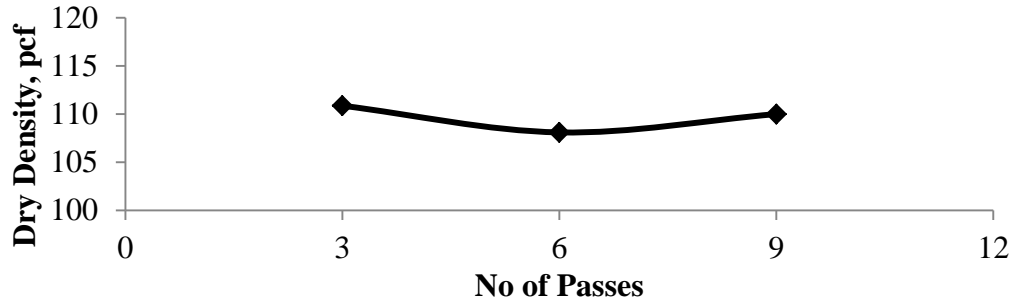


(c) Target LWD Modulus based on Target CMV

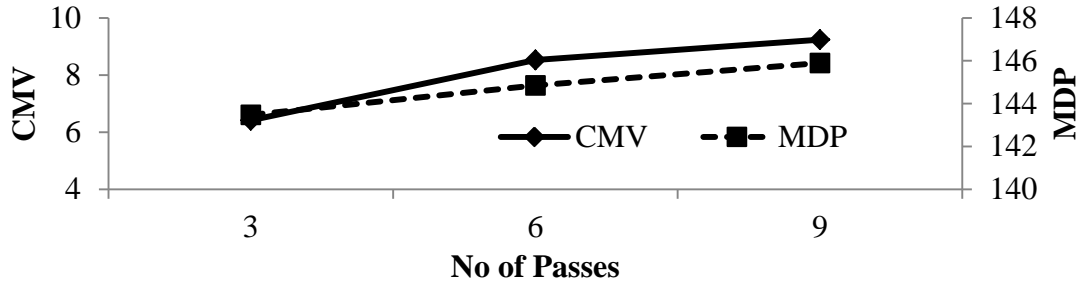


(d) Target PSPA values based on Target CMV

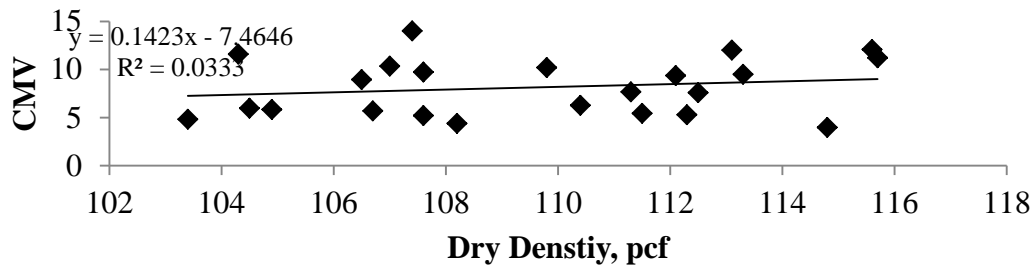
Figure C.4.2-Target RMV Estimation Process for OMC Subgrade Section of IH 35W Site



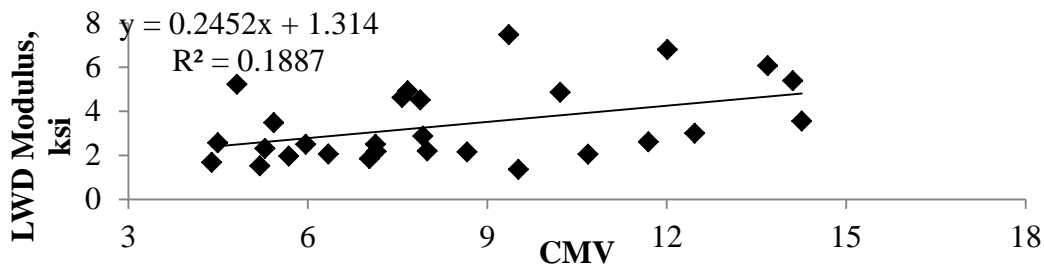
(a) Optimal Number of Passes based on Density Growth Curve



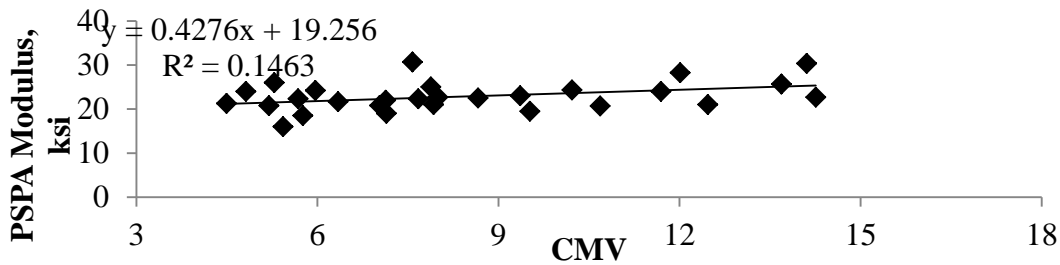
(b) CMV and MDP Sensitivity with Number of Passes



(c) Target CMV based on Target Dry Density



(d) Target LWD Modulus based on Target CMV



(e) Target PSPA values based on Target CMV

Figure C.4.3- Target RMV estimation Process for Wet Subgrade Section of IH 35W Site

## **Appendix D**

### **MEANS OF SETTING TARGET VALUES-ALTERNATE APPROACH**

## MEANS OF SETTING TARGET VALUES-ALTERNATE APPROACH

### D.1 Introduction

This Appendix presents the alternate approach proposed (Chapter 6) for the data collected from the first and second field evaluation activities on SH 267 and IH 35W.

### D.2 Case Study: SH 267

**Subgrade Layer** - Figure D.2.1 to D.2.3 shows the CMV color map of the dry subgrade section from the SH 267 site before the subgrade layer was placed. The statistical distributions of the CMVs are shown in Figure D.2.1b. Similarly Figures D.2.4 to D.2.6 and Figures D.2.7 to D.2.9 present the CMV variation estimated using the kriging technique and the lift contribution to the CMV. The percentages of the passing and marginal areas of each subgrade section are given in Table 6.4. The total percent passing based on the difference in the roller measurement in the case of the wet subgrade section is 42% against more than 80% for the OMC and production sections. This signifies the importance of moisture control during layer compaction.

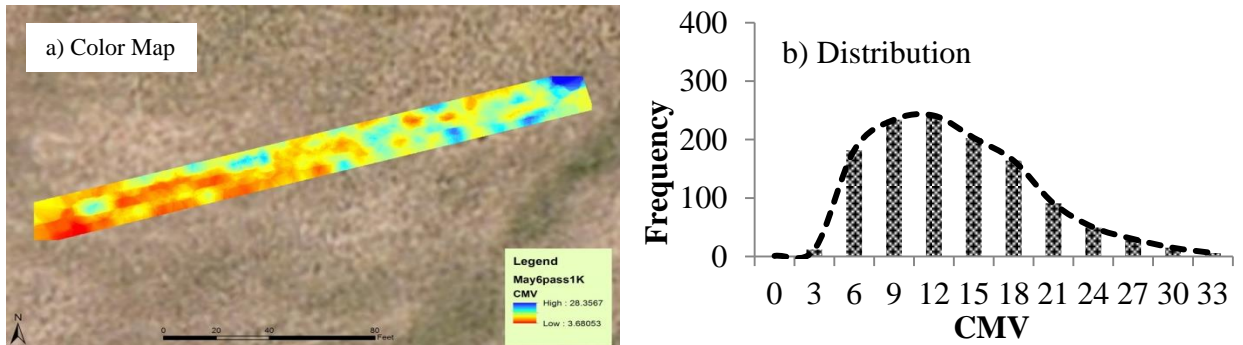


**Figure D.2.1- Variation of the CMV before Lift Placement**

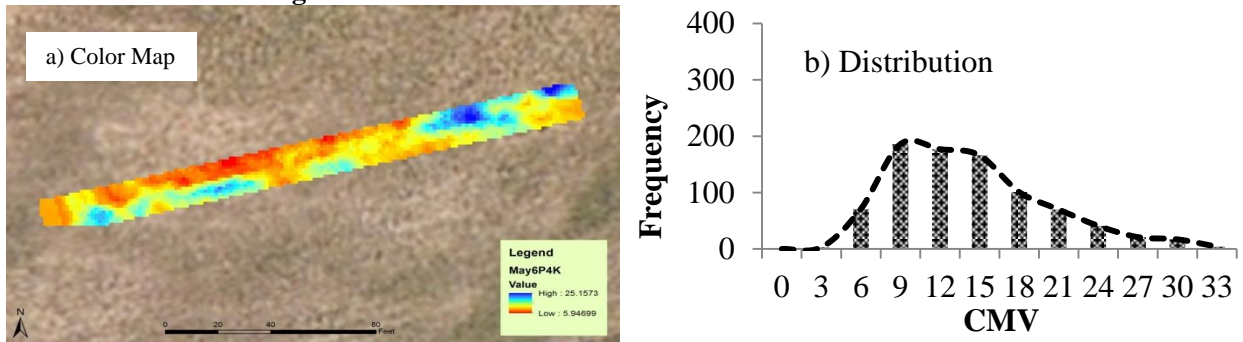


**Figure D.2.2 - Variation of the CMV After Placement and Compaction of the Next Lift**

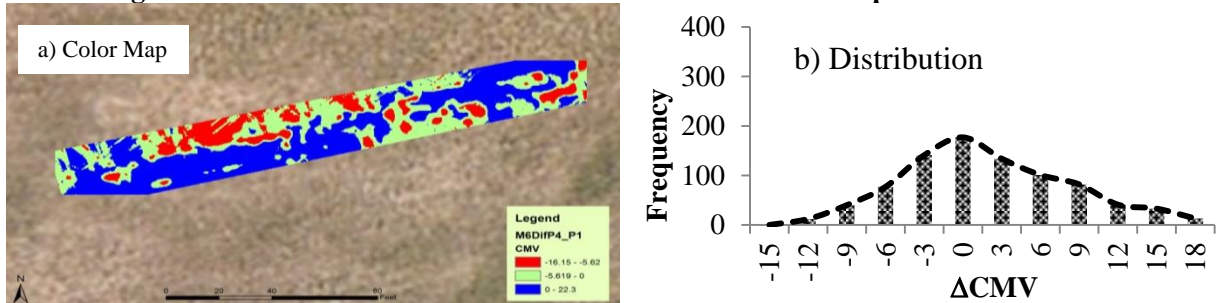


**Figure D.2.3 - Variation of the Differences in CMVs ( $\Delta$ CMV) After Placement and Compaction of the Next Lift and Foundation Layer for Dry Subgrade Section**

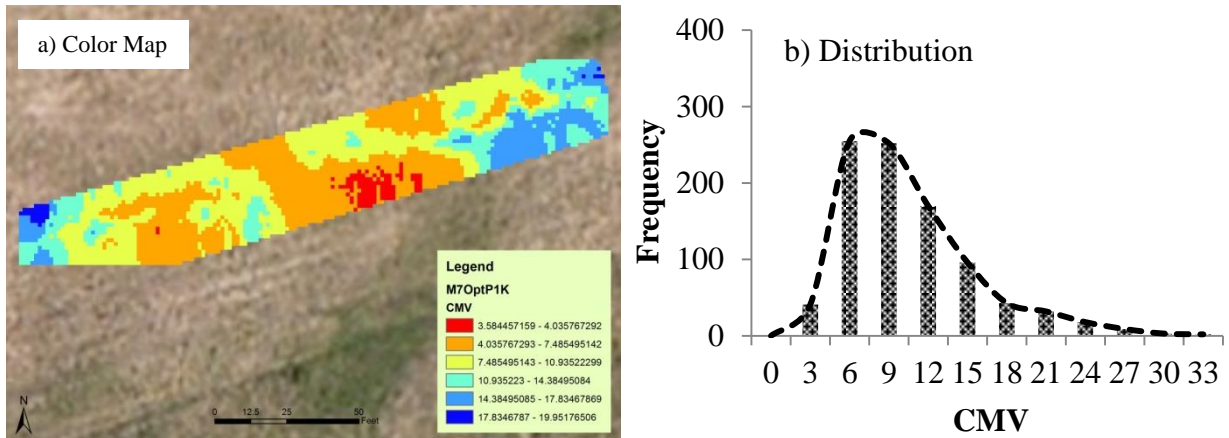


Figure D.2.4- Variation of the CMV before Lift Placement

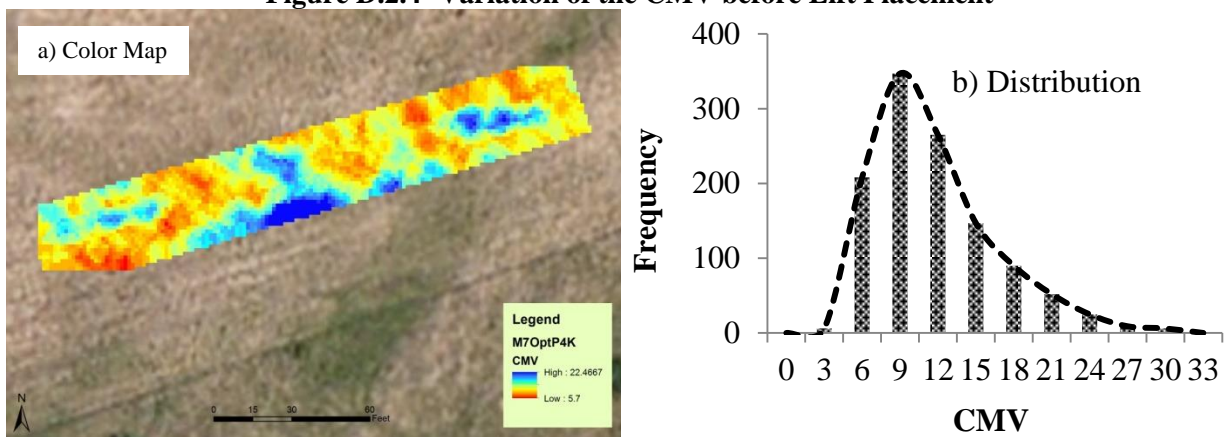


Figure D.2.5 - Variation of the CMV After Placement and Compaction of the Next Lift

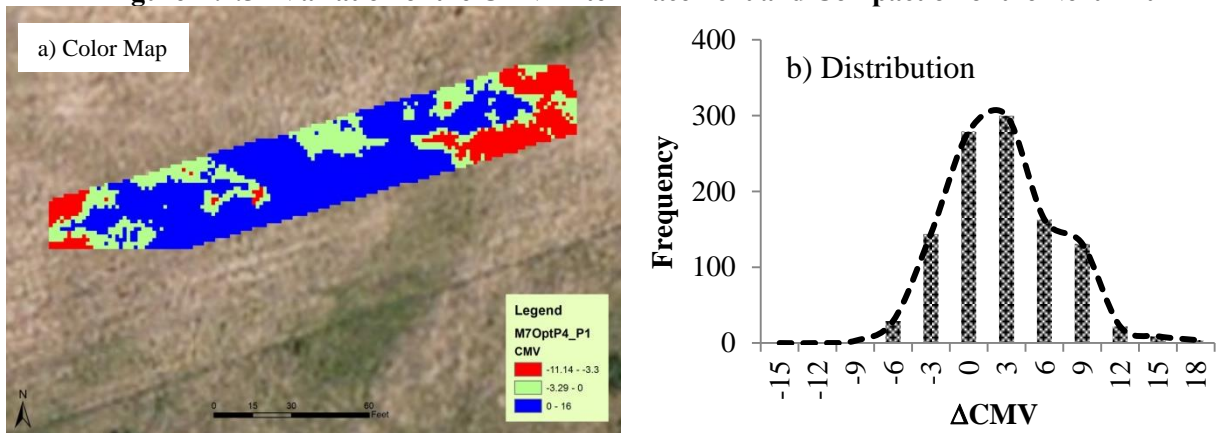


Figure D.2.6 - Variation of the Differences in CMVs ( $\Delta$ CMV) After Placement and Compaction of the Next Lift and Foundation Layer for OMC Subgrade Section

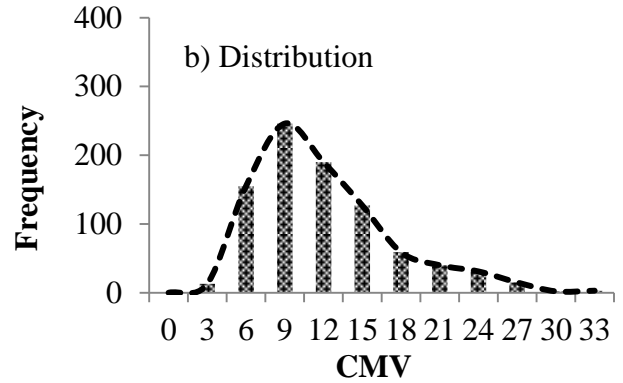
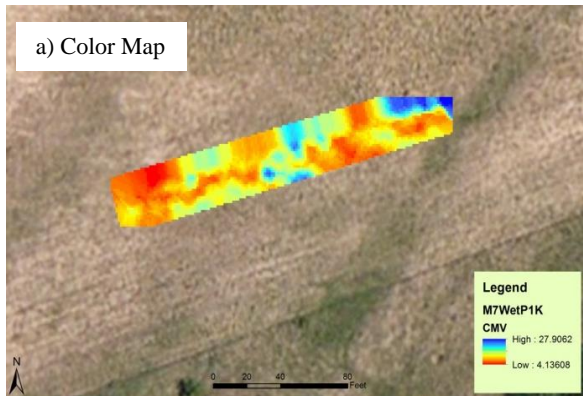


Figure D.2.7- Variation of the CMV before Lift Placement

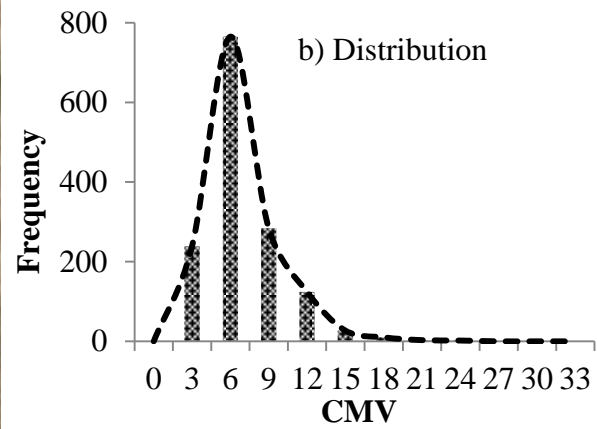
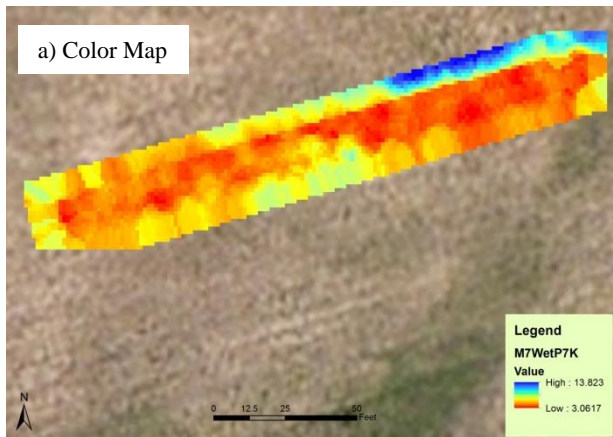


Figure D.2.9 - Variation of the CMV After Placement and Compaction of the Next Lift

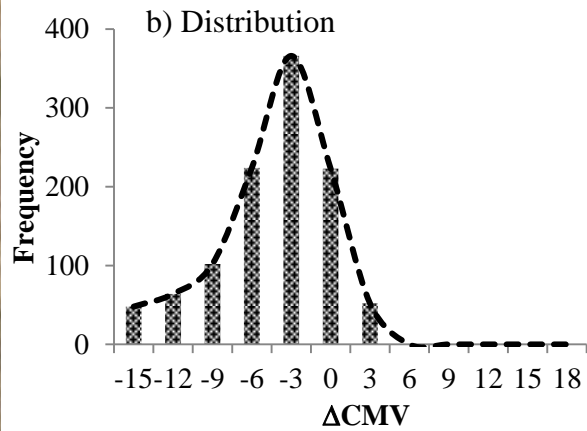
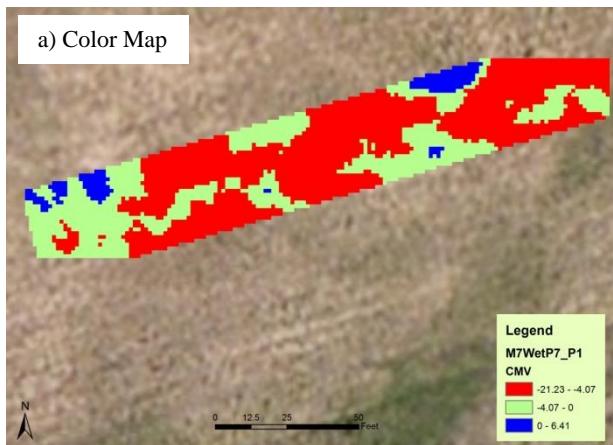
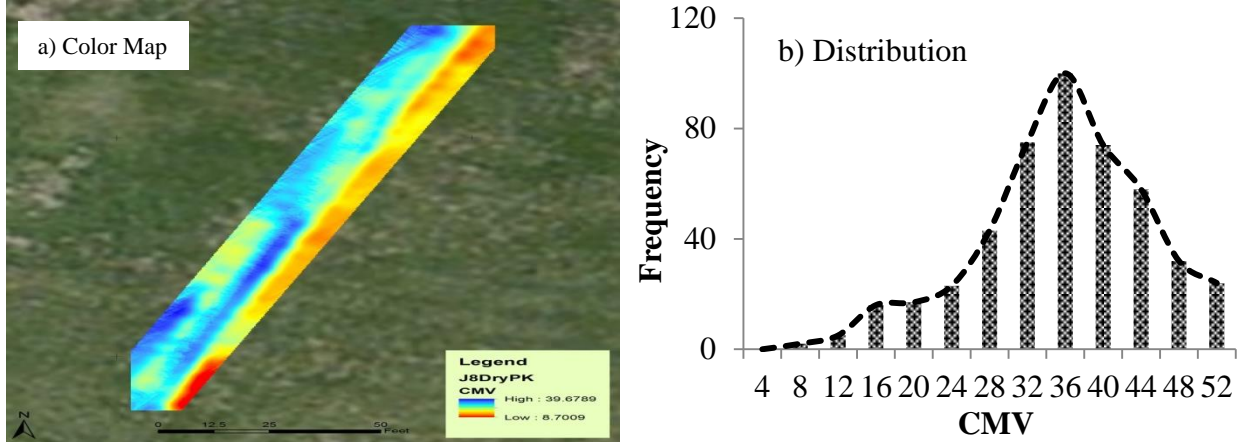
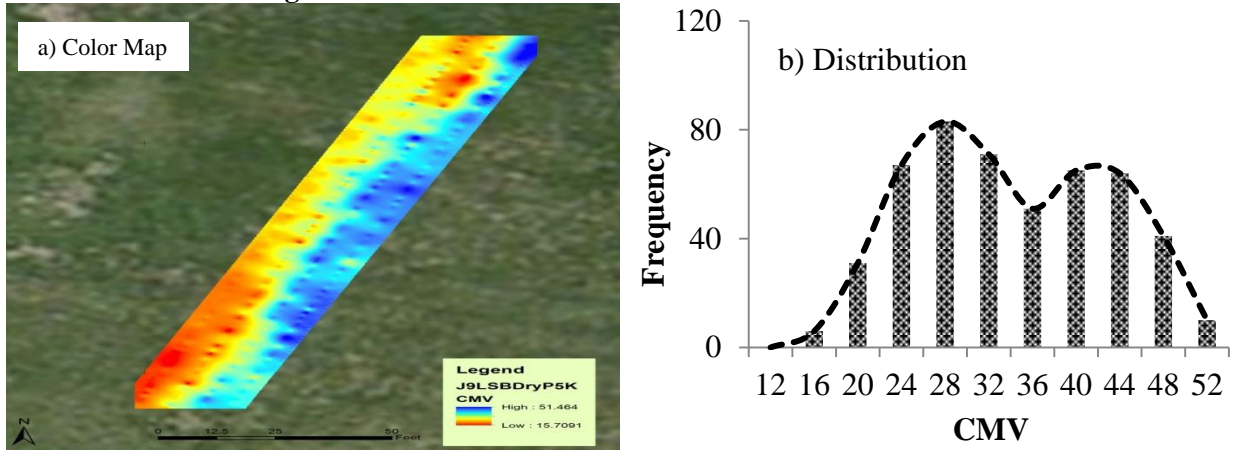


Figure D.2.9 - Variation of the Differences in CMVs ( $\Delta$ CMV) After Placement and Compaction of the Next Lift and Foundation Layer for Wet Subgrade Section

**Base Layer** - Figure D.2.10 to D.2.12 shows the CMV color maps for the dry base section from the SH 267 site before the base layer was placed. The statistical distributions of the CMVs are shown in Figure D.2.10b. Similarly Figure D.2.13 to D.2.15 and Figure D.2.16 to D.2.18 presents the CMV variation estimated using the kriging technique and the lift contribution to the CMV for the OMC and wet sections respectively. The percentage passing and marginal areas of the base sections are given in Table 6.4.



**Figure D.2.10- Variation of the CMV before Lift Placement**



**Figure D.2.11 - Variation of the CMV After Placement and Compaction of the Next Lift**

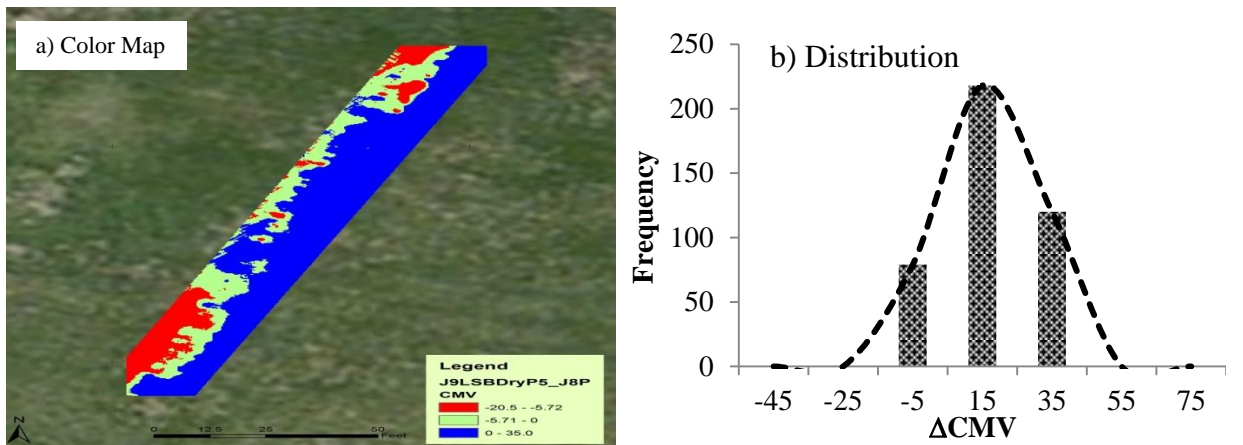


**Figure D.2.12 - Variation of the Differences in CMVs ( $\Delta$ CMV) After Placement and Compaction of the Next Lift and Foundation Layer for Dry Base Section**

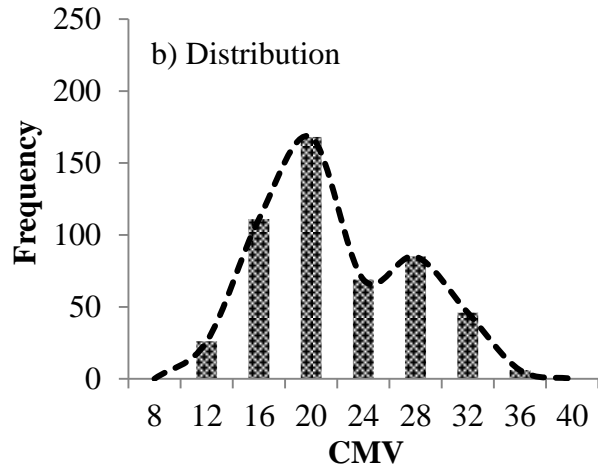
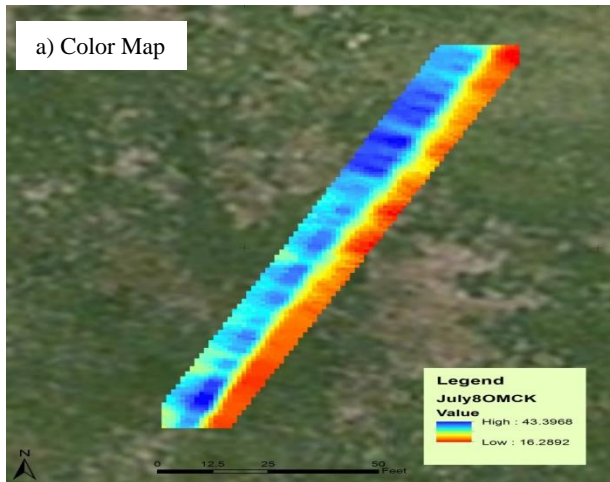


Figure D.2.13- Variation of the CMV before Lift Placement

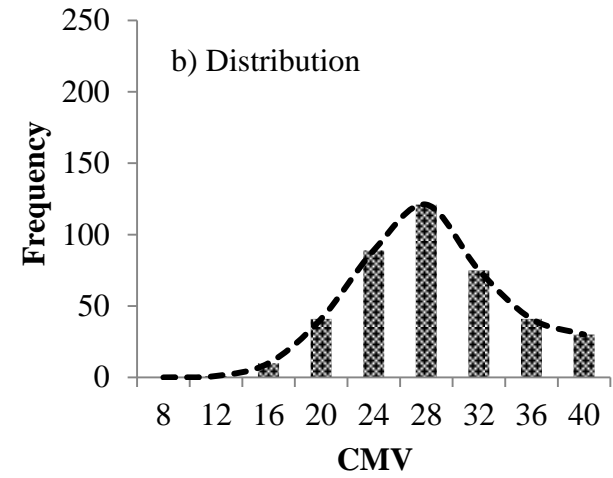
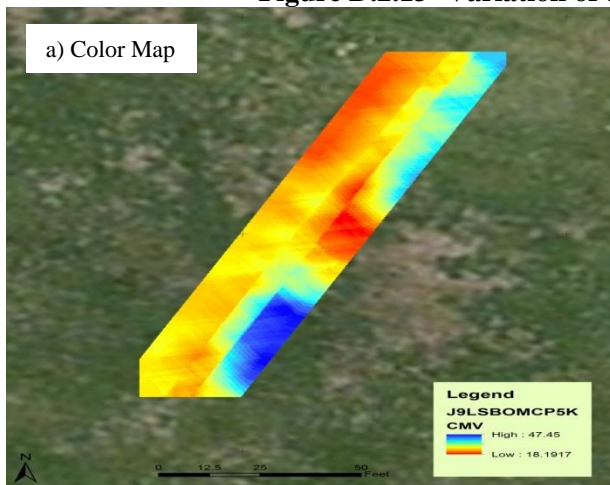


Figure D.2.14 - Variation of the CMV After Placement and Compaction of the Next Lift

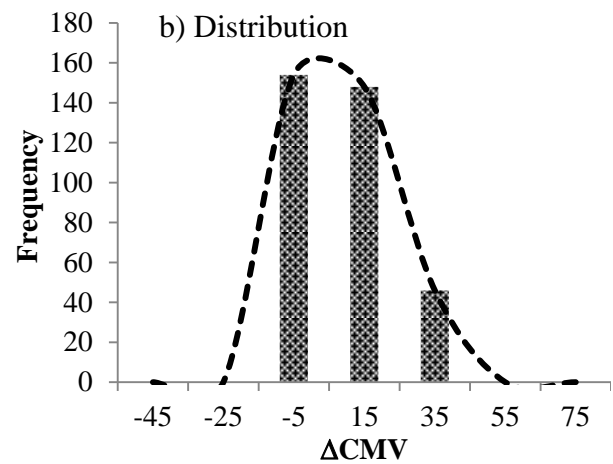
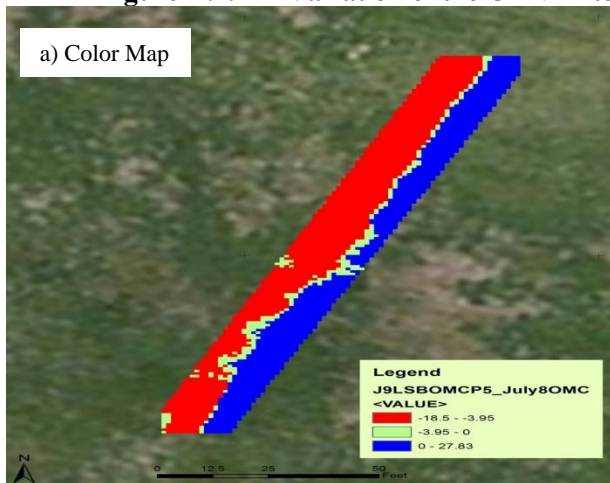


Figure D.2.15 - Variation of the Differences in CMVs ( $\Delta$ CMV) After Placement and Compaction of the Next Lift and Foundation Layer for OMC Base Section

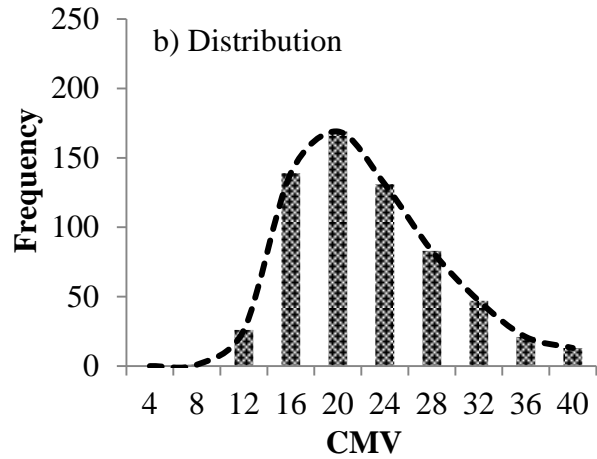
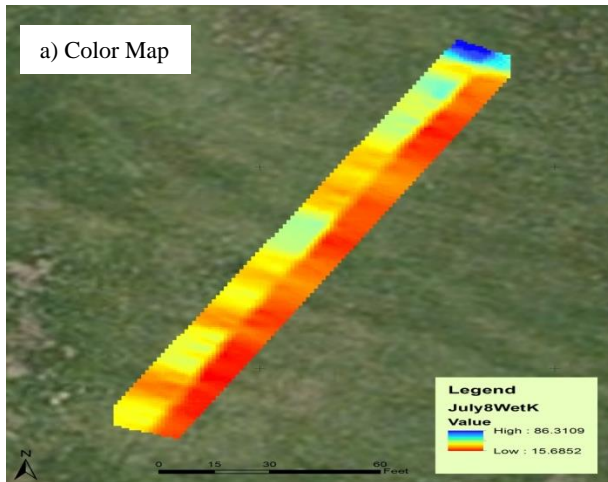


Figure D.2.16- Variation of the CMV before Lift Placement

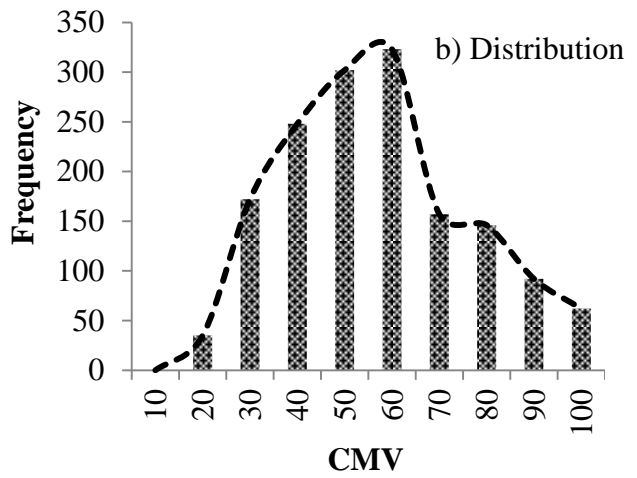
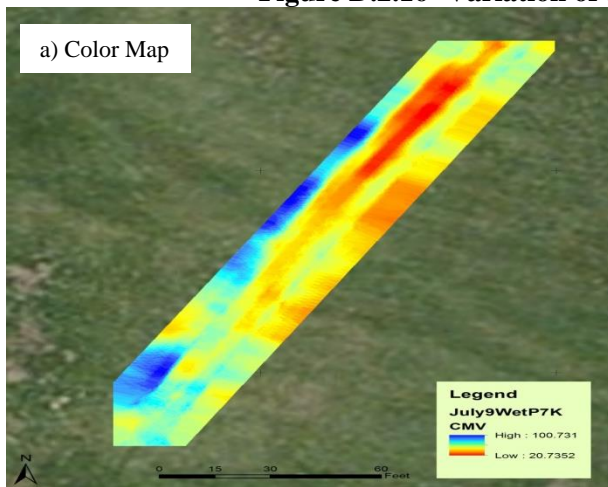


Figure D.2.17 - Variation of the CMV after Placement and Compaction of the Next Lift

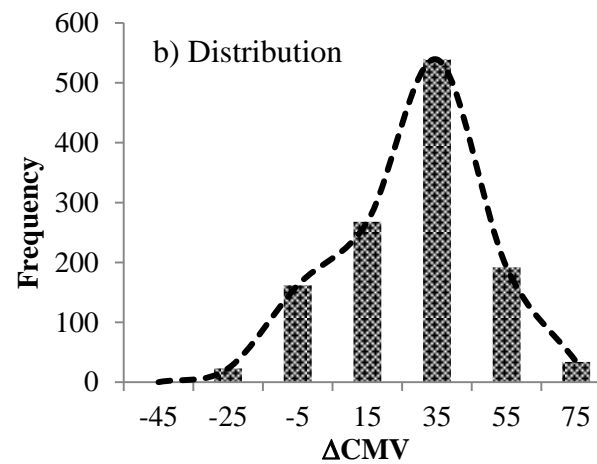
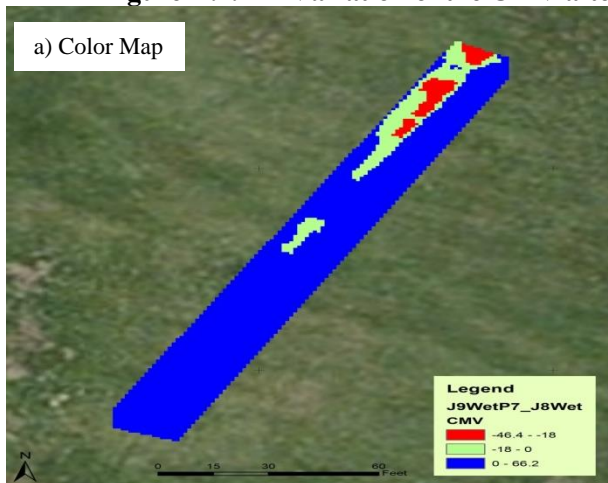
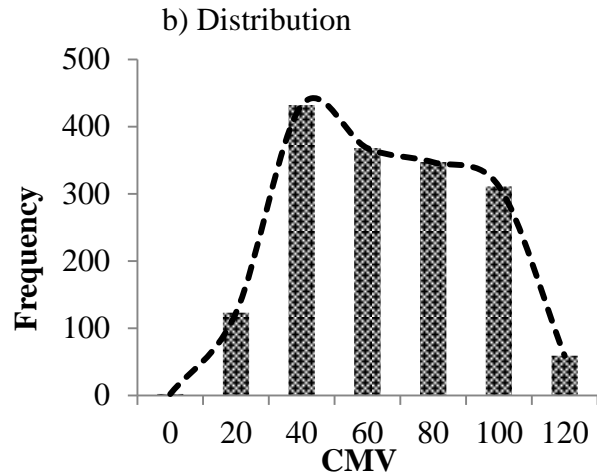
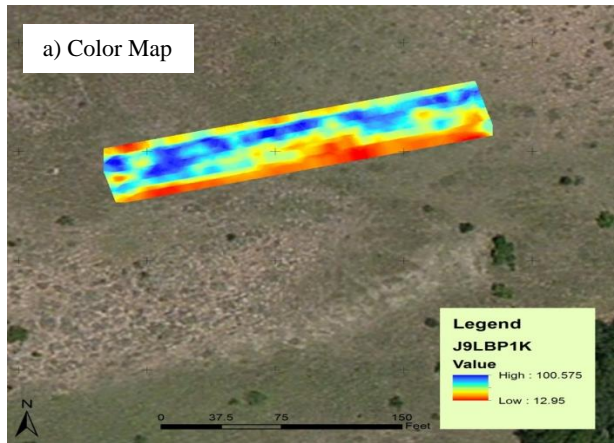
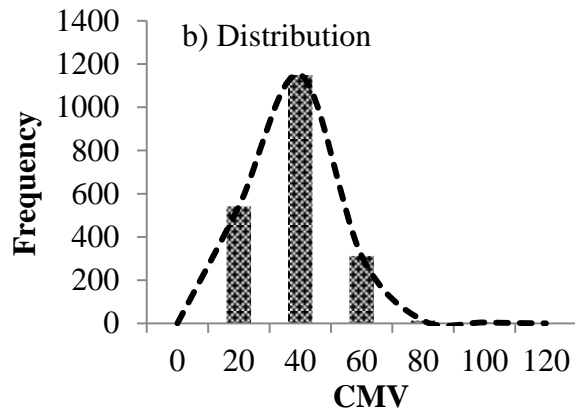
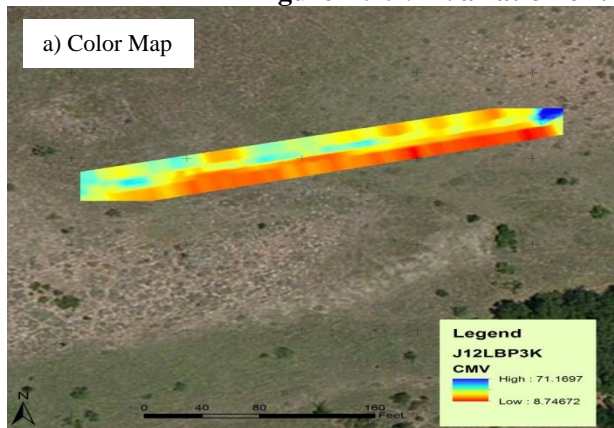


Figure D.2.18 - Variation of the Differences in CMVs ( $\Delta$ CMV) After Placement and Compaction of the Next Lift and Foundation Layer for Wet Base Section

**Lime-Treated Subgrade Layer** - Figure D.2.19 to D.2.21 shows the CMV color map of the lime-treated subgrade section from the SH 267 site. The statistical distributions of the CMVs are shown in Figure D.2.19b. The CMV variation estimated using the kriging technique and the lift contribution to the CMV are shown in Figure D.2.20 and D.2.21. The percentage passing and marginal areas of each subgrade section are given in Table 6.4. The total percent passing based on the difference in the roller measurement in the case of the lime-treated subgrade section is around 20%. The lower percentage of passing may be due to the time required for the lime-treatment. Hence, testing at a later time could result in an acceptable passing percentage.



**Figure D.2.19- Variation of the CMV before Lift Placement**



**Figure D.2.20 - Variation of the CMV after Placement and Compaction of the Next Lift**

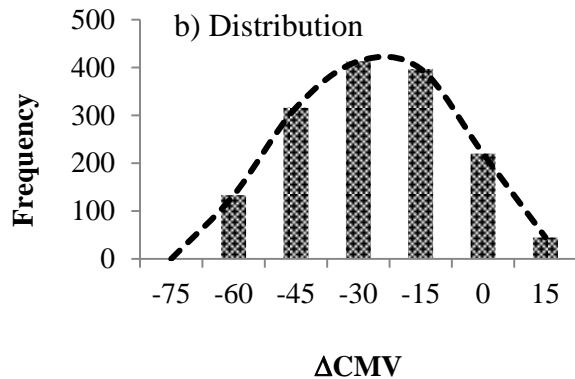
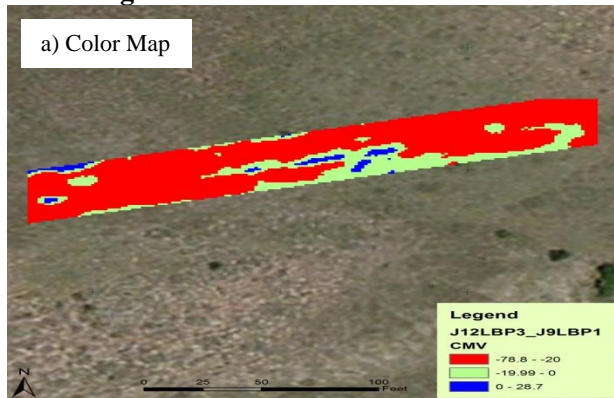


**Figure D.2.21 - Variation of the Differences in CMVs ( $\Delta$ CMV) After Placement and Compaction of the Next Lift and Foundation Layer for Lime Treated Subgrade Section**

### D.3 Case Study: IH 35W

**Subgrade Layer** - Figure D.3.1 to D.3.3 shows the MDP color map of the dry subgrade section from the IH 35W site before the subgrade layer was placed. The statistical distributions of the MDPs are shown in Figure D.3.1b. The MDP variation estimated using the kriging technique and the lift contribution to the MDP are shown in Figure D.3.2 and D.3.3. The percentage passing and marginal areas of each subgrade section are given in Table 6.5. The total percent passing based on the difference in the roller measurement in the case of the dry subgrade section is 82%. As mentioned in Appendix B, the roller measurements on the OMC and wet sections were not recorded due to the malfunction of the IC instrumentation.

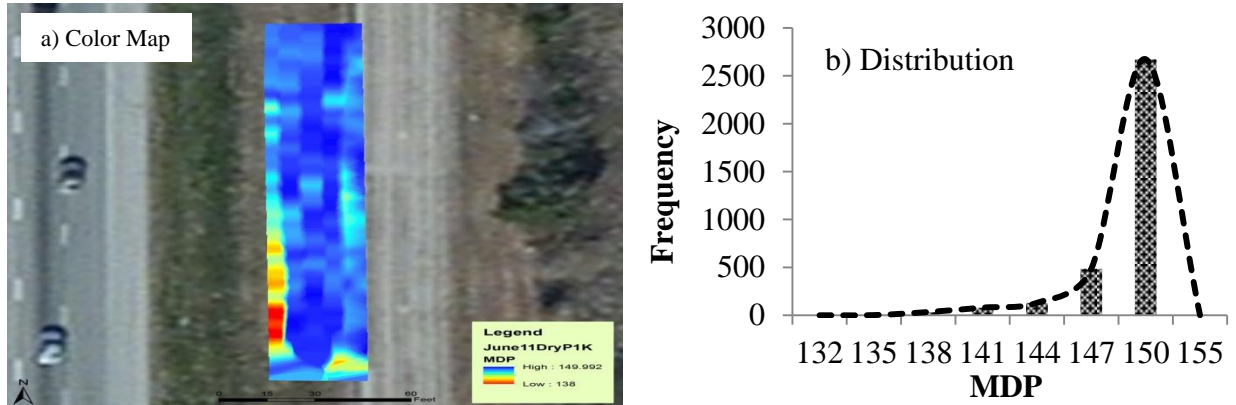


**Figure D.3.1- Variation of the MDP before Lift Placement on Dry Subgrade Section-IH 35W**

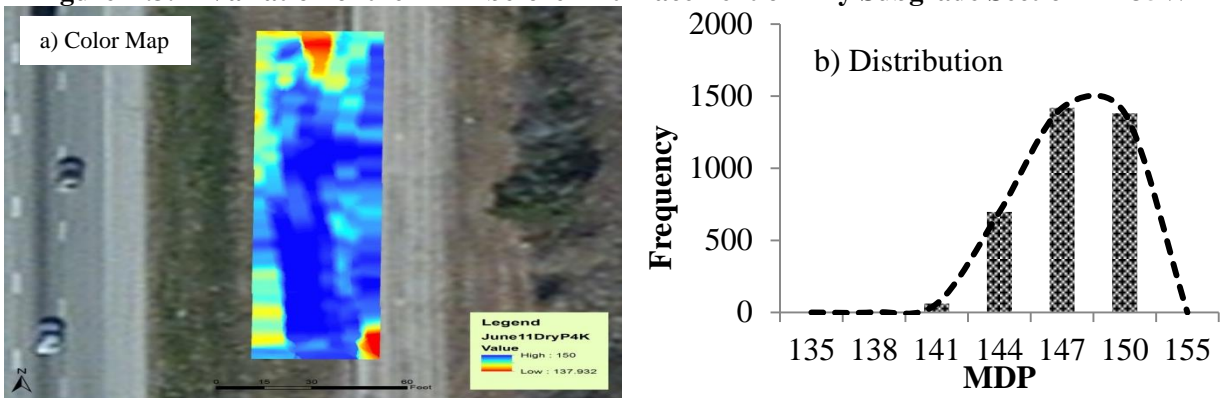


**Figure D.3.2 - Variation of the MDP after Placement and Compaction of the Next Lift on Dry Subgrade Section-IH 35W**

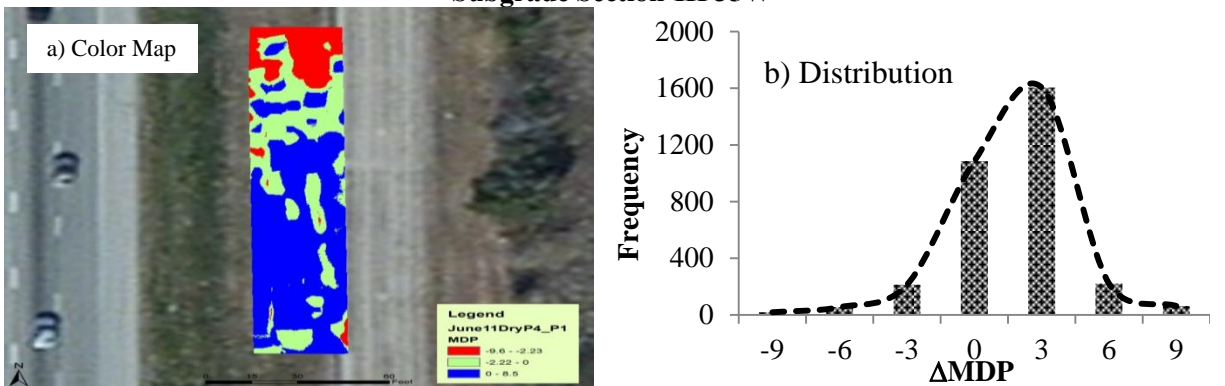


**Figure D.3.3 - Variation of the Differences in MDPs ( $\Delta$ MDP) After Placement and Compaction of the Next Lift and Foundation Layer for Dry Subgrade Section-IH 35W**

# Appendix E

## Proposed Specification

*Preliminary Draft, Not endorsed by TxDOT*



## **Quality Compaction of Soil and Base Using Intelligent Compaction Rollers**

- 1. Description.** Construct roadway embankment, subgrade soil and flexible base (treated or untreated) using intelligent compaction (IC) rollers within the limits of the work described in the plans or provisions. Provide the IC system integrated directly from the roller manufacturer or equipped with field IC retrofit kits. IC rollers consist of a stiffness type measuring system that records compaction parameters and a Global Positioning System (GPS) or equivalent system that records and documents roller location to ensure that optimum compaction and uniformity is achieved through continuous monitoring of operations.
- 2. Materials.** Furnish uncontaminated materials of uniform quality that meet the requirements of the plans and specifications in accordance with Item 110, "Excavation;" Item 132, "Embankment;" Item 247, "Flexible Base;" Item 251, "Reworking Base Courses;" Item 260, "Lime Treatment (Road-Mixed);" and Item 263, "Lime Treatment (Plant-Mixed)." Notify the Engineer of the proposed material sources. Notify the Engineer before changing any material source. The Engineer may sample and test project materials at any time throughout the duration of the project to assure specification compliance. Use Tex-100-E for material definitions.
- 3. Equipment.** Furnish machinery, tools, and equipment necessary for proper execution of the work in accordance with the plans and the applicable Specification Items listed in Section 2013.2, "Materials."

Provide rollers in accordance with the rollers shown on the Department's Approved Product List, "[Intelligent Compaction Rollers](#)." Only accelerometer-based IC systems are acceptable unless the sensitivity of other IC systems can be demonstrated at the project site and are satisfactory to the Engineer.

Provide IC rollers that have the capability to measure, record, and export compaction parameters in the Comma Delimited Separated Values (\*.csv) format data files. Deliver the IC data file to the Engineer within 24 hours from the end of each working day. The IC data file shall include, but not limited to, the following parameters:

- Roller Model
- Roller Type
- Roller Drum Width
- Roller Drum Diameter
- Roller Weight
- File Name
- Date Stamp
- Time Stamp
- GPS Measurement Coordinates (includes the coordinate system configuration information and zone number, if applicable)
- Roller Pass Count
- Roller Travel Direction (forward or reverse)

- Roller Travel Speed
- Vibration Setting (on or off)
- Vibration Frequency
- Vibration Amplitude
- Intelligent Compaction Measurement Values (ICMV)
- Intelligent Compaction Target Value (ICTV)

Provide a knowledgeable representative from the manufacturer of the IC system in the first two days of construction to ensure proper installation, calibration, and operation of the equipment. Provide certified personnel capable to operate and maintain the equipment, collect, save, and provide the data to the Engineer. Ensure that these certified personnel attend the on-site training of the IC roller operation provided by the manufacturer's representative.

Provide a GPS or equivalent system to record IC roller locations with detailed coordinate system information required to generate a color-coded map from the IC data. Furnish a GPS or equivalent reference base station required by the IC roller(s).

4. **Construction.** Construct each layer uniformly, free of loose or segregated areas, and with the required density and moisture content in accordance with the plans and the applicable Specification Items listed in Section 2013.2, "Materials." Provide a smooth surface that conforms to the typical sections, lines, and grades shown on the plans or as directed.
  - A. Preparation of Subgrade or Existing Base.** Prepare each area to be excavated or to receive embankment or base in accordance with Item 100, "Preparing Right of Way." Proof map the finished surface of the existing ground prior to placement of any material using the IC roller. Deliver the electronic compaction IC data files to the Engineer in the format specified in Section 2013.3, "Equipment."
  - B. Placing.** Spread and shape the materials into a uniform layer in accordance with the plans and the applicable Specification Items listed in Section 2013.2, "Materials."
  - C. Pulverization.** Pulverize or scarify existing materials in accordance with the plans and the applicable Specification Items listed in Section 2013.2, "Materials."
  - D. Application of Treatments or Stabilizers.** Uniformly apply treatments or stabilizers in accordance with the plans and the applicable Specification Items listed in Section 2013.2, "Materials."
  - E. Mixing.** Thoroughly mix the materials with treatments or stabilizers in accordance with the plans and the applicable Specification Items listed in Section 2013.2, "Materials."
  - F. Compaction.** Compact the material per the applicable Items specified in Section 2013.2, "Materials." Supply a sufficient number of rollers and other associated equipment necessary to complete the compaction requirements for the specific materials based upon the scope of the project. The IC roller(s) may be utilized during production with other standard compaction equipment. When tamping rollers, such as sheepfoot or padfoot rollers are used, blade off the depressions upon completion of compaction to provide a smooth surface, without depressions, for proof mapping. Use

IC rollers to proof map each completed layer. Provide access to the computer program used to generate the color-coded map when required by the Engineer.

- 1. Control Strip Compaction.** Construct a Control Strip using the IC roller to determine the level of compaction necessary to achieve 100% of the maximum dry density in accordance with applicable Test Procedures depending on the materials being compacted, unless otherwise shown on the plans. The Contractor and Engineer will agree on location(s) within the project to construct the control strip(s). Leave each Department accepted Control Strip in place to become part of the project.

Complete at least one Control Strip to establish a rolling pattern for each layer material and a roller Intelligent Compaction Target Value (ICTV) as the acceptance value for further construction compaction. Construct additional Control Strips whenever a change is made in the material source, gradation, type of material, layer thickness, IC roller, or as directed by the Engineer.

1. Construct the Control Strip to a minimum length of 500 feet and to the full width of the material course, unless otherwise approved by the Engineer. Place the material in layers and limit the thickness of compacted material, without depressions, to 12 in. for soil and 8 in. for base material, unless otherwise approved by the Engineer. Use the same IC roller and procedures to perform all proof mapping during construction. Perform all proof mapping operations within 24 hours upon the completion of compaction of each layer.
2. Place the first layer of material, upon complete preparation and proof mapping of the existing ground surface according to Section 2013.4.A, "Preparation of Subgrade or Existing Base," and Section 2013.4.B, "Placing." Start compaction of the material and stop after completing two passes using the IC roller. Mark three random locations at least 2 feet from any edge of the compaction area and take density and moisture content measurements in accordance with Tex-115-E, Part I at all three locations.
3. Continue the compaction process, stop after every two subsequent passes of the roller, and take additional density and moisture content measurements at the same three locations. The Engineer will witness the tests performed and confirm the material achieves the density and moisture content requirements, if applicable. Continue to compact and test the first layer until 100% of the target maximum dry density is obtained.
4. Proof map the first layer and collect the IC data. Deliver the electronic IC data files to the Engineer. The Engineer will establish a roller Intelligent Compaction Target Value (ICTV) for the first layer. The ICTV is the average of the total roller Intelligent Compaction Measurement Values (ICMV) from the electronic IC data files.
5. Construct additional layers, when necessary, using the same IC roller and mapping pattern used to construct the first layer. The Engineer will determine the new ICTV for subsequent layers. The new ICTV for the subsequent layer will be 1.05 times the ICTV from the previous layer. This assumes the stiffness of the subsequent layer increases 5% compared to the previous layer. Proof

map and collect the IC data upon completion of compaction for each layer. Deliver the electronic IC data files to the Engineer.

6. Proof map and collect the IC data when compaction of the entire layer is completed. Deliver the electronic IC data files and a hard copy of the color-coded map to the Engineer. The IC data will be color-coded using green, yellow, and red colors as shown in Table 1.

Table 1. Color-coded Map Requirements

| Green  | Yellow                           | Red           |
|--------|----------------------------------|---------------|
| $>\mu$ | $\mu-\sigma < \text{ and } <\mu$ | $<\mu-\sigma$ |

- Note: 1.  $\mu$  is the ICTV (average of total ICMV in the IC data file).  
 2.  $\sigma$  is one standard deviation of total ICMV in the IC data file.

## 2. Project Production Compaction

1. Compact the materials for each layer using density control unless otherwise shown on the plans. Compact the materials in accordance with the plans and the applicable Specification Items listed in Section 2013.2, “Materials.”
2. Upon completion of compaction, proof map the finished layer over the full length and width using the same IC roller used for the Control Strip. Use the final ICTV calculated from the entire layer of the Control Strip and use as the beginning ICTV for further compaction. Deliver the electronic IC data files and a hard copy of the color-coded map to the Engineer. Provide the IC color-coded map using the same legend as shown in Table 1 in Section 2013.4.F.1.a.6.
3. Final compaction acceptance by the Engineer will be based on the Department-performed field density and moisture content measurements within 24 hours after completion of compaction. The density and moisture measurements shall be taken by the Engineer within the red color areas identified by the IC color-coded map. The Engineer may accept the section if no more than one of the five most recent density tests are below the target density and the failing test is no more than 3 pcf below the target density. In cases of dispute, the sand cone method may be used to determine density in accordance with Tex-115-E, Part II, and moisture content may be determined in accordance with Tex-103-E, Part I.
4. Rework, recompact, and refinish material that fails to meet the applicable Specification Items listed in Section 2013.2, “Materials.” or that loses required moisture, density, stability, or finish before the next layer is placed or the project is accepted. Continue work until specification requirements are met. Perform the work at no additional expense to the Department.

G. **Finishing.** Immediately after completing compaction of the final layer, finish the final section in accordance with the plans and the applicable Specification Items listed in Section 2013.2, “Materials.”

- H. **Curing.** Cure the finished section in accordance with the plans and the applicable Specification Items listed in Section 2013.2, “Materials.”.
- 5. **Measurement and Payment.** The work performed, materials furnished, equipment, labor, tools, and incidentals will not be measured or paid for directly but will be subsidiary to the pertinent Items.